NUREG/CR–6074
04–4448–010
Vol. 2

Sealed Source and Device Design Safety Testing

Technical Report on the Findings of Task 4

Investigation of Failed Nitinol Brachytherapy Wire

Prepared by
D. J. Reese, H. C. Burghard

Southwest Research Institute

Prepared for
U.S. Nuclear Regulatory Commission

AVAILABILITY NOTICE

Availability of Reference Materials Cited in NRC Publications

Most documents cited in NRC publications will be available from one of the following sources:

1. The NRC Public Document Room, 2120 L Street, NW., Lower Level, Washington, DC 20555-0001
2. The Superintendent of Documents, U.S. Government Printing Office, P. O. Box 37082, Washington, DC 20402-9328
3. The National Technical Information Service, Springfield, VA 22161-0002

Although the listing that follows represents the majority of documents cited in NRC publications, it is not intended to be exhaustive.

Referenced documents available for inspection and copying for a fee from the NRC Public Document Room include NRC correspondence and internal NRC memoranda; NRC bulletins, circulars, information notices, inspection and investigation notices; licensee event reports; vendor reports and correspondence; Commission papers; and applicant and licensee documents and correspondence.

The following documents in the NUREG series are available for purchase from the Government Printing Office: formal NRC staff and contractor reports, NRC-sponsored conference proceedings, international agreement reports, grantee reports, and NRC booklets and brochures. Also available are regulatory guides, NRC regulations in the *Code of Federal Regulations*, and *Nuclear Regulatory Commission Issuances*.

Documents available from the National Technical Information Service include NUREG-series reports and technical reports prepared by other Federal agencies and reports prepared by the Atomic Energy Commission, forerunner agency to the Nuclear Regulatory Commission.

Documents available from public and special technical libraries include all open literature items, such as books, journal articles, and transactions. *Federal Register* notices, Federal and State legislation, and congressional reports can usually be obtained from these libraries.

Documents such as theses, dissertations, foreign reports and translations, and non-NRC conference proceedings are available for purchase from the organization sponsoring the publication cited.

Single copies of NRC draft reports are available free, to the extent of supply, upon written request to the Office of Administration, Distribution and Mail Services Section, U.S. Nuclear Regulatory Commission, Washington, DC 20555-0001.

Copies of industry codes and standards used in a substantive manner in the NRC regulatory process are maintained at the NRC Library, Two White Flint North, 11545 Rockville Pike, Rockville, MD 20852-2738, for use by the public. Codes and standards are usually copyrighted and may be purchased from the originating organization or, if they are American National Standards, from the American National Standards Institute, 1430 Broadway, New York, NY 10018-3308.

DISCLAIMER NOTICE

This report was prepared as an account of work sponsored by an agency of the United States Government. Neither the United States Government nor any agency thereof, nor any of their employees, makes any warranty, expressed or implied, or assumes any legal liability or responsibility for any third party's use, or the results of such use, of any information, apparatus, product, or process disclosed in this report, or represents that its use by such third party would not infringe privately owned rights.

NUREG/CR–6074
04–4448–010
Vol. 2

Sealed Source and Device Design Safety Testing

Technical Report on the Findings of Task 4

Investigation of Failed Nitinol Brachytherapy Wire

Prepared by
D. J. Benac, H. C. Burghard

Southwest Research Institute

Prepared for
U.S. Nuclear Regulatory Commission

DF02 1/1

AVAILABILITY NOTICE

Availability of Reference Materials Cited in NRC Publications

Most documents cited in NRC publications will be available from one of the following sources:

1. The NRC Public Document Room, 2120 L Street, NW., Lower Level, Washington, DC 20555-0001

2. The Superintendent of Documents, U.S. Government Printing Office, P. O. Box 37082, Washington, DC 20402-9328

3. The National Technical Information Service, Springfield, VA 22161-0002

Although the listing that follows represents the majority of documents cited in NRC publications, it is not intended to be exhaustive.

Referenced documents available for inspection and copying for a fee from the NRC Public Document Room include NRC correspondence and internal NRC memoranda; NRC bulletins, circulars, information notices, inspection and investigation notices; licensee event reports; vendor reports and correspondence; Commission papers; and applicant and licensee documents and correspondence.

The following documents in the NUREG series are available for purchase from the Government Printing Office: formal NRC staff and contractor reports, NRC-sponsored conference proceedings, international agreement reports, grantee reports, and NRC booklets and brochures. Also available are regulatory guides, NRC regulations in the *Code of Federal Regulations*, and *Nuclear Regulatory Commission Issuances*.

Documents available from the National Technical Information Service include NUREG-series reports and technical reports prepared by other Federal agencies and reports prepared by the Atomic Energy Commission, forerunner agency to the Nuclear Regulatory Commission.

Documents available from public and special technical libraries include all open literature items, such as books, journal articles, and transactions. *Federal Register* notices, Federal and State legislation, and congressional reports can usually be obtained from these libraries.

Documents such as theses, dissertations, foreign reports and translations, and non-NRC conference proceedings are available for purchase from the organization sponsoring the publication cited.

Single copies of NRC draft reports are available free, to the extent of supply, upon written request to the Office of Administration, Distribution and Mail Services Section, U.S. Nuclear Regulatory Commission, Washington, DC 20555-0001.

Copies of industry codes and standards used in a substantive manner in the NRC regulatory process are maintained at the NRC Library, Two White Flint North, 11545 Rockville Pike, Rockville, MD 20852-2738, for use by the public. Codes and standards are usually copyrighted and may be purchased from the originating organization or, if they are American National Standards, from the American National Standards Institute, 1430 Broadway, New York, NY 10018-3308.

DISCLAIMER NOTICE

NUREG/CR-6074
04-0448-010
Vol. 2

Sealed Source and Device Design Safety Testing

Technical Report on the Findings of Task 4

Investigation of Failed Nitinol Brachytherapy Wire

Manuscript Completed: March 1996
Date Published: March 1996

Prepared by
D. J. Benac, H. C. Burghard

Southwest Research Institute
6220 Culebra Road
San Antonio, TX 78238-5166

D. H. Tiktinsky, NRC Project Manager

Prepared for
Division of Industrial and Medical Nuclear Safety
Office of Nuclear Material Safety and Safeguards
U.S. Nuclear Regulatory Commission
Washington, DC 20555-0001
NRC Job Code D2553

PREVIOUS DOCUMENTS IN SERIES:

Document Number	Issuance Date
NUREG/CR-6074 Vol. 1	*April 1994*

NUREG/CR–6074, Volume 2, has been reproduced from the best available copy.

ABSTRACT

This report covers an investigation of the nature and cause of failure in Nitinol brachytherapy sourcewires. The investigation was initiated after two clinical incidents in which sourcewires failed during or immediately after a treatment.

The investigation determined that the two clinical Nitinol sourcewires failed in a brittle manner, which is atypical for Nitinol. There were no material anomalies or subcritical flaws to explain the brittle failures. The bend tests also demonstrated that neither moist environment, radiation, nor low-temperature structural transformation was a likely root cause of the failures. However, degradation of the PTFE was consistently evident, and those sourcewires shipped or stored with PTFE sleeves consistently failed in laboratory bend tests.

On the basis of the results of this study, it was concluded that the root cause of the in-service failures of the sourcewires was environmentally induced embrittlement due to the breakdown of the PTFE protective sleeves in the presence of the high-radiation field and subsequent reaction or interaction of the breakdown products with the Nitinol alloy.

TABLE OF CONTENTS

TABLE OF FIGURES

TABLE OF TABLES

EXECUTIVE SUMMARY

As a result of two clinical incidents which involved the failure of two Nitinol brachytherapy sourcewires, an investigation of the nature and cause of the sourcewire failures was conducted by Southwest Research Institute (SwRI) under the direction of the Nuclear Regulatory Commission (NRC).

The failed sourcewires were extensively examined using the Scanning Electron Microscope (SEM) to establish overall fracture features and fine-scale topographic features. In addition, X-ray spectrographic techniques, chemical analyses, metallographic examination, microhardness measurements and thermal analyses were conducted on the failed sourcewires and on the Nitinol wire.

A bend test program was pursued to evaluate the material properties of the Nitinol wire and to establish fracture characteristics of clinical sourcewires. As part of the test program, dummy and active sourcewires were exposed to environments of moisture, teflon, and temperatures below 10°C. In addition, solid wires were electrolytically charged with hydrogen.

The investigation determined that the Nitinol sourcewires failed in a brittle manner which is atypical for Nitinol. There was no material anomaly or subcritical flaw to explain the brittle failures. It was determined that the brittle failure resulted because of environmentally- induced-embrittlement. Results of additional tests on other sourcewires indicated that moisture, radiation, or temperature below 10°C was likely not a cause of failure. However, teflon degradation was evident on service failures and other sourcewires. Consistently, sourcewires shipped or stored with a teflon-liner either failed in the storage cask or failed in a brittle manner during a bend test.

On the basis of the results of this study, it is concluded that the root cause of the in-service failures of the sourcewires was environmentally-induced-embrittlement due to the breakdown of the PTFE protective sleeves in the presence of the high-radiation field and subsequent reaction or interaction of the breakdown products with the Nitinol alloy. It is likely that the embrittlement occurred by a classic hydrogen-embrittlement process or by a process with very similar characteristics.

INTRODUCTION

Failures of two brachytherapy sourcewires were recently encountered at two separate cancer treatment facilities. For the purposes of this report, the two treatment centers are identified as Facility A and Facility B. The failure at Facility A occurred in December 1992 during an actual treatment procedure. The second failure occurred at Facility B in January 1993, at the completion of a procedure.

The sourcewires involved in both incidents were 0.59 mm (0.023 in) diameter Nitinol wire, shown in Figure 1-1(a), and contained a 10 Ci Ir-192 radiation source. The iridium source measured 0.34 mm (0.014 in.) in diameter x 10 mm (0.394 in.) In length and was encapsulated in an axial cavity at one end of the sourcewire. Nitinol is a NiTi shape memory alloy, see Section 1.2 for more details. Prior to May 1992, the sourcewires for this particular system were fabricated from Type 316L stainless steel wire.

As a result of the two clinical incidents, an investigation of the nature and cause of the sourcewire failures was initiated at Southwest Research Institute (SwRI) at the direction of the Nuclear Regulatory Commission (NRC).

The investigation of the sourcewire failures conducted at SwRI included examinations and tests of the two failed wires as well as a test program to investigate the fracture characteristics of other selected sourcewires and Nitinol wire samples.

1. BACKGROUND

1.1 Brachytherapy Treatment and Equipment

Brachytherapy treatment involves the insertion of a sealed radiation source into a patient's body to provide direct radiation to cancerous tumors, and is accomplished by extension of an active sourcewire from an afterloader storage and control device through one or more catheters to needles or applicators, which have been previously implanted at treatment sites (see Figure 1-1(b)).

Both failure incidents involved identical 10-channel afterloader systems produced by the same manufacturer. The system employs dual wires, one dummy and one active, each with a separate drive mechanism, a dedicated control and monitoring system, an activation and safety circuit, and a lead safe for storage of the active radiation source. A schematic diagram of the particular afterloader in use at Facilities A and B is shown in Figure 1-2.

The computer system, activating the drive mechanism, controls the extension and retraction of sourcewires. The dummy sourcewire (non-radioactive) is extended to the treatment site prior to extension of the active sourcewire. This feature verifies the integrity of the catheter connections and the sourcewire path prior to extension of the active source from its lead storage safe. The 10-channels allow for sequential treatments at multiple treatment sites. The active sourcewire can be positioned incrementally in each needle or applicator for specified times to provide prescribed radiation doses.

1.2 Characteristics and Properties of Nitinol Alloy

Nitinol was the material used for the failed brachytherapy wires. Nitinol (Nickel Titanium Naval Ordance Laboratory)[1] is not a conventional material, but a NiTi shape memory alloy (SMA) with the ability to restore itself to a previous shape with specific thermal treatments. The material, developed in the early 1960s, has found extensive use in military, industrial, and medical applications. This particular Nitinol alloy, often referred to as 55-Nitinol, has a nominal chemical composition of 55% nickel and 45% titanium. The properties are shown in Table 1-1.

Two unique characteristics of Nitinol determine how the material acts at various strains and temperatures:

(1) The material can be deformed plastically at temperatures below a specific transformation temperature and the original shape can be restored upon heating above that transformation temperature. This type of behavior is known as shape memory effect or thermal memory.

(2) The material can undergo unusually large mechanical strains at temperatures above the transformation temperature without displaying plasticity. When the strain is removed, the shape is then restored. This behavior is known as pseudoelasticity (PE) or superelasticity (SE).

Table 1-1. Typical Properties for Nitinol

Property	Units	Value
Young's Modulus[2]	ksi (kg/mm^2)	10.2×10^3
Minimum Ultimate Tensile Strength at 20°C[3]	ksi (kg/mm^2)	199.1 (140)
Minimum Yield Strength at 20°C[3]	ksi (kg/mm^2)	78.2 (55)
Minimum Elongation at Failure[2]	%	12
Density[2]	g/cm^3	6.4
Transformation[3]	°C	15±5°

1. 55-Nitinol - The Alloy with a Memory: Its Physical Metallurgy, Properties, and Applications, NASA, SP. 5110.
2. High Technology Handbook, Volume II, Chapter 11 Shape Memory Alloys, 1993. Prepared by SwRI under Contract No. F41608-87-A237.
3. Vendor Data.

The reason Nitinol has shape memory abilities and superior elastic behavior is because of a phase transformation that occurs at a specified transformation temperature. The transformation temperature is often referred to as the M_S, the martensite start, or A_F, the austenite finish temperature. The transformation from austenite to martensite is what allows the material to restore its shape. Figure 1-3(a) shows a diagram indicating the transformation effects on structure as a function of temperature. In the case of the brachytherapy wire used in the mechanical device, the Nitinol had a transformation temperature specified as 15°C ± 5°C. So, above 15°C (59°F), Nitinol is stable in the austenite crystal structure. At temperatures below 10°C (50°F), the austenite undergoes a phase transformation to another crystal structure, called martensite. For clinical usage, the operating temperatures are typically above 15°C (59°F), so the Nitinol wire is constantly in the austenite crystal structure. So, the sourcewire application does not take advantage of the thermal memory effects.

As noted, the thermal memory was not a factor in selection of Nitinol. However, the materials pseudoelastic behavior and ability to withstand high strains while still maintaining elasticity makes it a good candidate for medical devices. Figure 1-3(b) shows how the material responds as a function of stress and strain. When the wire is extended and retracted from the afterloader, the wire goes through multiple bends. The wire needs to return to its linear shape without distortion after it is deflected. Nitinol can be strained to about 8% and still return to its original shape. A conventional stainless steel material will incur permanent plastic deformation after about 0.1% strain. Figure 1-4 shows a typical stress strain curve for a conventional material.

Although thermal memory was not a consideration in the decision to use Nitinol, in the investigation of the failed wires, the transformation temperature was determined because the transformation temperature is an indication of material quality. In addition, bend properties, both in the austenite and the martensite structure, were analyzed to determine if one of the structures was more susceptible to brittle failure.

1.3 Handling and Storage of Sourcewires

Because of the high level radioactivity, brachytherapy sourcewires are shipped and stored in specifically designed lead casks. A photograph of a typical shipping cask is shown in Figure 1-5, and the design is detailed in Figure 1-6. The cask consists of a two-part lead cylinder 4 inches in diameter x 5 inches high. A tungsten cylinder is embedded in the central portion of the cask for further shielding. The lower part of the cask contains a 0.190-inch diameter stainless steel tube extending into the tungsten block. The stainless steel tube has a jog which prevents radiation from escaping directly up the tube. The stainless steel tube is embedded into a tungsten cylinder for further shielding. A sectioned cask is shown in Figure 1-7.

Typically, the brachytherapy wires are shipped to the clinic in the lead casks prior to use and then stored in the cask after approximately three months of service. The earlier shipments, before 28 September 1992, which included the failed wires, were shipped and stored with a teflon sleeve. The teflon sleeve was used to transfer the wire remotely into the cask. The sleeved wire was inserted into the stainless tube, then forced past the jog until the wire was bottomed out in the tungsten cylinder. The wire was held in place with a compression fitting. After the service failures occurred, the wires were no longer stored with a teflon-sleeve. Instead, the wires are inserted into a stainless steel needle, shown in Figure 1-8, which in turn is inserted into the lead cask.

1.4 Scope of Investigation

From the onset of the investigation, determination of the failure mechanism on these failures was a very complex process. There are several reasons for the complexity of the investigation.

(1) The sourceswires were at high levels of radioactivity. This required special handling procedures and limited fractographic examination.

(2) The Nitinol wire is a shape memory alloy that does not behave like conventional materials. So, the effects of transformation on susceptibility to failure had to be evaluated.

(3) There are a very limited number of documented failure cases involving Nitinol. This required additional testing to understand the possible embrittlement phenomenon of Nitinol.

The wire sides of each of the failed sourcewires were extensively examined in the scanning electron microscope (SEM) to establish the overall features of the failed wire as well as the fine-scale topography of the fracture surfaces. In addition, X-ray spectographic techniques were employed to analyze surface deposits. Chemical analyses, metallographic examinations, microhardness measurements, and thermal analyses were also performed on specimens from the same lot of wire.

A bend test program was organized and pursued to establish the fracture characteristics of selected sourcewire samples and identify the susceptibility of the sourcewires to embrittlement processes. This test program included active sourcewire that had been subjected to varying environments in service and in subsequent storage as well as solid wire samples that had been electrolytically charged with hydrogen.

The procedures used and the results obtained in these tests and examinations are presented in the following section of this report.

a) Nitinol Wire

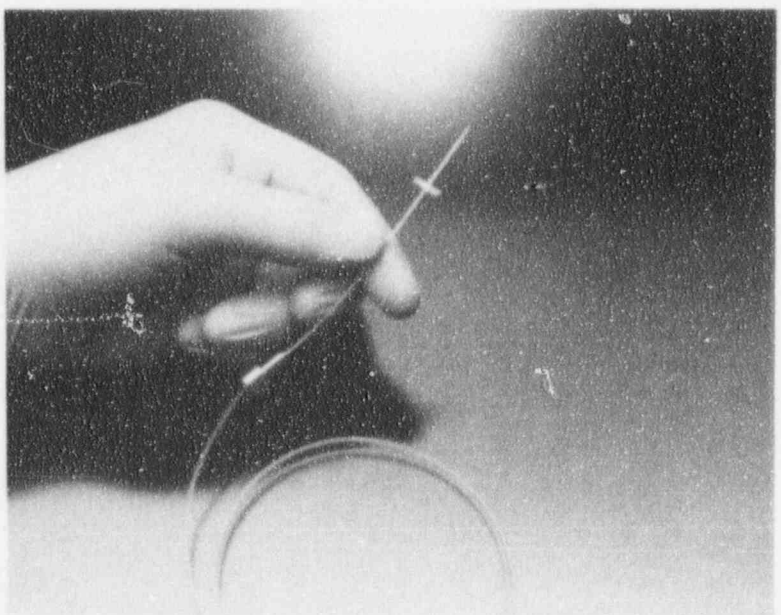

b) Catheter and Needle

Figure 1-1 Photograph of the Nitinol Wire, Needle,and Catheter.

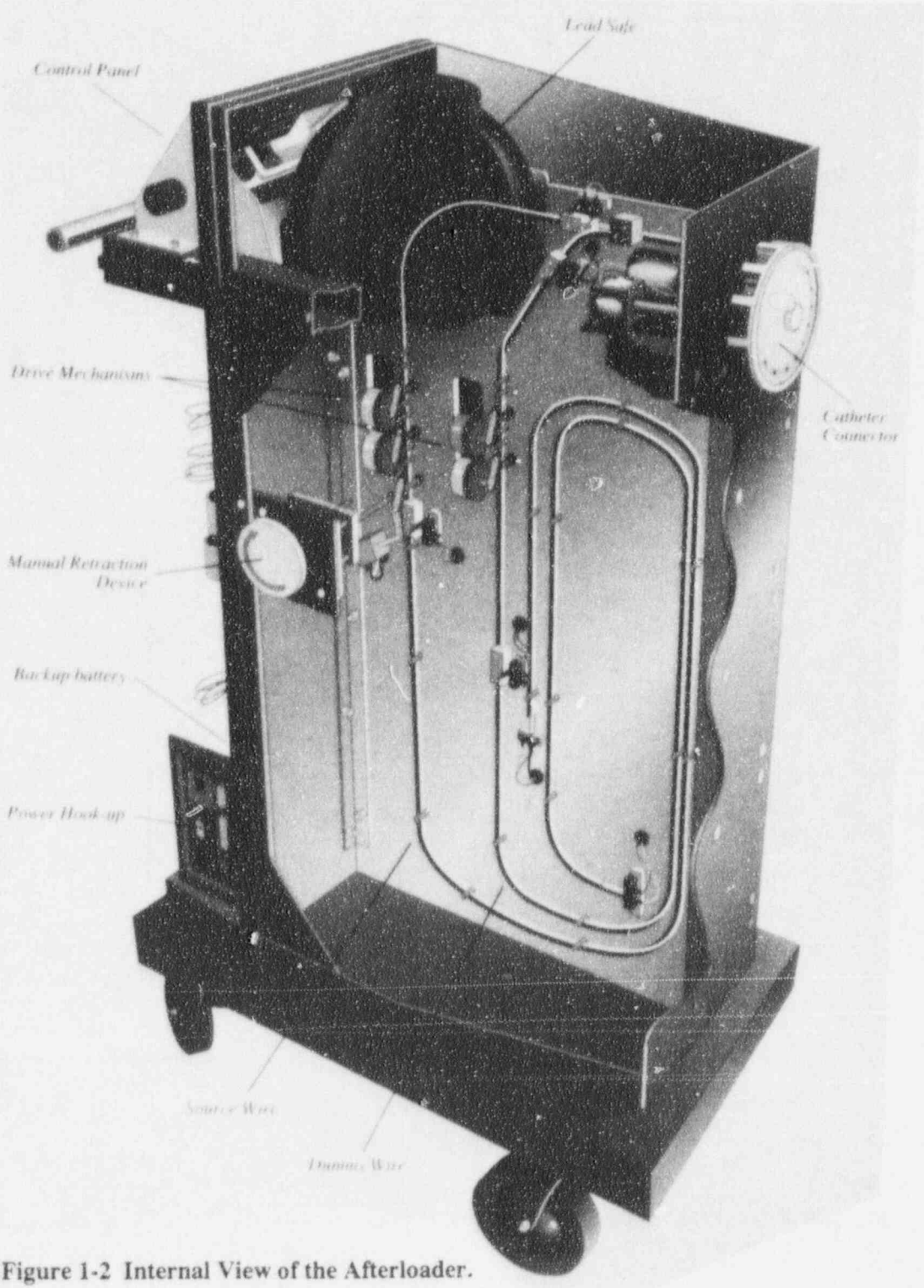

Figure 1-2 Internal View of the Afterloader.

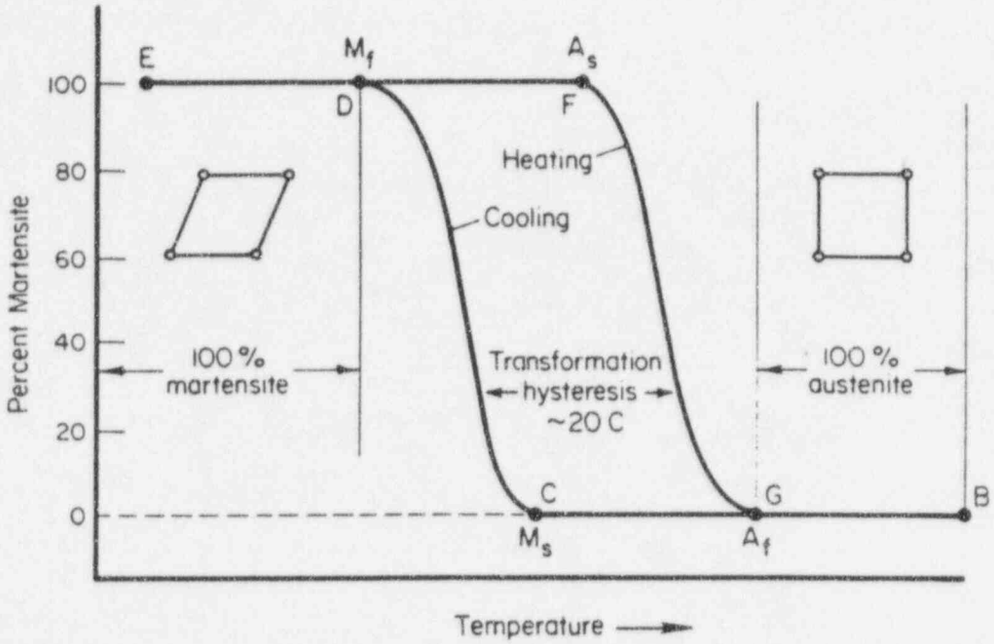

a) Thermal Memory

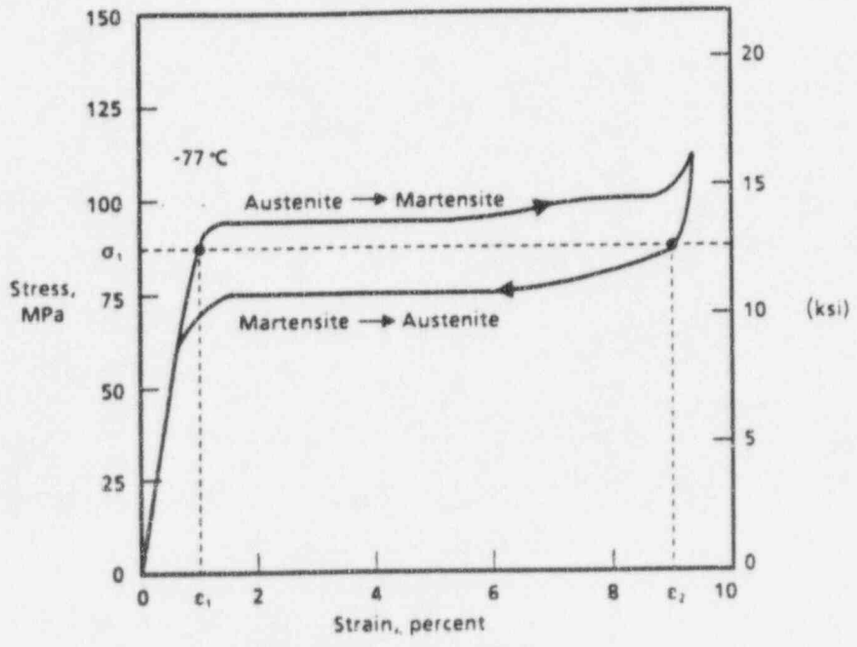

b) Pseudoelastic Effect

Figure 1-3 Illustration of Austenite Transformation to Martensite in a Shape Memory Alloy.

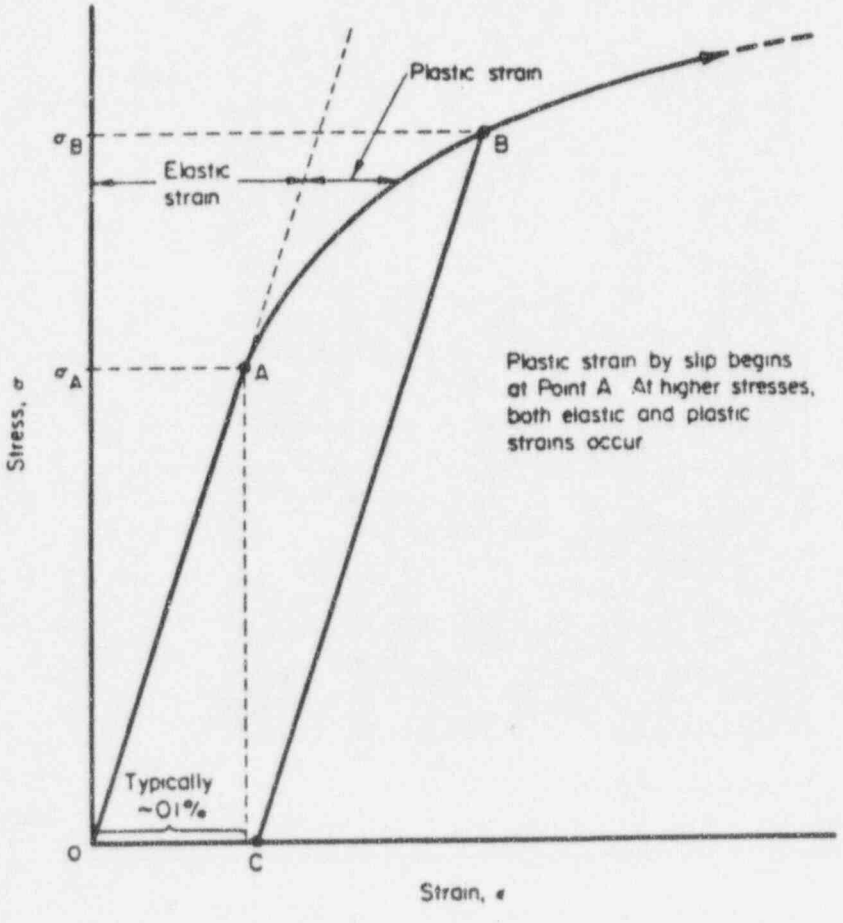

Figure 1-4 Stress-strain Response of Conventional Metals and Allows.

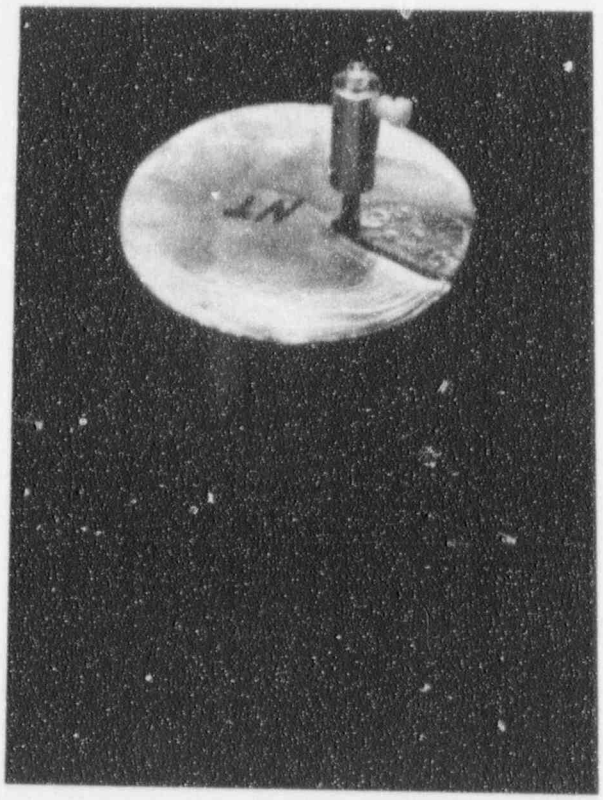

Figure 1-5 Photograph of a Lead Cask.

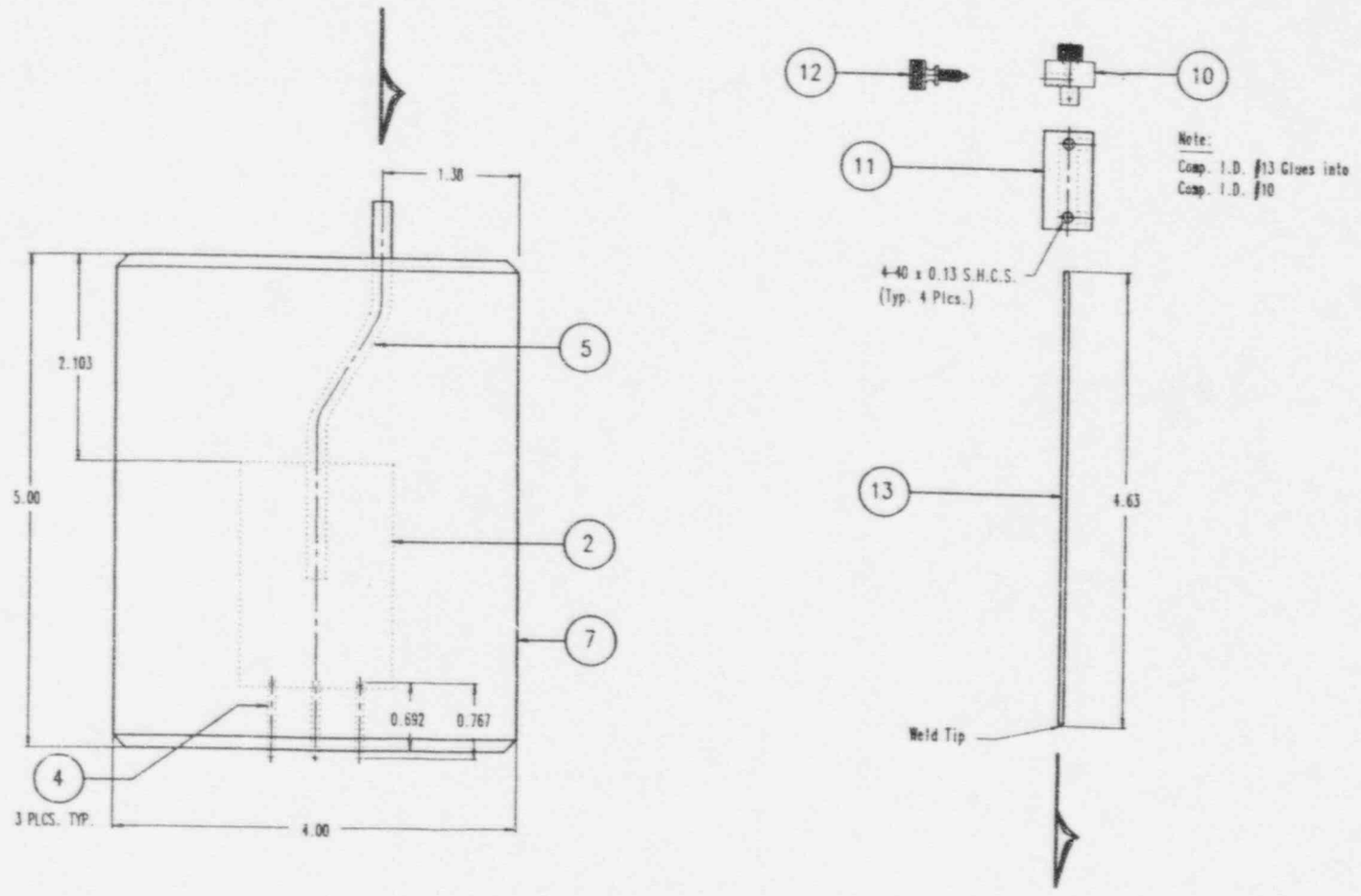

Figure 1-6 Engineering Drawing of a Cask.

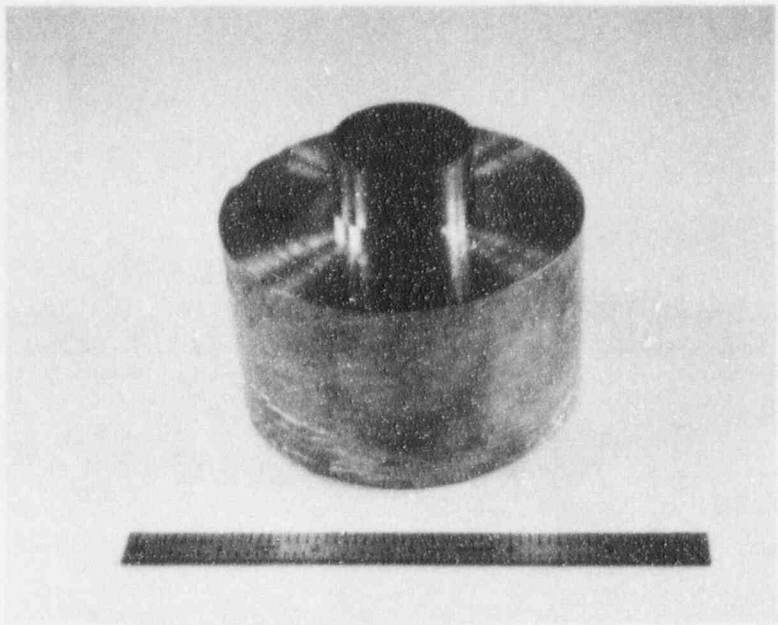

59693

a)

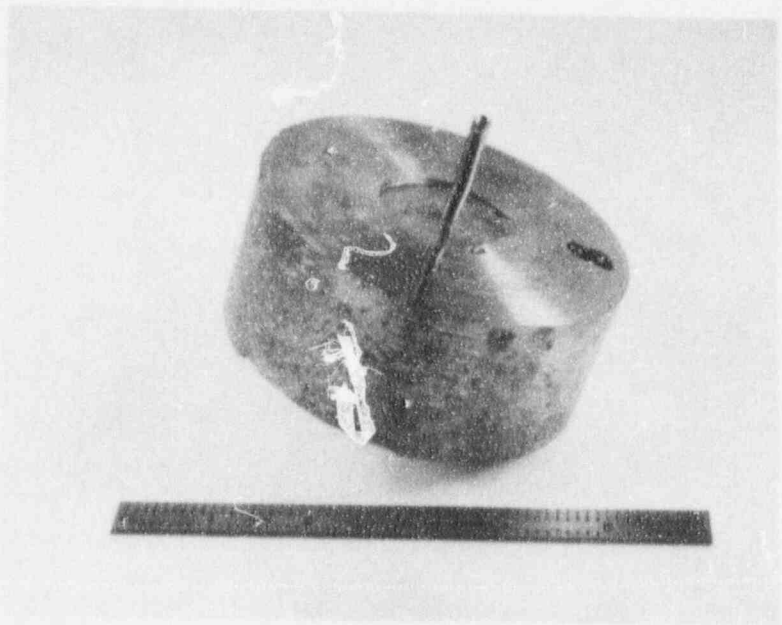

59694

b)

Figure 1-7 Photographs of a Cross Sectioned Cask.

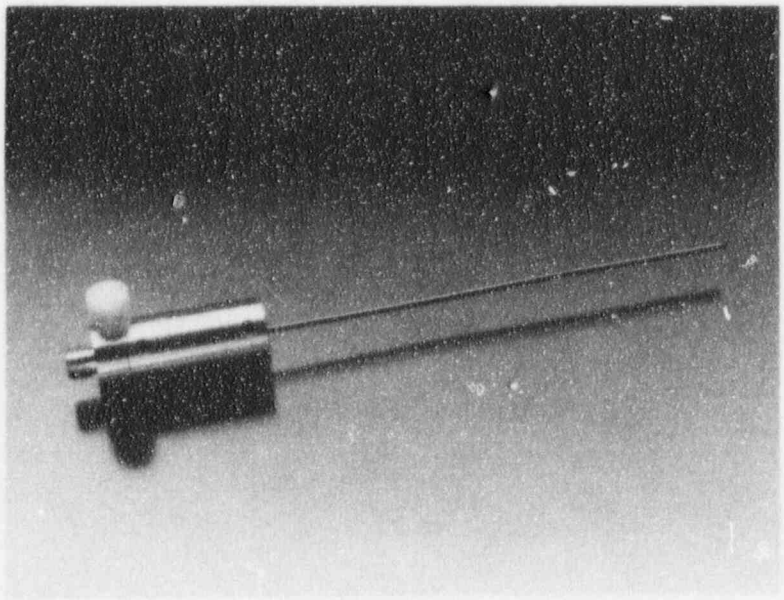

1X

Figure 1-8 Photograph of a Stainless Steel Needle for Storing Brachytherapy Wires.

2. EXAMINATIONS OF IN-SERVICE SOURCE FAILURES

The fracture surfaces on the wire side of each failure were examined in the SEM to establish the general character of the failures, as well as the fine-scale fractographic features. Energy dispersive X-ray spectroscopy was also employed to provide qualitative analyses of deposits on the fracture surfaces and deposits from wipes made on the outside surface of the failed sourcewires. Longitudinal metallographic sections of the wire side of each failure were also prepared and examined to identify the microstructural features and provide for microhardness measurements in the vicinity of the failure. Further characterization of the sourcewire material was accomplished by means of bulk chemical analyses to establish the material composition and thermal analysis to identify transformation characteristics. The results of these tests and examinations on the failed sourcewires are presented in the following subsections.

2.1 Sourcewire from Facility A

2.1.1 General Features

SEM photomicrographs of the complete fracture surface are shown in Figure 2-1. The fracture developed through the wall of the source cavity a short distance from the bottom of the cavity. The fracture surface was comprised of two major zones, each representing approximately 50% of the total fracture. One of the zones was extremely flat and oriented essentially normal to the axis of the wire. The remaining half of the fracture was a slant surface oriented approximately 45° to the wire axis. The slant fracture exhibited somewhat rougher features than the flat fracture. In the as-received condition, the end of the wire and the fracture surface were covered with a deposit material that had a non-metallic appearance. The SEM photomicrographs of Figure 2-1 and the subsequent detailed fractographs were taken after ultrasonic cleaning in deionized water and nonaggressive solvents.

Limited low-magnification examinations of the fracture surface on the source side of the failure also revealed approximately 50% flat fracture and 50% slant fracture.* However, the two parts did not provide an exact match in that the slant fracture zones were oriented in opposite directions. This feature indicates that a portion of the wire between the two slant fractures was broken loose and lost in the failure incident.

There were no general features to indicate any significant plastic deformation of the wire during the fracture process. On the basis of this feature, the failure may be classified as a brittle fracture.

2.1.2 Fractography

Representative SEM fractographs illustrating the fine-scale topographic features of the wire-side fracture surface of Sample No. 410 are shown in Figures 2-2 through 2-5. The flat zone exhibited uniform, generally equiaxed dimples indicative of fracture by microvoid growth and coalescence; see Figures 2-2 and 2-3. A very thin, continuous shear lip was present around the outer periphery of the flat zone [Figure 2-2(a)]. There were no fractographic features to identify any unique fracture initiation sites within the flat zone and no indications of any preferred direction of cracking in that zone.

The fractographic details of the slant zone are illustrated in Figures 2-4 and 2-5 [also see Figure 2-1(b)]. This zone was relatively flat and smooth, but exhibited numerous small steps emanating from the cavity surface [Figure 2-1(b) and Figure 2-4(c)]. The nature and orientation of these steps indicate that, within the slant zone, crack initiation occurred along the cavity wall and propagated outward through the wall thicknesses at central locations and back toward the flat zone at the extremities of the zone. There was some curvature to the surface at the bottom of the flat zone on the outside surface of the wire [Figure 2-4(a)]. This area also exhibited numerous fine-scale steps. The fractographic character of this area [Location 4, Figure 2-1(a)] is consistent with fracture in a through-wall direction from the inside out. Other step features were present at the outer periphery of the slant zone [Figure 2-5(a)], but there were no fine-scale features to identify the particular fracture mechanism involved for this zone. The intersection of the slant zone and flat zone is shown in Figure 2-5(b). A through-wall longitudinal crack was present at this location, but, again, there were no features to positively identify the mechanism of fracture in the slant zone or positively establish the sequence of the fracture process.

---

* Both iridium pellets were retained in the source side of the failure. As a result, the radioactivity level was too high to allow any direct evaluation other than very brief examination in the stereomicroscope.

2.1.3 Surface Deposits

Representative X-ray energy spectra from the fracture surface of Sample No. 410 are shown in Figures 2-7, 2-8, and 2-9. Note that in these analyses both the beryllium window technique, which detects elements down to Z = 11 (Na), and the ultra-thin window technique, which detects elements down to Z = 5 (B) were used.

As expected, peaks for nickel (Ni) and titanium (Ti), the two principal constituents of the Nitinol wire, were present in varying degrees in all of the spectra recorded. These could arise either from corrosion products on the surface or directly from the underlying Nitinol wire material. In this case, since relatively low oxygen levels were indicated, it is likely that the Ti and Ni peaks are associated with the base metal itself. Other than Ni and Ti, the elements detected among the several locations analyzed included aluminum (Al), silicon (Si), chlorine (Cl), potassium (K), calcium (Ca), and sodium (Na). These elements were common to a majority of the locations analyzed, but present in varying amounts. The indications for Al and Si were consistently small to very small while chlorine peaks were generally very small with one notable exception, see Figure 2-7. Ca and K peaks were generally small. In most cases where sodium was detected, the indicated amounts were very small (Figure 2-8), but at one location a moderate amount was observed (Figure 2-7). Fluorine was consistently present at all locations examined on the fracture surface and usually present in substantial quantity (Figures 2-8 and 2-9). In one instance, small quantities of copper (Cu) and zinc (Zn) were also detected, see Figure 2-8.

The deposit materials on the outside wire surface and in the source cavity surface were also analyzed; representative X-ray energy spectra are shown in Figures 2-10 and 2-11. On the outside, the only elements indicated, other than Ti and Ni, were barely detectable amounts of aluminum and silicon, see Figure 2-10. In the case of the inside cavity surface, very small quantities of Al, Si, S, Cl, and K were indicated along with moderate oxygen (O) and fluorine peaks, see Figure 2-11.

At the time of the initial on-site investigation of the sourcewire failure several wipe tests of the sourcewire were made. These tests are usually performed as a means of detecting radioactive contamination. In this case, small quantities of a dark gray or black deposit were collected on the cloth wipe patches. These were analyzed by EDS and the results are shown in Figures 2-12 and 2-13. The strongest peaks in the spectrum for the black deposit on the wipe were for oxygen, aluminum, and titanium. Small to moderate amounts of silicon, iron (Fe), nickel, copper, and zinc were also detected. An X-ray spectrum from a clean area on the wipe material is shown in Figure 2-4. This spectrum exhibits a strong aluminum peak with a small silicon peak and probably indicates that the Al and Si peaks obtained for the deposited coating can be attributed to the underlying wipe material

2.2 Sourcewire from Facility B

2.2.1 General Features

The overall features of the fracture in the sourcewire from Facility B (Sample No. 411) are illustrated by the SEM photomicrographs shown in Figures 2-15 and 2-16. In this case, the fracture was located very close to the bottom of the source cavity. This fracture was similar to that in Sample No. 410 in that it was comprised of a flat zone oriented normal to the wire axis and a slant zone. In this case, however, the flat zone was predominant, comprising approximately 75% of the total fracture surface.

The cross section at the fracture remained very round [Figure 2-16(a)] and there was no evidence of overall plastic deformation of the wire. The overall character of the failure serves to classify it as brittle fracture. At the fracture location, the cavity wall was not uniform in thickness [Figure 2-16(a)], but this feature is attributed to the cavity being slightly off center and does not indicate thinning due to plastic deformation.

In the as-received condition, the entire fracture surface, and the shallow depression corresponding to the bottom of the cavity were covered with a relatively thick deposit material with nonmetallic characteristics. The SEM photomicrographs and fractographs shown in Figures 2-15 through 2-19 were all taken after ultrasonic cleaning in nonaggressive solvents.

2.2.2 Fractography

The fine-scale fractographic features of the fracture surface are shown in Figures 2-17 and 2-18. Both the flat zone and the slant zone exhibited a distinct dimpled topography characteristic of fracture by microvoid growth and coalescence.

There were no clearly defined initiation sites or directional features, but the occurrence of a few small steps at the inside edge of the flat zone [Figure 2-17(b)] and the orientation of tear dimples [Figure 2-17(c)] suggests that, in the flat zone, fracture might have initiated at the cavity wall. The orientation of tear dimples in the slant zone (Figure 2-18) clearly indicates that the direction of fracture was down the slope, as viewed in Figure 2-15.

A distinct thin rim, resembling a shear lip, was present almost completely around the periphery of the fracture. This feature is evident in Figure 2-16(b) and detailed features are shown in Figure 2-19(a). Another feature noted in the examination was the presence of small subcritical cracks near the fracture surface, as shown in Figure 2-19(b). Those cracks in Figure 2-19(b) represent the largest of any outside surface defect noted and were confined to the immediate locale of the main fracture. The small gap in the rim, which is evident in Figure 2-19(a), could possibly represent a subcritical crack involved in the final fracture. However, this feature cannot be fully evaluated without direct comparison of the mating fracture surfaces.

The character of the inside surface of the source cavity is illustrated in Figure 2-19(c). This surface exhibited smooth, rounded features, and shallow surface cracks were evident. These features are consistent with a thin melted and resolidified surface layer as may be expected for electric discharge machining.

2.2.3 Surface Deposits

As noted above, the fracture surface of Sample No. 411 was originally covered with a relatively thick deposit material. Photomicrographs of the surface in the as-received condition are shown in Figure 2-20. Individual locations on the surface were analyzed by EDS in the as-received conditions and representative examples of the X-ray energy spectra obtained are shown in Figures 2-20 and 2-21.

A number of elements were detected other than the nickel and titanium of the base metal. These included carbon (C), oxygen (O), sodium (Na), aluminum (Al), silicon (Si), sulfur (S), chlorine (Cl), potassium (K), calcium (Ca), chromium (Cr), and iron (Fe). The indications are that the Al, Si, and S were present in small quantity among all of the locations examined. Na and Cl were present in substantial amounts at one location (Figure 2-21), and Fe and Cr were present in substantial amounts at another site (Figure 2-22). All of the elements detected, besides the Ni and Ti, can be attributed to extraneous deposit material from an outside source. None of these were detectable in EDS analyses on clean locations on the wire, see Figure 2-23. It should be noted, that in contrast to Sample No. 410, no fluorine was detected in the deposit material.

2.3 Material Characterization

Chemical analyses, metallographic examinations, microhardness measurements, and thermal analyses were performed to characterize the composition and properties of the sourcewire material. Although it was established that the wire material was specified as the 55Ni45Ti alloy Nitinol, the actual material specification was not available for review. A mill test report for the particular heat was available, however, and typical composition and properties were available from the literature. The results of these tests and analyses are presented in the follow subsection.

2.3.1 Chemical Composition

Specimens from two different sourcewire samples, Samples No. 410 and No. 414, were analyzed to establish the chemical composition. The results are presented in Table 2-1 and are compared with typical values and the composition stated in the mill test report in that table.

Table 2-1. Chemical Composition

Sample No.	Composition - wt.%										
	Ni	Ti	C	Al	Zn	Fe	Zr	Cu	O	H	All Other
No. 411	54.59	44.93	0.29	<0.01	<0.01	<0.01	<0.01	<0.01	N/A	N/A	--
No. 414	54.10	45.65	0.10	<0.01	<0.01	<0.01	<0.01	<0.01	N/A	N/A	--
Mill Test	56.03	43.85	0.039	--	--	--	--	--	0.063	0.0018	0.0162

The compositions determined for the two specimens are very similar and are comparable to that presented in the mill test report. The differences evident in Table 2-1 are not unusual between different specimens of a single heat and are not unusual between mill analyses and product analyses.

2.3.2 Thermal Transformation

Differential scanning calorimetry (DSC) techniques were employed to identify the transformation temperature for the Nitinol wire. In this procedure, a small specimen (≈ 40 mg) is heated through a given temperature range at a closely controlled rate. The occurrence of endothermic or exothermic reactions or transformations during the heating process alters the heat input necessary to maintain a constant heating rate and measurements of the heat input in any temperature range below melting provides indications of solid-state transformation.

In this case, specimens taken from Sample No. 414 were analyzed in the Perkin Elmer DSC-4 thermal analyzer over a temperature range of -20 to 80°C at a scanning rate of 30°C/min. A DSC curve representative of the results obtained is shown in Figure 2-24. A distinct peak is evident over the temperature range of 10-20°C, which indicates a solid-state transformation within that range. The maximum of the peak occurs at 20°C, which indicates conformance to the transformation temperature value of 15±5°C presented in the mill test report.

2.3.3 Microstructure and Microhardness

Longitudinal metallographic sections were taken through the fractured end of each of the two failed sourcewires (Samples No. 410 and 411). In each case, the end containing the wire side of the fracture was cut off and mounted in clear mounting compound. Each specimen was mounted intact with an orientation so that subsequent grinding would create a longitudinal section intersecting both the flat zone and slant zone. Both mounted specimens were then progressively ground and polished. The microstructure and microstructural character of the fracture were examined in sequential sections down to the centerline. Photomicrographs illustrating the pertinent features observed are shown in Figures 2-25 through 2-29.

The overall configuration of the cross sections through the sourcewire from Facility A is shown in Figure 2-25. The relative positions of the flat and slant zones and the position of the fracture relative to the bottom of the cavity are readily evident. The microstructure consists of uniformly distributed, elongated particles and dispersed smaller particles in a generally featureless matrix, see Figure 2-26(a). No grain boundaries were evident in the matrix. This two-phase structure is consistent with the composition and the elongated particles are typical of drawn wire. In the course of the metallographic examination, the thin altered case on the inside of the cavity and several small crack-like defects in the cavity wall were evident. These features are illustrated in Figures 2-26(b) and (c). Figure 2-27 shows the longitudinal crack at the junction of the slant and flat zones. This is the crack that was observed in the fractographic examinations and illustrated earlier in Figure 2-5(b). The crack extended only 0.01 inch beyond the fracture surface in the longitudinal direction.

Representative microstructural features of the sourcewire from Facility B (Sample No. 411) are shown in Figures 2-28 and 2-29. The proximity of the fracture to the bottom of the cavity is evident in Figure 2-28(a) and the section shows the relationship of the flat and slant zones. The microstructure is identical to that of Sample 410 [Figure 2-28(b)] and a few similar cavity surface defects were noted (Figure 2-29).

Vickers microhardness measurements were made on the longitudinal sections of each sample. Hardness indentations were made in the immediate vicinity of the cavity and at remote locations using a standard 136° diamond pyramid indentor with a 500 gm load. The locations of the indentations in the vicinity of the cavity in Sample No. 410 are shown in Figure 2-25. Other measurements were remote to the cavity. In the case of Sample 411, three indentations were made across the section immediately below the cavity and three more sets of indentations were made at positions progressively further from the cavity. The results of all measurements are presented in Table 2-2. The hardness values obtained were very uniform over the multiple indications in each sample and the values for the two separate samples were comparable. For Sample No. 410, the measured hardness was in the range of VHN 396-427 and the values determined for Sample 411 were in the range of VHN 409-426. These values correspond to approximately HRC 40 and a variation of 20 points on the VHN scale represents approximately 2 points on the HRC scale.

2.4 Summary of Observations

The principal observations made in the examination of the two failed sourcewires are itemized below.

1) Both failures were brittle in nature without any evidence of plastic deformation of the cavity wall or of the wire itself.

2) Both fractures were comprised of a flat zone oriented normal to the wire axis and a slant zone. The flat zone in the wire from Facility A comprised approximately 50% of the total fracture and that in the Facility B sample amounted to nearly 75% of the fracture.

3) The flat zones in both failures were characterized by fine-scale dimples typical of microvoid growth and coalescence. Dimples were also evident in the slant zone of the wire from Facility B but the fine-scale features of the slant zone in the wire from Facility A were indeterminant except for small steps and direction markings.

4) Fluorine was consistently detected in the surface deposits on the sample from Facility A. It was not possible to determine the form of the fluorine, however. Other extraneous elements such as aluminum and silicon were also detected but none of these, except possibly chlorine, were indicative of a corrosive environment.

5) In the case of the Facility B sample, no fluorine was detected in the deposit analyses. Numerous other elements, including sodium, chlorine, iron, and chromium were present in the deposits.

6) The chemical compositions were normal for 55-Nitinol and comparable to that reported in the mill test report. The microstructure was normal for this alloy and the hardness was uniform and consistent with the strength values listed in the mill test report. DSC indicated a transition temperature consistent with the mill test report.

7) The cavity in the wire from Facility B was slightly misaligned but there was no evidence to indicate that this was a causitive factor in the failure.

8) There was no evidence to indicate that any form of mechanically induced damage was involved in either failure.

Table 2-2. Microhardness Data

Indentation No.	Hardness (VHN)*	
	Sample 410	Sample 411
1	416	409
2	418	409
3	402	409
4	396	409
5	396	409
6	408	409
7	396	417
8	427	417
9	408	409
10	409	417
11	427	417
12	402	426
13	408	--
14	422	--

* All measurements made with 500 gm load.

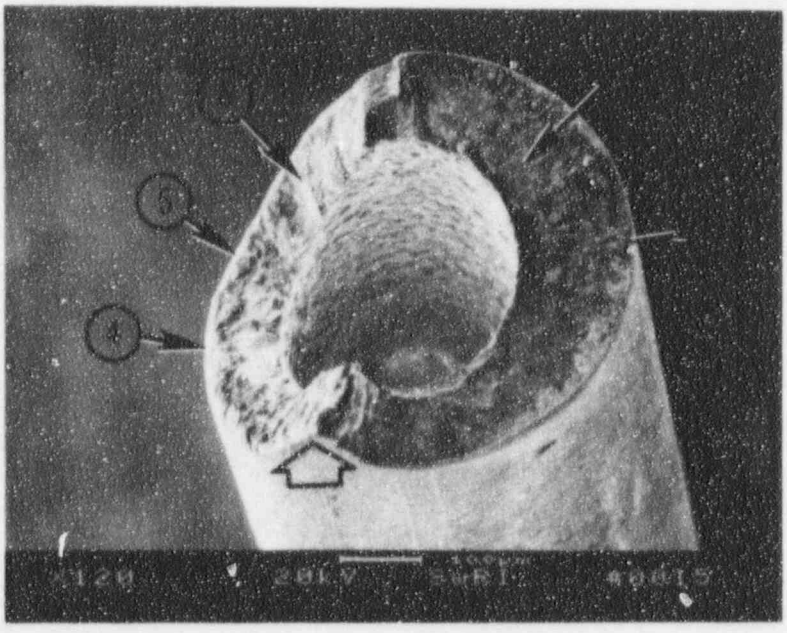

59474

(a)

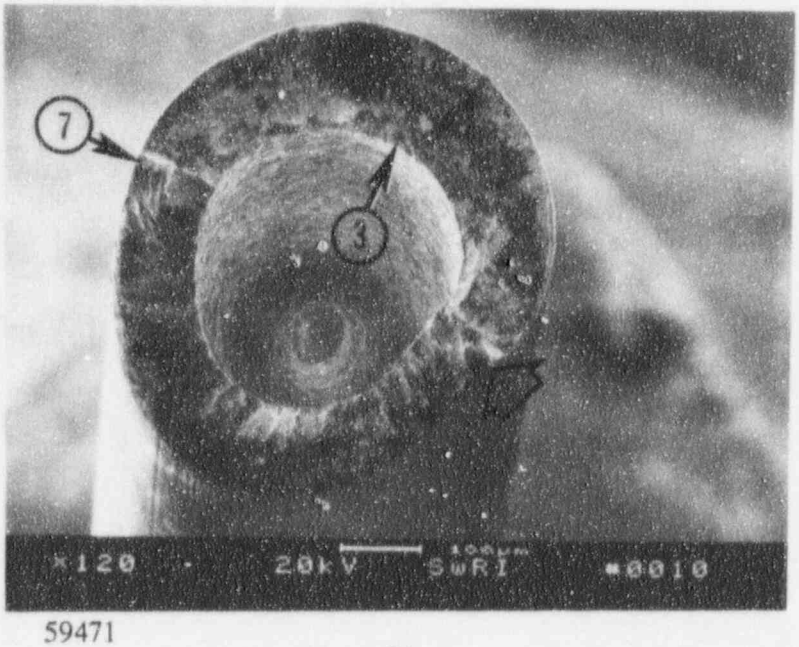

59471

(b)

Figure 2-1 SEM Photomicrographs of Failed Source Wire from Facility A (Sample No. 410). Fracture surface on wire side of failure. Bottom of source cavity is evident in (b). Block arrows mark match points for two views.

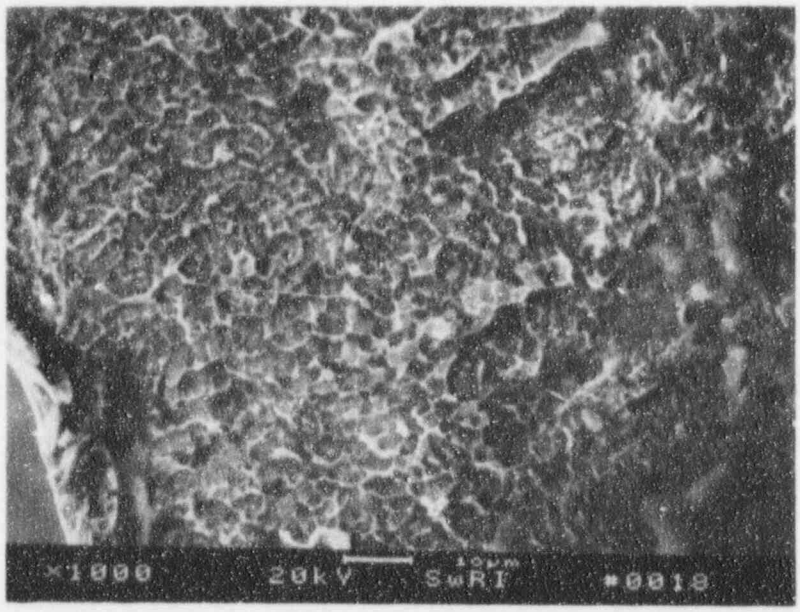

59481

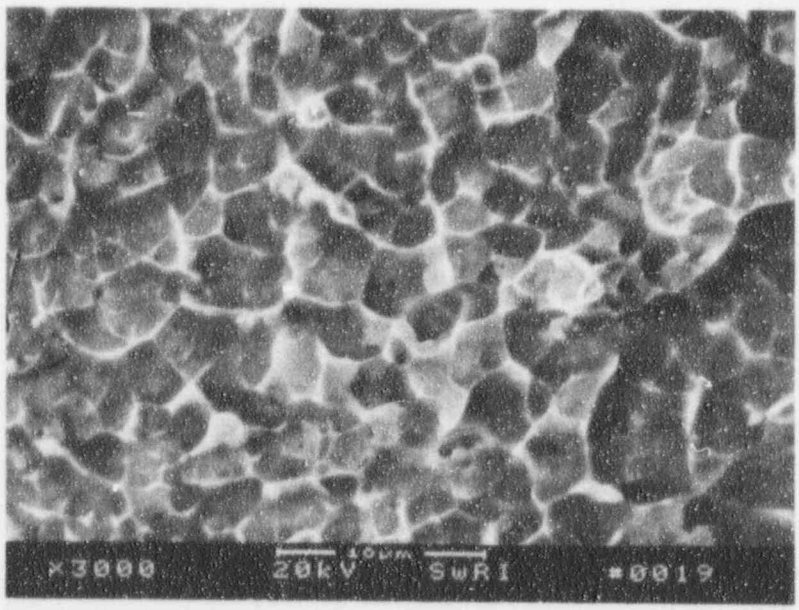

59482

Figure 2-2 Photomicrographs from Flat Zone of Sample No. 410. Location 1, Figure 2-1.

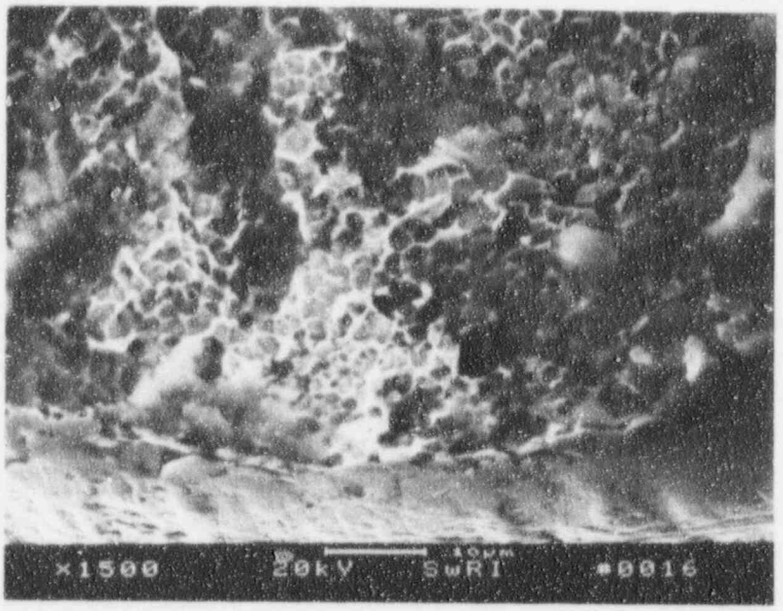

59477

(a) Location 2, Figure 2-1.

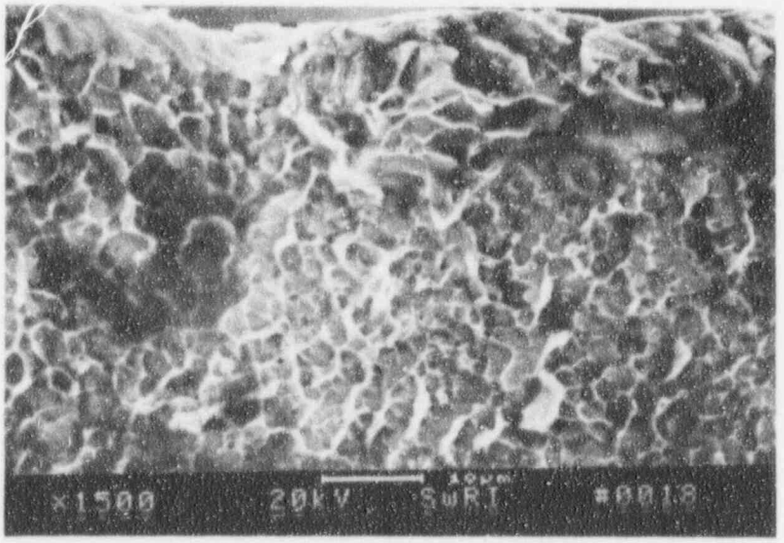

59480

(b) Location 3, Figure 2-1.

Figure 2-3 SEM Fractographs from Flat Zone of Sample 410.

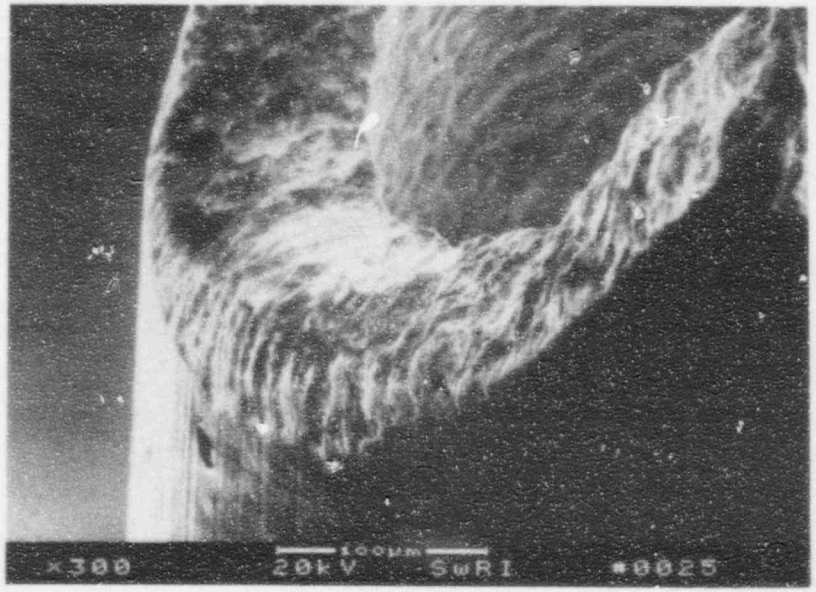

59484 (a) Location 4

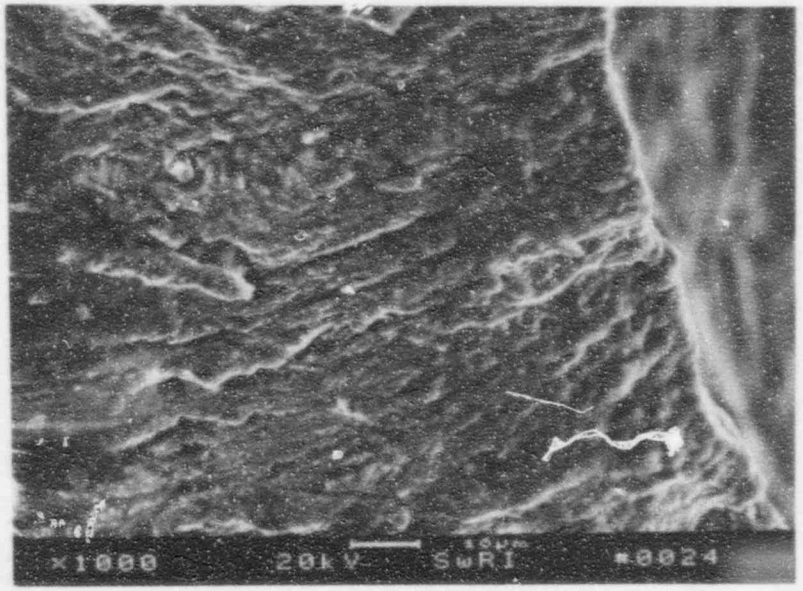

59486 (b) Location 5

Figure 2-4 SEM Fractographs from Slant Fracture Zone of Sample 410. See Figure 2-1 for locations.

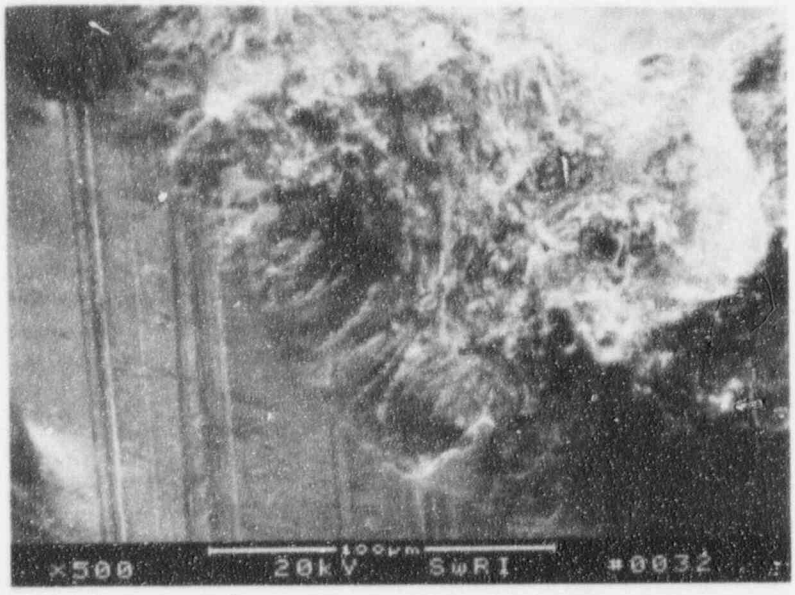

59494

(a) Location 6

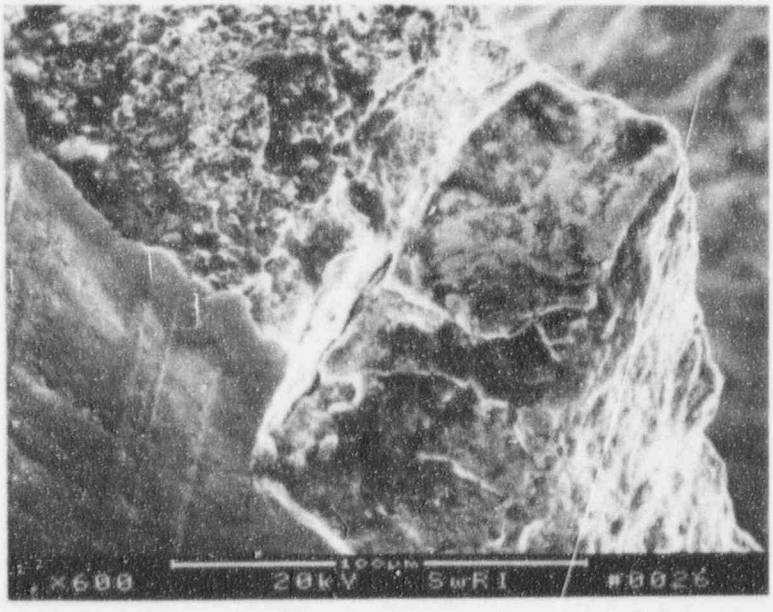

59490

(b) Location 7

Figure 2-5 SEM Fractographs from Slant Fracture of Sample No. 410.

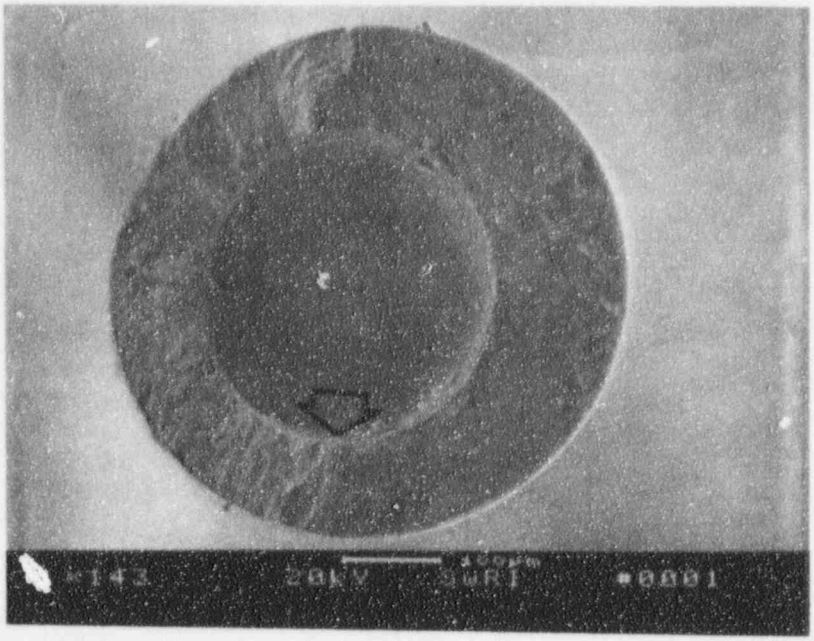

59467

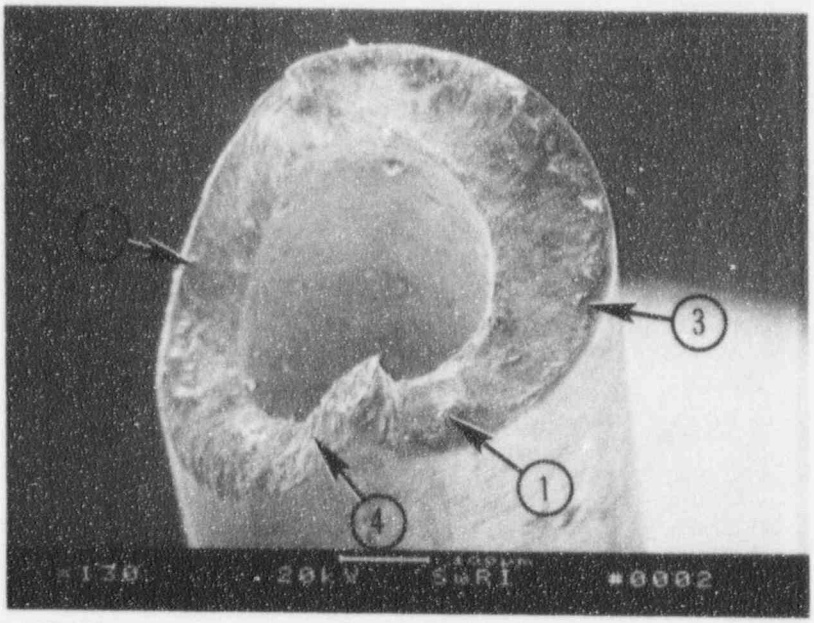

59473

Figure 2-6 SEM Photomicrographs of Failed Source Wire in As-Received Condition. Sample No. 410. Block arrows mark match points for two views.

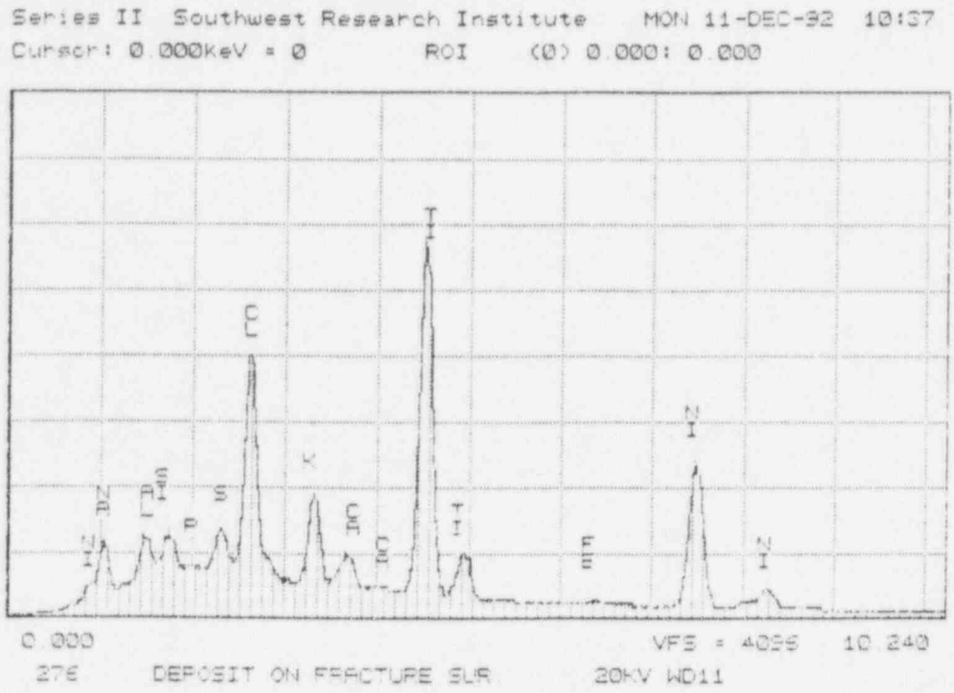

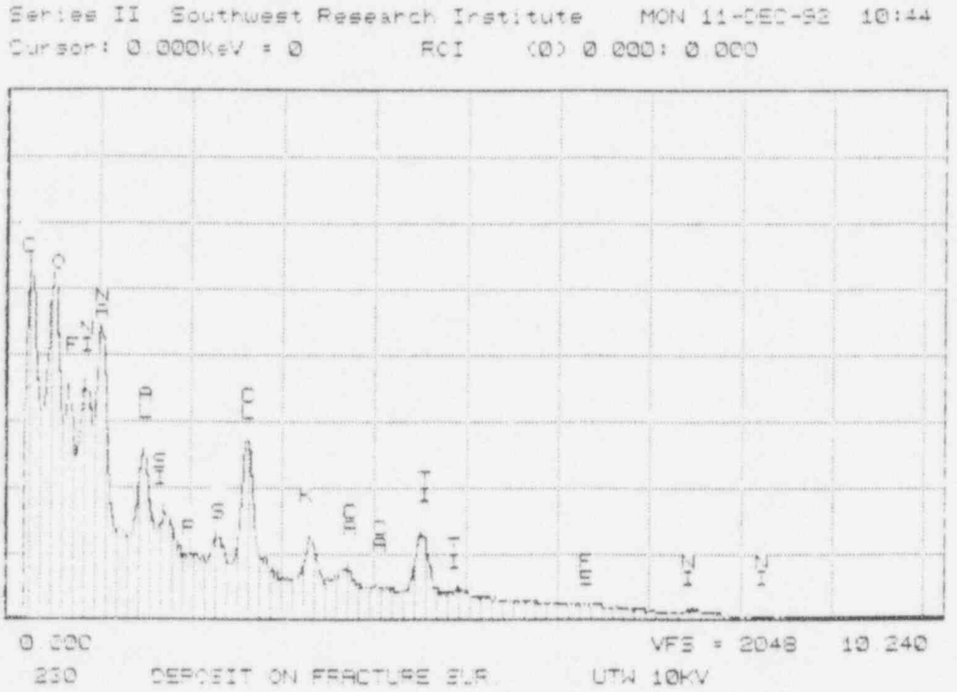

Figure 2-7 X-ray Energy Spectra from Fracture Surface. Sample No. 410. Location 1, Figure 2-6. **Upper: βe window, 20 kV; Lower: Ultra-thin window, 10 kV**

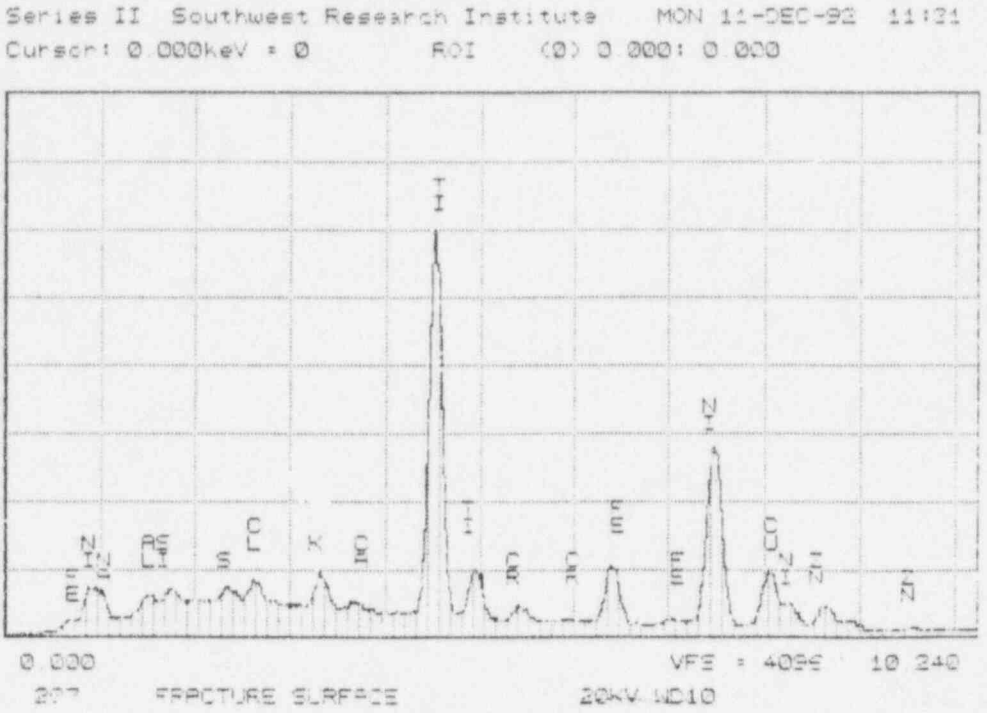

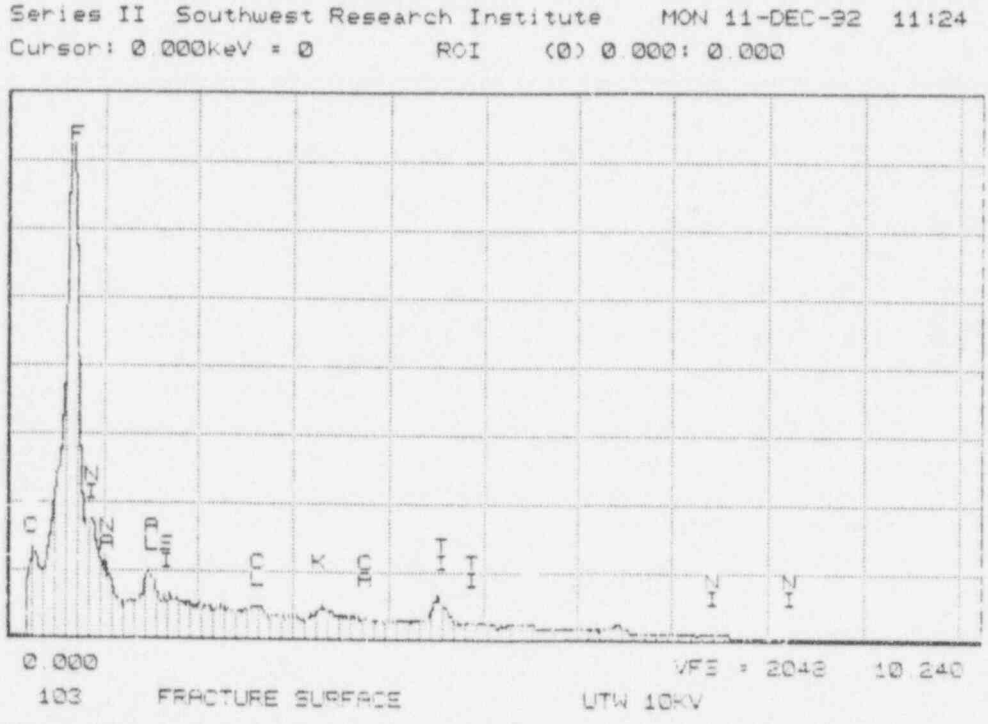

Figure 2-8 X-ray Energy Spectra from Fracture Surface. Sample No. 410. Location 2, Figure 2-6. **Upper: βe window, 20 kV; Lower: Ultra-thin window, 10 kV**

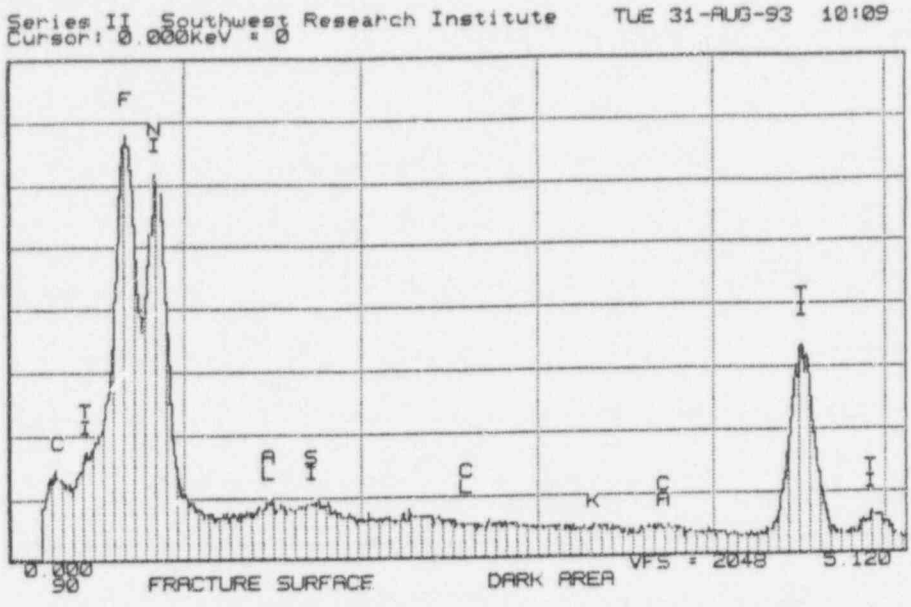

(a) Location 3, Figure 2-6

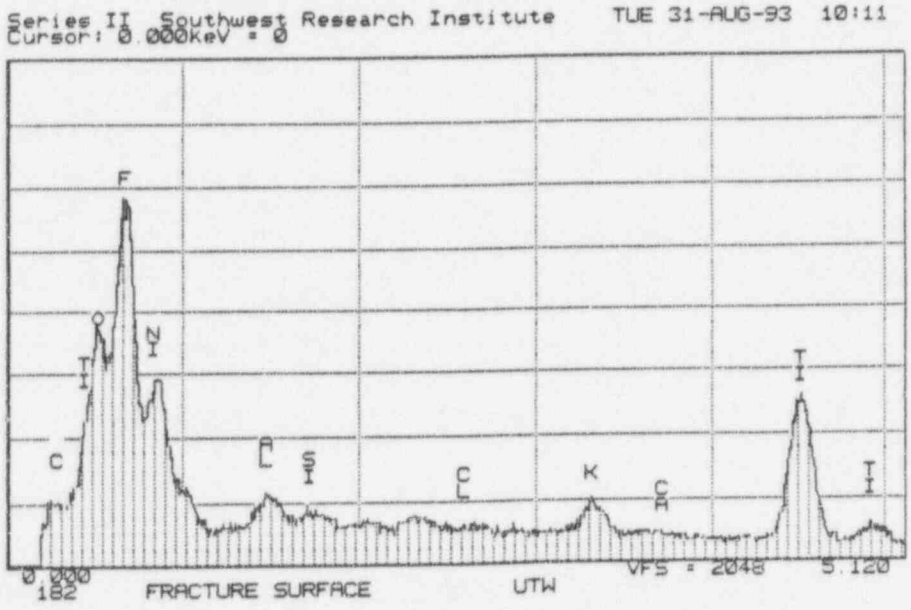

(b) Location 4, Figure 2-6

Figure 2-9 X-ray Energy Spectra from Fracture Surface. Sample No. 410. **Both spectra are for light element window with 10 kV potential.**

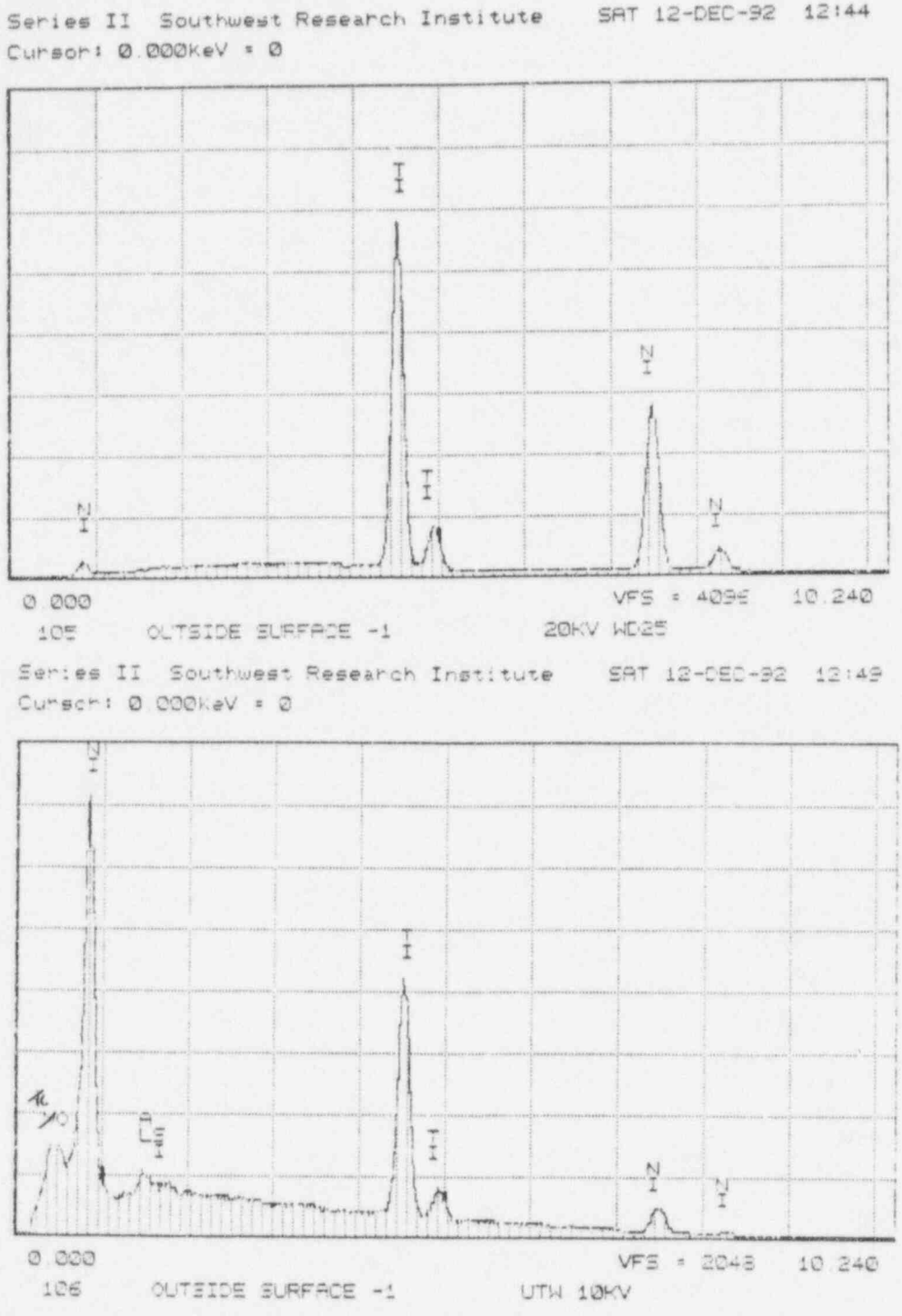

Figure 2-10 X-ray Energy Spectra from Outside Surface. Sample No. 410. **Upper: βe window, 20 kV; Lower: Ultra-thin window, 10 kV**

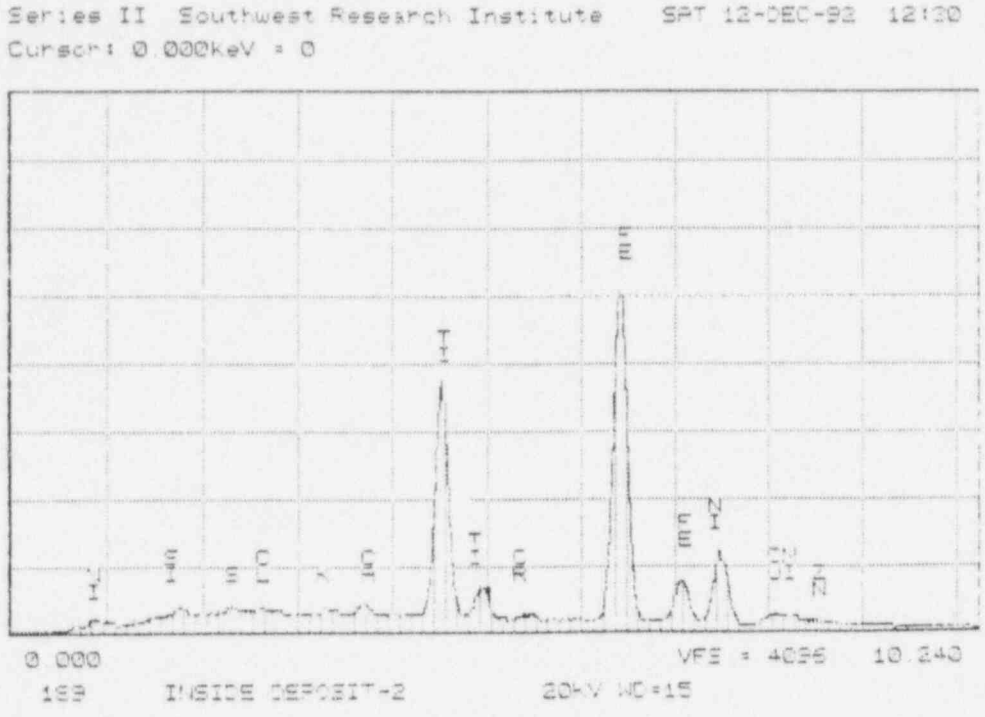

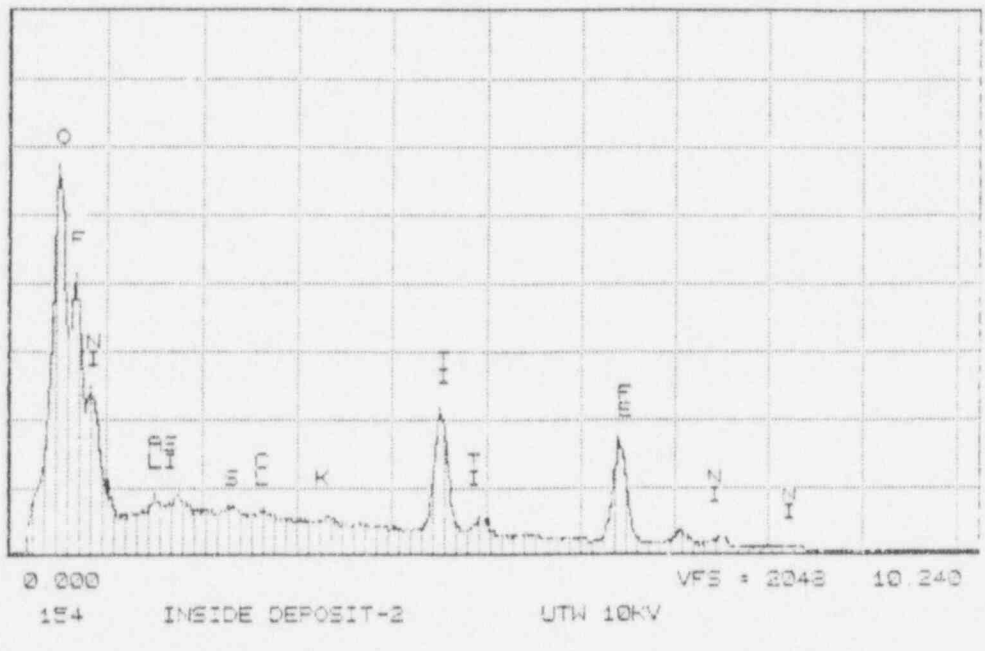

Figure 2-11 X-ray Energy Spectra from Inside Surface of Cavity. Upper: βe window 20 kV; Lower: Ultra-thin window, 10 kV

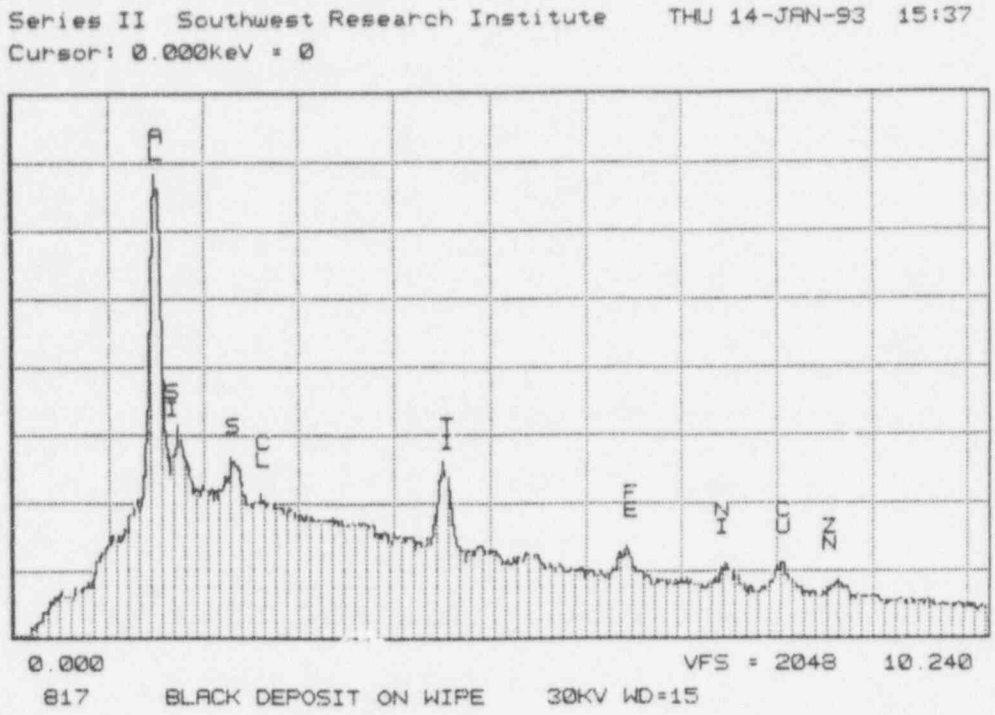

(a) Location 1, βe window

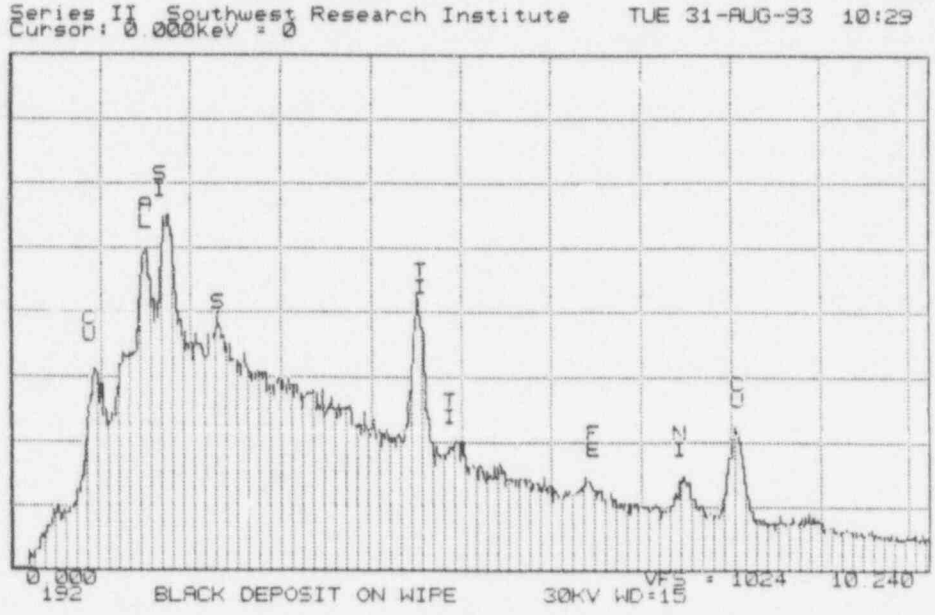

(b) Location 2, βe window.

Figure 2-12 X-ray Energy Spectra for Black Deposit on Wipe from Failed Source Wire at Facility A (Sample No. 410)

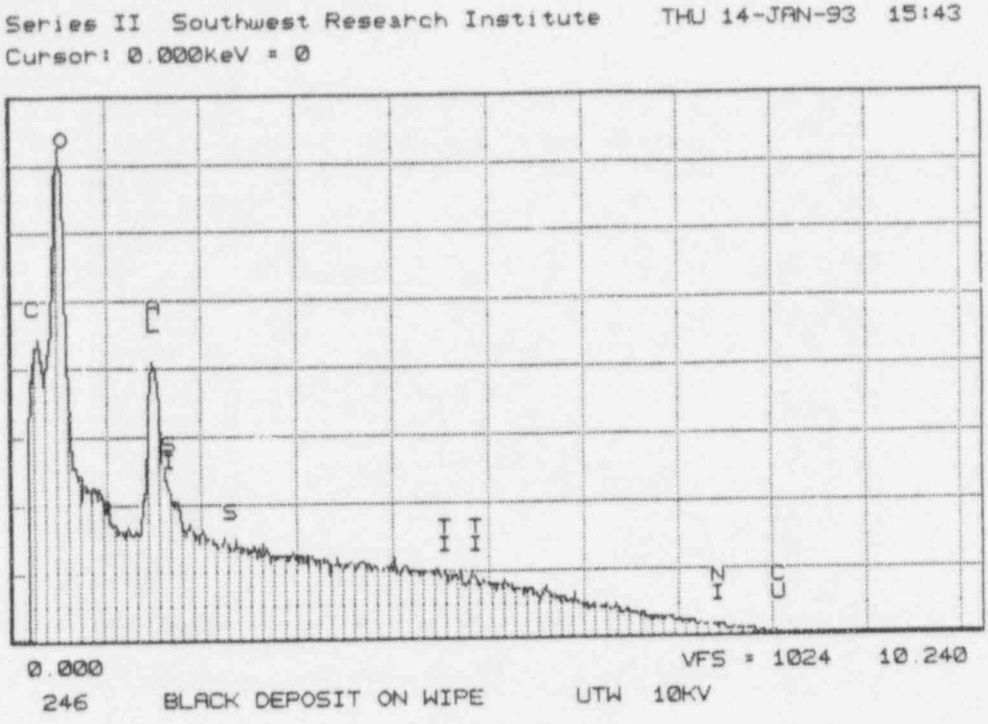

(a) Location 1, Ultra-thin window

Figure 2-13 X-ray Energy Spectra for Black Deposit on Wipe from Failed Source Wire at Facility A (Sample No. 410)

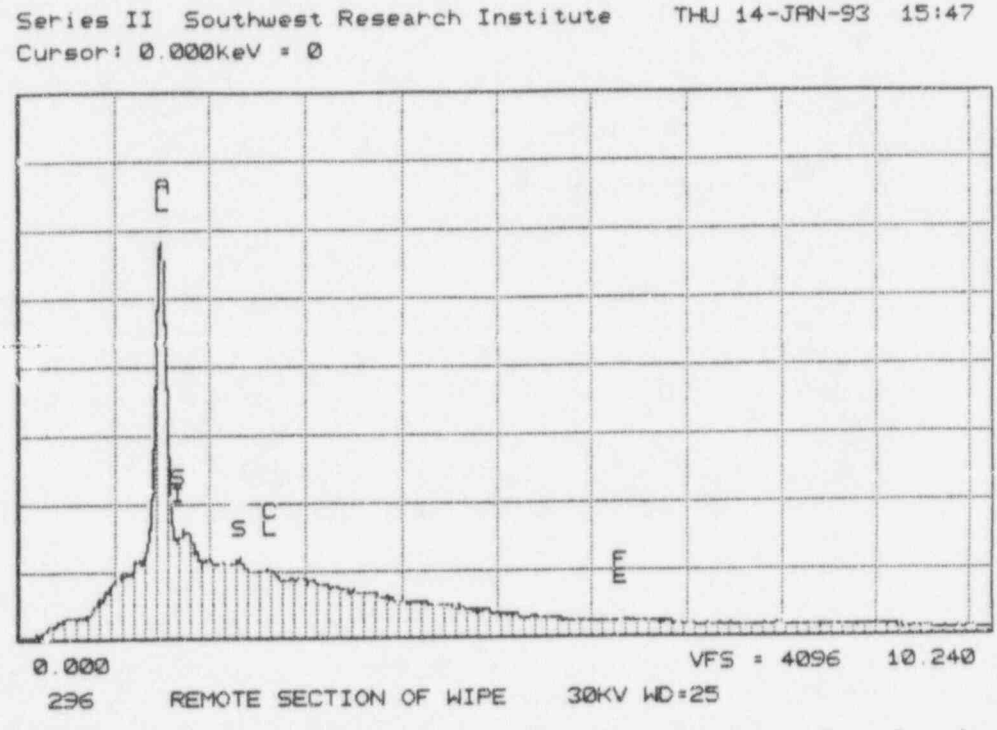

Figure 2-14 X-ray Energy Spectra from Wire Cloth. Location remote from deposit. Upper: βe window; Bottom: Ultra-thin window

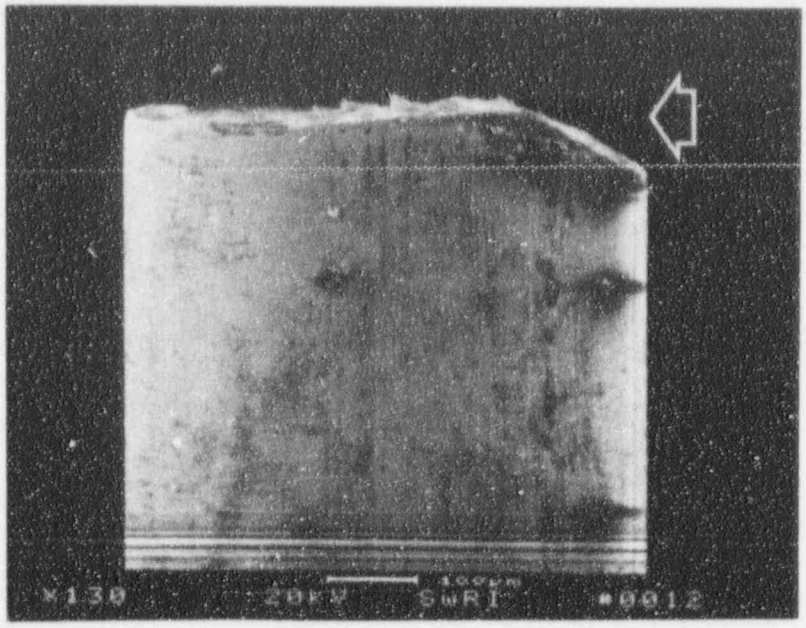

59519

(a) Side view.

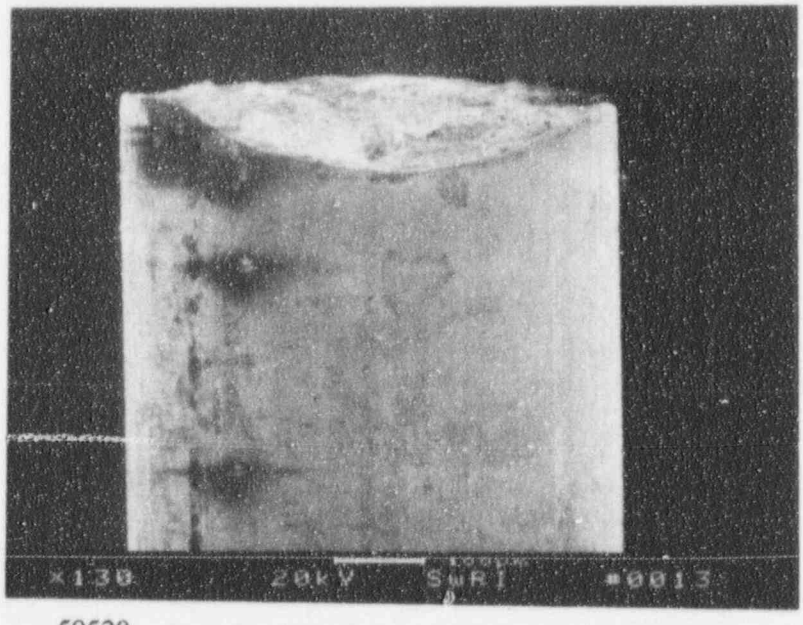

59520

(b) Front view. In direction of arrow in (a).

Figure 2-15 SEM Photomicrographs of Failed Source Wire from Facility B (Sample No. 411). Wire side of fracture.

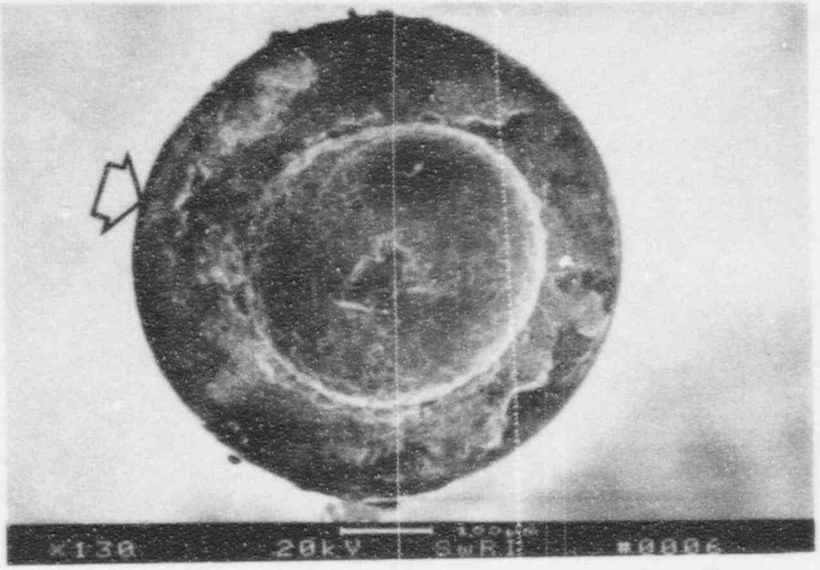

59517 (a)

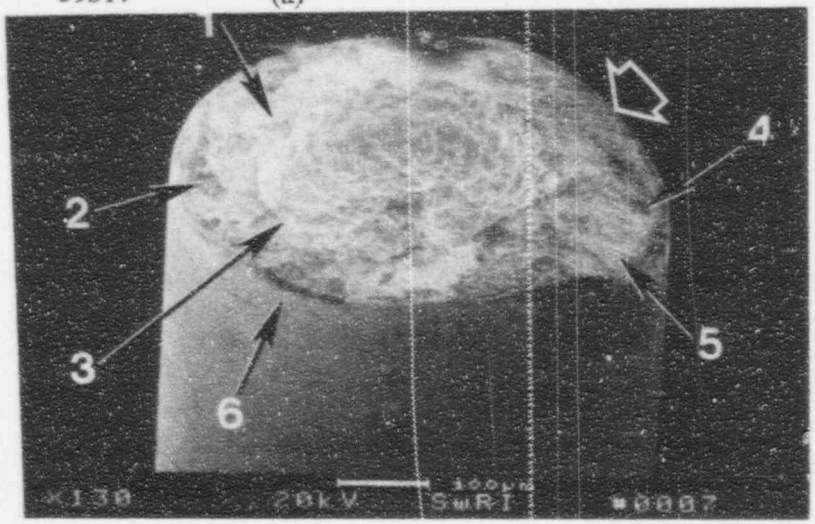

59518 (b)

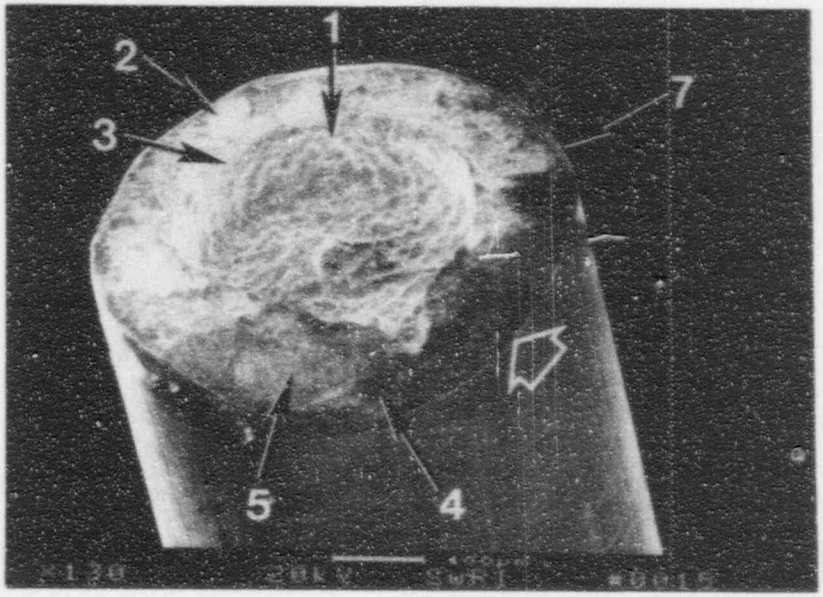

59521 (c)

Figure 2-16.SEM Photomicrographs of Failed Source Wire from Facility B (Sample No. 411). Fracture surface on wire side of failure. After cleaning. Block arrows indicate match points for three views.

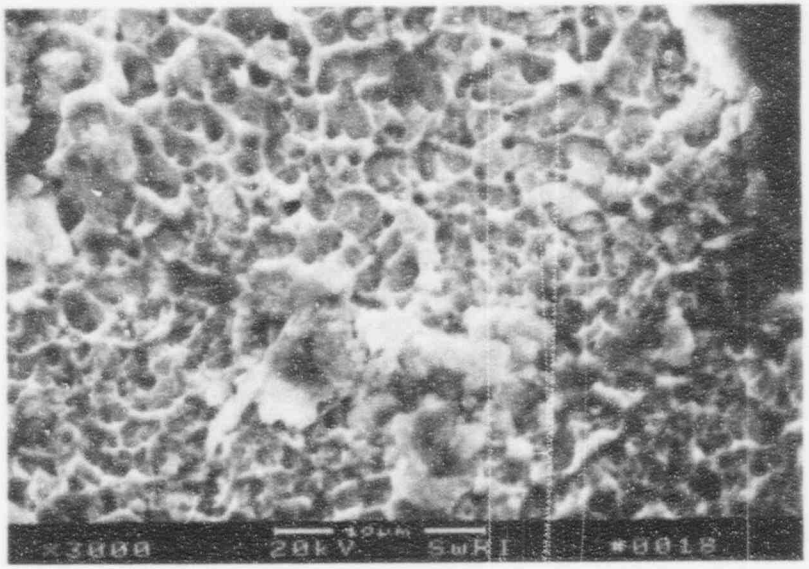

59525 (a) Location 1

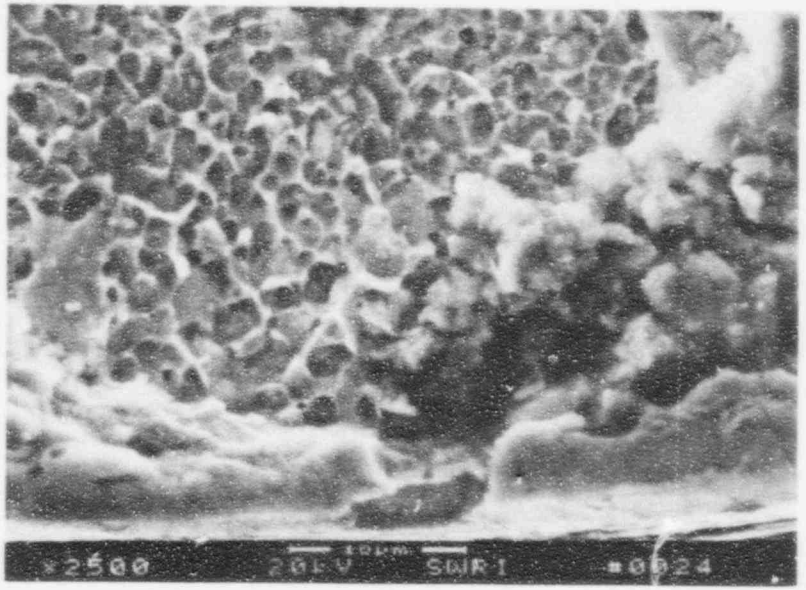

59587 (c) Location 3

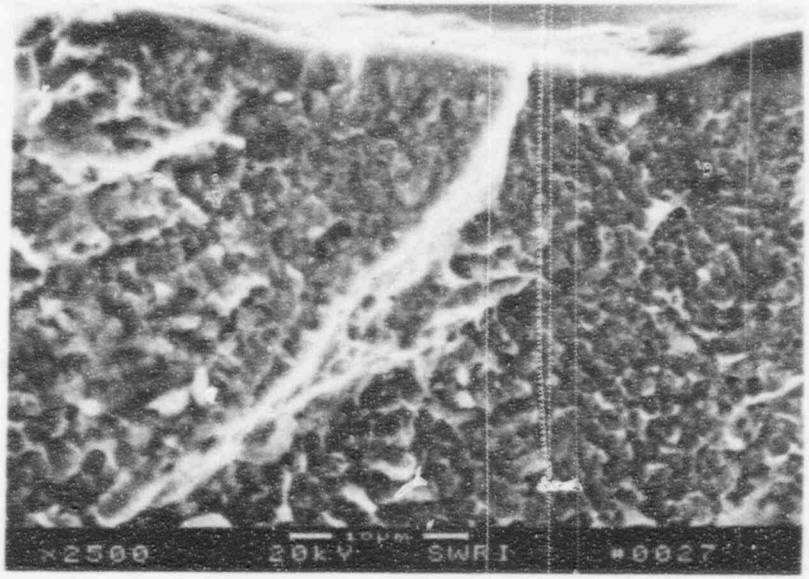

59588 (b) Location 2

Figure 2-17.SEM Fractrographs From Failed Sourcewire From Facility B. See Figure 2-16 for locations.

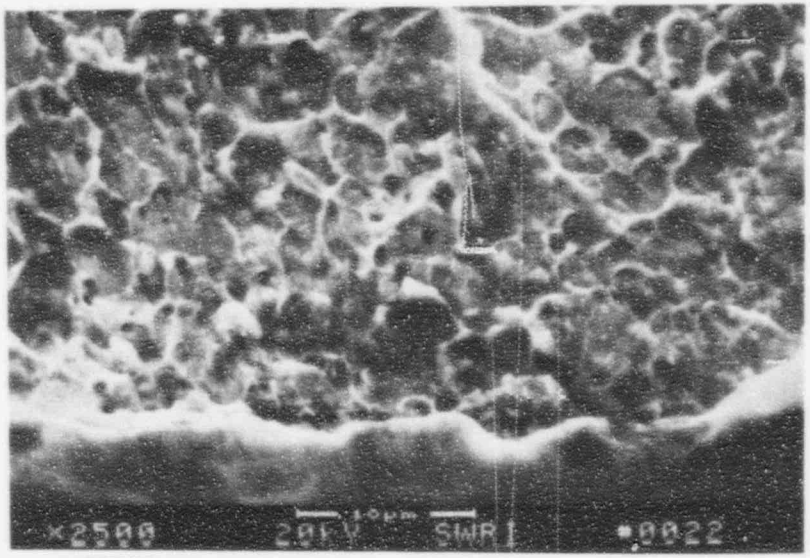

59583

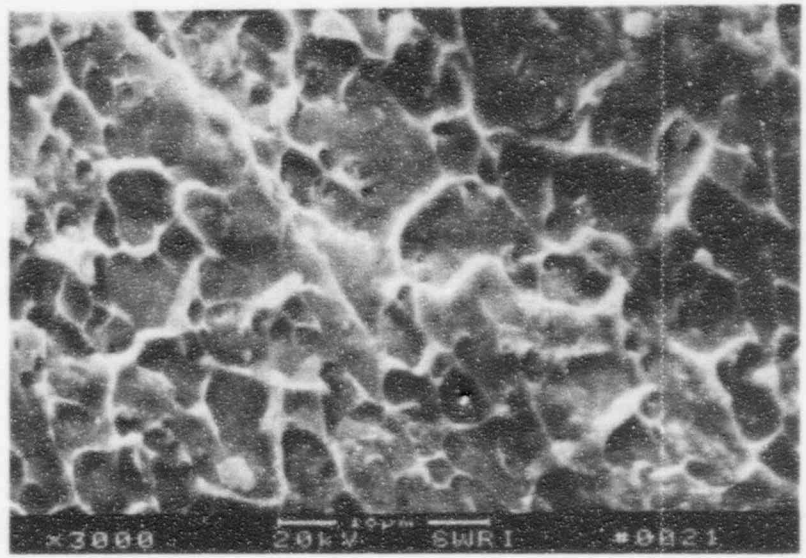

59582 (b) Location 5

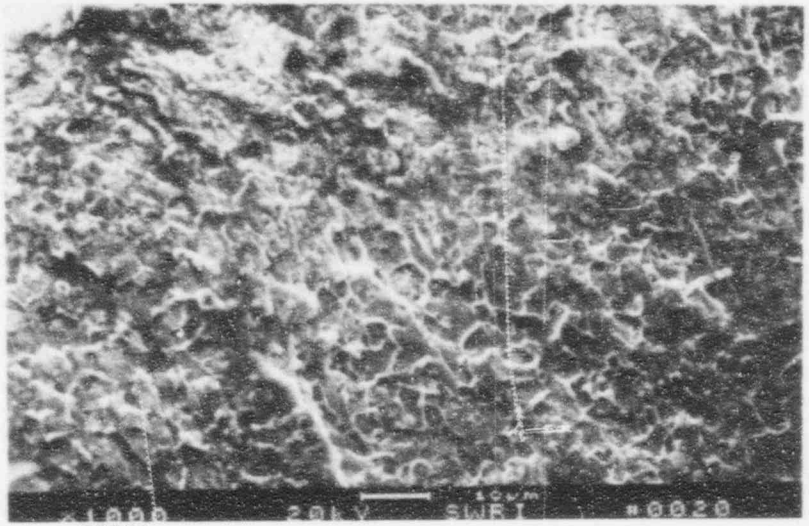

59581

Figure 2-18. SEM Fractographs from Failed Sourcewire From Facility B. See Figure 2-16 for locations.

59528 (a) Location 5

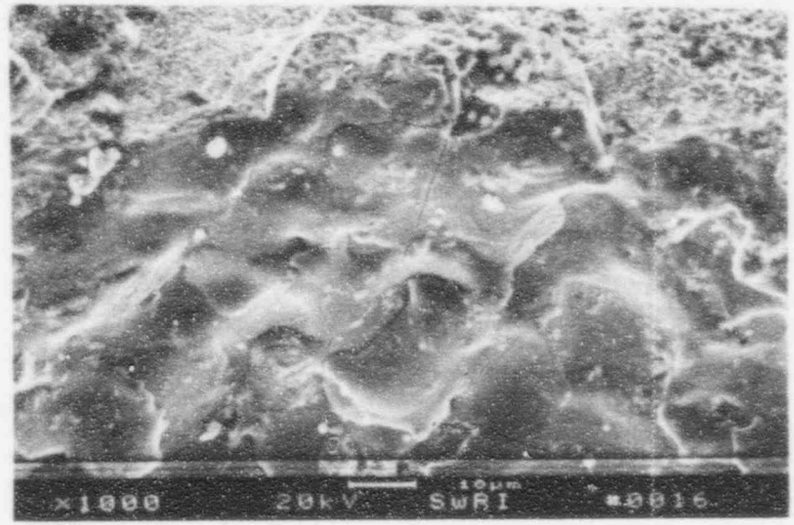

59521 (c) Location 7. Inside surface of cavity.

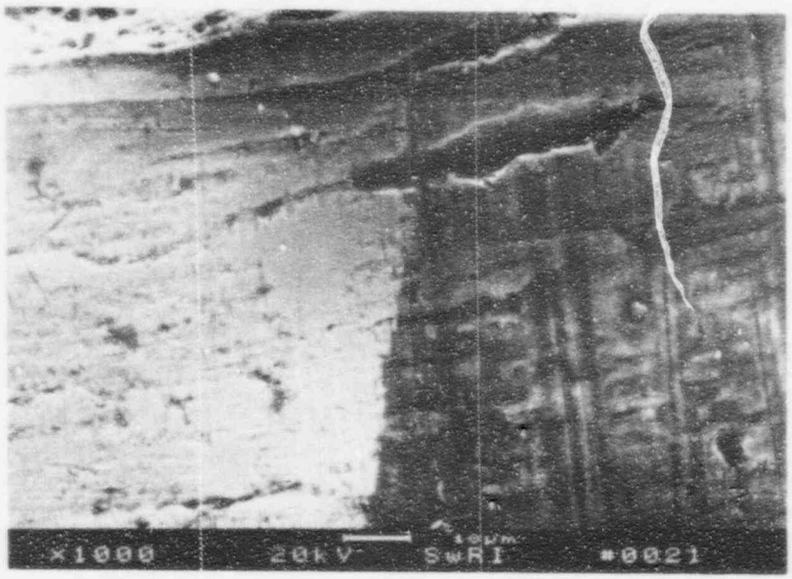

59527 (b) Location 6. Outside surface or wire

Figure 2-19. SEM Photomicrographs of Failed Source Wire from Facility B (Sample No. 411). See Figure 2-16.

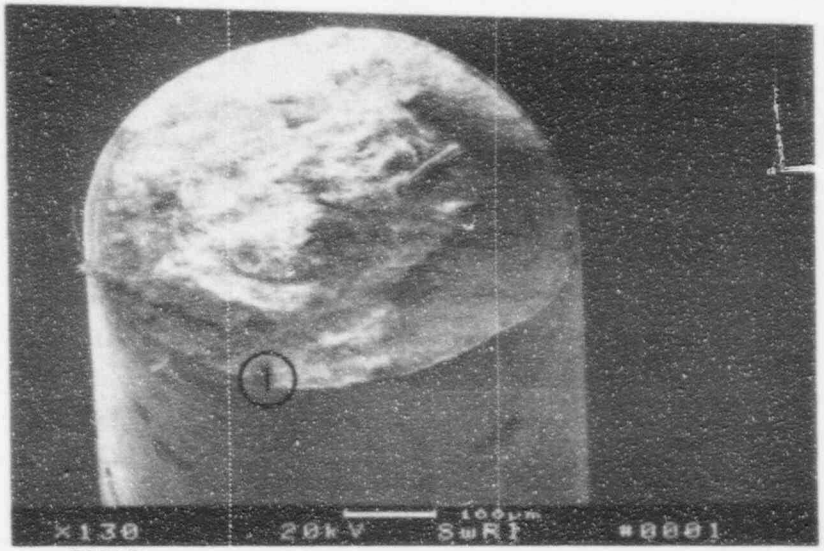

59512 (a)

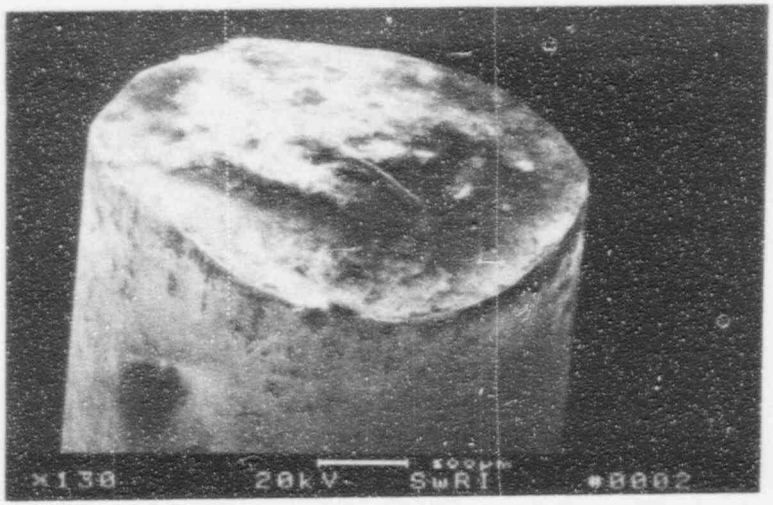

59513 (b) View in direction of block arrow in (a).

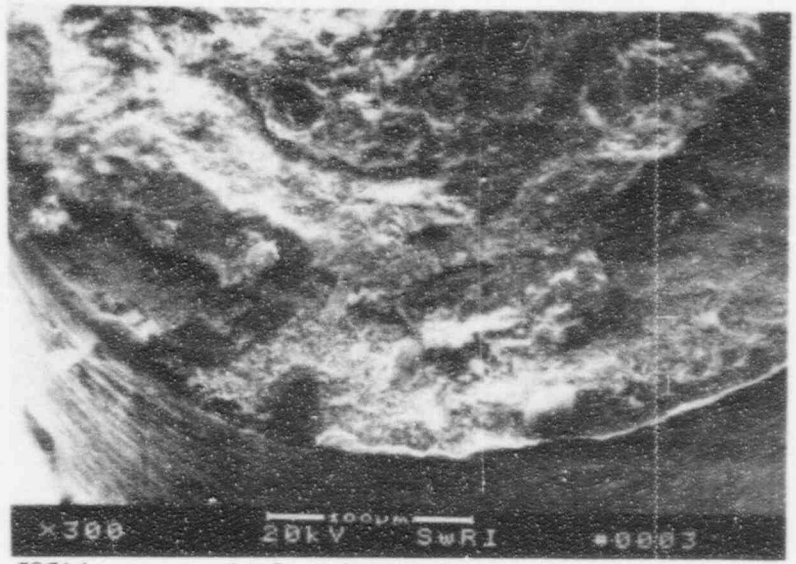

59514 (c) Location 1 in (a).

Figure 2-20. SEM Photomicrographs of Failed Source Wire from Facility B (Sample No. 411). As received.

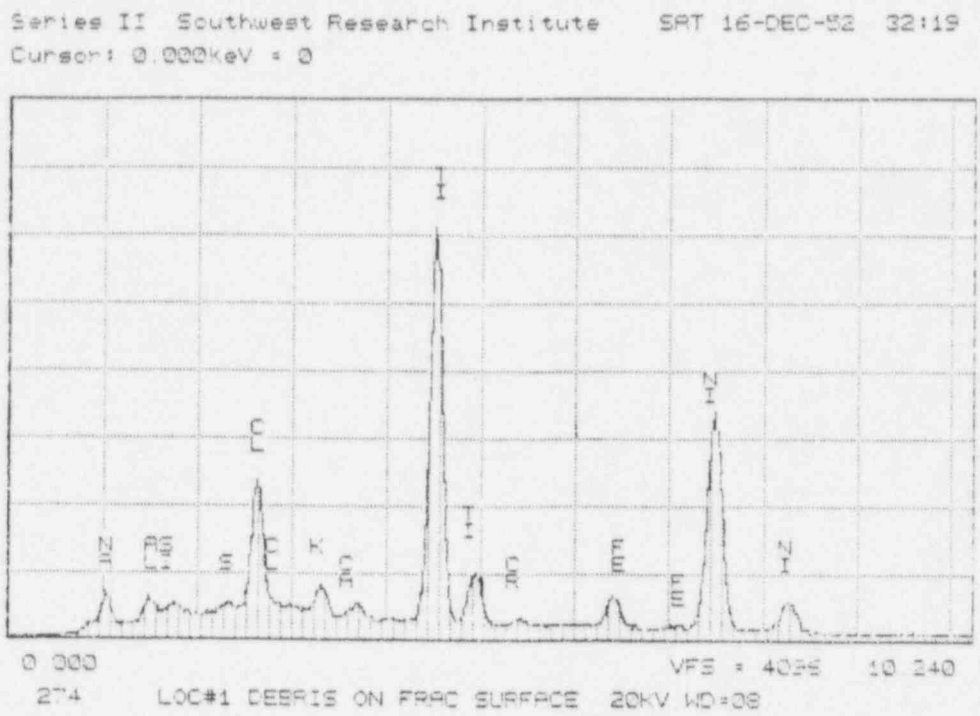

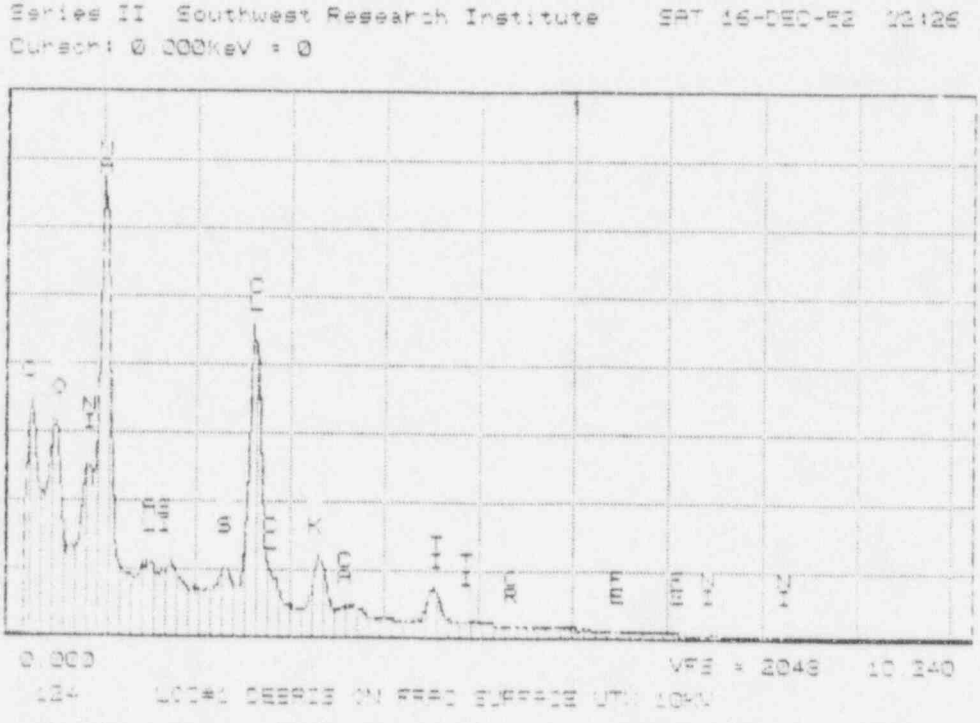

Figure 2-21 X-ray Energy Spectra for Debris on Fracture Surface. Sample 411. See Figure 2-20. Upper: βe window; Bottom: Ultra-thin window

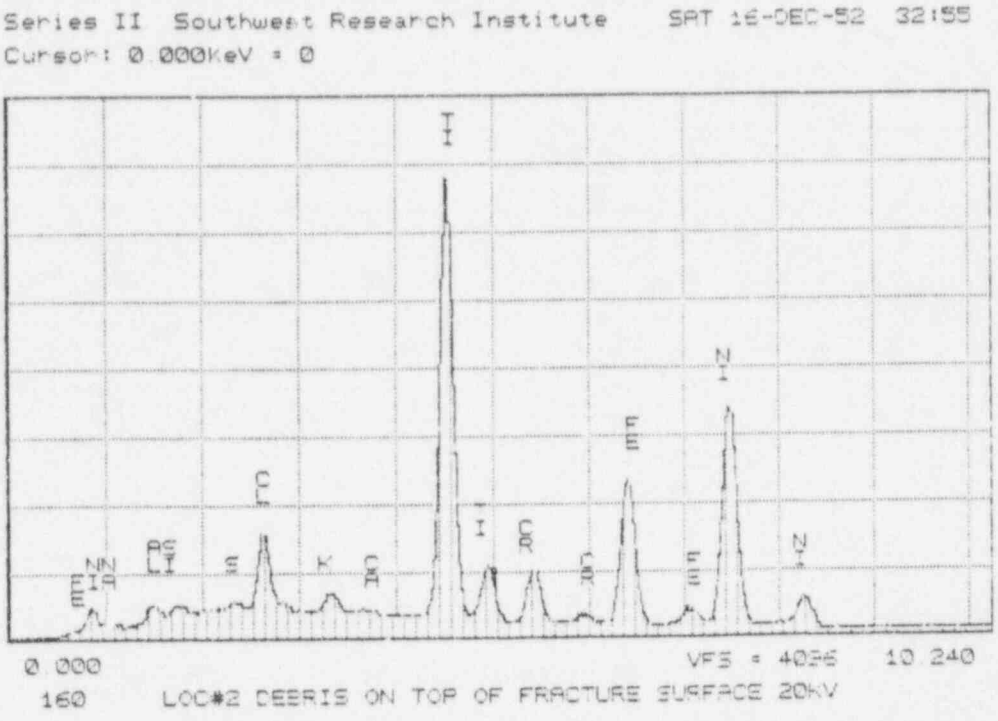

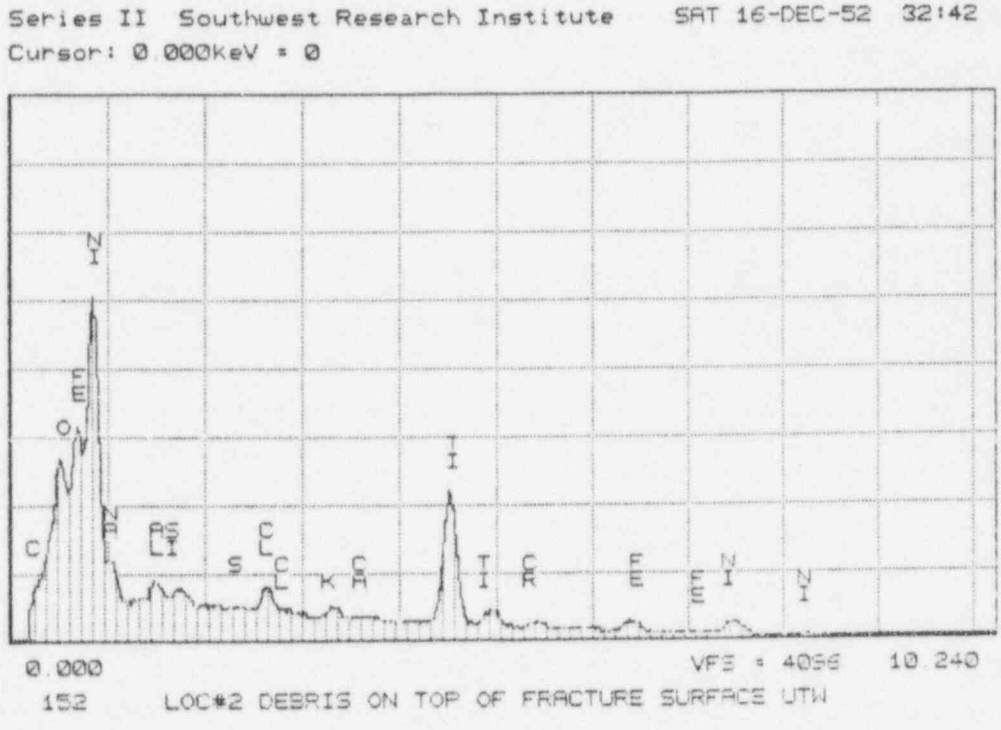

Figure 2-22 X-ray Energy Spectra for Debris on Fracture Surface. Sample 411. See Figure 2-20. Upper: βe window; Bottom: Ultra-thin window

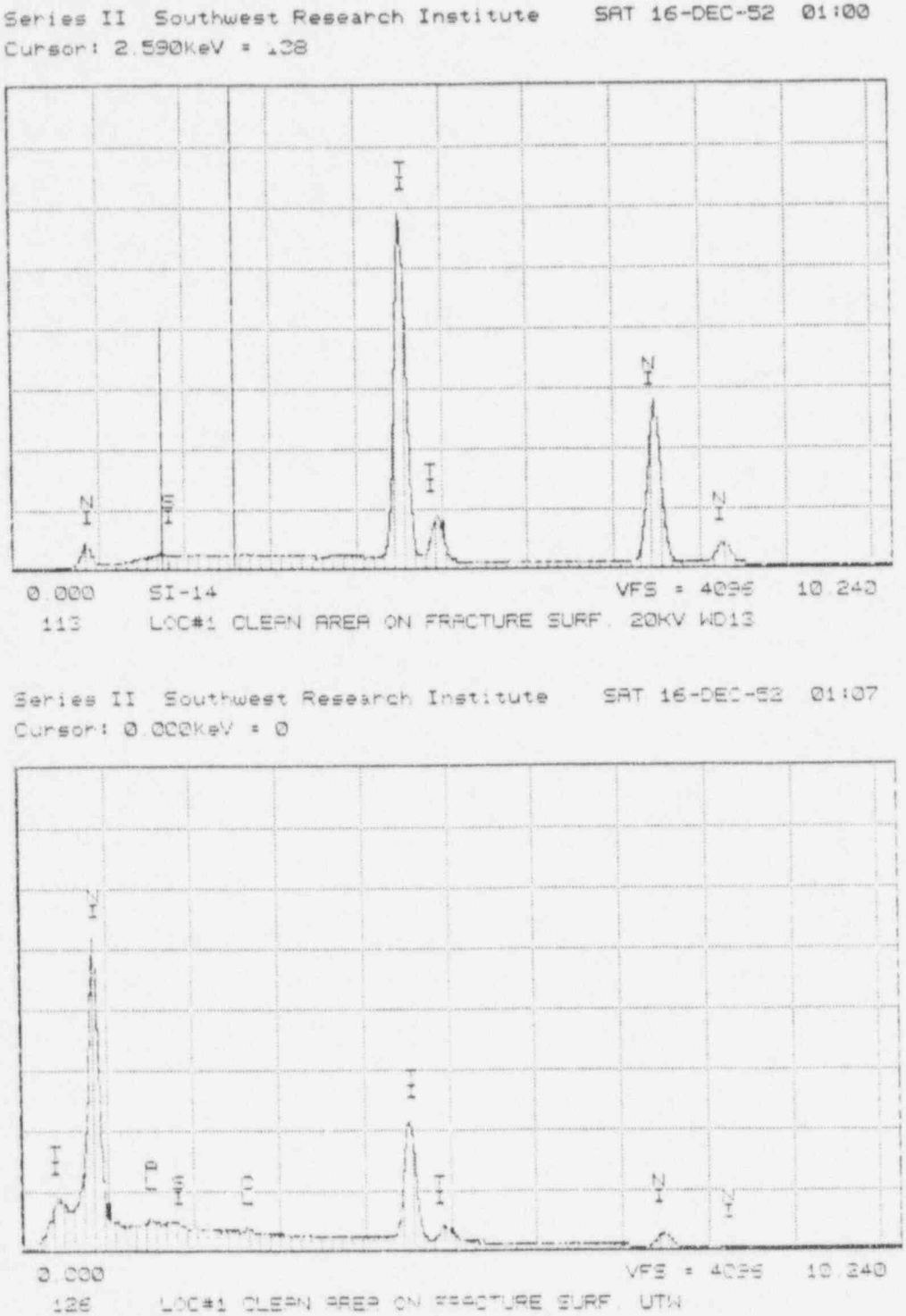

Figure 2-23 X-ray Energy Spectra for Clean Nitinol Wire. Sample 411. See Figure 2-20. Upper: βe window; Bottom: Ultra-thin window

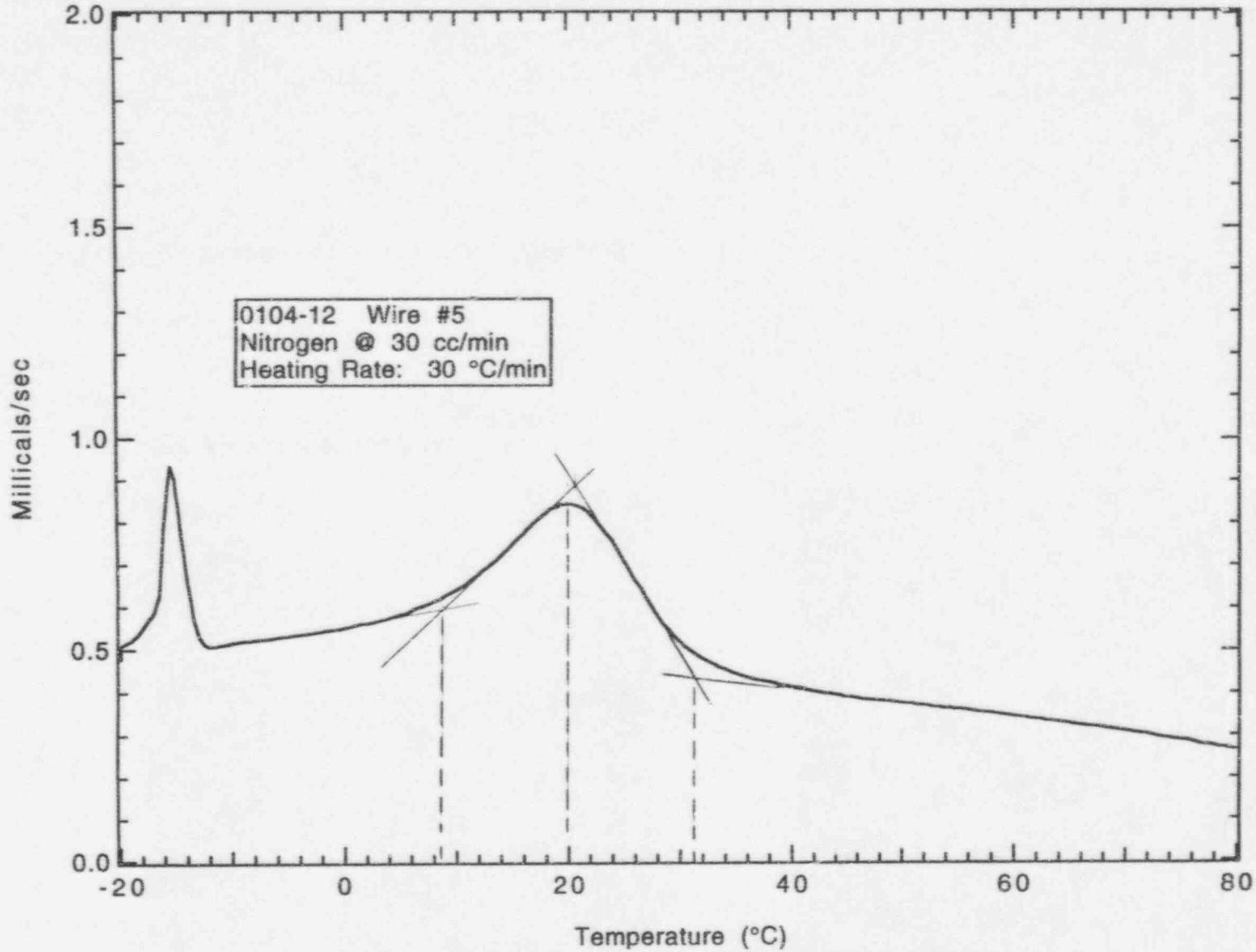

Figure 2-24. DSC Curve for Nitinol Wire Specimen. Sample No. 414

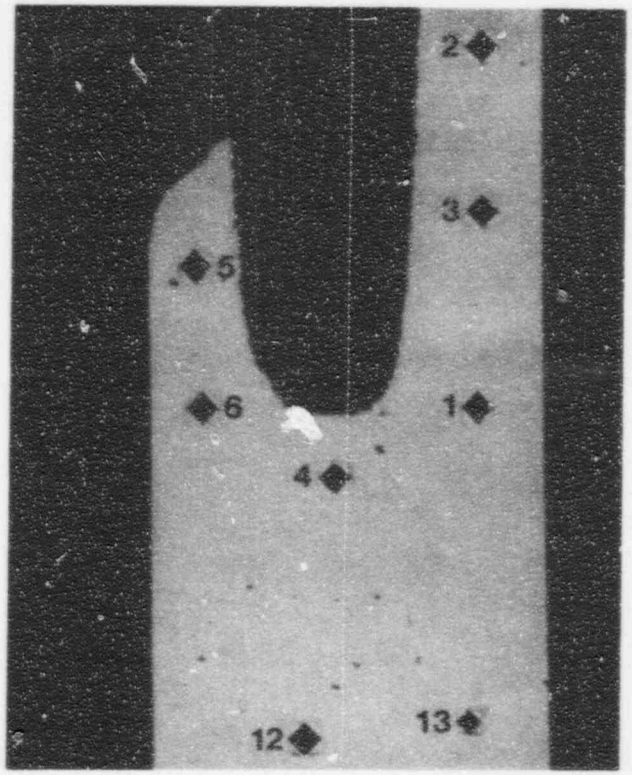

60773-774 100X
(a)Section between centerline and outer limit of cavity. As polished. 500 gm hardness indentations.

60775 100X
(b) Section near centerline Etchant: HF +HNO_3 200 gm hardness identations.

Figure 2-25. Longitudinal Cross Sections of Sample No. 410. Wire side of fracture.

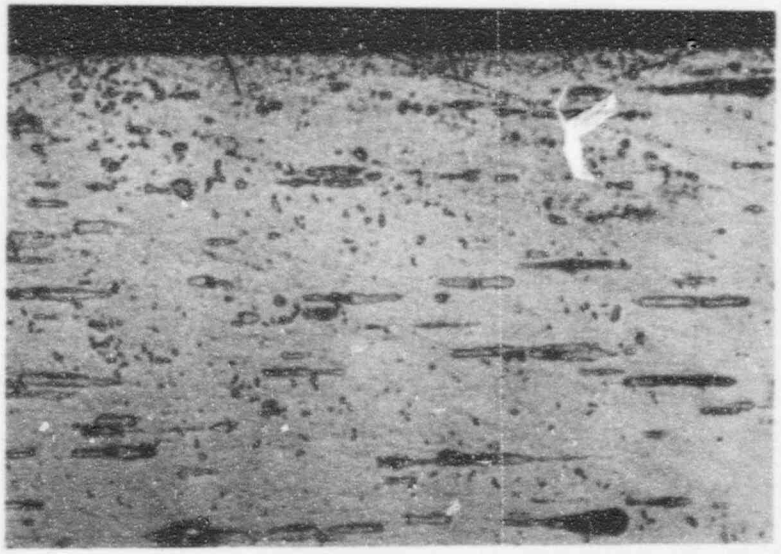

60782

(a) Typical microstructure

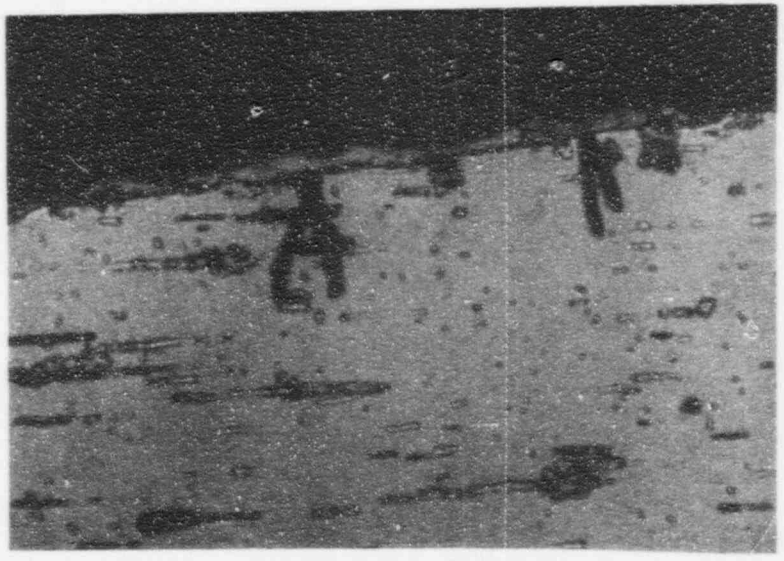

60783 (b) At inside of cavity wall.

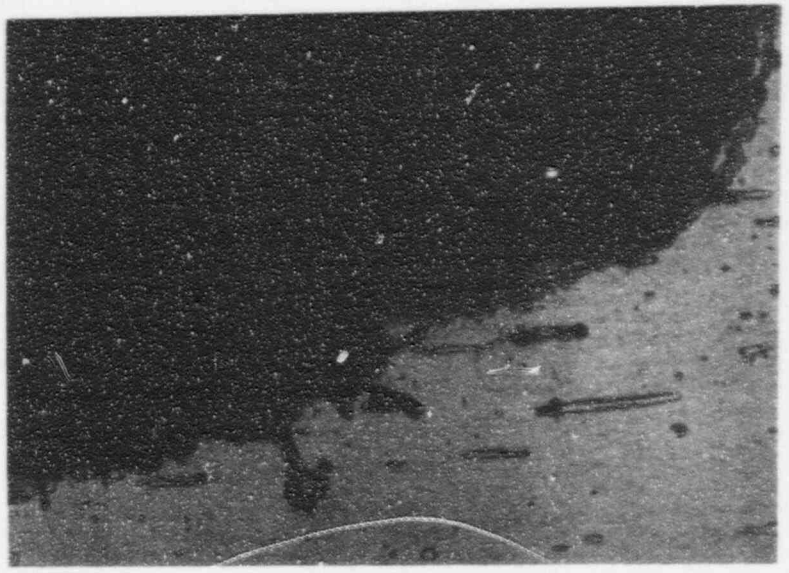

60784 1000X

(c) Near bottom of cavity

Figure 2-26. Photomicrographs from Longitudinal Sections through Sample No. 410. Etchant: HF +HNO_3

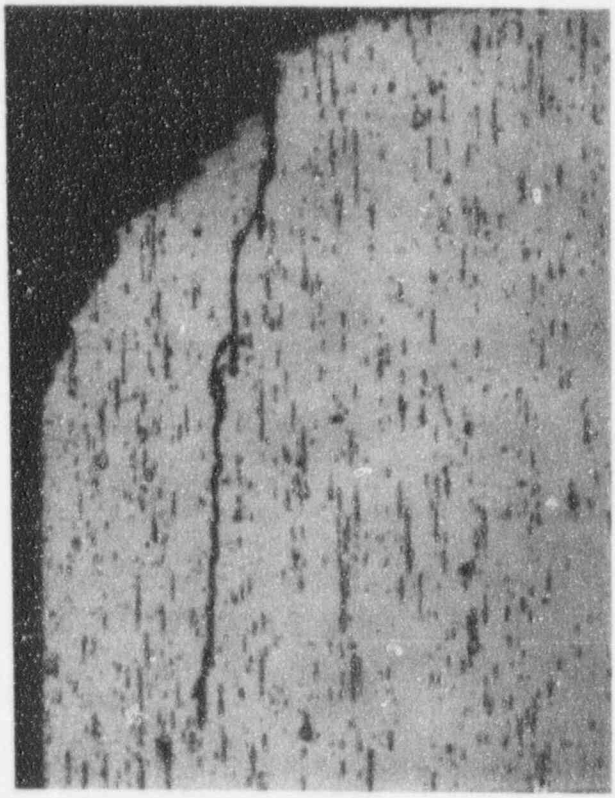

60781 400X

Figure 2-27. Photomicrograph from Longitudinal Section through Sample 410. Location at intersection of flat fracture and slant fracture. Section within wall thickness prior to grinding into cavity.

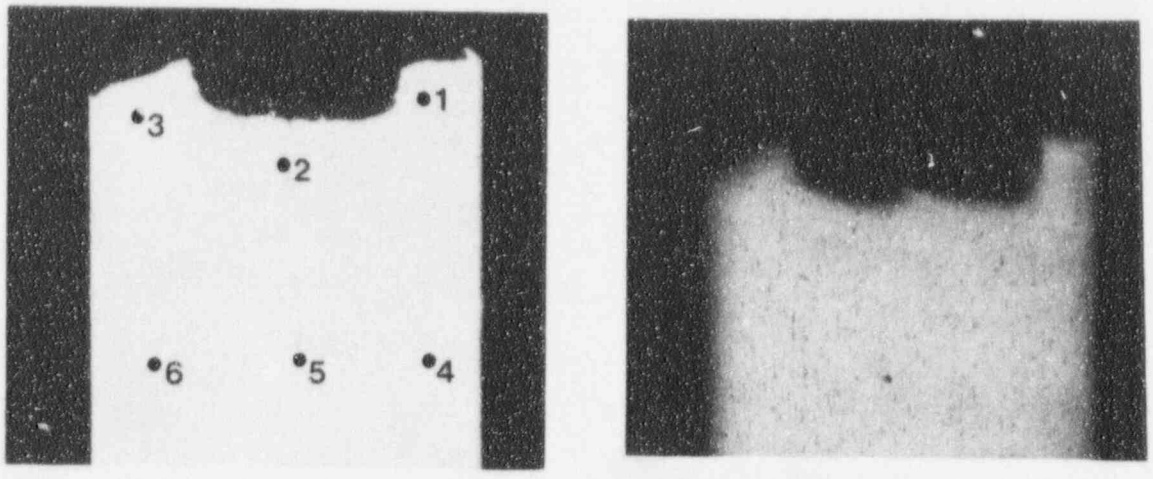

59627 100X
As polished

63312 100X
Etched after additional polishing

(a) Wire side of fracture.

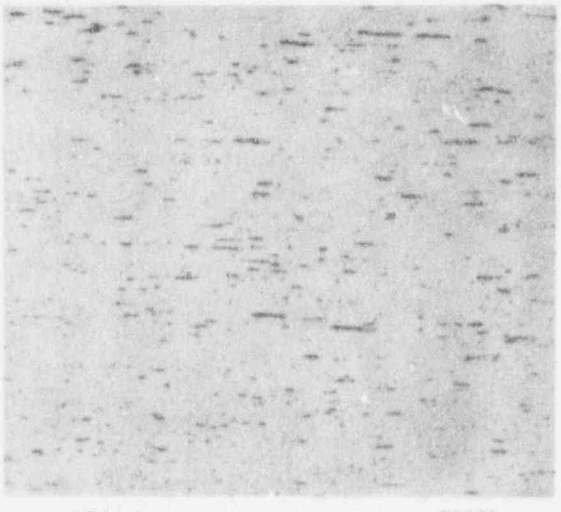

63314 500X

(b) Typical Microstructure

Figure 2-28. Photomicrograph from Longitudinal Section of Sample 411. Etchant: HF $+HNO_3$.

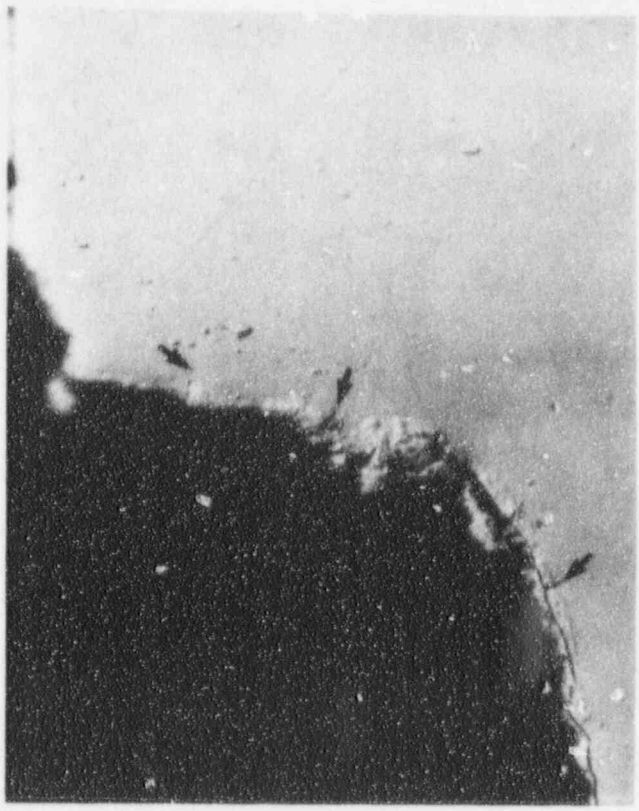

59622 1000X

Figure 2-29. Photomicrographs from Longitudinal Section of Sample No. 411. As polished. Arrows mark small defects at cavity surface.

3. PRELIMINARY TESTS

Three types of preliminary tests were conducted on Nitinol wire to determine possible mechanisms of failure. One condition involved a simple bend overload of a solid wire, SwRI Wire No. 412. Another condition included exposing solid wires to dilute hydrogen fluoride. A third condition involved hydrogen charging a solid wire.

3.1 Simple Bending Overload Failure (SwRI Wire No. 412)

A one-inch section of solid wire was cut form the wire that failed at Facility A. The wire was gripped with a pair of pliers and intentionally reverse flexured until the wire failed. The wire did not fail easily. The ends of the wire touched, when crimped, then the wire was reverse flexed. Figure 3-1 shows the failed wire that had some permanent set indicated by the curvature of the wire. The fracture surface had microfeatures of dimples. The fracture planes were slanted at the OD where the wire was flexed. The middle section was flat. The simple bend test of a solid wire indicated the Nitinol wire was very ductile. The permanent set and dimples were characteristic of overload.

3.2 Hydrogen Fluoride Tests

Solid wires were exposed to 0.1% hydrogen fluoride for various time periods. The first exposed sample, SwRI Wire No. 415, was exposed to 0.1% HF for 24 hours.

Figure 3-2 shows the wire failed in a brittle manner with a flat fracture across the section of the wire. Fracture flow marks proceeded across the cross section. Figure 3-3 shows fracture surface microfeatures were predominantly dimpled. However, around the periphery at the OD surface was a rim that was not dimpled. The rim was feathery in appearance and the features had a slight curvature which may indicate crack direction around the periphery. The HF test indicated that Nitinol wire was embrittled.

Another test included exposing solid wires for 6 hrs. and 45 minutes to 0.1%HF, then manually bent. Figure 3-4 shows the fracture surface which was flat and covered with some residual product. Figure 3-5 shows the EDX spectra of the residual product on the fracture surface. Expected elements of nickel and titanium where identified and potassium, sodium, sulfur, chlorine, and oxygen. The source of all these elements is uncertain. Fluorine was not identified as a by-product. An interesting note was microcracks identified on the compression side of the wires shown in Figure 3-6. The microcracks indicate that the OD was embrittled; the cracks had a slight angle. The cracks on the compression side is not a normal occurrence in conventional loading conditions. Two possible explanations to consider; first, cracks may initiate because the shear strength of the brittle layer is low. When the wire is initially flexed, shear stresses are present on 45° planes on the compression side. Therefore, shear cracks could develop in the brittle layer on the inside of the bend. Alternatively, the microcracks may have occurred when the wire was reverse flexed. In either case, the microcracks indicate HF had an embrittling effect on the Nitinol wire.

3.3 Hydrogen Charged Tests

A solid wire was electrolytically charged for two hours with hydrogen at SwRI (see Appendix D for details on charging procedure) then manually bent, either instantly with no delays or with a five hour delay or with a seventy hour delay. Figure 3-7 shows that all the specimens failed in a brittle manner. Each of the fractures had a flat fracture plane with flow lines from one side of the fracture to the other side of the fracture, micro-dimples on the fracture, and a rim or shell on the OD of the wire, shown in Figures 3-7 and 3-8. In some cases, longitudinal microcracks were evident and a separation or delamination occurred. Also noted was smaller dimples adjacent to the initiation site.

3.4 Summary

- A simple bend test of a solid wire indicated that the Nitinol wire was very ductile and did not fail until crimped, then reverse flexured. The macrofeatures of the overload condition included permanent set with microfeatures of dimples.
- The preliminary HF exposure tests indicated the Nitinol wire was embrittled by HF.

- The specimens that were hydrogen charged failed in a brittle manner.
- In view of these preliminary results, it was concluded that Nitinol can be embrittled by HF or hydrogen. A more comprehensive test plan, discussed in Section 5.0, was developed.

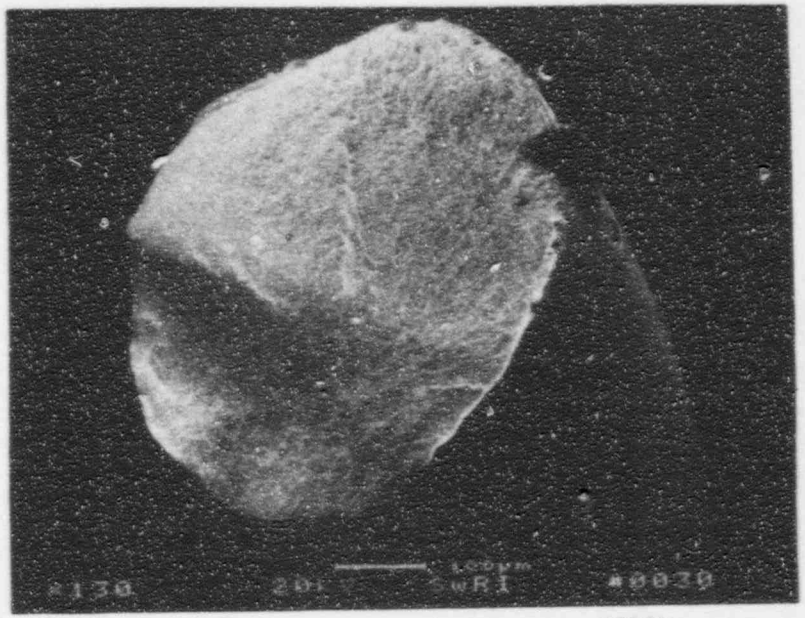

59493 130X

a)

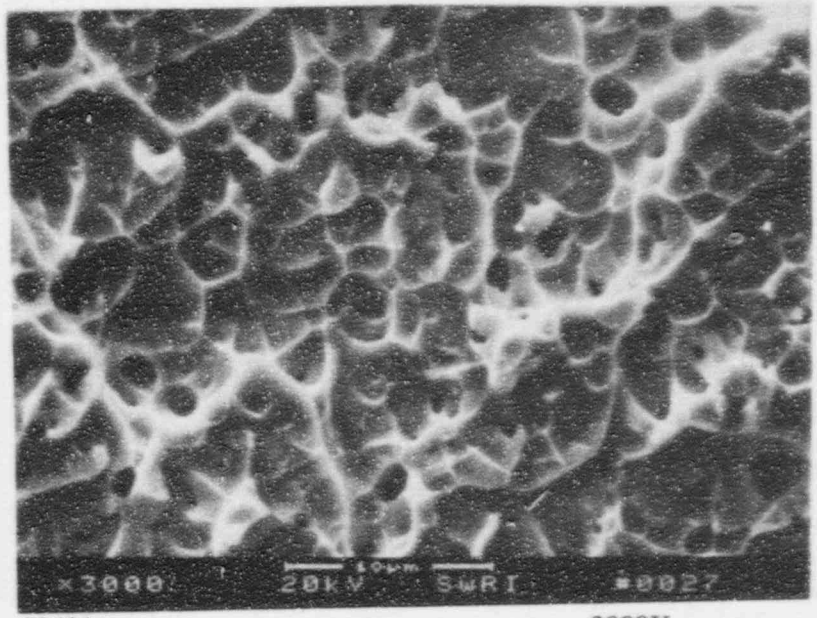

59491 3000X

c)

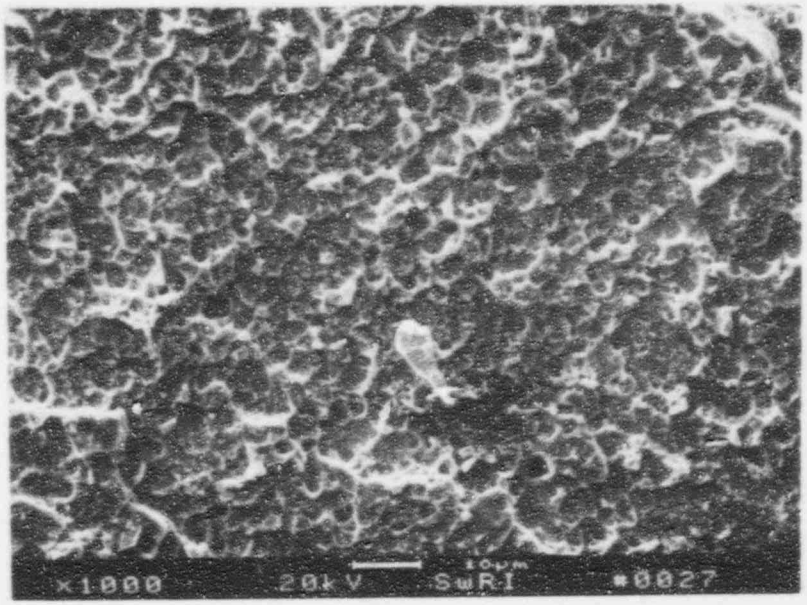

59492 1000X

b)

Figure 3-1. SEM Fractographs of SwRI Wire No. 412.

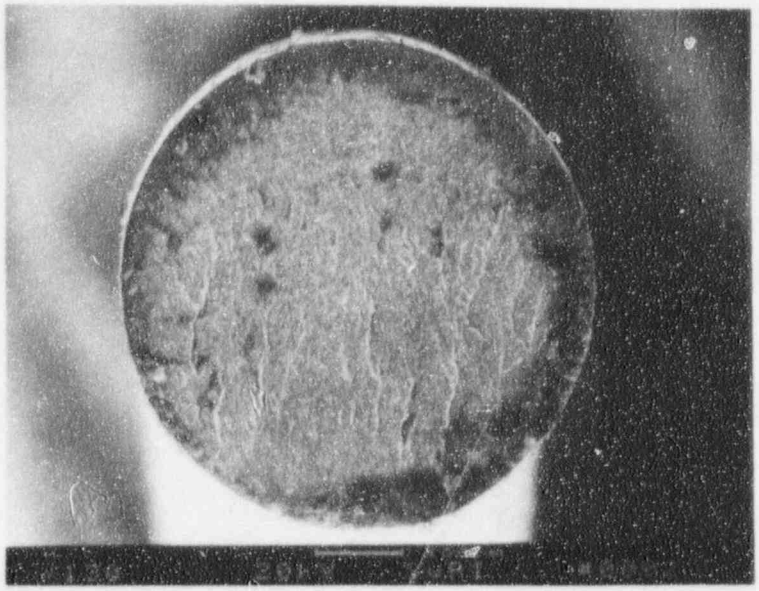

59655 130X

a)

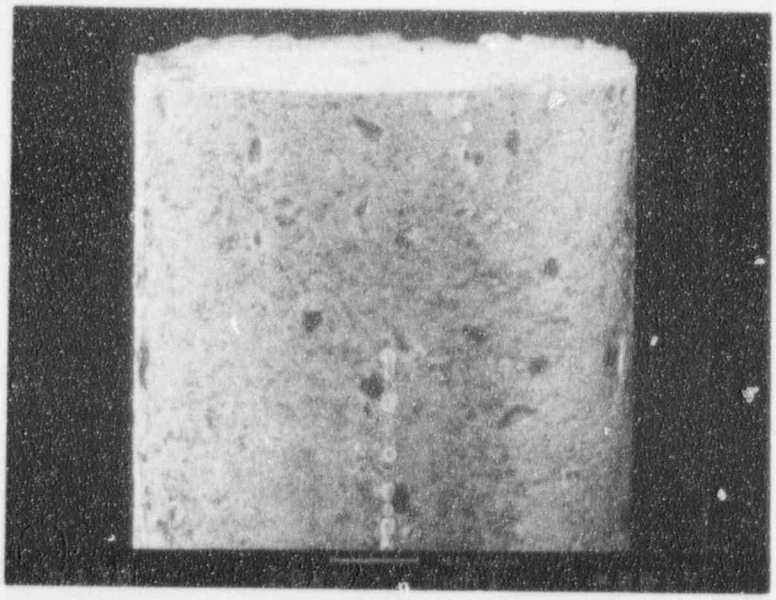

59667 130X

b)

Figure 3-2. SEM Fractographs of SwRI Wire No. 415.

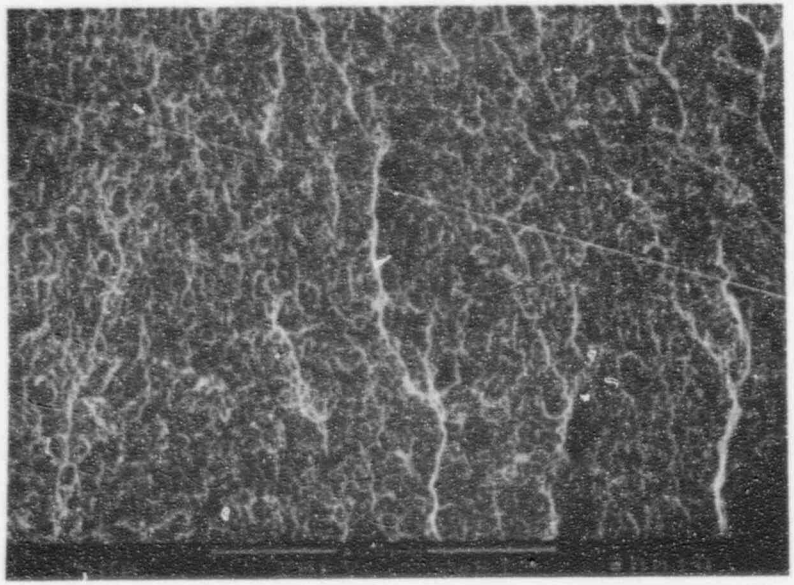

59659 500X

a)

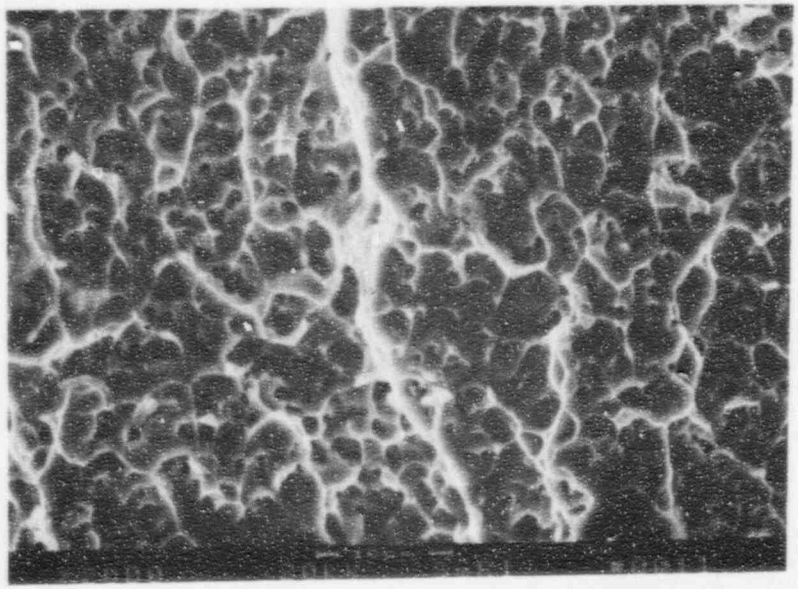

59660 2000X

b)

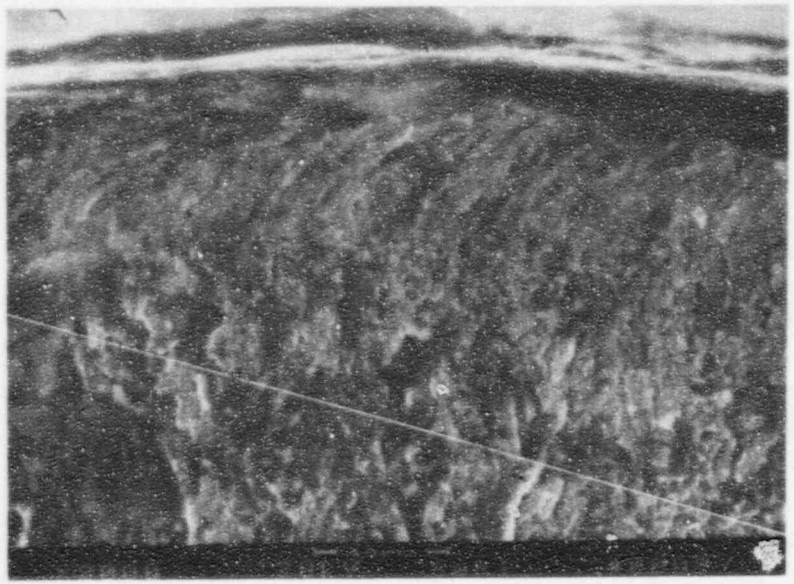

59658 2000X

c)

Figure 3-3. SEM Fractographs of SwRI Wire No. 415.

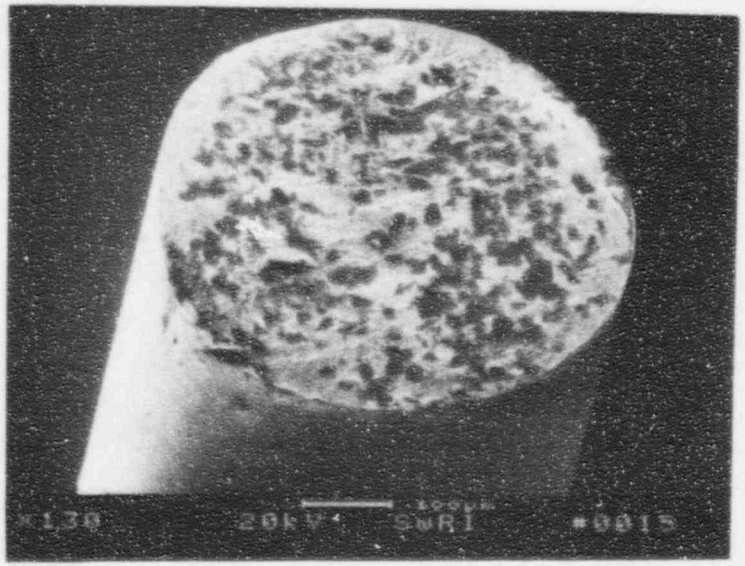

59784 130X

a)

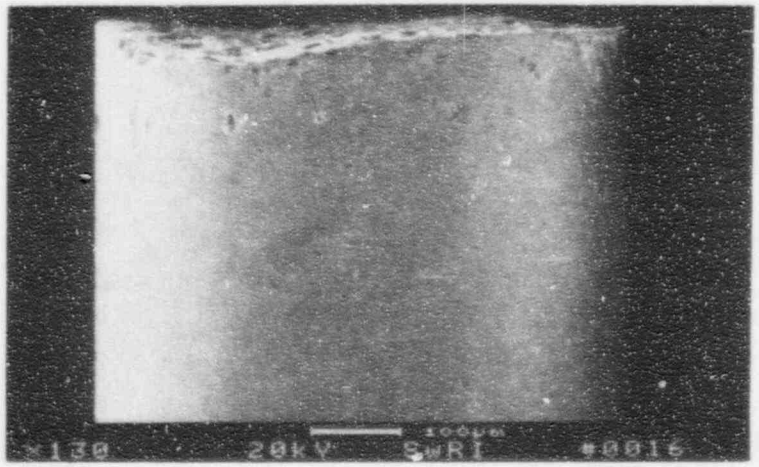

59787 130X

b)

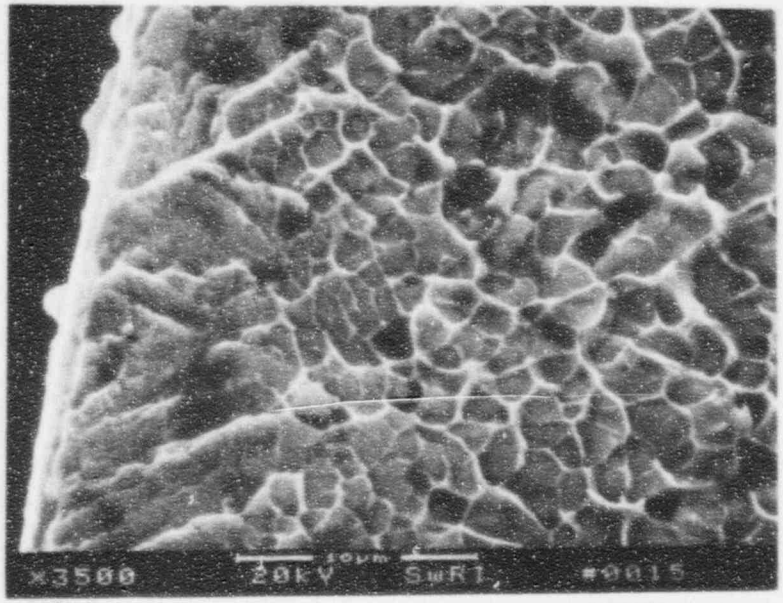

59786 3500X

c)

Figure 3-4. SEM Fractograph of Wire Exposed to .1% HF Acid.

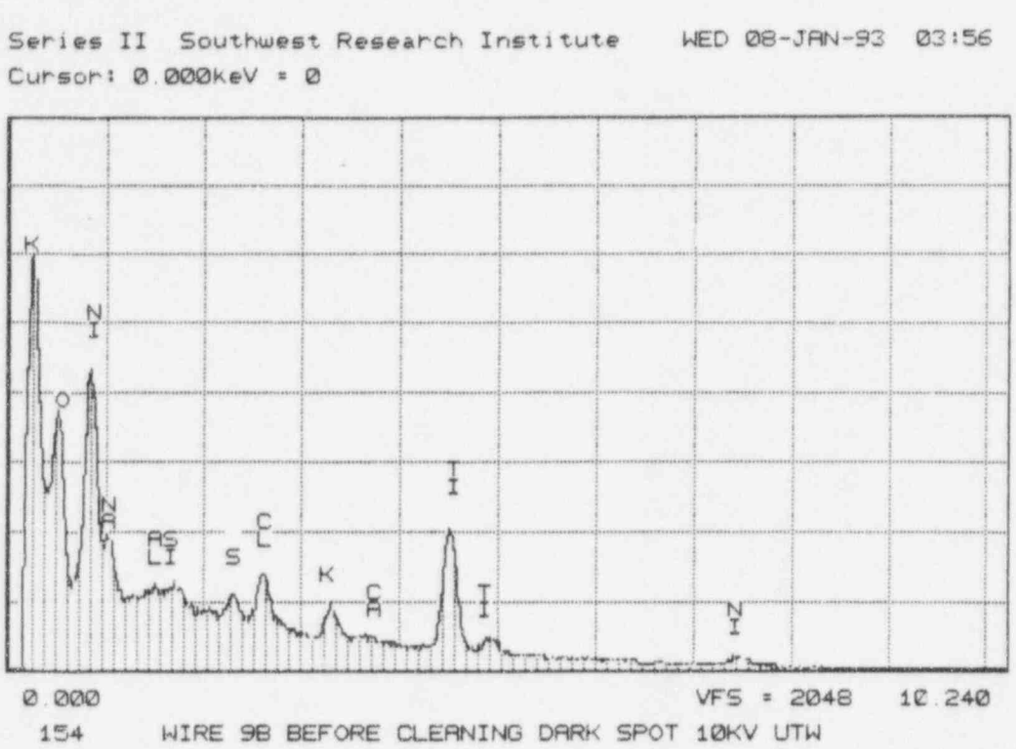

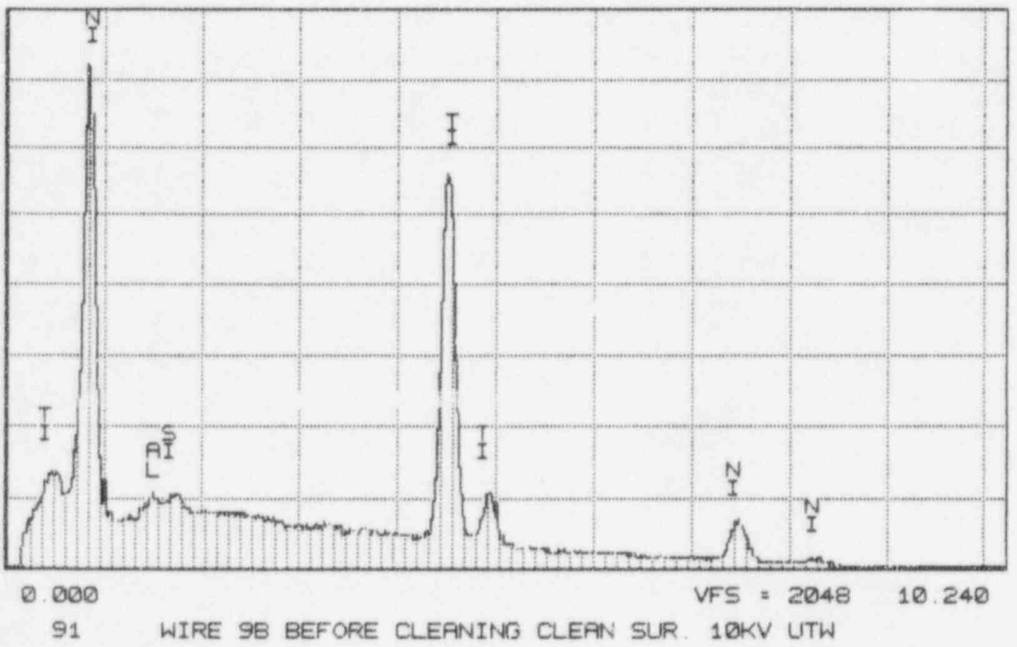

Figure 3-5. EDX Spectra of Residual Product on the Fracture Surface.

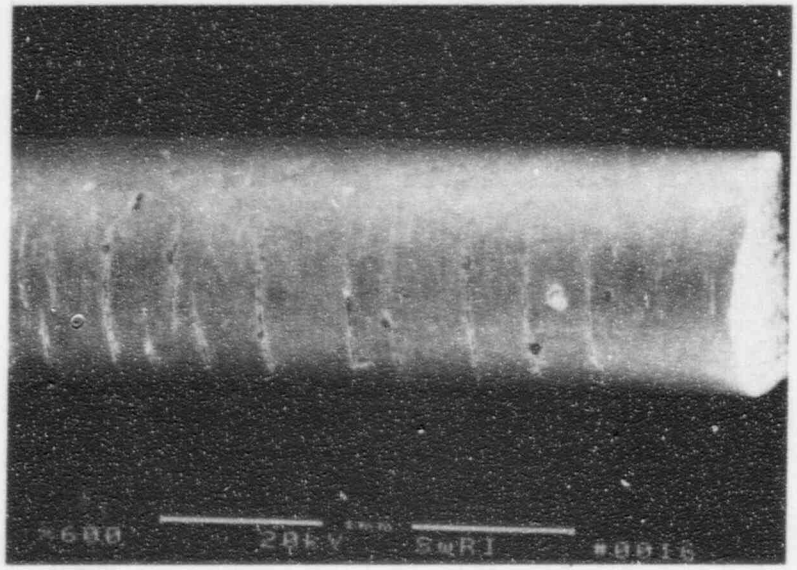

59788 60X

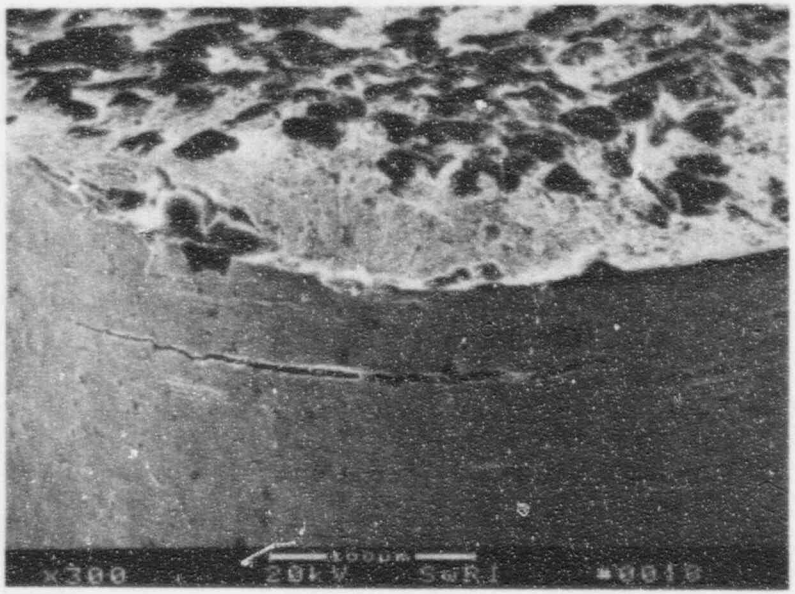

59790 300X

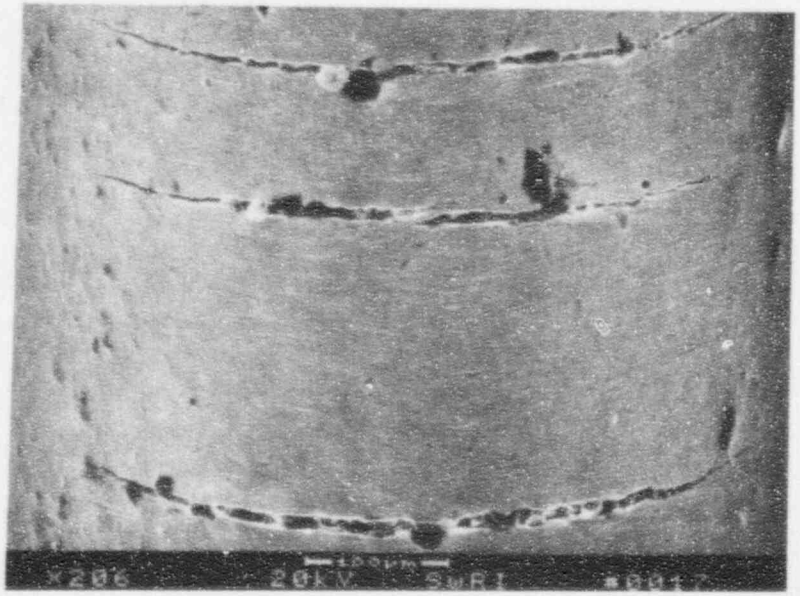

59789 200X

Figure 3-6. SEM Photographs of the OD Compression Side of the Specimen.

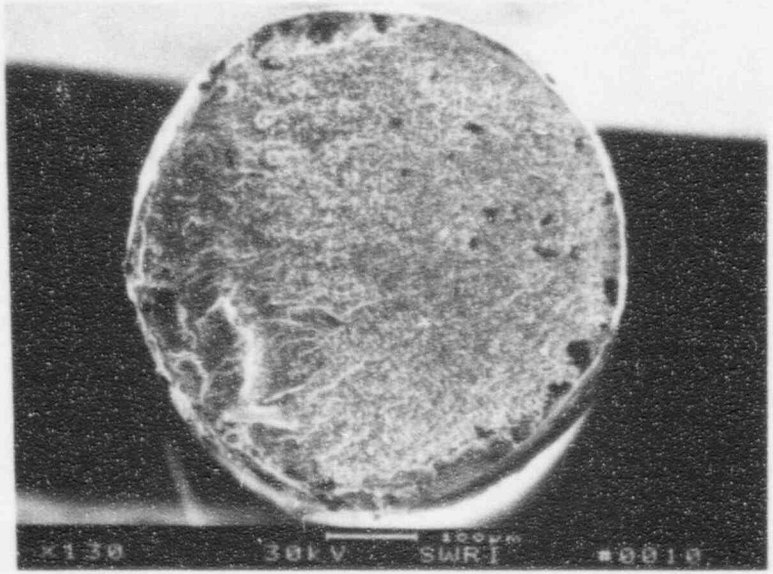

60205 130X

a) No Delay

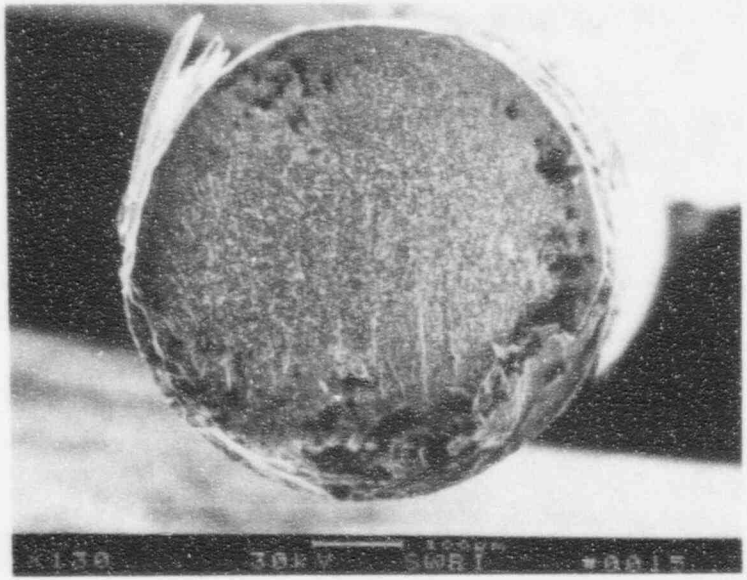

60210 130X

b) 5-hr. Delay

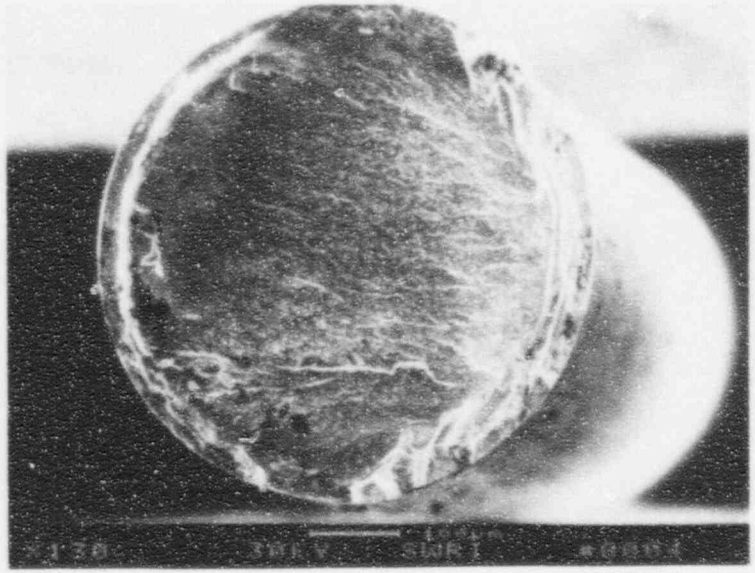

60200 130X

c) 70-hr. Delay

Figure 3-7. SEM Fractographs of Hydrogen Charged Specimens.

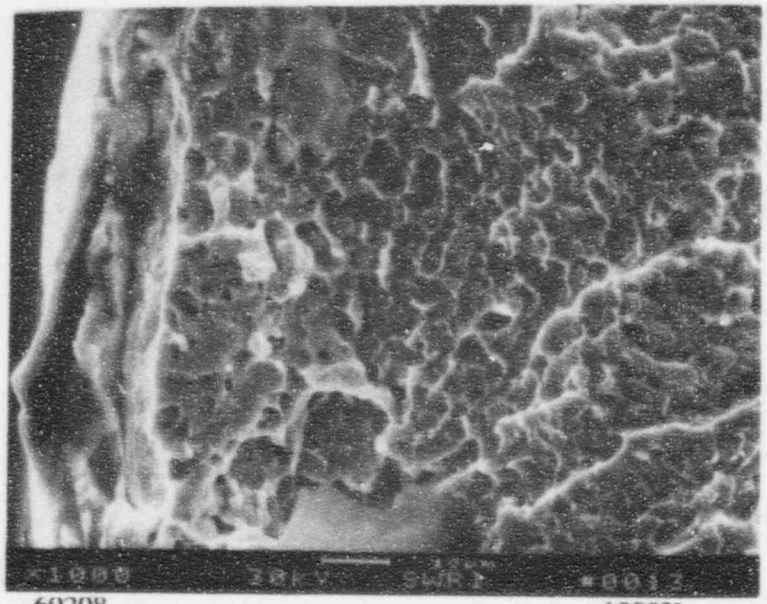

60208 1000X

a) No Delay

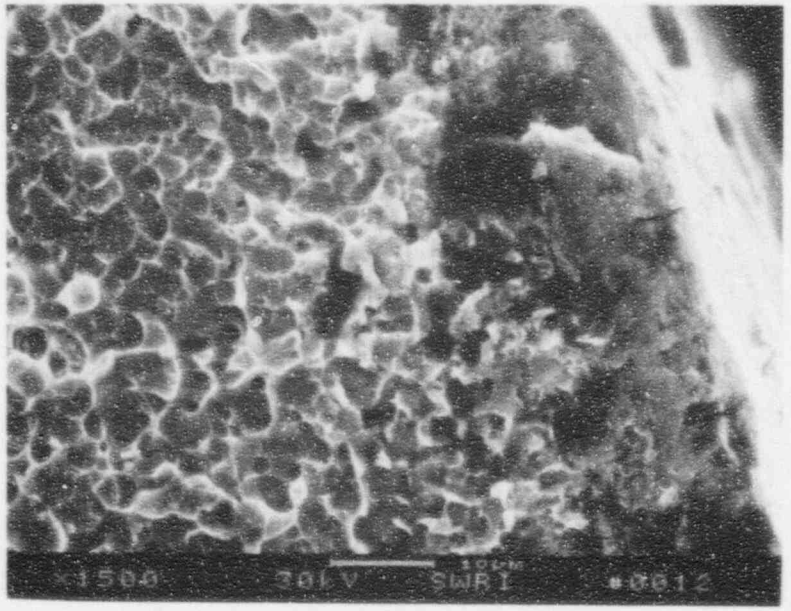

60207 1500X

b) No Delay

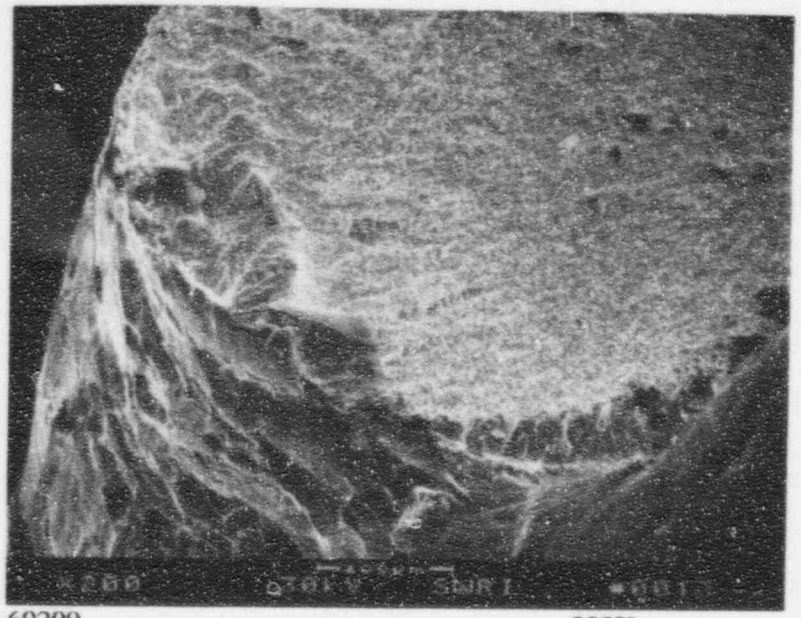

60209 200X

c) No Delay

Figure 3-8. SEM Fractographs of Hydrogen Charged Specimens.

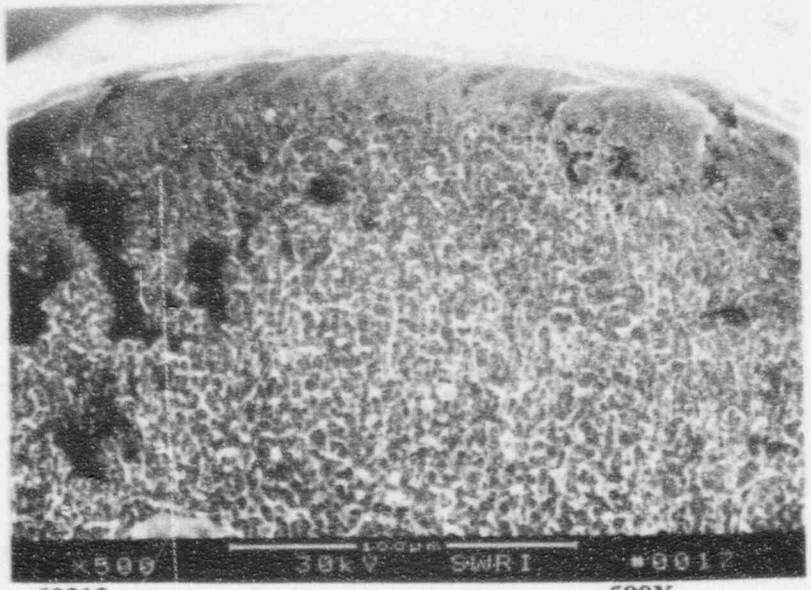

60213 500X

a) 5-hr.

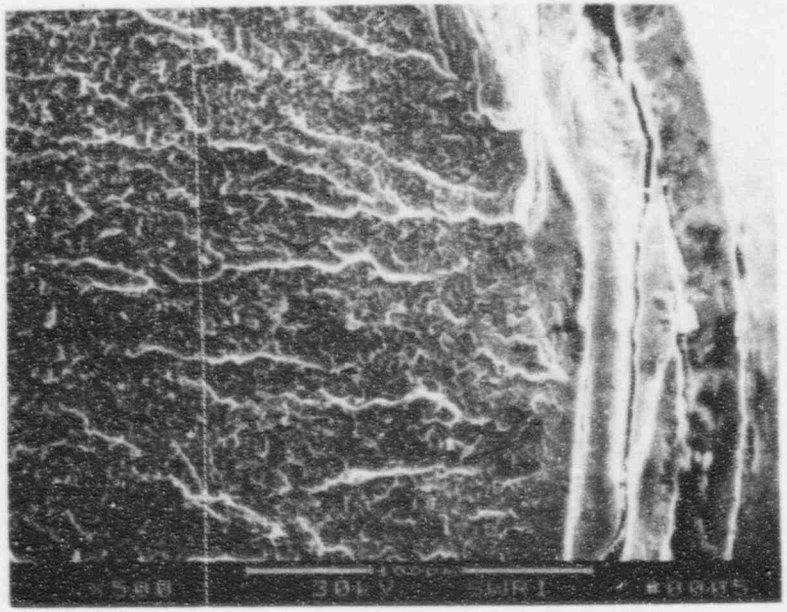

60201 500X

b) 70-hr. Delay

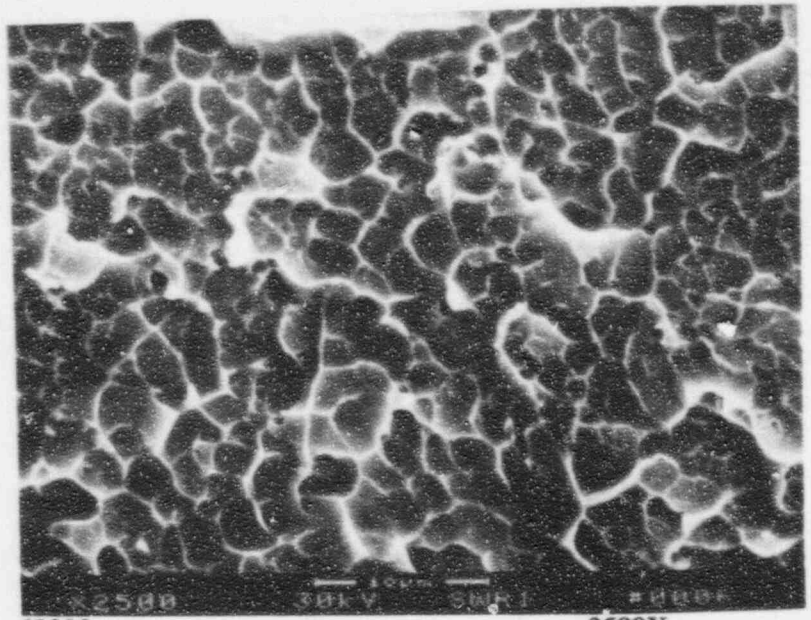

60202 2500X

c) 70-hr Delay Near Initiation

Figure 3-9. SEM Fractographs of Hydrogen Charged Specimens.

4. MANUFACTURER SAMPLES

This section discusses macrofeatures of three fractured wires: SwRI Wire Nos. 416, 417, and 419. SwRI Wire No. 416 was used in clinical applications for three months, then lined with teflon while stored in a lead cask. When the sample was extracted from the cask at the manufacturer, the wire had failed. Subsequently, the cask and wire were forwarded to SwRI for examination. SwRI Wire No. 417 was a Nitinol sourcewire exposed to wet teflon for 8 days at the manufacturer; the wire then failed when bend tested by the manufacturer.

SwRI Wire No. 419 was used successfully in service, then stored 36 days in a teflon-lined condition. The wire fractured during a bend test conducted by the manufacturer. The manufacturer's bend test consisted of clamping the sourcewire firmly in a test fixture (Figure 4-1). The wire was then pressed against a rigid glass surface until it deflected 60° or greater. The wire deflected around a 0.1 inch radius.

4.1 SwRI Wire No. 416

SwRI No. 416 was used successfully in clinical applications for three months. When the wire was extracted from its storage cask, it was severed and severely deteriorated. Figure 4-2 shows the end of the teflon catheter with the teflon lining removed. The teflon sheathing was degraded, brown in color, and cracked. Figure 4-3 shows the end of the failed wire filled with debris. The wire was cleaned first with acetone. Some of the debris was removed, but not completely, as shown in Figure 4-3(b). The wire was ultrasonically cleaned in hexane, and most of the debris was removed (Figure 4-4).

The fracture had two distinct planes with a slight angle. The two planes intersected mid-axis of the wire. The fracture surfaces were smooth and burnished with no distinct features, indicating probable sourcewire failure prior to extraction.

In order to determine the state of the sourcewire remaining in the cask, the cask was machined to section the cask into two halves, similar to the sections in Figure 1-7. After sectioning, it was observed that the stainless steel tube was packed with degraded teflon, metallic debris, and that the iridium pellets were no longer in the wire. The tip of the wire (Figure 4-5) was deteriorated, split, and severed. Figure 4-6 shows the welded plug in the center. It appeared that the cavity region between the tip and the fractured end, Figure 4-2, had completely deteriorated.

Energy dispersive X-ray analysis was conducted on the deposit found in the sectioned cask, on the fracture surface in the cleaned and uncleaned condition, and on the EDM surface. Figures 4-7 and 4-8 show the EDS spectra for the cleaned and uncleaned fracture surface. In addition to the base metal elements of titanium and nickel, fluorine (F), silicon (Si), chlorine (Cl), potassium (K), calcium (Ca), aluminum (Al), magnesium (Mg), and zinc (Zn) were detected. Figures 4-9 and 4-10(a) show the EDS spectra of the center region, which identified oxygen, fluorine, aluminum, silicon, calcium, and sulfur.

Figure 4-10 shows the EDS spectrum for the deposit found in the sectioned cask. The deposit was collected with acetate replica tape, then analyzed. Identified elements included carbon, fluorine, aluminum, nickel, phosphorous, and titanium. A higher oxygen peak than in the other EDS spectra was observed. Identification of carbon and fluorine indicates teflon was present in the deposit.

4.2 SwRI Wire No. 417

SwRI Wire No. 417 was exposed to a wet teflon environment for 8 days, then failed in a bend test at the manufacturer. Figure 4-11 shows multiple fracture planes formed during bending of the wire. Two flat areas appeared to have initiation sites at the ID surface. The wire diameter was uniform and the hole centered. The flat regions transitioned to a slant fracture, then a final fracture, shown in Figure 4-11(c). The fracture was characteristic of a brittle failure. Figure 4-12 shows a side view of the failed wire. The OD surface appeared to be covered with some debris. No cracks were noted on the OD surface. Figure 4-13 shows the microfracture features at three locations. The fracture had characteristic dimples in all locations. In Location No. 1, the dimples were elongated, indicating the direction of the failure away from the initiation sites. The EDM surface of the cavity did not have cracks that would have caused the failure.

4.3 SwRI Wire No. 419

SwRI Wire No. 419 was successfully used in clinical applications, subsequently stored in teflon for 36 days, then fractured in a bend test at the manufacturer. Figure 4-14 shows that the fracture was predominantly flat with a slight slant fracture on one side. The fracture was brittle looking in nature. The diameter of the wire was 0.021 inch. The cavity through the center was slightly offset. The thinned side was 0.0032 inch thick, while the thicker side was 0.0052 inch thick. Figure 4-15 shows flow lines radiating from the ID of the wire at the thinned region. Fracture initiated at the ID, then propagated until complete failure had occurred through the cross section. In the initiation region, the dimples were small and flat, shown in Figure 4-15(b). Figure 4-16 shows the fracture features at other locations on the fracture. The elongated dimples in Figure 4-16(a) indicate that the crack propagated from the initiation site towards the opposite side. The fracture flow lines at the final fracture region, shown in Figure 4-16(b), extended from the ID to the OD surface at a slight angle.

4.4 Summary

The following observations were made on the sourcewires by the manufacturer:

1) Complete degradation, deterioration occurred of a teflon-lined wire stored in a cask for three months.

2) One end of the wire had a fracture surface coated with debris, suggesting the failure probably occurred prior to extraction from the cask.

3) EDS analysis identified several elements in the deposit on the failed wires. The elements included oxygen, fluorine, aluminum, silicon, calcium, sulfur, chlorine, potassium, and phosphorus.

4) SwRI Wire Nos. 417 and 419, exposed to teflon had a brittle fracture that initiated on the ID surface. There was no abnormal feature on the ID that would have caused failure.

5) The cavity in Sample No. 419 was slightly off center. There was no indication that it was a cause for failure.

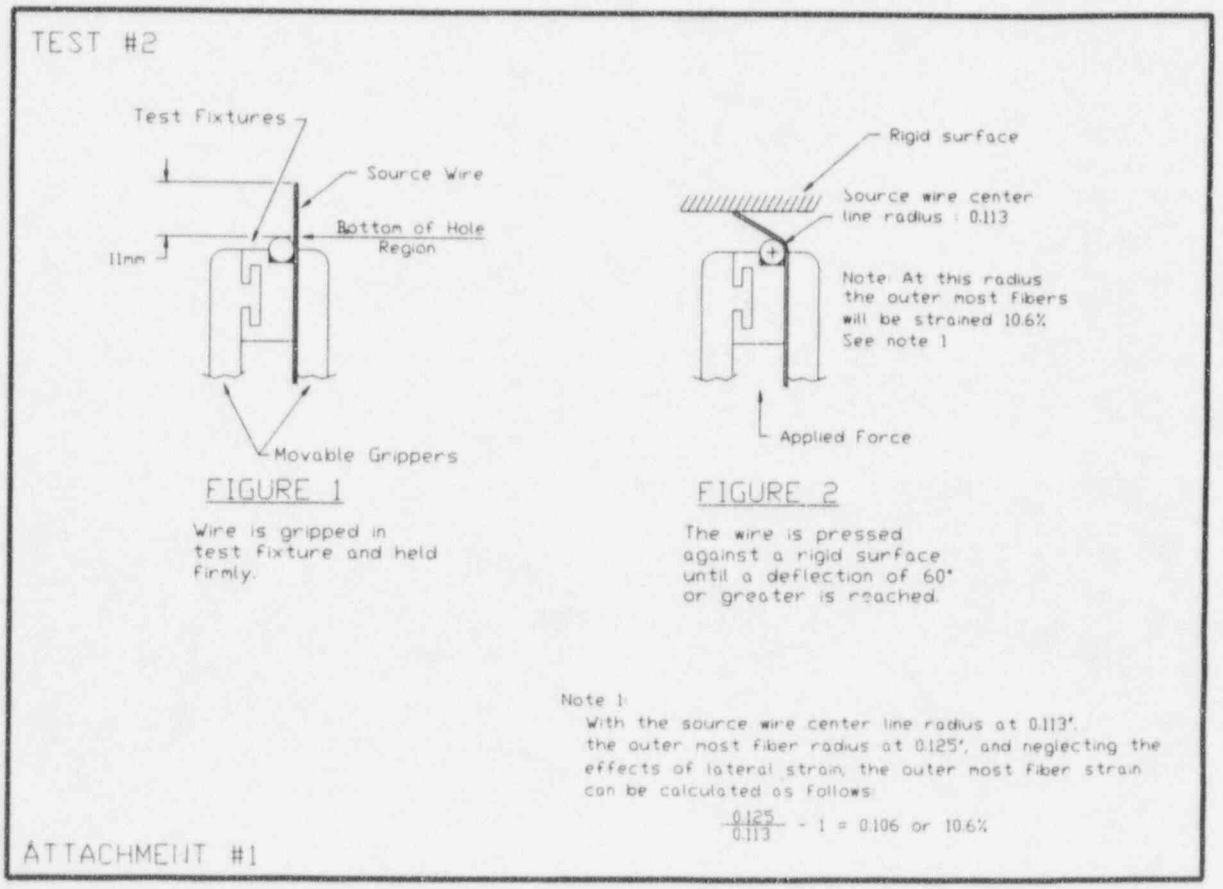

Figure 4-1. Illustration of Manufacturer's Bend Test Fixture.

59644 15X

a) Side View of Wire

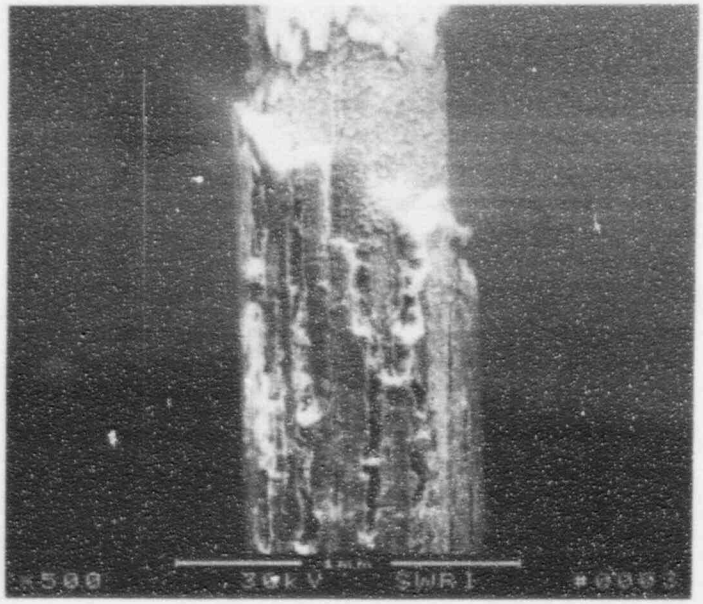

59708 50X

b) Close-up of OD

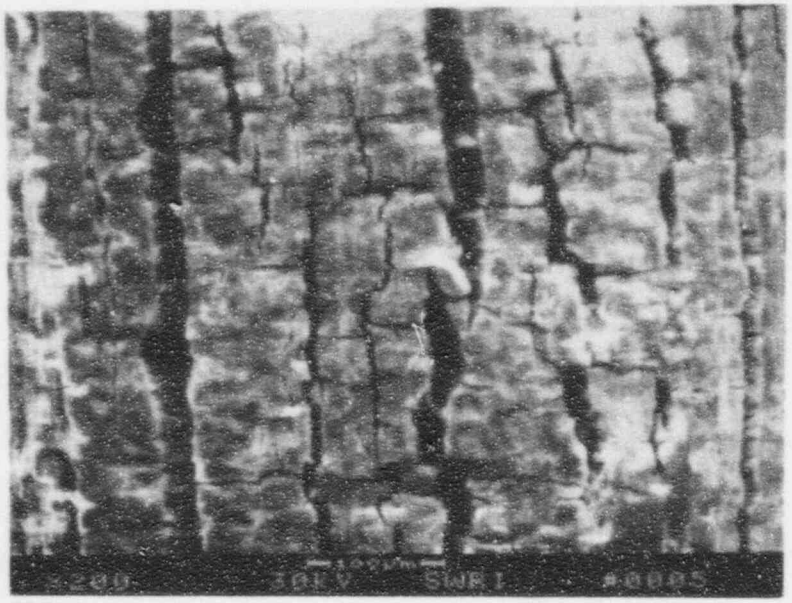

59710 200X

c) Degraded teflon

Figure 4-2. Photographs of SwRI Wire No. 416.

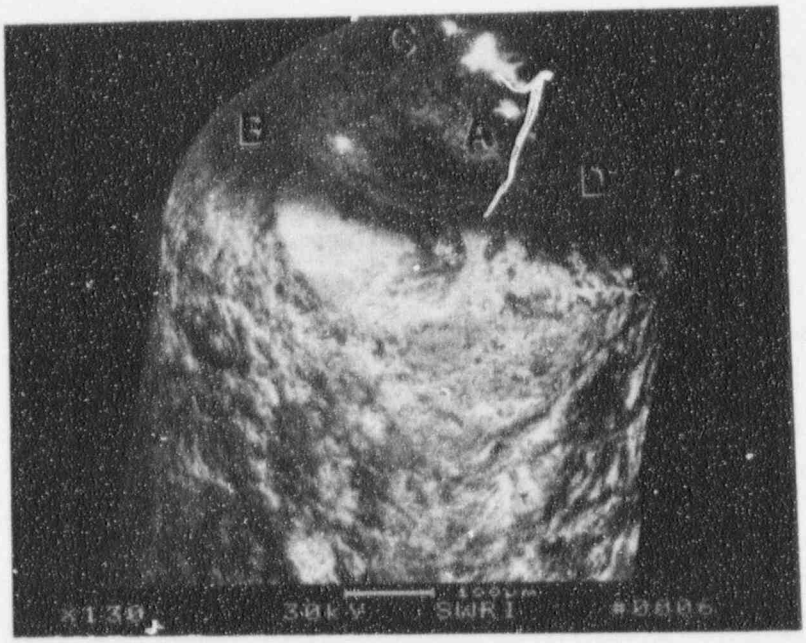

59737 130X

a) First Clean

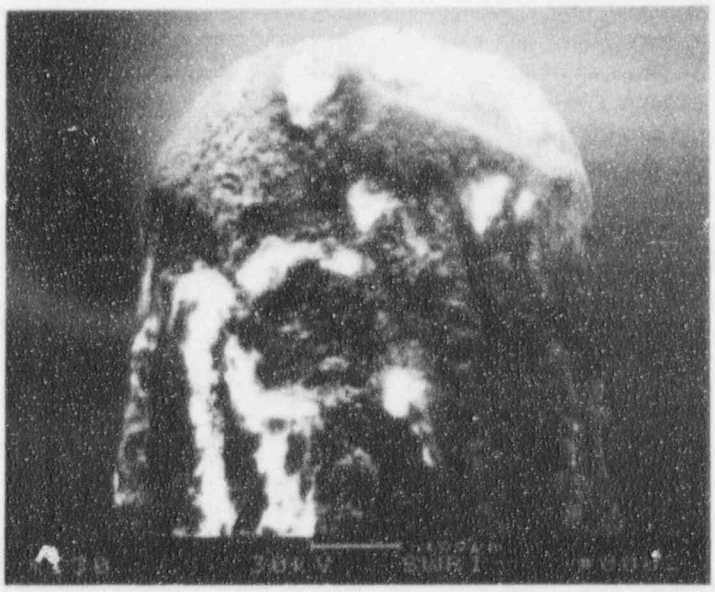

59707 130X

b) Uncleaned

Figure 4-3. SEM Photographs of the Wire End of SwRI Wire No. 416.

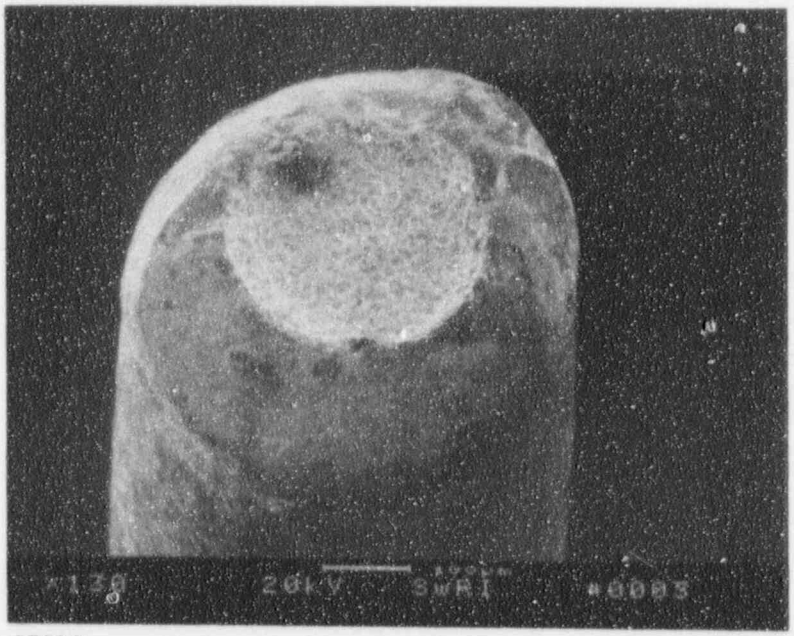

57909 130X

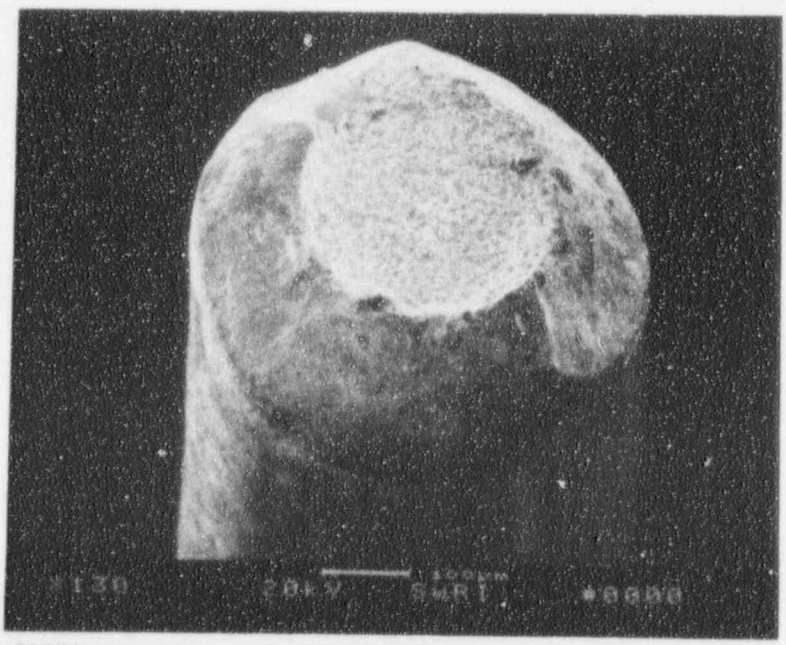

59309 130X

Figure 4-4. SEM Photograph of the Tip of SwRI Wire No. 416.

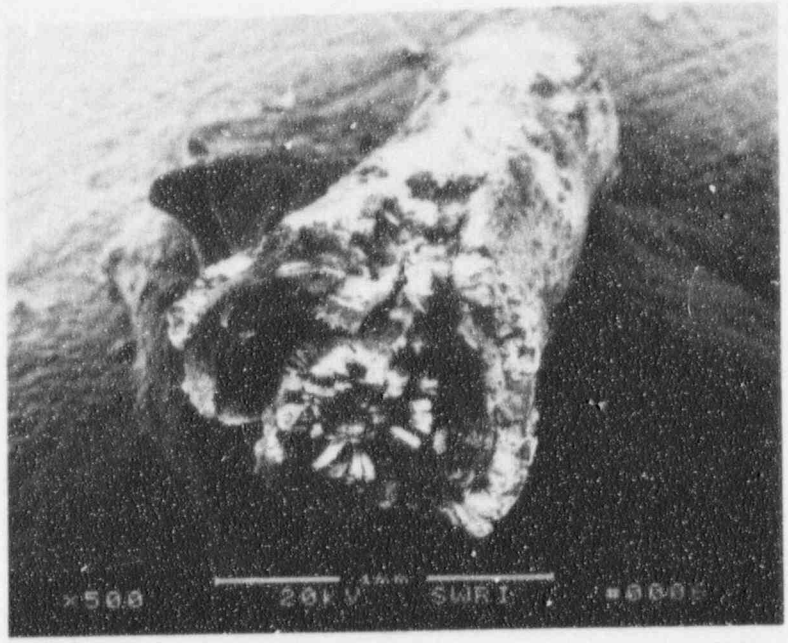

59894 50X

a)

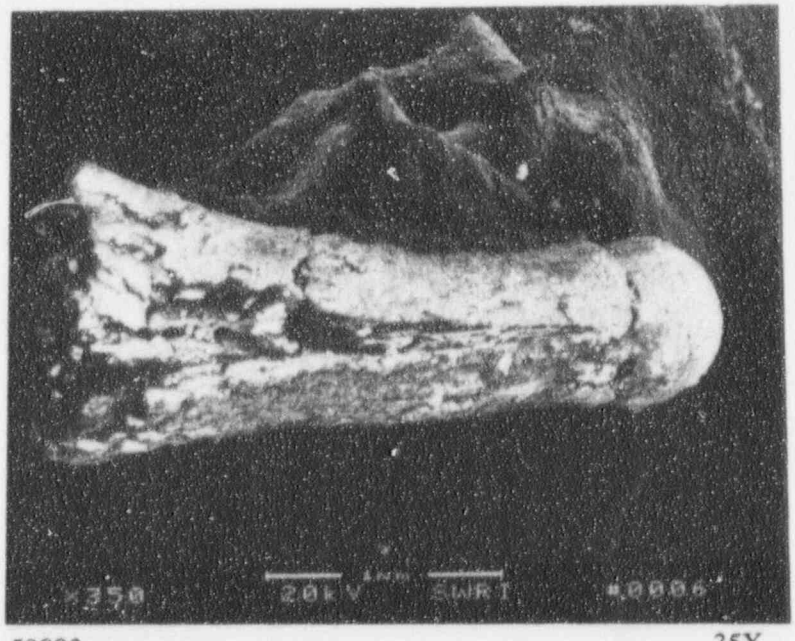

59893 35X

b)

Figure 4-5. SEM Photographs of the Tip of SwRI Wire No. 416.

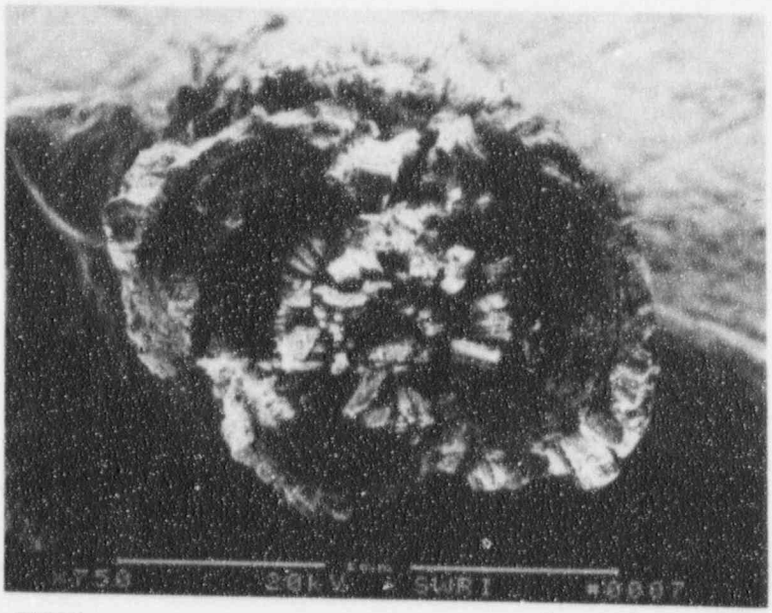

59896 75X

a)

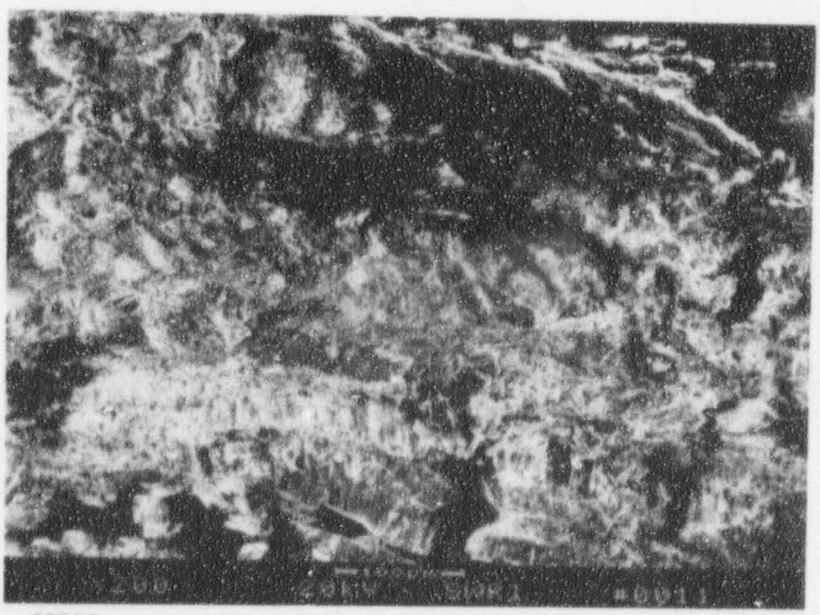

59899 200X

b)

Figure 4-6. SEM Photographs of the Tip of SwRI Wire No. 416.

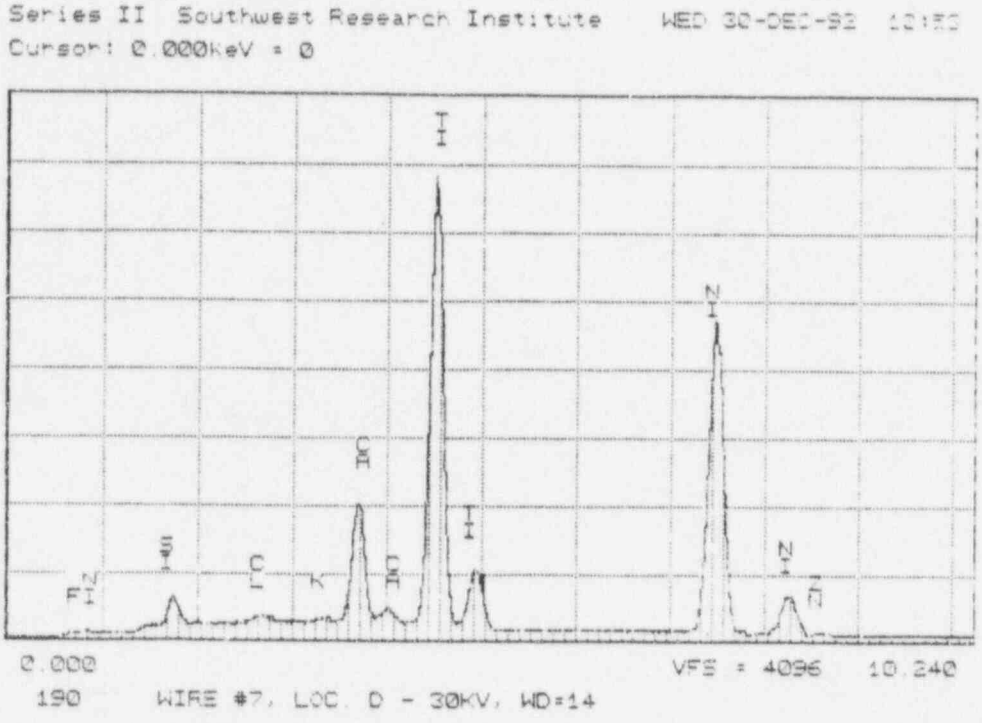

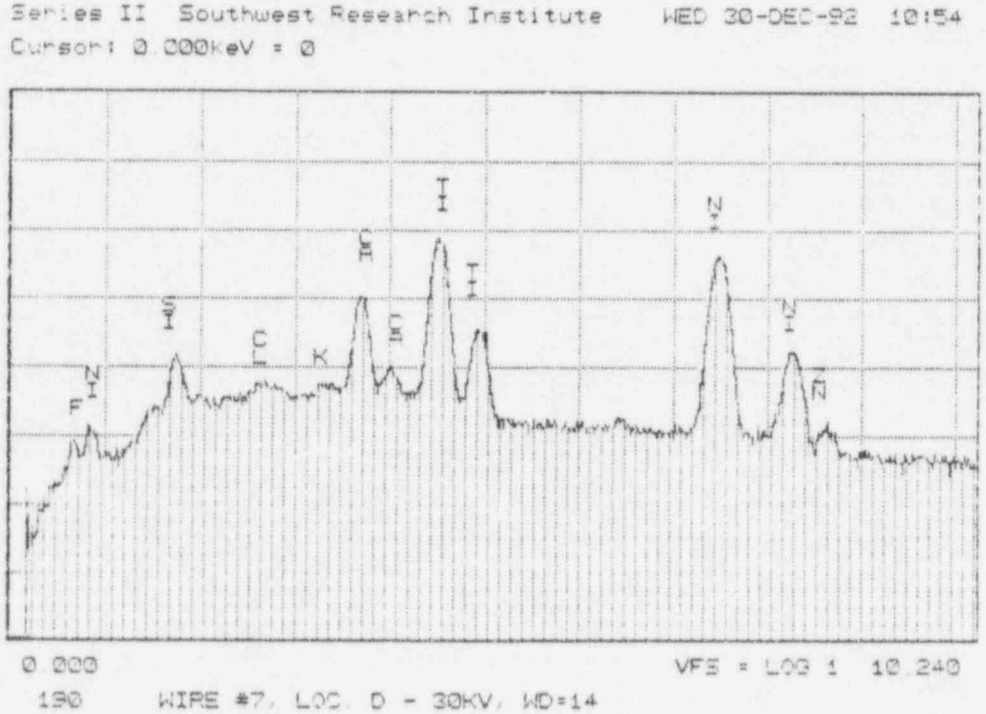

Figure 4-7. Energy Dispersive X-Ray Spectra of the Uncleaned Fracture Surface of SwRI Wire No. 416.

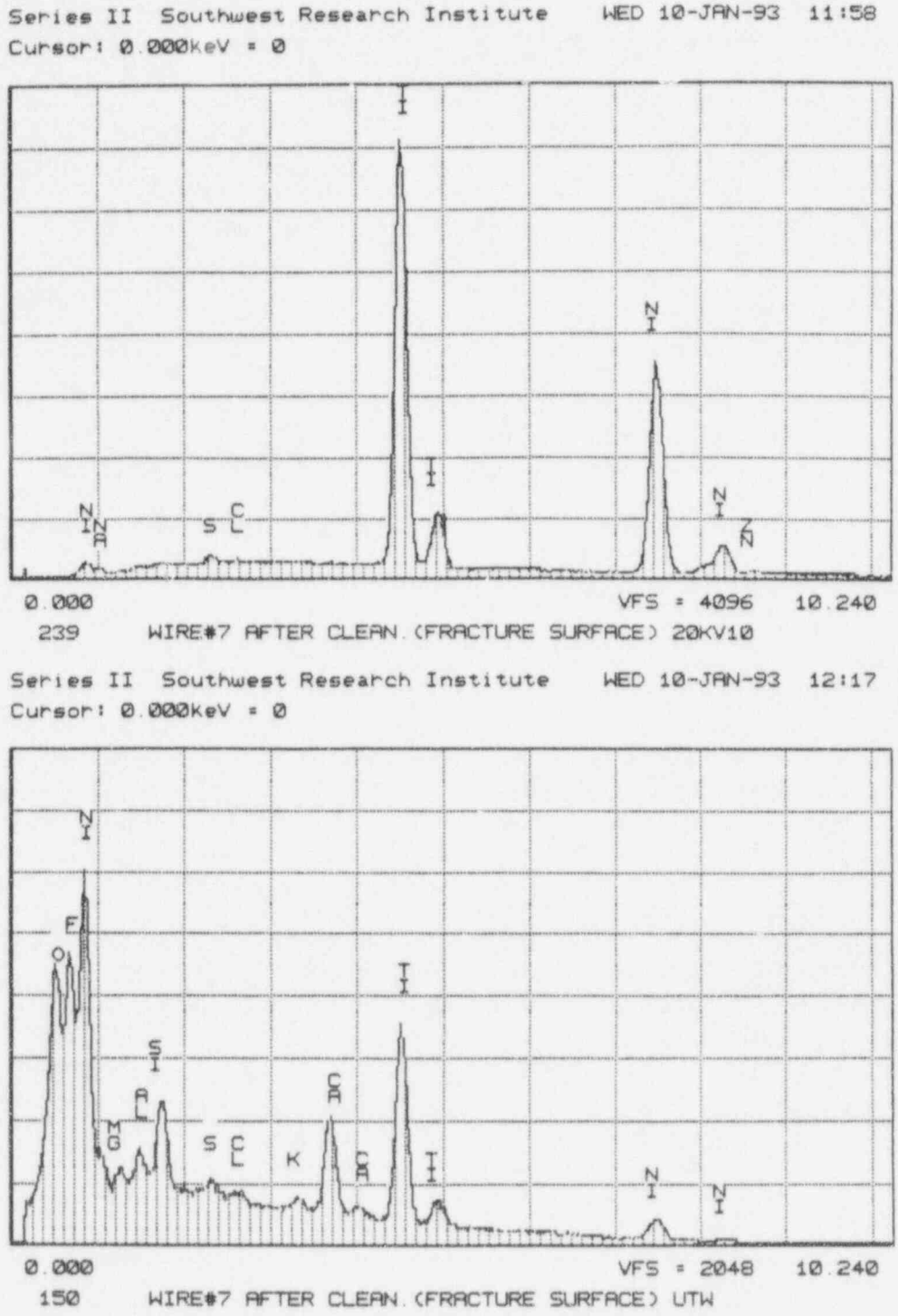

Figure 4-8. Energy Dispersive X-Ray Spectra of the Cleaned Fracture Surface For SwRI Wire No. 416.

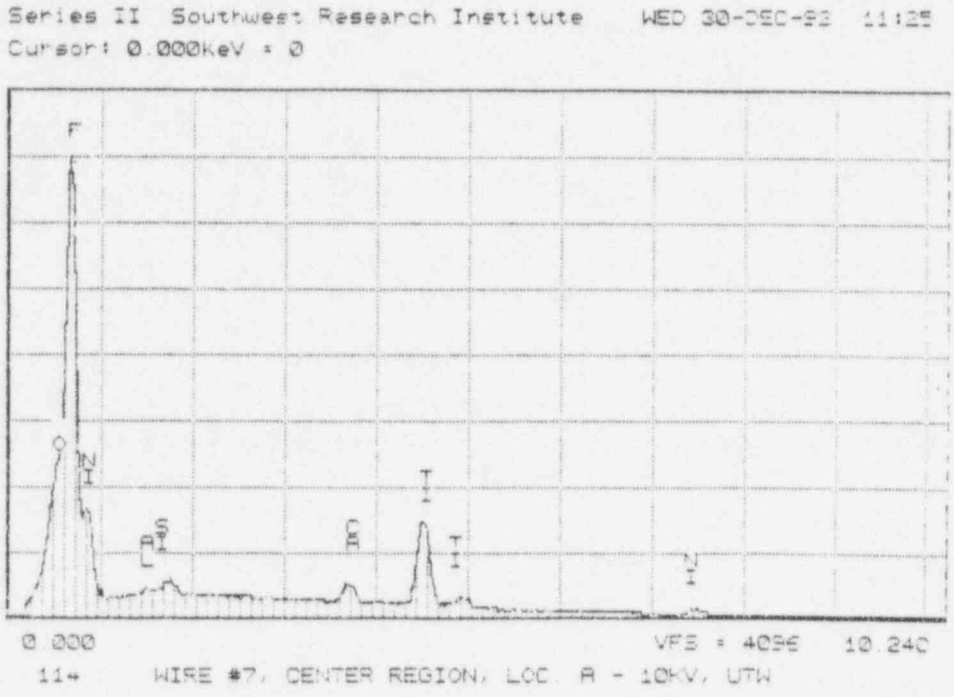

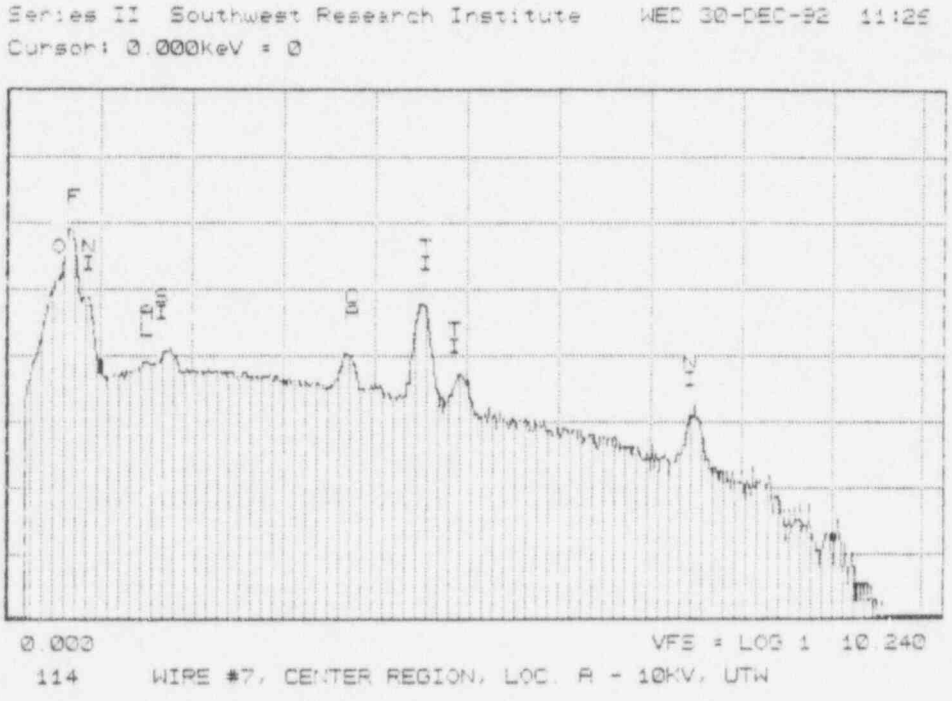

Figure 4-9. Energy Dispersive X-Ray Spectra of the Center Portion of Failed SwRI Wire No. 416.

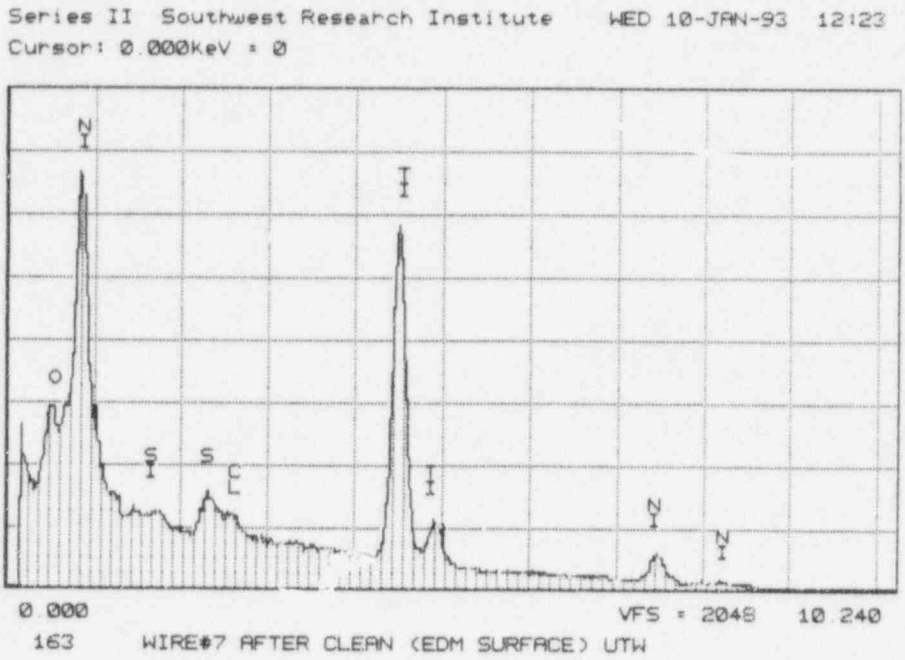

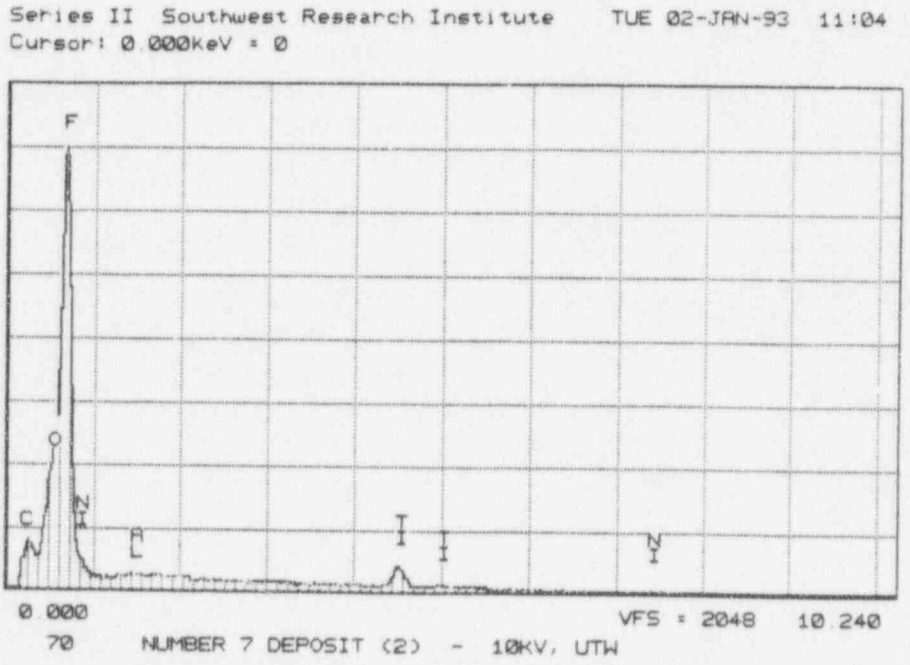

Figure 4-10. Energy Dispersive X-Ray Spectra of the EDM Surface and Deposit for SwRI Wire No. 416.

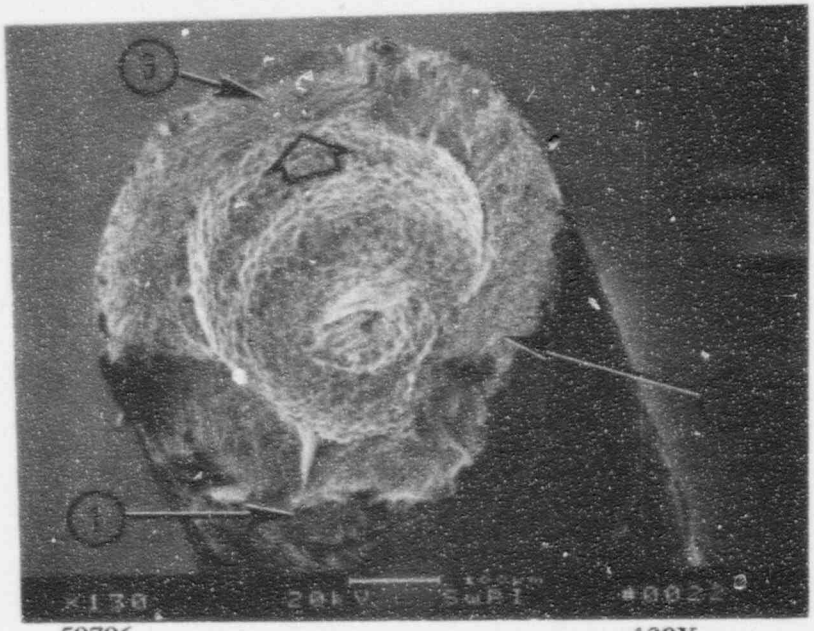

59796 130X

a) View Looking Down

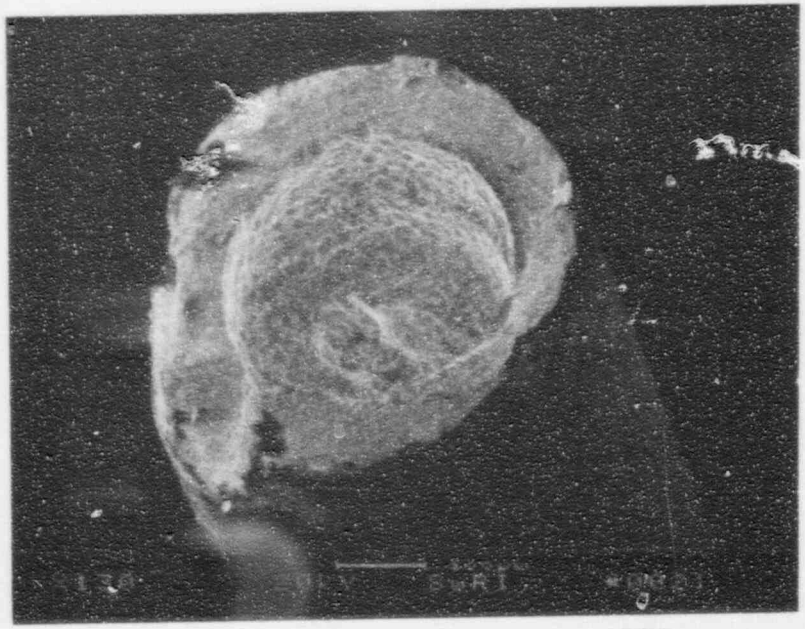

59797 130X

b) View Looking Down

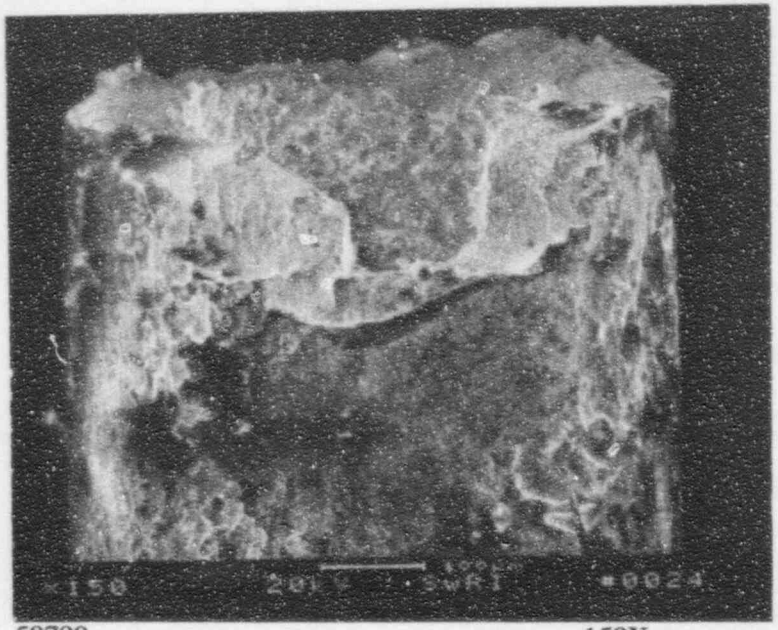

59799 150X

c) View of the Side

Figure 4-11. SEM Fractographs of SwRI Wire No. 417.
Arrow shows origin.

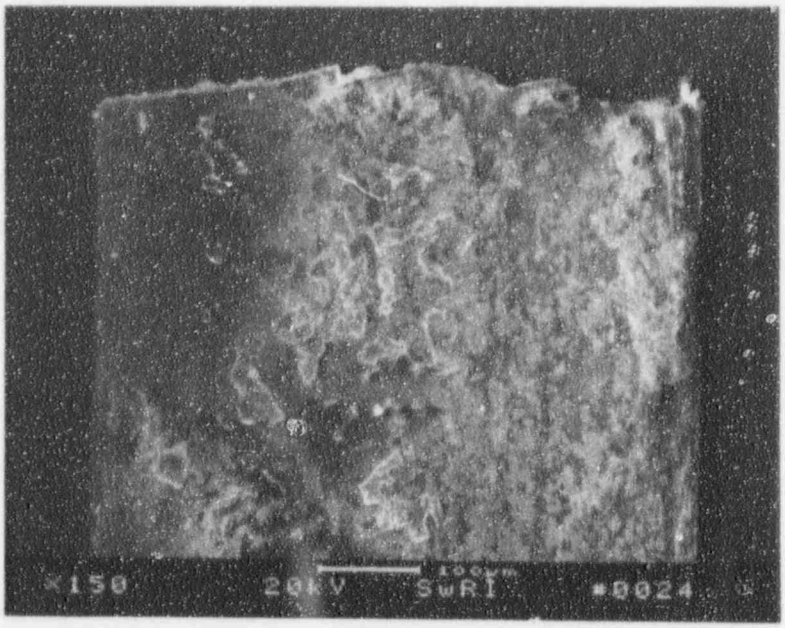

59800 150X

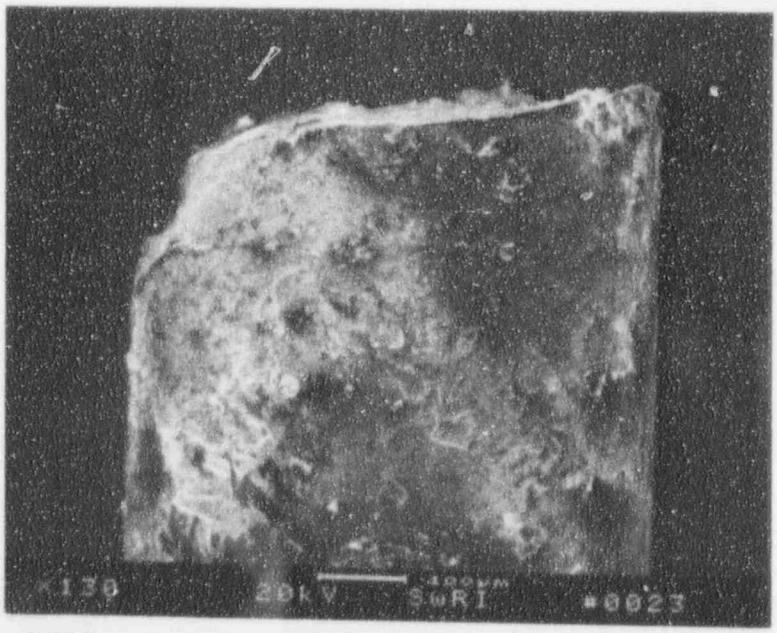

59798 130X

Figure 4-12. SEM Photographs of SwRI Wire No. 417.

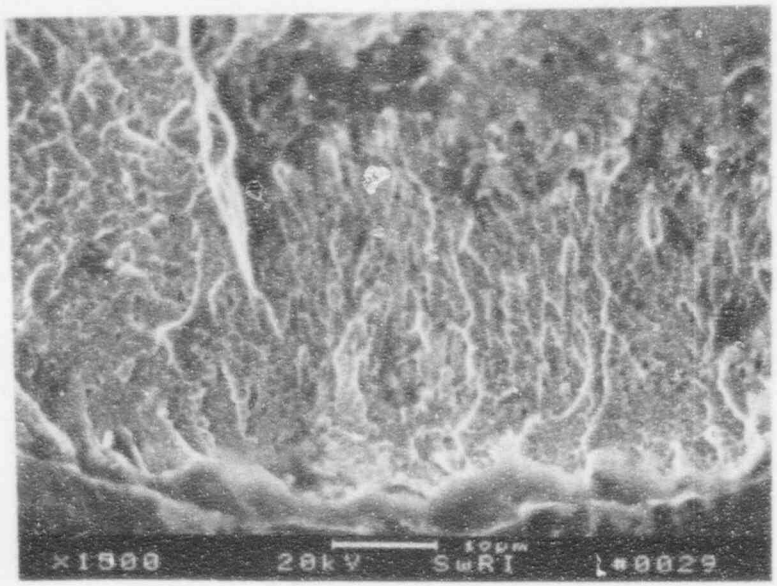

59806 1500X

a) Location 3

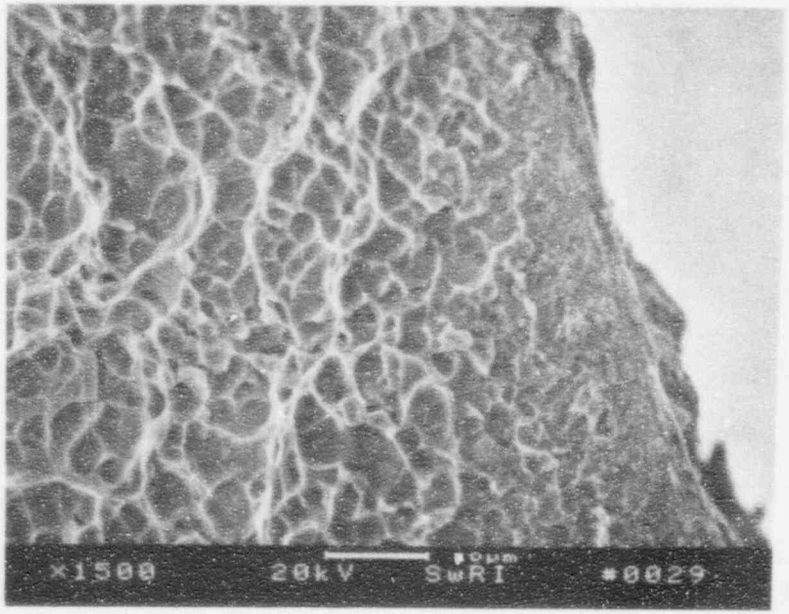

59807 1500X

b) Location 2

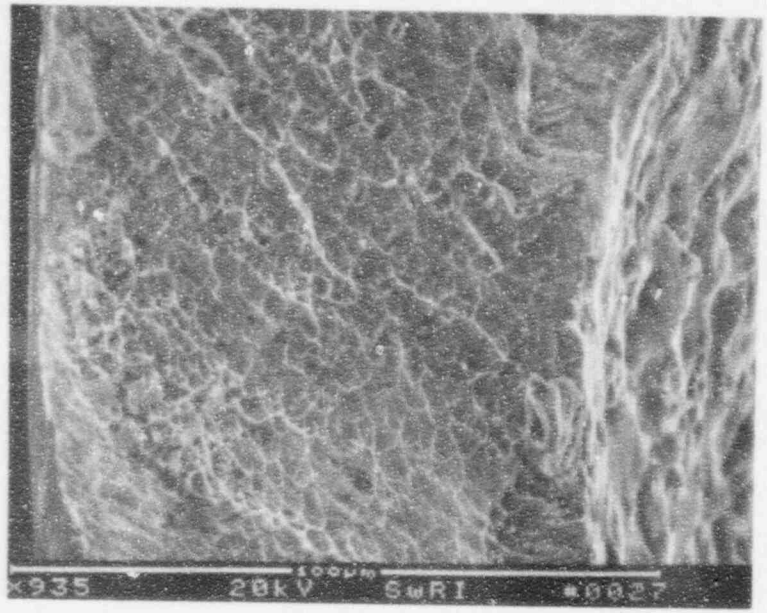

59803 935X

c) Location 1

Figure 4-13. SEM Fractographs of Fracture Features on SwRI Wire No. 417.

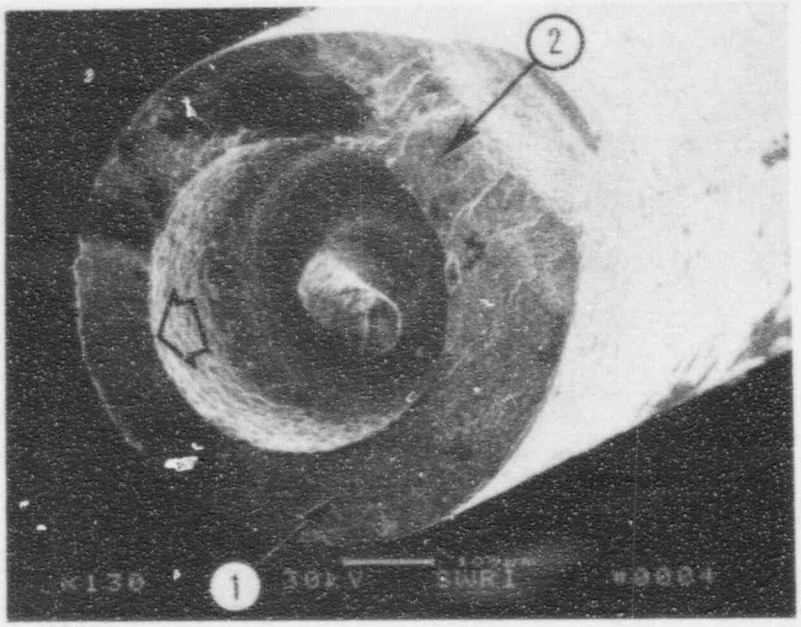

59938 130X

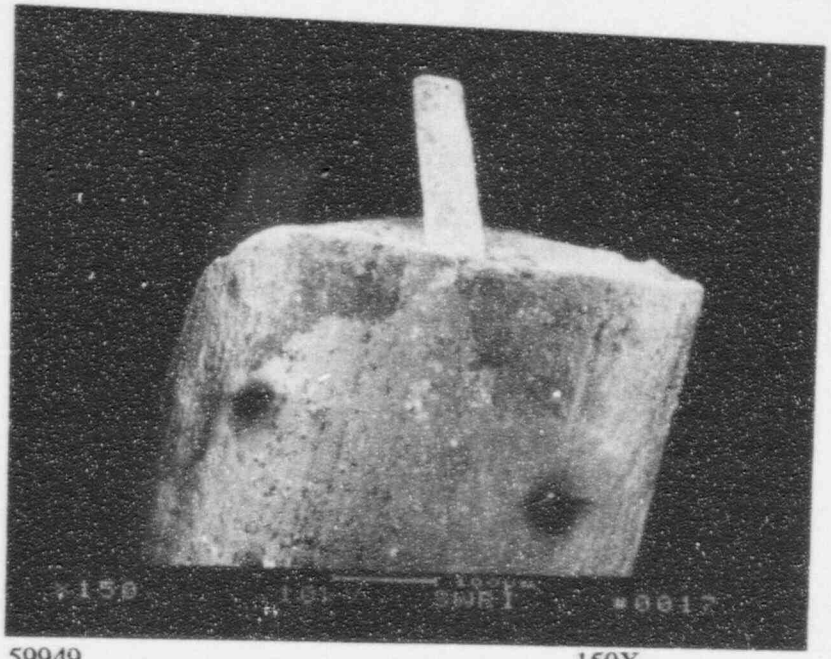

59949 150X

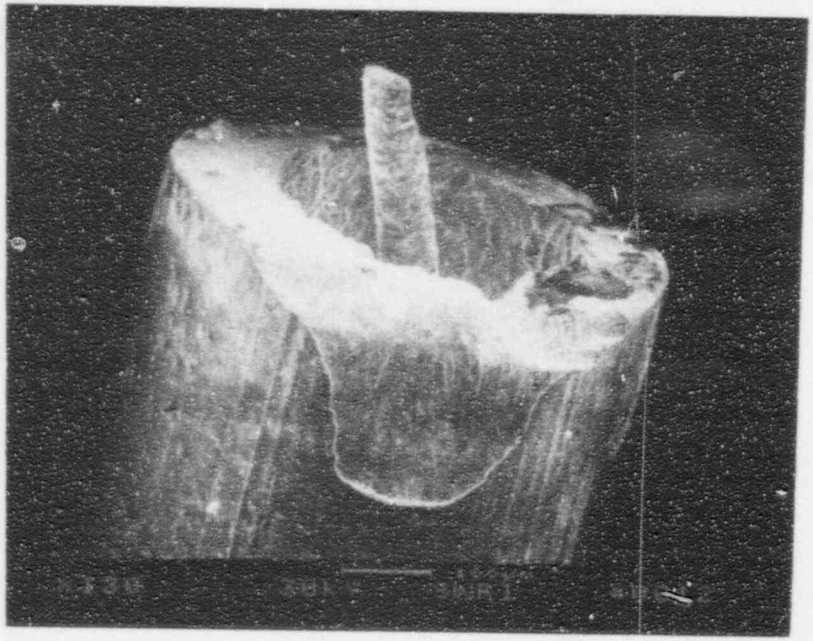

59947 130X

Figure 4-14. SEM Fractographs for SwRI Wire No. 419.

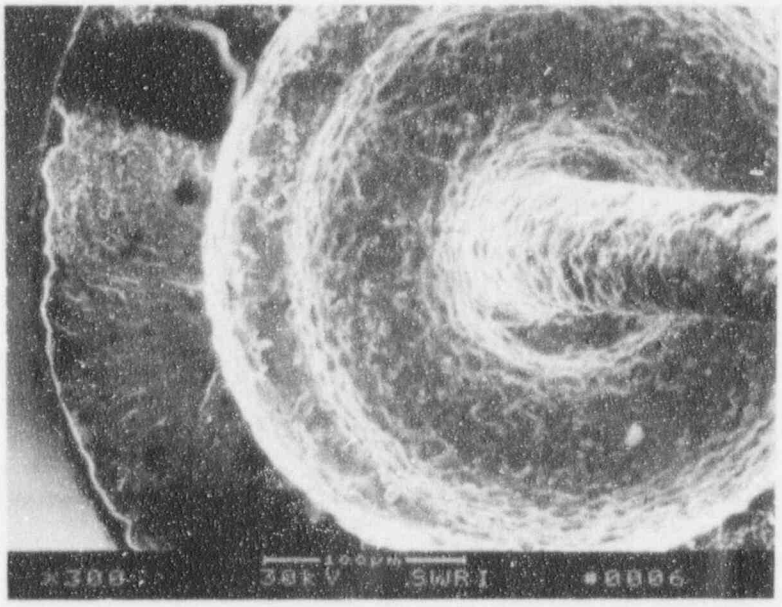

59441 300X

a) Thinned Wall

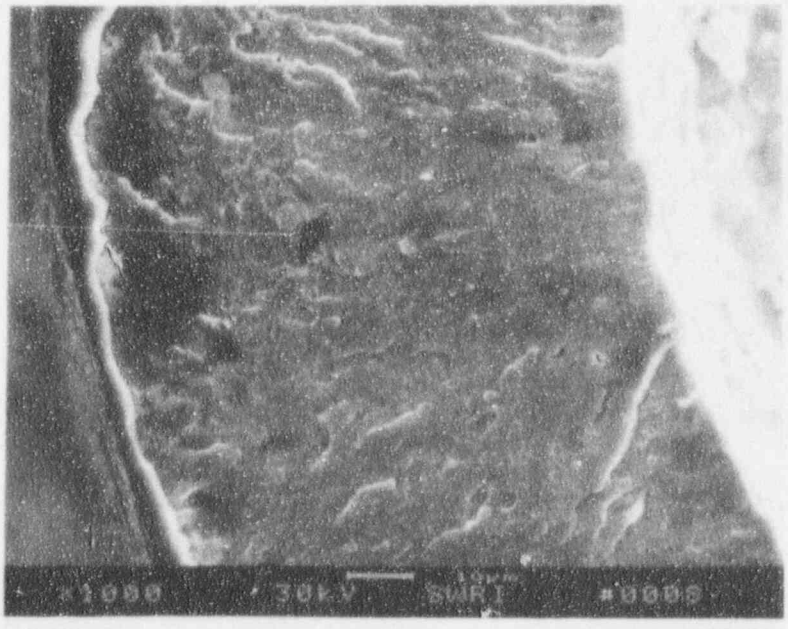

59942 1000X

b) Initiation Site

Figure 4-15. SEM Fractographs of the Initiation Site on SwRI Wire No. 419.

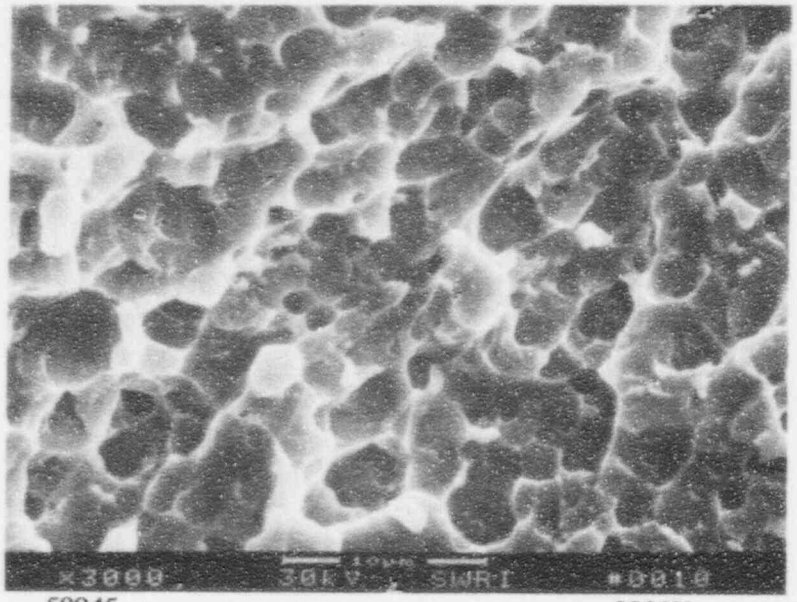

59945 3000X

a) Location 1

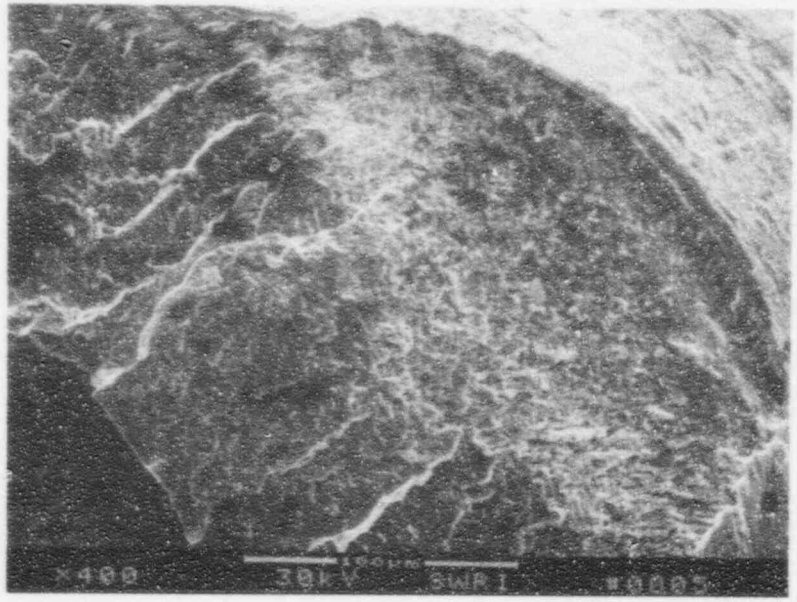

59939 400X

b) Location 2

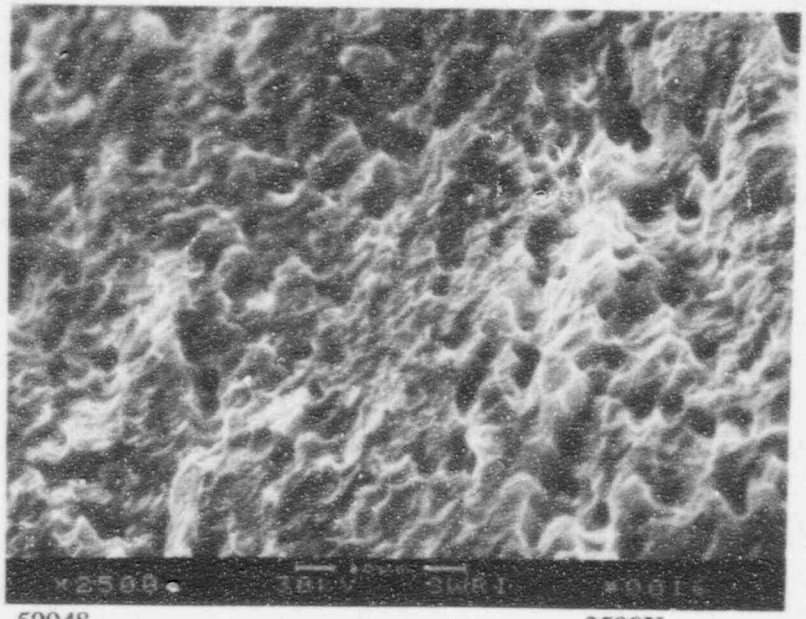

59948 2500X

c) Location 2

Figure 4-16. SEM Fractographs at Location Nos. 1 and 2 of SwRI Wire No. 419.

5. LABORATORY BEND TESTS

A bend test program on Nitinol wire was established to determine if Nitinol could be embrittled due to either hydrogen, moisture, teflon, radiation exposure or the combination of the environments. Nitinol wires in various pre-test conditions were exposed to these environments, then the wires were tested in a bend test fixture. A flow diagram, Figure 5-1, shows the different test conditions. Additional tests were conducted on solid wire charged with hydrogen. SwRI designed a bend test fixture that provided the control needed to deflect the wire, then measure the deflection. Section 5.1.2. has additional discussion on the bend test fixture. If a wire failed prematurely at a lower angle of deflection, it was an indication that a wire was embrittled. If a Nitinol wire was indeed embrittled, the deflection angle could be measured, then compared to the deflection angle for a ductile condition. If a wire failed, fractographic examination was conducted. The fractographic features and bend test results were compared to the clinical failures discussed in Section 2.0.

5.1 Procedures and Equipment

5.1.1 Sourcewire Conditions

When the wire samples were shipped to SwRI, the sourcewire remained in the lead storage cask until the time of testing. The wires were radioactive and handled according to SwRI radiation safety procedures discussed in Appendix F. To determine if the wire was deteriorated or broken, the wire was removed from the cask. If the wire was not broken, the wire was bend tested to determine if the as-received condition was still ductile or if it was embrittled.

Table 5-1 shows a listing of the bend test samples and exposure conditions for the sourcewires. The test samples were identified with a SwRI lab number to maintain records of samples received and tested. The numbers were not specifically ordered for any condition. If a number is not identified, for example, SwRI No. 433, it is because that number was used for another SwRI project. The dashed number after a wire number represents the test sequence on a particular wire, for example 424-1, is the first test and 424-3 is the third test, etc.

The majority of the tests on the sourcewire was conducted in lab air at the SwRI radiation lab facility at which the temperature ranged from 70° to 80°F with a relative humidity of 62%. The only tests not conducted in lab air were the tests conducted below 50°F (10°C).

The sourcewires stored in a stainless steel needle had additional environment conditioning of the wires before the final bend test. The wires were exposed to moisture for at least 100 days, then tested in lab air or tested below 50°F (10°C), see Section 5.4 for more details.

Bend tests were conducted on the Nitinol wire in various pre-test conditions. The conditions included:

1) Unradioactive dummy wires with a cavity. These wires were identical to a production wire except the cavity was filled with two nonradioactive iridium pellets.

2) Unradioactive solid wires charged with hydrogen. These wires were charged with hydrogen in the SwRI laboratory, then tested.

3) Post-service radioactive wires stored in teflon. These wires were used in clinical applications, removed from service, then stored with a teflon liner in a lead cask.

4) Post-service radioactive sourcewires stored in a stainless steel needle with no teflon. These wires were used in clinical applications, removed from usage, then stored in a stainless steel needle in a lead cask.

5) Non-service radioactive sourcewires stored in stainless steel with no teflon. These wires were production wires never used in a clinical application. They were shipped to SwRI in a stainless steel needle in a lead cask.

Each bend test had a load verses angle of deflection plot. If the wire failed, the angle was noted and recorded.

Table 5-1. Listing of Sourcewires and Identification Numbers

Manufacturer ID. No.	SwRI ID. No.	Sample Identification
92-57	421	Service wire stored in teflon for 222 days.* (Received 2/16/93)
92-66	422	Service wire stored in teflon for 142 days.* (Received 2/16/93)
92-91	423	Service wire stored in teflon for 103 days.* (Received 2/16/93)
92-113	424	Service wire with no teflon. Stored in SS for 70 days.* (Received 2/16/93)
92-114	425	Service wire with no teflon. Stored in SS for 70 days.* (Received 2/16/93)
92-117	426	Production sourcewire. Never installed. Stored in SS for 131 days.* (Received 2/16/93)
92-118	427	Service wire with no teflon. Stores in SS for 76 days.* (Received 2/16/93)
93-2	428	Production sourcewire. Never installed. Stored in SS for 91 days.* (Received 2/16/93)
92-88	429	Service wire shipped in teflon for 6 days. Stored in SS for 199 days.* (Received 2/16/93)
120492-2	435	Dummy wire.
111292-1	436	Dummy wire.
92-111	441	Service wire. 202 days in SS.** (Received 5/25/93)
92-123	442	Service wire. 183 days in SS.** (Received 6/8/93)
92-100	443	Service wire. 226 days in SS.** (Received 6/8/93)
93-01	444	Service wire. 154 days in SS.** (Received 6/8/93)
92-121	445	Service wire. 183 days in SS.** (Received 5/25/93)
92-108	446	Service wire. 202 days in SS.** (Received 5/25/93)
93-10	447	Service wire. 91 days in SS.** (Received 5/25/93)
92-115	448	Service wire. 195 days in SS.** (Received 5/25/93)

* Time in storage (including shipping) for all of the samples based on date of initial bend test (4/16/93).
** Exposure time counted through 6/7/93.

Table 5-2. Bend Test Specimens, Conditions, and Test Results

SwRI ID No.	Test Date	Exposure Conditions	Test Results			
			Fracture	Displacement		Load vs. Angle
				x (in.)	$\theta^{\Delta\circ}$	Figure No.
DUMMY						
435-1	4/6/93	Shop Air & Lab Air Solid wire	No	>0.33	64	C-11
435-2	4/693	Shop Air & Lab Air Solid wire	No	>0.39	90	C-11
435-3	4/6/93	Shop Air & Lab Air/Cavity	No	>0.39	90°	C-12
436-1	4/6/93	Shop Air & Lab Air/Cavity	No	>0.39	90°	C-13
436-2	4/6/93	Shop Air & Lab Air/Solid wire	No	>0.39	90	C-13
TEFLON-LINED						
421	4/6/93	222 days in PTFE	Failed during* extraction	--	--	--
422-1	4/6/93	142 days in PTFE	Yes	0.153	28	C-1
423	4/6/93	103 days in PTFE	Failed during* extraction	--	--	--
429-1	4/6/93	6 days in PTFE 199 days in SS	Yes	0.201	37	C-10
STORED IN STAINLESS STEEL NEEDLE						
424-1	4/6/93	70 days in SS	No	> 0.39	90°	C-2
425-1	4/6/93	70 days in SS	No	> 0.39	90°	C-4
426-1	4/6/93	131 days in SS	Yes	> 0.39	90°	C-5
427-1	4/6/93	76 days in SS	No	> 0.39	90°	C-6
428-1	4/6/93	91 days in SS	No	> 0.39	90°	C-8
424-2	6/16/93	70d SS + 65d SS/H_2O	No	0.36	70°	C-2
425-2	6/16/93	70d SS + 65d SS/H_2O	No	0.36	68°	C-4
427-2	6/16/93	76d SS + 65d SS/H_2O	No	0.36	70°	C-6
428-2	6/16/93	71d SS + 65d SS/H_2O	No	0.36	70	C-8

* Sample was completely fractured when withdrawn from shipping cask. End containing iridium source pellets remained in cask.

Δ Angle of displacement of 90° indicates that wire was bent to extremity of test device (almost flat).

Table 5-2. Bend Test Specimens, Conditions, and Test Results (Continued)

SwRI ID No.	Test Date	Exposure Conditions	Test Results			
			Fracture	Displacement		Load vs. Angle
				x (in.)	$\theta^{\Delta\circ}$	Figure No.
STORED IN STAINLESS STEEL NEEDLE						
441	6/16/93	210 days in SS	Yes	0.37	35	C-14
441-2	6/16/93	108 days in moist air tested in lab air (solid)	No	0.36	70	C-14
442-1	6/18/93	193 days in SS	Yes	0.30	58	C-15
443-1	6/18/93	236 days in SS	No	0.36	70	C-15
444-1	6/18/93	164 days in SS	No	0.36	70	C-16
445-1	6/18/93	193 days in SS	No	0.36	≈70	C-16
446-1	6/18/93	212 days in SS	No	0.36	67	C-17
447	6/18/93	101 days in SS	Yes	0.32	35	C-17
448-1	6/18/93	205 days in SS	No	0.36	68	C-18
424-3	7/29/93	108 days in moist air	No	0.36	70	C-3
425-3	No Test	108 days in moist air	—	—	—	—
424-4	8/2/93	108 days in moist air reverse bend	No	0.36	70	C-3
427-3	7/29/93	108 days in moist air tested < 5°C	No	0.36	68	C-7
427-4	8/2/93	108 days in moist air tested in lab air	No	0.36	64	C-7
428-3	7/29/93	108 days in moist air tested <5°C	No	0.36	70	C-9
428-4	8/2/93	108 days in moist air tested in lab air	No	0.36	70	C-9

5.1.2 Test Fixture

To simulate a worst-case bending scenario of the wire near the source tip, a bend test fixture, shown schematically in Figure 5-2, was designed and constructed by SwRI. It consisted of an aluminum support block, which in addition to serving as a mounting base for the actuator assembly and the displacement measuring system, also incorporated the wire clamping assembly.

The clamping system consisted of three major components: a reaction-block, a jack-screw activated clamping block, and a contoured disk-die, as shown in the exploded view in Figure 5-3. An aperature, slightly larger than the diameter of the test wire was machined into the support block and the clamping block, centered on the interface between the two. The clamping assembly was made self-opening using two sets of properly sized and assembled disk-spring stacks sandwiched between the support and the clamping blocks.

The test wire was inserted into the aperature through the orifice of the die, until bottoming was obtained. Bottoming the specimen in the aperature assures that the radius of the die is always located at 0.512-inch (13 mm) from the tip of the specimen. This dimension was selected to locate the maximum bending train at the bottom of the source cavity in the test specimens. The specimen was secured by activating the clamping block using the reaction-block mounted jack-screw. The elastomer insert in the clamping block assures positive clamping of the specimen without damaging its surface.

A gear-motor driven actuator assembly, shown in Figures 5-2 and 5-4, was used to apply the necessary bending loads to the test cavity. By transversing the actuator assembly, the specimen was bent as the slotted wheel rolled over the wire; see Figure 5-5. Travel of the actuator system was controlled to obtain a predetermined displacement that generated a fixed angle of deflection.

Displacement measurements were obtained using a laster/photo-diode measuring system attached to the support block, as shown in Figure 5-2. The "flag" affixed to the load transducer provided the means of determining the real-time position of the actuator system.

Real-time output voltages from the displacement measuring system and the load transducer were recorded using a NICOLET Model 4094 digital data acquisition system. For redundancy these signals were also recorded on an analog strip-chart recorder, shown in Figure 5-6. The recorder voltages were converted to load, displacement, and angular deflection using the appropriate calibration curves shown in Figures 5-7. Zero displacement or angular deflection for each test was defined as the position coincident with the initial indication of measurable load. Temperature profile curves for the tests below 10°C are shown in Figure 5-8.

A correlation was made of the displacement of the slotted wheel to the angle of deflection. The deflection of the wire at a given displacement was photographed, as shown in Figure 5-9. Various displacement measurements were selected, then the angle of deflection measured. Figure 5-10 shows a plot of the displacement versus angle of deflection.

5.2 Dummy Wires

A finite element analysis, discussed in Appendix A, determined the maximum strain and stress on the wire in bending. It was determined that a deflection of 70° would produce about 10% strain at the bottom of the cavity.

Two unradioactive "dummy wires," Sample Nos. 435 and 436, were bend tested to establish the baseline or control for the environmental bend tests. Table 5-2 shows the results. The "dummy wires" were identical to a production wire except the cavity was filled with two nonradioactive iridium pellets. Each wire was inserted into the bend test fixture, then deflected nearly 90°. The wire deflection was not completely 90° due to a restriction by the radius of the dye. SwRI Sample No. 435 was deflected three times. The solid end, without a cavity, was deflected twice (SwRI Wire No. 435-1 and Wire No. 435-2). The end with the cavity, SwRI Wire No. 435-1, was also deflected about 90°. SwRI Wire No. 436 had the solid end tested, SwRI Wire No. 436-2, and the cavity end tested, SwRI Wire No. 435-1. No failure occurred on either end of the wire. Figure 5-11 shows an example of the bend test plots. The plot shows the load dropping at about 65° deflection. This is when the slotted wheel started to roll over the wire. The wire was not broken as indicated by the recovery of the wire demonstrated by the curve with the lower load. The OD surfaces of the wire had evidence of blemishes or transverse marks, shown in Figure 5-12. But these did not result in failure. Some of these may have been from the grinding operation used to remove the oxide. Figure 5-13 shows a cross section through a deflected wire, SwRI Wire No. 435-3, yielded plastically, but had no failure.

5.3 Sourcewires Stored in Teflon

In order to evaluate the effects of teflon exposure, bend tests were performed on post-service sourcewires that were received in two conditions. Four sourcewire samples, Nos. 421, 422, 423 and 429 were received at SwRI. The sourcewires were lined with teflon at some time during the life of the wire. Sample Nos. 421, 422, and 423 were in-service, then removed from service, then stored with a teflon liner in a stainless steel tube in a lead cask. The time exposed to teflon varied from 103 days exposure to as much as 222 days. For the other sample condition, Sample No. 429, the radioactive sourcewire was shipped in teflon, then used in service, then removed from usage, then stored in stainless steel needle in a lead cask. This wire was not stored with teflon. Both as-received conditions had no moisture added to them before removal. Any moisture present was naturally picked-up from the air. Table 5-2 shows the test results for these samples.

Two of the four wires, SwRI Wire Nos. 421 and 423, were noticed to be severed after extracting the wire from the lead storage cask. Figures 5-14 and 5-15 show the appearance of each severed wire. The fracture appearance of Wire Nos. 421 and 423 were not identical to the clinical failures. However, several common features were noted; the teflon was deteriorated, residual teflon was found on the fracture surface, and the fractures were brittle in nature. Sample No. 421 failed in the solid wire, while Wire No. 423 failed adjacent to the cavity bottom.

The other two wires, SwRI Nos. 422 and 429 were still intact when extracted from the cask. During bend testing of these wires, in accordance with Section 5.1.2., SwRI Wire No. 422 failed at 28° of deflection and SwRI Wire No. 429 failed at 37° of deflection. Figure 5-16 shows the bend test results plotted. The plots indeed indicate a drop in load when the wire broke. The angle of deflection at failure was significantly less than the control samples shown in Figure 5-11.

Figures 5-17 and 5-18 show the fractures had a flat zone, flattened dimple features on the fracture, and no material thinning. These are all indicative of a brittle failure. The fracture appearance of SwRI Wire Nos. 422 and 429 also had features similar to the clinical failures. Detailed fractographic evaluation of the wires is discussed in Appendix B.

5.4 Sourcewires Stored in Stainless Steel Needles

Wires stored in stainless steel needles without teflon were received at SwRI in two conditions. In one condition the wires had been in-service and had completed clinical usage. The wires were individually shipped and stored in a stainless steel needle in a lead cask. Specimens in this condition included SwRI Nos. 424, 425, 427, 428, 441, 442, 443, 444, 446, 447, and 448.

In the other condition, the as-received wires were never used in a clinical application. The wires were production sourcewires forwarded to SwRI for testing purposes. Samples in this condition included SwRI Nos. 426 and 428.

Some of the Nitinol wires stored in the stainless steel needles were bend tested as much as four times. Table 5-2 shows the test results. All the wires were pre-tested in lab air to determine if the wire was embrittled or in a defective condition. After exposing a number of wires to moisture for either 65 or 108 days, the wires were bend tested at room temperature. These moisture tests were conducted to evaluate if moisture combined with radiation could cause embrittlement of the wire. In the other test condition, where the wires were exposed to moisture, the Nitinol wire was tested below 50°F (10°C). This temperature was selected because at 15°C (59°F) ± 5°C, Nitinol wire transforms to martensite as part of the shape memory capabilities of the wire. The wire was bend tested in this martensitic condition to determine if the Nitinol wire would fail in a brittle manner.

5.4.1 Pre-Test Results

None of the wires that were pre-tested failed due to embrittlement or a material defect. Wire Nos. 426, 441, 442, and 447 inadvertently failed because of an abnormal test condition. SwRI Wire No. 426 failed because it was overloaded beyond the acceptable strength of the material. Figure 5-19 shows the macroscopic features indicating that the wire yielded and the wall thinned. This type of fracture was unlike the clinical service failures. During these preliminary tests, some of the other wires were deflected nearly 90°. Later it was determined, based on the surface appearance of the wires and the failure of SwRI Wire No. 426, that 90° may have been too severe and actually may have taken the wire to an overload condition. The purpose of the bend test was to evaluate embrittlement conditions and not the maximum bending load to

cause failure. In subsequent tests, the maximum deflection of the wire was reduced to 0.36 inch which was about 70°. Based on the stress and strain calculations detailed in Appendix A, a deflection of 70° is equivalent to a maximum strain of about 10%. A 10% strain exceeds the elastic limit at 8% strain, but does not approach strain to failure.

During the pre-test, Specimen Nos. 441, 442, and 447 broke. It later became evident that the wires were not completely bottomed out when inserted into the test fixture. There was a groove in the aperature that prevented the wire from going down. As a result, the wires were loaded in an abnormal way. Failure occurred at the midway portion of the cavity. This was verified on Specimen No. 441, which actually had the pellets fall out and Specimen No. 447, which was broken 9.5 mm from the tip. The fracture surfaces of SwRI Nos. 441 and 447 were not examined because both ends were too radioactive. Figure 5-20 shows failed SwRI Wire No. 442. Appendix B has a more detailed evaluation of SwRI No. 442. Sample Nos. 443, 444, 445, 446, and 448 were bend tested with no failure, then stored in moisture as backup. These specimens were never retested.

5.4.2 Moisture and Room Temperature Test

After the pre-test, Sample Nos. 424, 425, 427, and 428 were enclosed in moisture, as described in Section 5.4.1. The samples remained in the moisture for 65 days, then were tested. The purpose of the 65-day test was to determine if any of the wires had microcracks from the apparently extreme 90° bend that may result in failure. All the samples were bend tested to 0.36 inch displacement or 70°. No failures occurred. See the bend test results in Appendix C.

Post-service and unused radioactive wires were exposed to a moist air environment for at least 100 days. The moist air was obtained by bubbling air through water in a flask; the moistened air then circulated through an enclosed chamber, shown in Figure 5-21(a). The chamber surrounded the lead casks, which contained the sourcewires stored in the stainless steel needles. Adequate space was provided for the moistened air to circulate through the chamber and above the sourcewires. The radioactive wire was inserted in a lead cask that had a stainless steel tube filled with 0.5 cc of water. This quantity of water provided moisture in the tube but prevented submersion of the wire. When the wire was inserted in the stainless steel tube, the wire did not submerge in the water. The wire was held in place with an inverted clamp from the stainless steel needle, see Figure 5-21(b). Since the cut off sourcewires did not go deep into the cask, the environment chamber was surrounded with 2-inch thick lead to reduce radiation leakage. The test samples were kept at least 100 days under moisture to simulate a three-month service exposure at a clinic.

The room temperature, 108-day moisture test was to be conducted on Sample Nos. 424 and 425. However, Sample No. 425 sheared off in the cask; the Nitinol wire and the iridium pellet were both sheared. The wire sample was too radioactive to examine with the SEM, however, three observations indicate that the cask and wire had been inadvertently hit. The tape that secured the lead shielding had been torn, both halves of the fracture were extremely radioactive, and visual examination at about 20X revealed a portion of a pellet was in the cavity. The end removed form the cask was at least 1.8 r/hr. at 18 inches. This indicates part of a pellet had been lodged in the cavity. Visual examination at about 20X revealed a portion of a pellet was indeed in the cavity.

As a result of Sample No. 425 not being available, Sample No. 424 was tested and Sample Nos. 427 and 428 were retested at room temperature. All three samples were tested to a displacement of 0.36 inches and a deflection of 70°. Again, none of the samples failed. Sample No. 424 was bend tested two times. Figure 5-22 shows a slight load drop occurred at 16° deflection. To confirm that the wire was not cracked, the sample was rotated 180° then retested. No failure occurred, indicating that moisture alone had no detrimental effect on the Nitinol wire.

5.4.3 Moisture and Below 10°C Test

In order to maintain the wire below 50°F (10°C), the bend test fixture was chilled with dry ice and the wire was pre-chilled with dry ice. The temperature of dry ice is -78°F (-61°C). Because the base of the test fixture was aluminum, which has excellent thermal conductivity, the test fixture was easily maintained below 50°F (10°C). The bend test fixture acted as a heat-sink to keep the wire chilled. Thermocouples on the top surface of the base plate, the location where the wire bends, measured 32°F (0°C). Figure 5-8 shows the actual temperature profiles obtained on the bend test fixture chilled with dry ice. The temperature was monitored during the bend test. Because of the high humidity in the lab, the test fixture was enclosed with plastic, then purged with argon. This kept the fixture from condensing moisture, then freezing. Before the wire was bend tested, it was inserted into a lead base chilled with dry ice. This wire was pre-chilled 5 minutes to assure that the wire was below 50°C (10°C). The wire was manually transported to the chilled bend test fixture before the test was started. The time from the pre-chilled condition to the start of the test was 33 to 35 seconds. The actual bend test lasted from 50 to 60 seconds.

After 108 days exposure to moisture, Sample Nos. 427 and 428 were extracted from the lead casks and tested at temperatures below the transformation temperature in accordance with the description in Section 5.4.1. Figure 5-23 shows that both the wires deflected 70° with no failure.

5.5 Hydrogen Charged Specimens

In view of the results of the bend tests on actual sourcewires (Sections 5.3 and 5.4) and the results of the preliminary hydrofluoric acid exposure and preliminary hydrogen-charged tests (Sections 3.0), a series of controlled bend tests was performed on solid wire specimens that had been electrolytically charged with hydrogen. The overall objective of these tests was to demonstrate the hydrogen embrittlement susceptibility of the Nitinol wire, and compare the fractographic features of the hydrogen-charged specimens with those of the in-service failures and the actual sourcewires that failed in the controlled bend tests.

The bend test procedures were the same as those used for the tests on actual sourcewires (see Section 5.1), and the specimens were electrolytically charged in a 0.5% acetic acid solution in the same manner as the preliminary tests (see Section 3.4.1). In this case, the charging potential and charging time were varied to establish optimum test conditions. Bend tests were also performed with controlled delays after the completion of charging and after a 2-hr. post-charging bake-out at 450°F.

5.5.1 Optimization Tests

The results of the tests performed to establish the optimum test conditions are listed in Table 5-3 as Test Nos. HC-1 through HC-9 and presented graphically in Figures 5-24 and 5-25. Load/deflection curves for all of the tests are presented in Appendix E.

Initially, three tests were performed with a charging potential of -0.5v and a charging time of 120 minutes (Nos. HC-1, HC-2, and HC-3). None of the three specimens failed, indicating that the charging conditions were not adequate for significant embrittlement. A representative load/deflection curve from this group is shown in Figure 5-24(a). A second set was then tested after charging for 120 minutes at a potential of -1.0v (Nos. HC-4, HC-5, and HC-6). The results of these tests are included in Table 5-3 and presented graphically in Figure 5-24(b). Two of these three tests resulted in brittle fracture at bend angles of 28° and 34°. The low bend angle at fracture clearly demonstrates the embrittling effect of the charging conditions.*

The third set of three tests maintained the charging potential of -1.0 volt, but employed successively shorter charging times of 100, 80, and 60 minutes. These results are included in Table 5-3 as Nos. HC-7, HC-8, and HC-9. Test No. HC-7 resulted in brittle fracture at a low bend angle, see Figure 5-25(a). Tests No. HC-8 and No. HC-9 both survived the full bend angle without fracture, [Figure 5-25(b)].**

The results of the entire group of optimization tests established that charging conditions of -1.0 volt and 120 minutes consistently embrittled the Nitinol wires to a substantial degree and that reduction of the charging time to 80 minutes or less sharply reduced the embrittling effect. On the basis of these results, a charging potential of -1.0v and a charging time of 120 minutes were selected as the standard charging procedure for all subsequent tests.

5.5.2 Test Matrix

Fourteen tests were performed on hydrogen-charged specimens to provide for triplicate tests at any one set of test conditions and to investigate the tendency for recovery of original properties after delay at room temperature and after a bake-out procedure. These test results are presented in Table 5-4 as Tests Nos. HC-12 through HC-23, and representative load/deflection curves are shown in Figures 5-26 and 5-27. The first three of these (HC-12, HC-13, and HC-14) constituted repeat tests for the particular charging conditions chosen (-1.0v, 120 min.). All three of these resulted in brittle fracture at low angles of deflection (19°-26°); see Figure 5-26(a).

---

* Test No. HC-5 did not result in a fracture even after bending to the limit of the test device (≈ 90°). However, subsequent SEM examinations revealed subcritical cracks and this anomalous test result is attributed to inadvertent variation in the charging procedure for this particular specimen, see Appendix D.

** SEM examination of the specimen from Test No. HC-8 revealed subcritical cracking on the tension side of the bend and a subsequent bend test in the opposite direction resulted in brittle fracture at a low angle of deflection. These factors are discussed in Appendix D.

Six other tests in this group (HC-15 through HC-20) were performed with planned delays of 16 hours and 52 hours after completion of the charging procedure. As may be noted in Table 5-4, all three specimens tested after a 16-hour delay failed at a low angle of deflection (24°-36°), see Figure 5-26(b). Those representing a 52-hour delay survived the full deflection angle without cracking or fracture; see Figure 5-27(a). Tests HC-21, HC-22, and HC-23 were performed after the charged specimens were baked out at 450°F for 2 hours. In all three cases, the full-bend angle (70°) was attained without cracking or fracture. A representative load/deflection curve for this group of three tests is shown in Figure 5-27(b). These results together with those from the test with a 52-hour delay demonstrate that the embrittlement process is reversible and of the same nature as the classic hydrogen embrittlement process involving the absorption of nacent hydrogen.

Table 5-3. Bend Test Results
Hydrogen-Charged Specimens

Test No.[3]	Charging Conditions		Bend Test		Notes
	Potential Volts	Time Min.	Displacement Degrees	Fracture	
HC-1	-0.5	120	≈ 90	No	--
HC-2	-0.5	120	≈ 90	No	--
HC-3	-0.5	120	≈ 90	No	--
HC-4	-1.0	120	31	Yes	--
HC-5	-1.0	120	≈ 90	No	(1)
HC-6	-1.0	120	26	Yes	--
HC-7	-1.0	100	29	Yes	--
HC-8	-1.0	80	≈ 90	No	(1)
HC-9	-1.0	60	≈ 90	No	--
HC-5R	---	---	14.0	Yes	(2)
HC-8R	---	---	15.0	Yes	(2)

(1) Subcritical cracks were observed in post-test SEM examinations. See Appendix D.

(2) Retest of specimens from HC-5 and HC-8. Specimen bent in opposite direction from first test. See Appendix D.

(3) All specimens for this series of tests were taken from Wire No. 424.

Table 5-4. Bend Test Results
Hydrogen-Charged Specimens

Test No[6]	Charging Conditions		Bend Test		Notes
	Potential Volts	Time Min.	Displacement Degrees	Fracture	
HC-12	-1.0	120	26	Yes	(1)
HC-13			25	Yes	
HC-14			19	Yes	
HC-15	-1.0	120	36	Yes	(2)
HC-16			28	Yes	
HC-17			24	Yes	
HC-18	-1.0	120	68	No	(3)
HC-19			68	No	
HC-20			68	No	
HC-21	-1.0	120	68	No	(4)
HC-22			68	No	
HC-23			68	No	
HC-10	-1.0	120	17.0	Yes	(5)
HC-11			17.0	Yes	

(1) Specimens tested immediately after charging.
(2) Specimens tested 16 hours after completion of charging.
(3) Specimens tested 52 hours after completion of charging.
(4) Specimens tested after 2-hr. bake-out at 450°F.
(5) Test Nos. HC-10 and HC-11 were performed on dummy sourcewires fabricated from tubing.
(6) All specimens for this series of tests (except HC-10 and HC-11) were taken from Wire No. 426.

Two additional hydrogen-charged bend tests were performed on specialized specimens fabricated to simulate actual sourcewires. These specimens were fabricated from 0.023 in. x 0.004 wall Nitinol tubing. A 1 1/4-inch long section of this tubing formed the principal component of the specimen. A stainless steel filler wire was then cemented into the tubing in a manner to leave a 13 mm long cavity at one end. Two inactive production iridium pellets were then inserted into the cavity and the end was sealed with a stainless steel plug and epoxy. The resulting specimens were then hydrogen charged by the standard procedure and tested in the bend test fixture. The results of these two tests are listed in Table 5-4 as Tests Nos. HC-10 and HC-11. Both tests resulted in brittle fracture at a bend angle of 17°.

5.5.3 Fractographic Examinations

Selected specimens from the series of hydrogen-charged bend tests were examined in the SEM to identify the fractographic features of fractured specimens and to determine the surface condition and presence or absence of subcritical cracks in those that survived the bend test. Representative SEM fractographs and photomicrographs are shown in Figures 5-28 and 5-29. Additional fractographic data are presented in Appendix D.

In each case where fracture occurred, the fracture was very brittle in nature with little or no evidence of deformation of the wire. Each fracture surface was very flat and oriented essentially normal to the axis of the wire, see Figure 5-28. Typically, a small slant fracture developed on the inside of the bend. The fracture surfaces were generally fine textured and some steps and river marks were evident on the side corresponding to the inside of the bend. Although there were no unique features to identify a specific fracture origin, the smooth features at the outside of the bend and the location and nature of the steps and river marks established that fracture progressed through the section from the outside of the bend (tension side) to the inside (compression side).

The fine-scale topography consisted of well-developed, generally equiaxed dimples characteristic of fracture by microvoid growth and coalescence, see Figure 5-29. Localized tear dimples also confirmed the direction of crack propagation as from the tension side to the compression side of the bend.

Another feature common to the fractures in the hydrogen-charged specimens was the presence of a distinct rim around the periphery of the fracture surfaces in which the fine-scale topography was essentially featureless [Figure 2-29(a)]. The nature of this rim suggests the presence of a very brittle layer at the outer surface.

It should be noted that these test fractures all represent cases where brittle fracture occurred by the microvoid growth and coalescence mechanism. This was also a characteristic feature of the two clinical failures.

The two simulated sourcewires (Test Nos. HC-10 and HC-11) exhibited essentially identical fractographic features. SEM photomicrographs and fractographs from one of these tests (HC-10) are shown in Figures 5-30 and 5-31. Figure 5-30 demonstrates that the fracture was very brittle in nature, the fracture surface was very flat and oriented normal to the wire axis and there was no evidence of deformation of the cavity wall or cross section.

The fine-scale topographic features are illustrated in Figure 5-31. Distinct dimpled features characteristic of microvoid growth and coalescence were evident completely around the fracture surface. A distinct rim with a nearly featureless topography, similar to that observed in the solid wires was also evident at the outer periphery of the fracture. In both of these cases, the orientation of tear dimples indicated a direction of fracture from the outer rim inward through the cavity wall [Figure 5-31(b)].

5.6 Summary of Bend Test Results for Sourcewires and Hydrogen Charged Specimens

Based on the bend test results for the dummy wires, the teflon-lined wires, the wires stored in a stainless steel needle, and the solid wires charged with hydrogen, the following conclusions are made:

1) The bend tests of the control samples determined that the Nitinol wire in the as-received condition was indeed very elastic and can endure high strains with no catastrophic failure.

2) The surface imperfections, nicks, scratches, and blemishes, probably produced from a grinding operation, did not result in failure at high strain rates.

3) The dummy wire test results indicate that for a Nitinol sourcewire to fail prematurely, a unique phenomenon would have to occur, i.e., environmental embrittlement or a material flaw.

4) Two Nitinol sourcewires exposed to teflon, then bend tested, failed prematurely in a brittle manner, indicating the wires were embrittled. The wires failed after only 28° of deflection. Similar microscopic features existed that were present on the clinical failures.

5) Two Nitinol wires exposed to teflon had failed prior to extraction from the lead storage cask. The macroscopic fracture features were indicative of a brittle failure, there was no evidence of wall thinning or yielding. Microscopic fracture features were either destroyed or covered up by residual by-products on the fracture surface.

6) Analytical modeling of the Nitinol sourcewire in a bending condition determined that a deflection of 70° would be about 10% strain which is above the elastic limit of 8% strain.

7) If the Nitinol wire fails because of excessive bending (greater than 8% strain), the wire has a permanent set, yielding occurs, and the cavity wall thins. These macrofeatures were not the same as the macrofeatures of the clinical wire failures.

8) One of the wires, SwRI No. 426, was inadvertently overloaded resulting in wall thinning. This failure mode was not similar to the service failures. The service failures did not have any indication of wall thinning or yielding.

9) The 108-day moisture exposure, followed by bend testing at room temperature and below 10°C, indicated that moisture alone did not cause failure of the wire.

10) Since the Nitinol wires did not fail during the low temperature test, the temperature of operation of the wire had no effect on the failure. The Nitinol wire should not be more susceptible to failure because of a shift in temperature.

11) The sourcewires stored in the teflon-lined condition consistently showed that the Nitinol wire was embrittled. The specimens either failed prior to extraction from the cask or at a low level of strain. The teflon liner was degraded, and residual by-products were found on the fracture surface. The macroscopic features on the bend test samples were indicative of a brittle failure. This was also evident on the service failures.

12) Electrolytic hydrogen charging of solid Nitinol wires resulted in marked embrittlement as evidenced by brittle fracture at low deflection angles.

13) The major portion of each fracture surface in the solid wires exhibited fine-scale dimples characteristic of fracture by microvoid growth and coalescence, and a thin outer rim with a nearly featureless topography.

14) Simulated sourcewire specimens also failed in a brittle fashion after hydrogen charging. The fine-scale topography consisted of a distinct dimples.

15) Delayed tests and tests after a bake-out procedure indicated that the hydrogen embrittlement process is completely reversible.

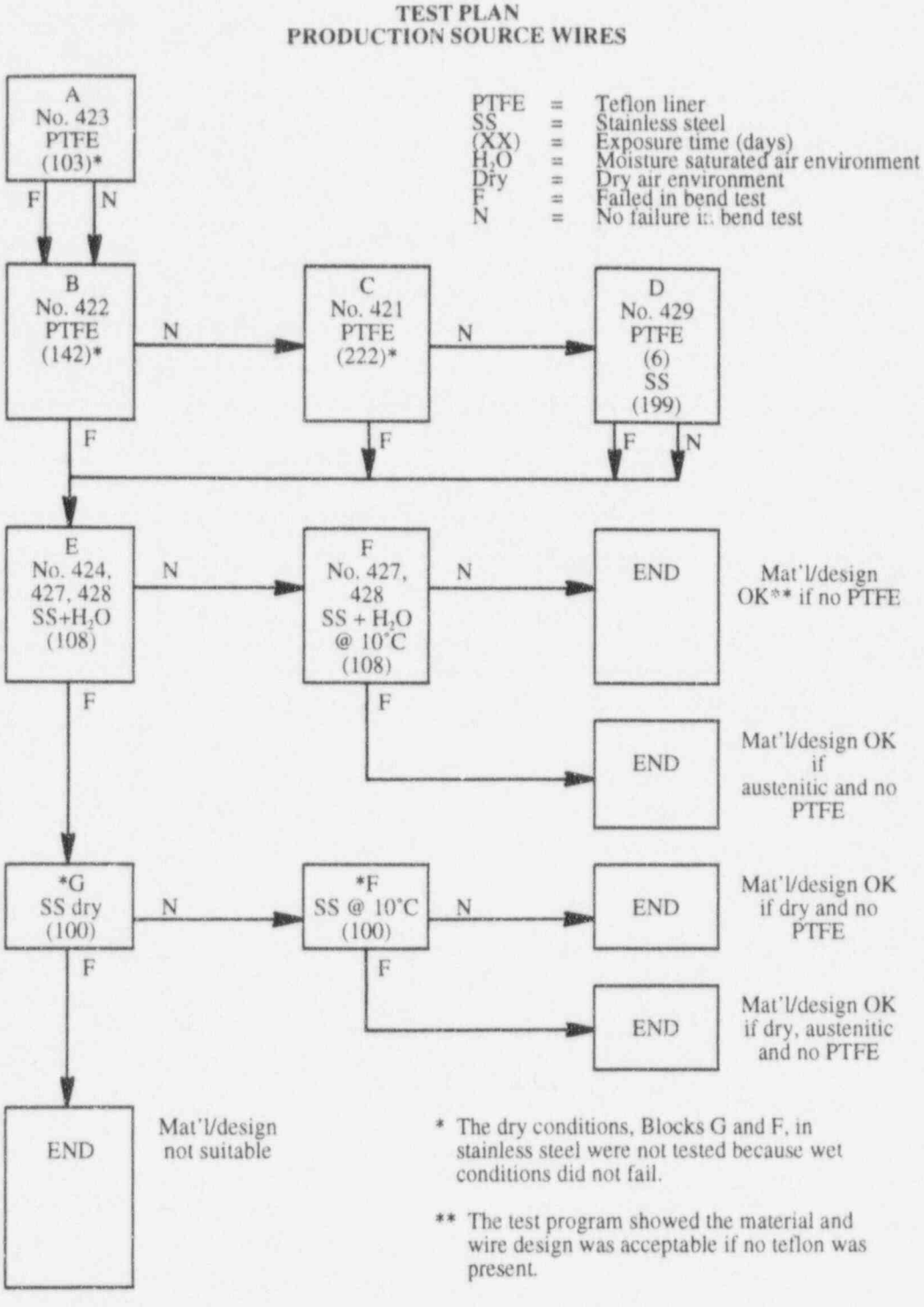

Figure 5-1. Production Source Wires

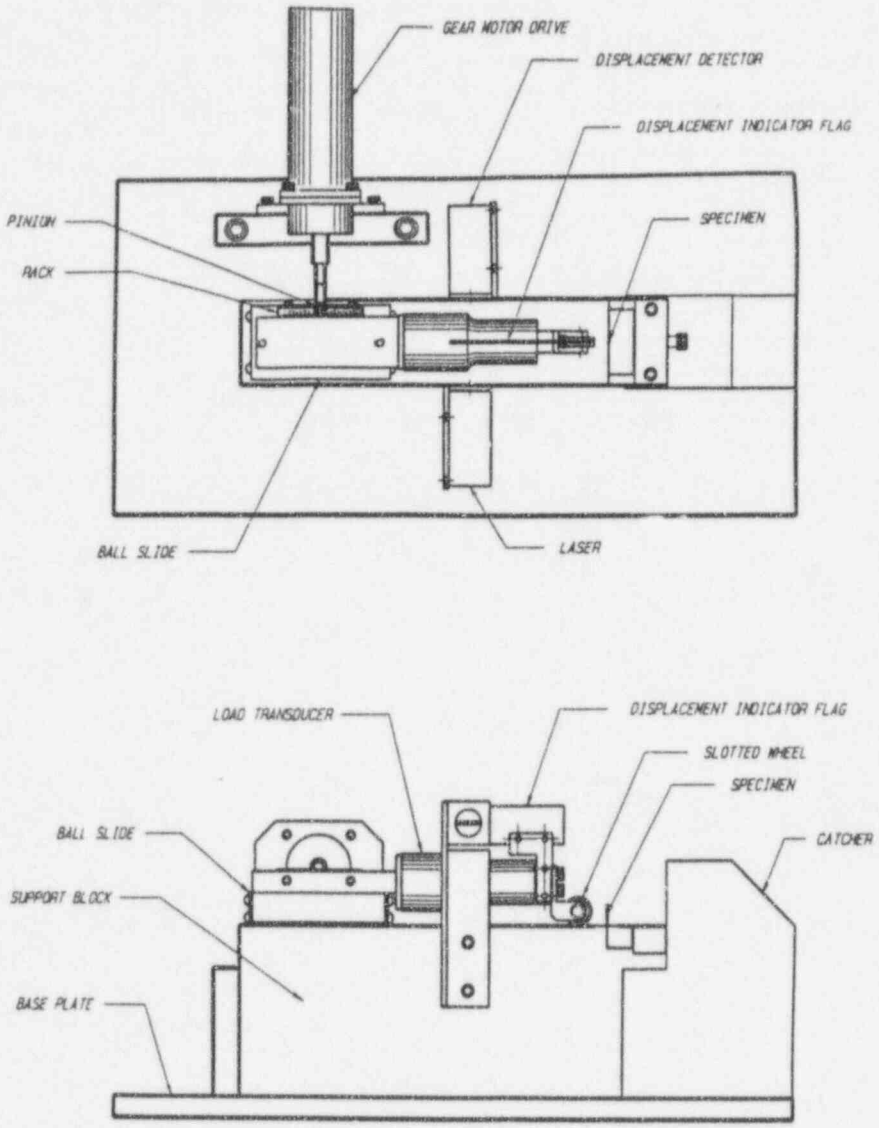

Figure 5-2. Schematic of the Bend Test Fixture

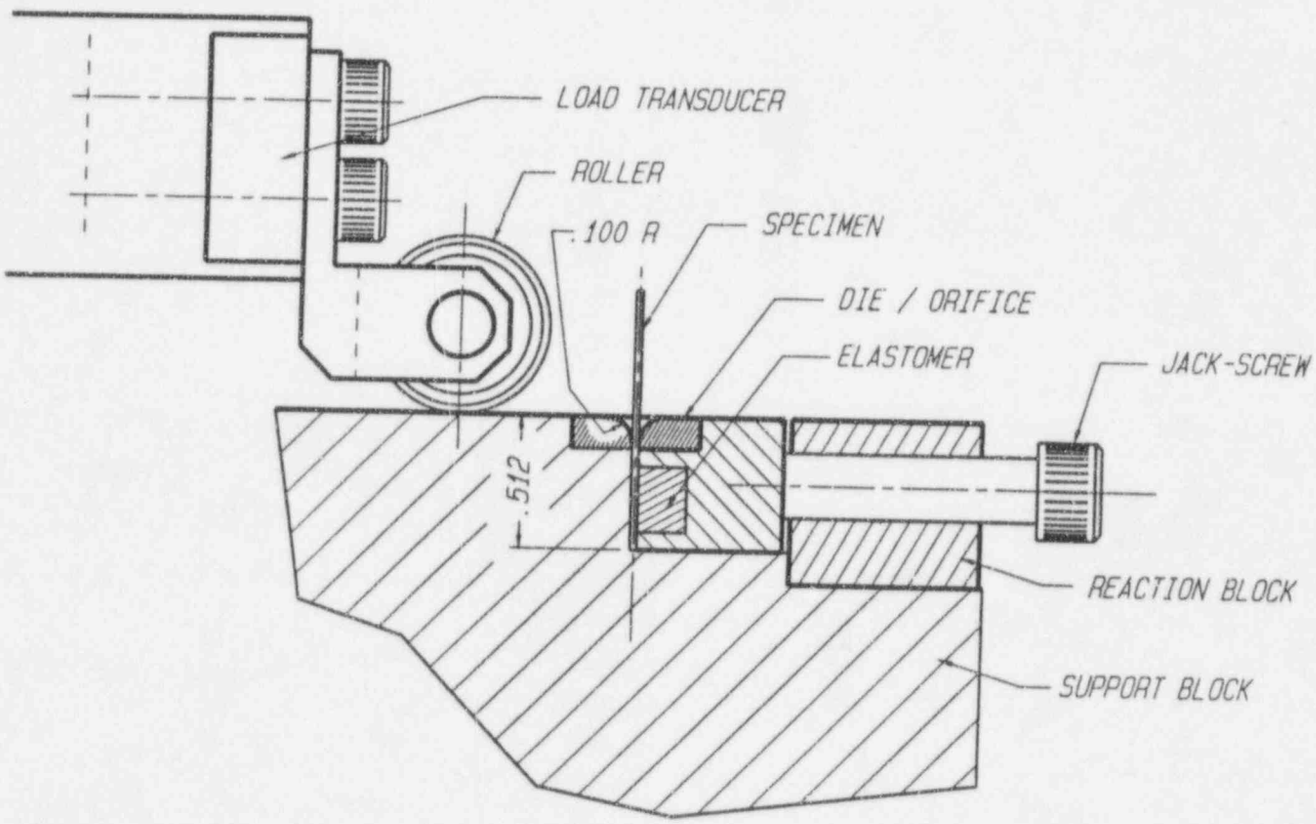

Figure 5-3. Exploded View of the Wire and Radius Die

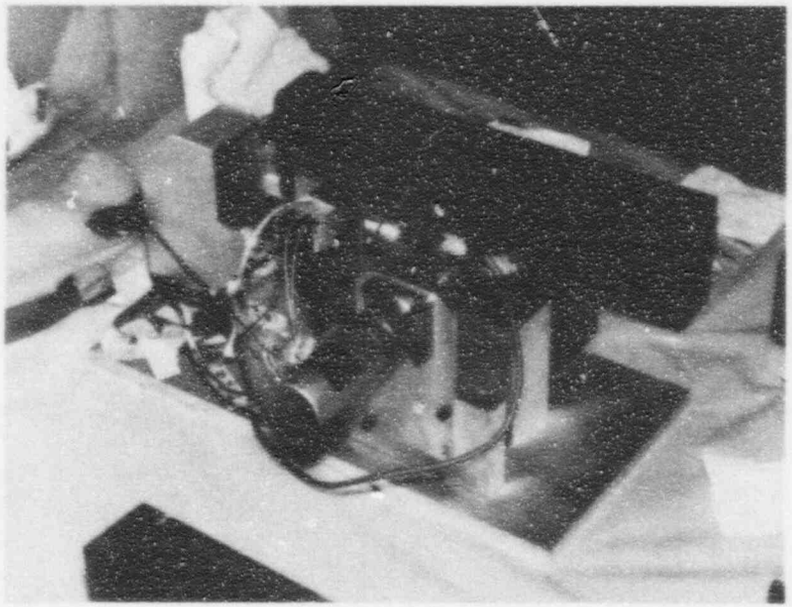

a) Front View

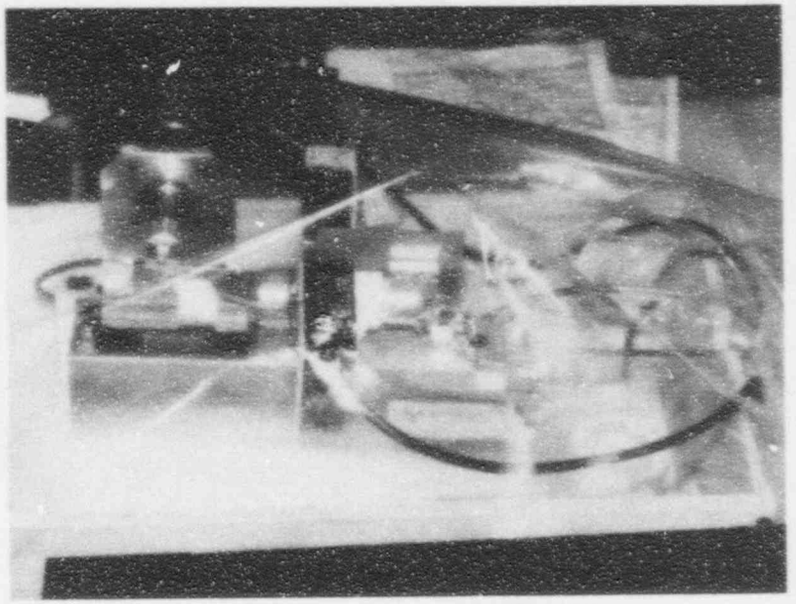

(c) Environment Chamber for Cold Test

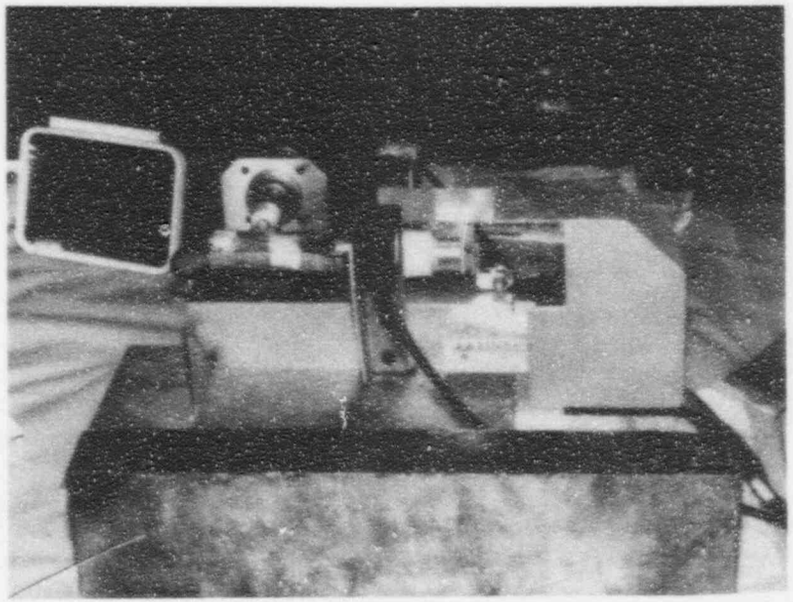

b) Back View

Figure 5-4. Photographs of the Bend Test Fixture

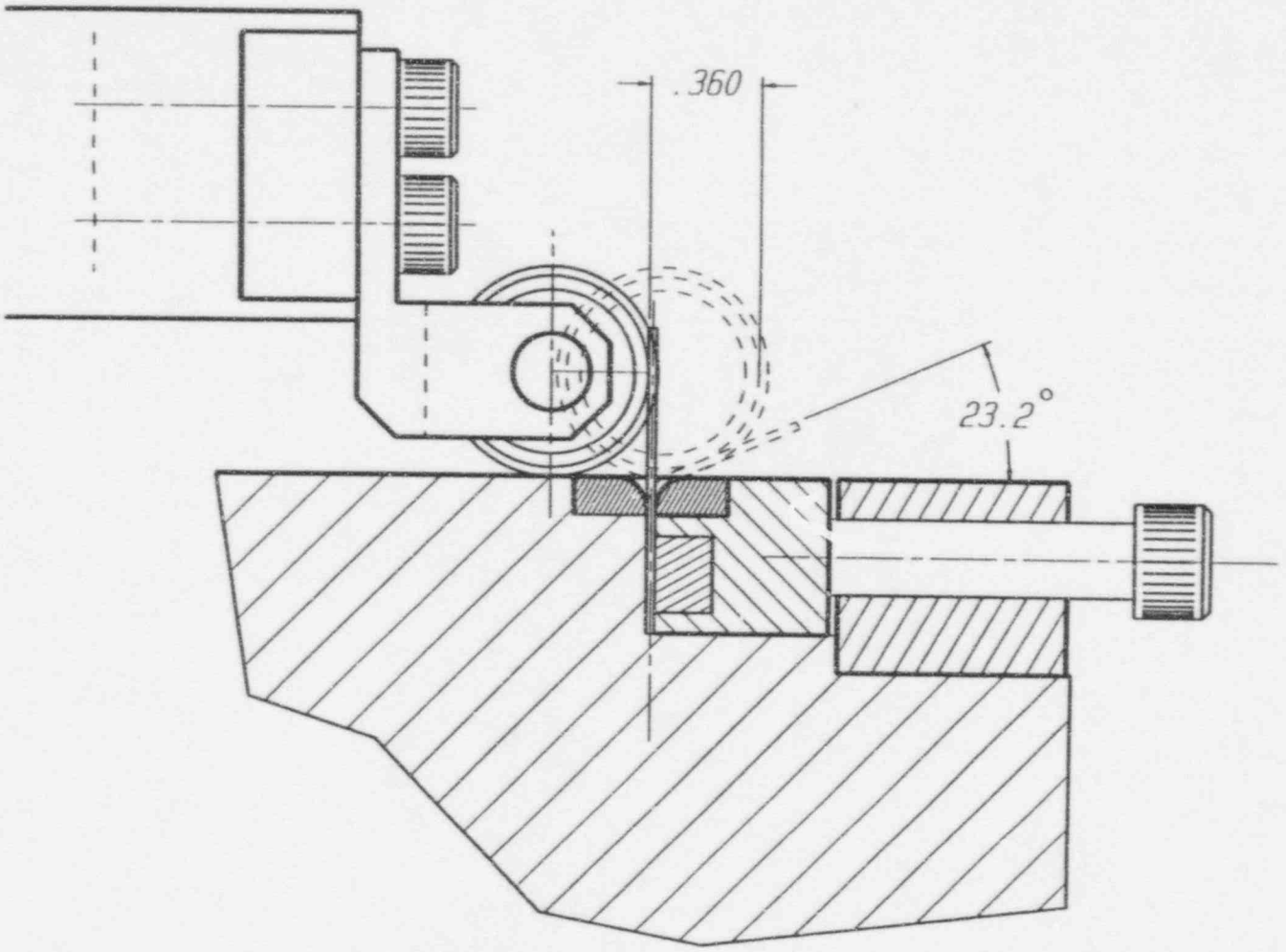

Figure 5-5. Schematic of the Wire Bending as When Deflected by the Wheel

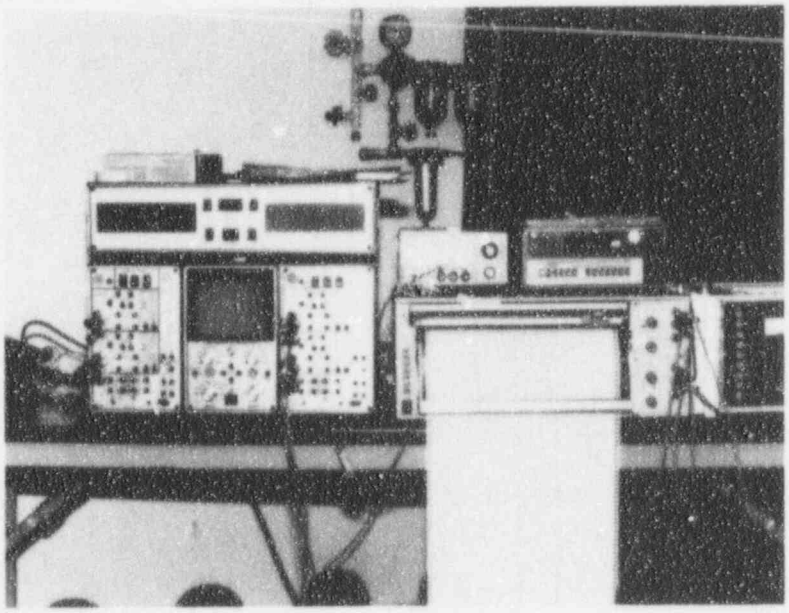

Figure 5-6. Photograph of the Support Electronic Equipment for the Bend Test

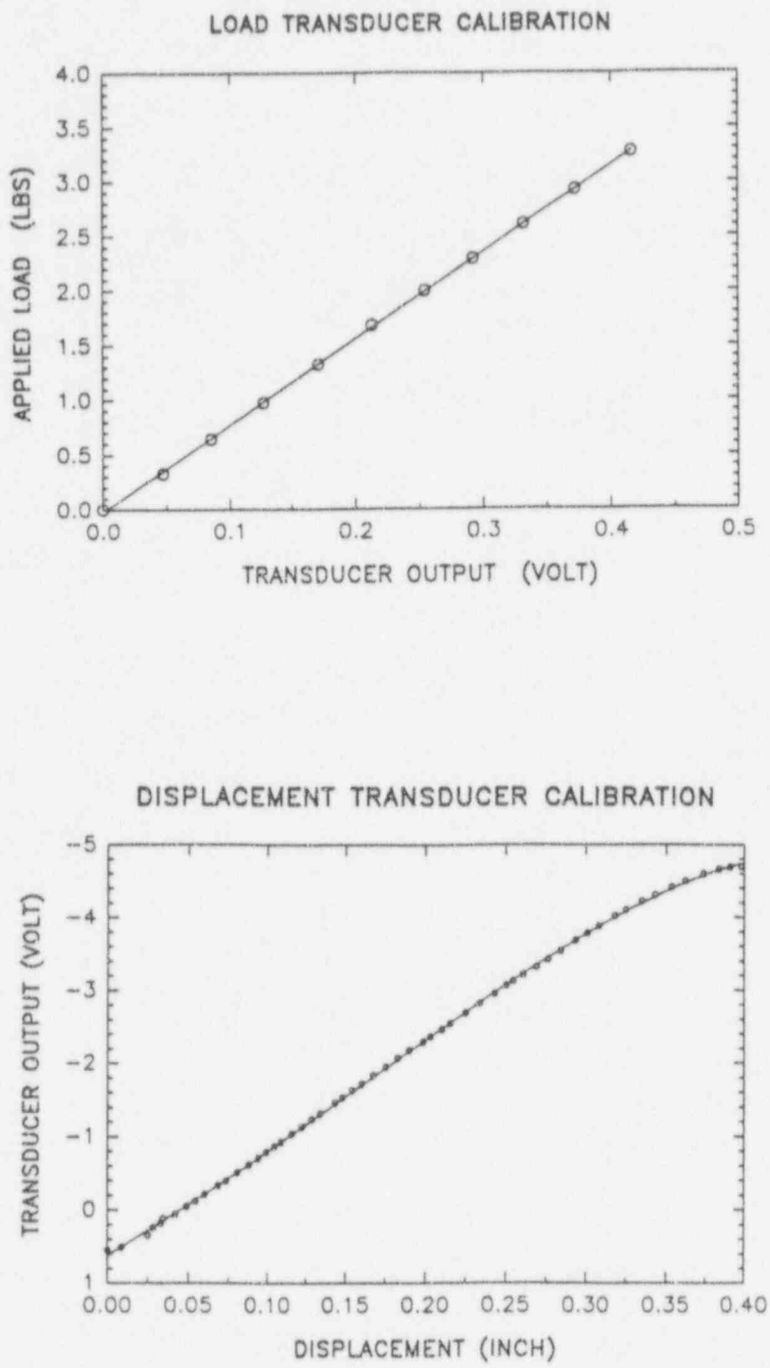

Figure 5-7. Plot of the Load and Displacement Calibration

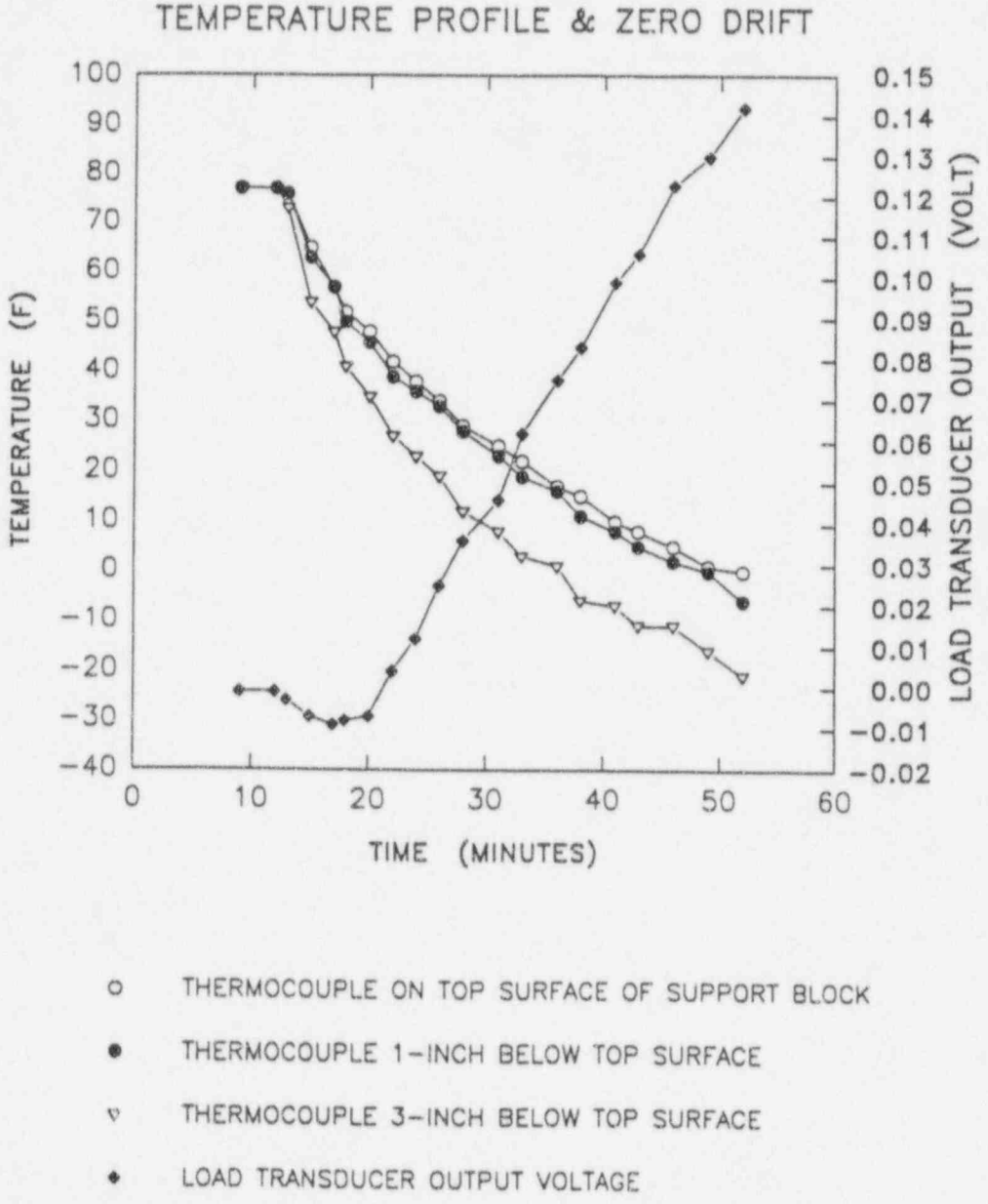

Figure 5-8. Plot of the Temperature Profile vs. Time Figure 5-8 for the Less than 10°C Test

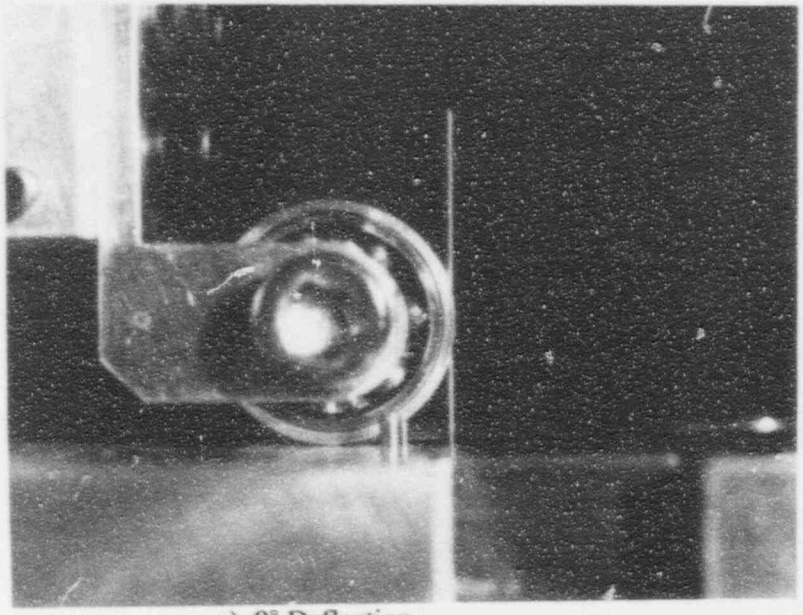

a) 0° Deflection

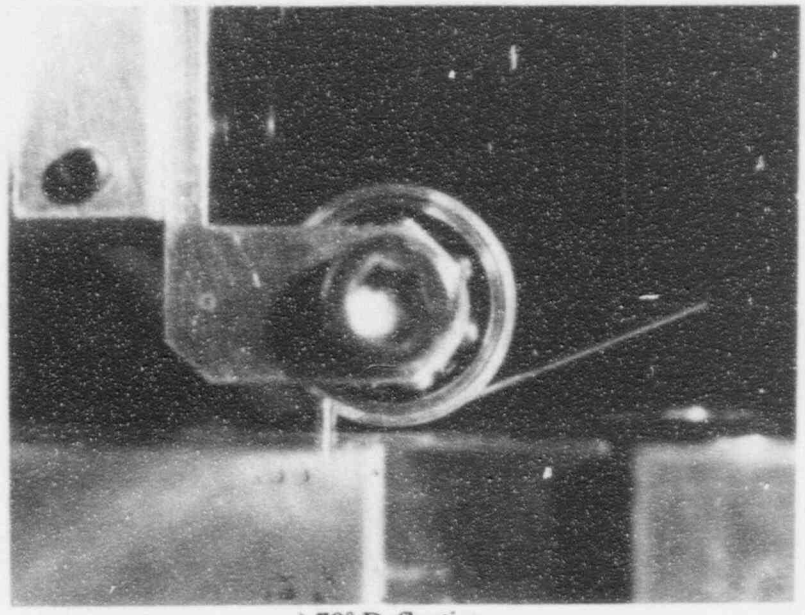

c) 70° Deflection

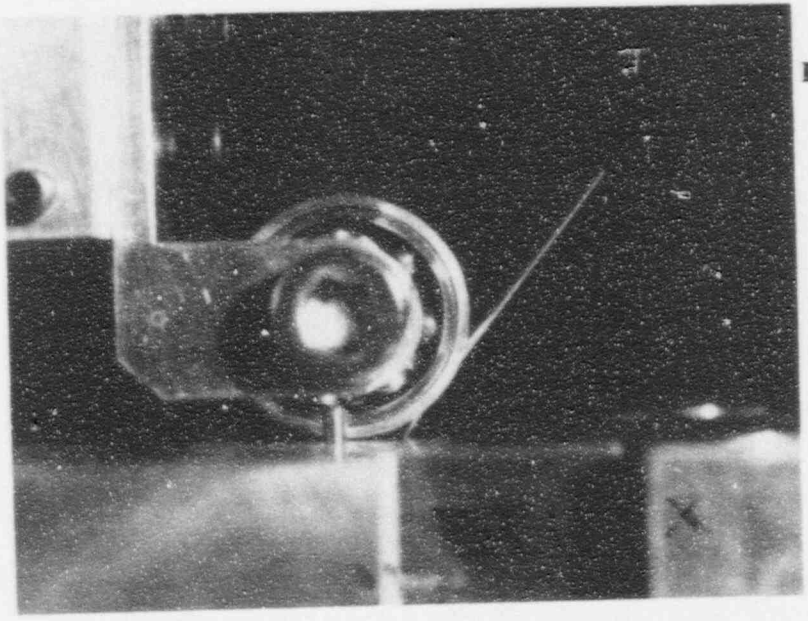

b) 38° Deflection

Figure 5-9. Photographs of the Wire Deflected During the Bend Test

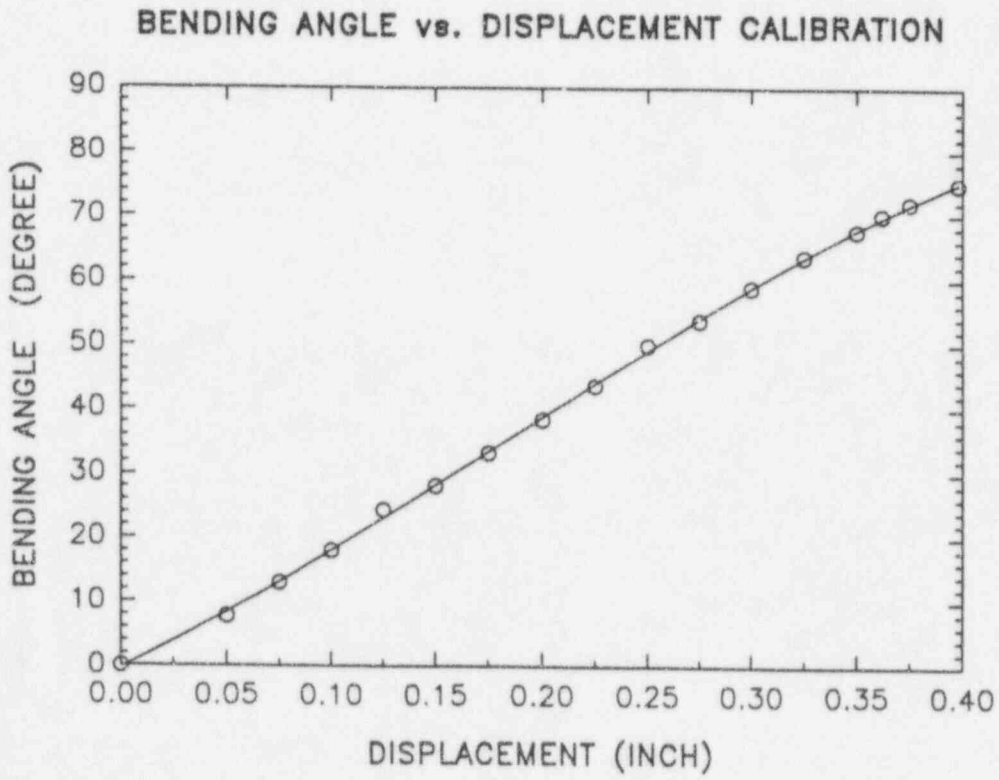

Figure 5-10. Displacement of the Wheel vs. the Angle of Deflection of the Wire

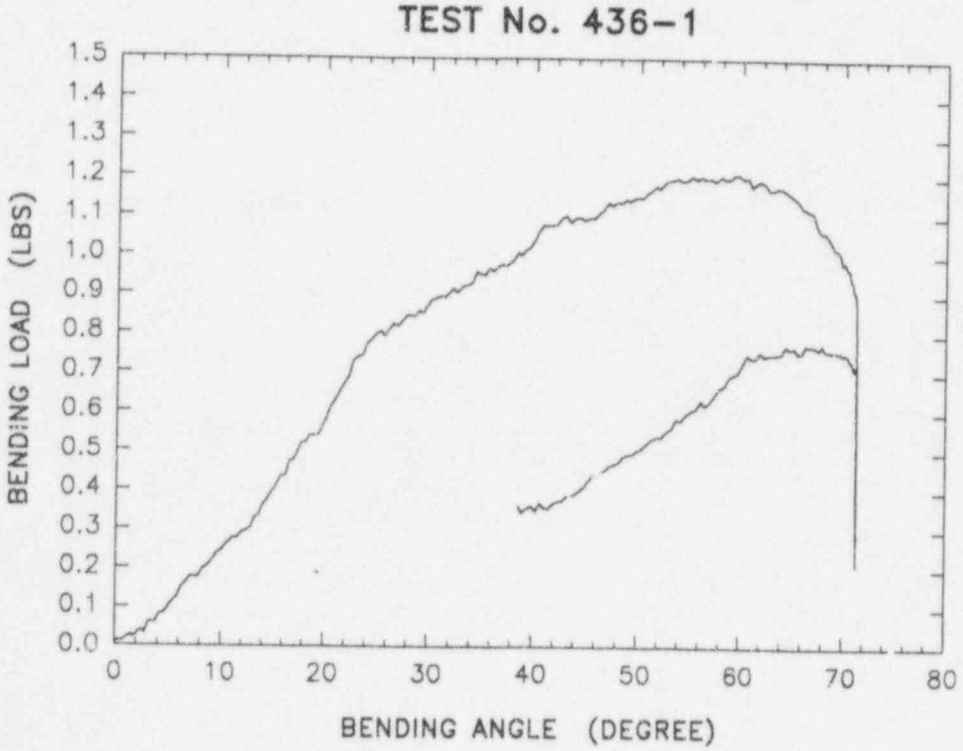

Figure 5-11. Bend Test Plot of Load vs. Angle of Deflection for SwRI Wire No. 436-1.

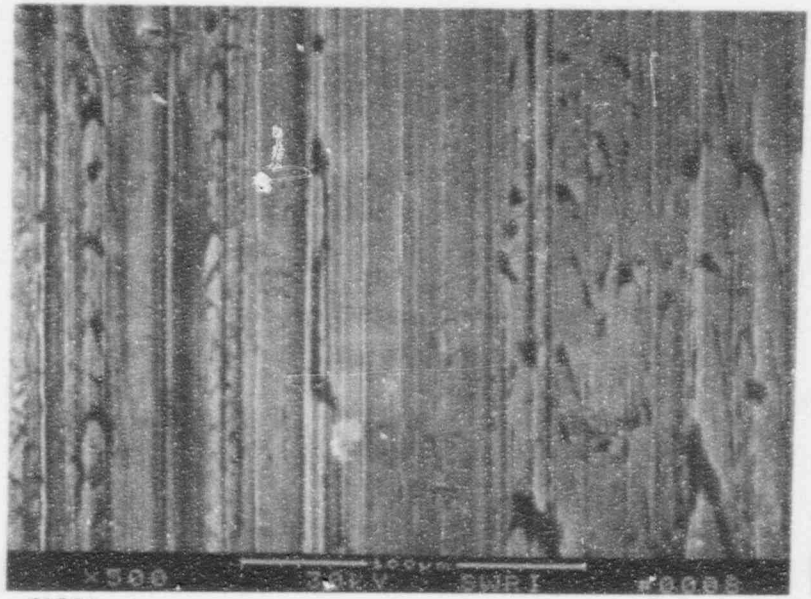

61921 500X

a) Inside Bend

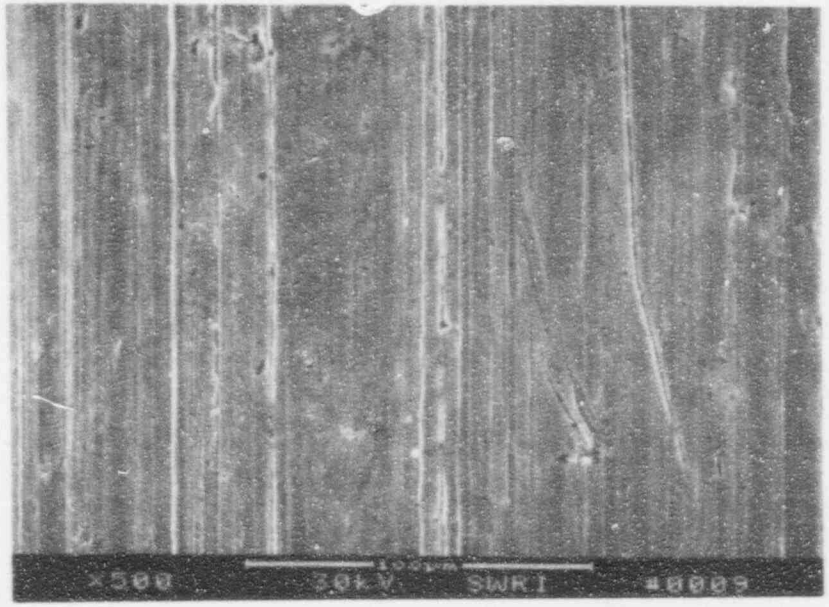

61923 500X

b) Outside Bend

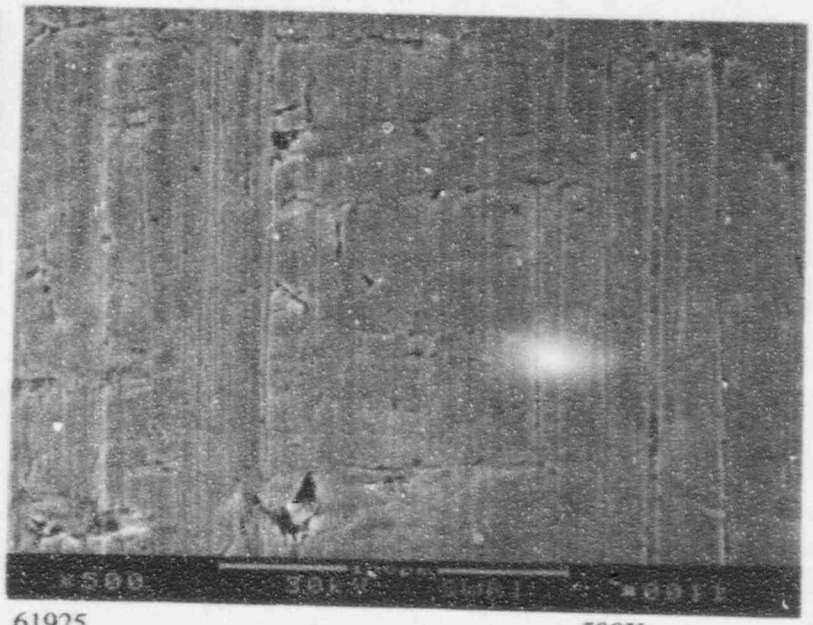

61925 500X

c) Remote from Bend

Figure 5-12. SEM Fractographs of the OD Surface for SwRI Wire No. 436-1.

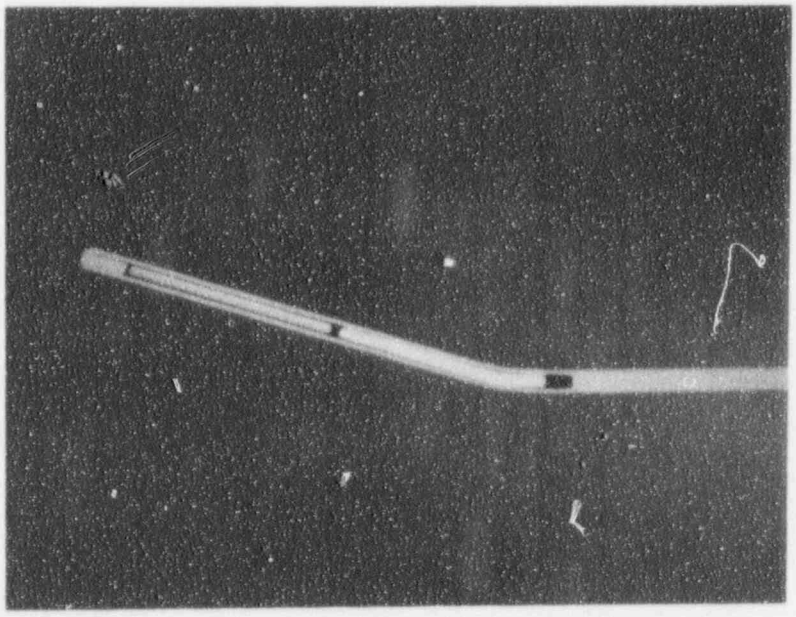

Figure 5-13. Photomacrograph of a Cross Section of SwRI Wire No. 435-3 that Had Plastic Deformation but No Failure

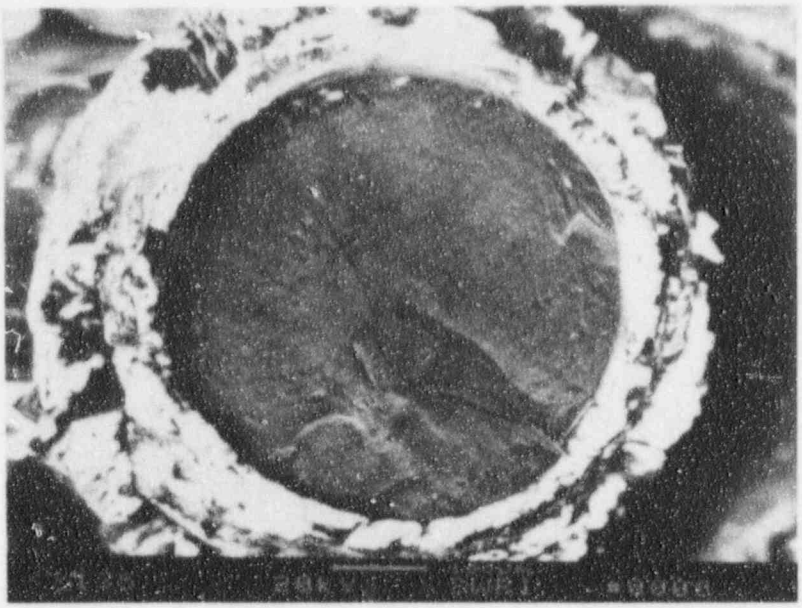

61943 135X

a) View Looking Down on Fracture

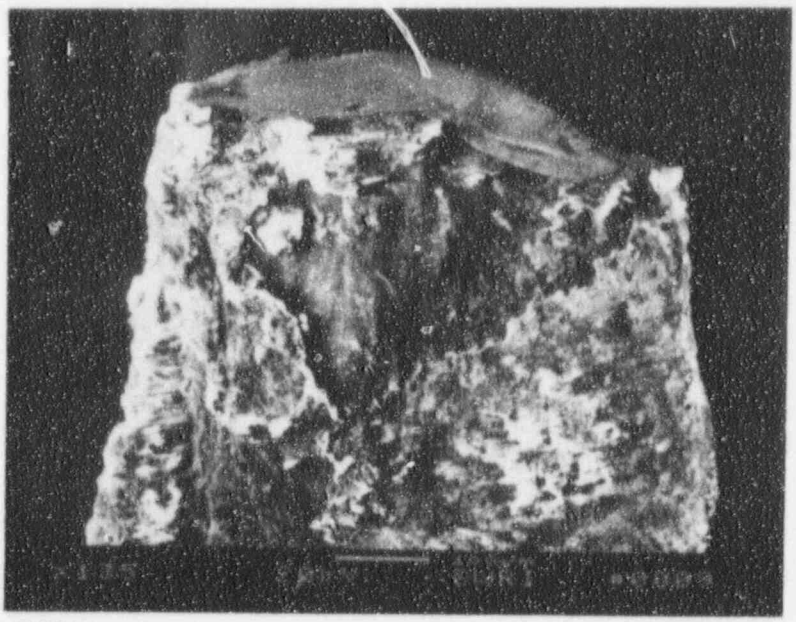

61951 135X

b) Side View

Figure 5-14. SEM Fractographs of SwRI Wire No. 421-1

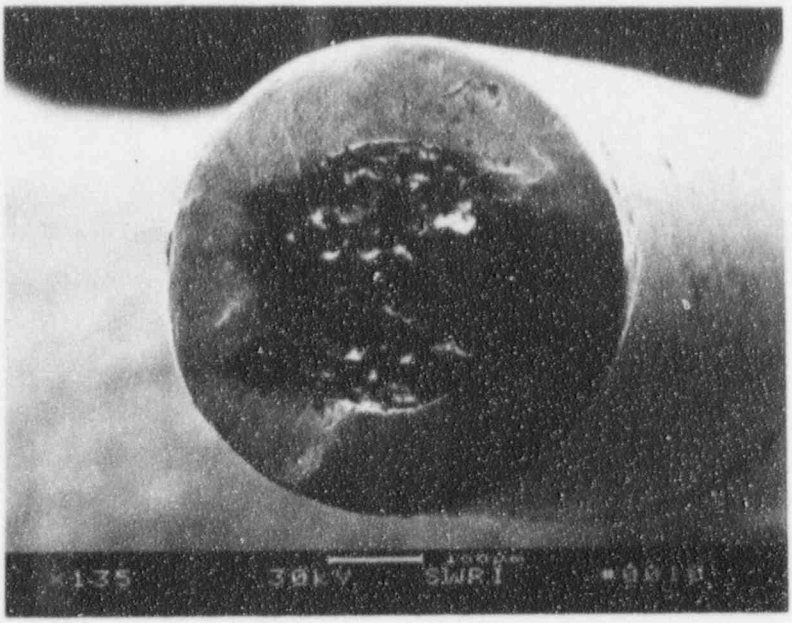

61926 135X

a)

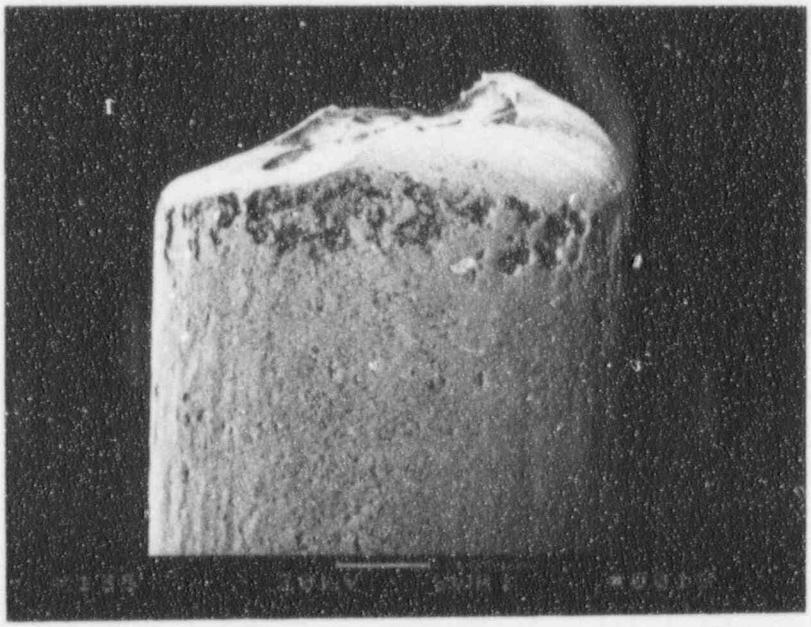

61932 135X

b)

Figure 5-15. SEM Fractograph of SwRI Wire No. 423-1

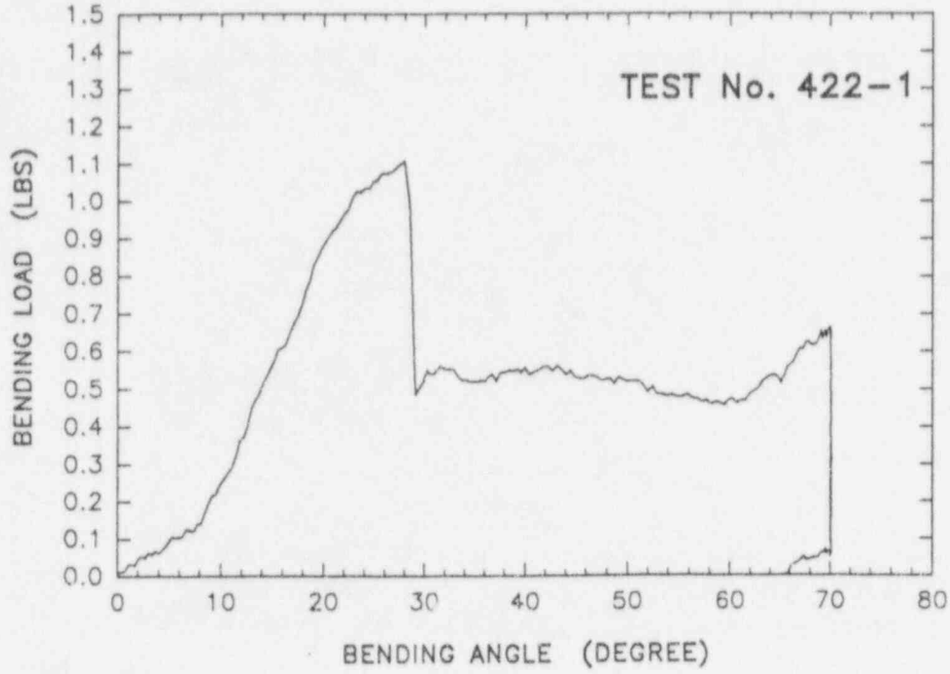

a)

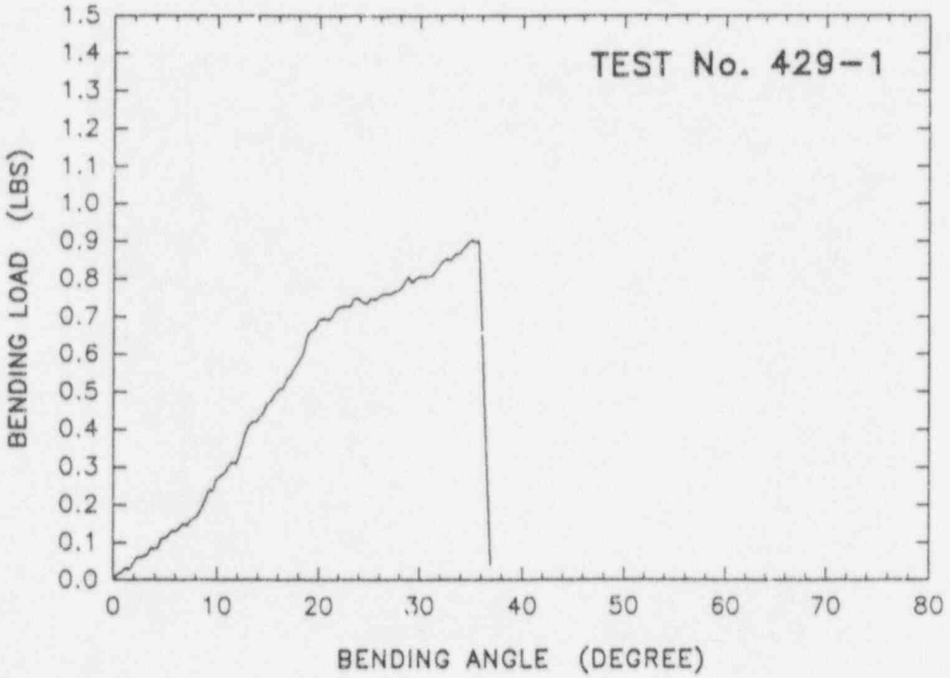

b)

Figure 5-16. Bend Test Plot of Load vs. Angle of Deflection for SwRI Wires, Nos. 422-1 and 429-1

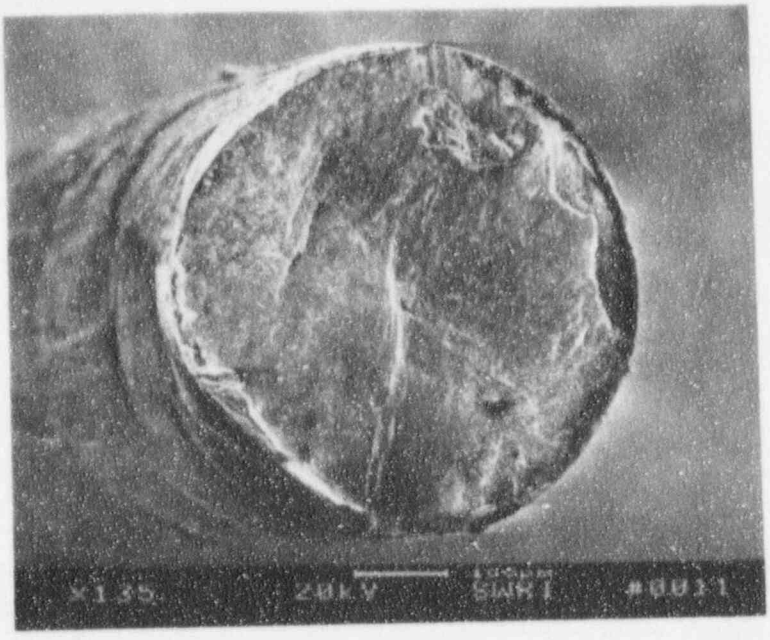

61952 135X

a) View Looking at Fracture Surface

61955 135X

b) Side View

Figure 5-17. SEM Fractographs of SwRI Wire No. 422-1

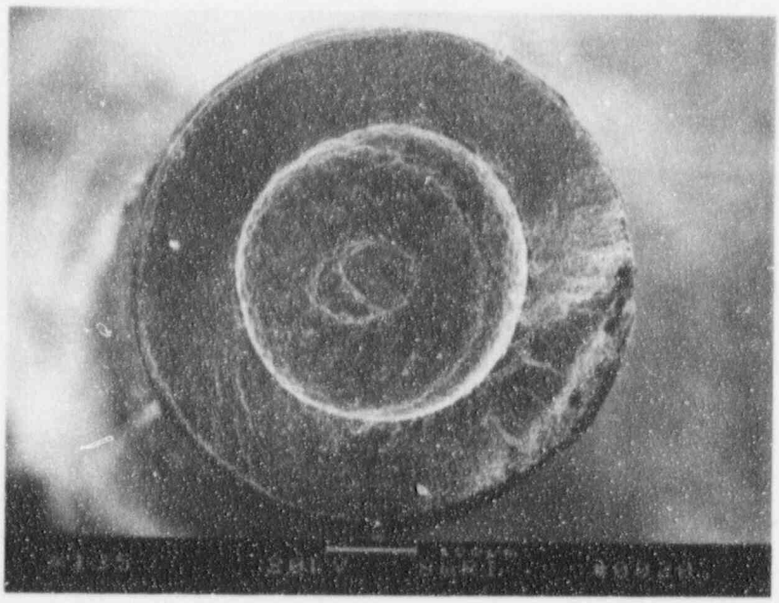

61365 135X

a) View Looking Down at the Wire

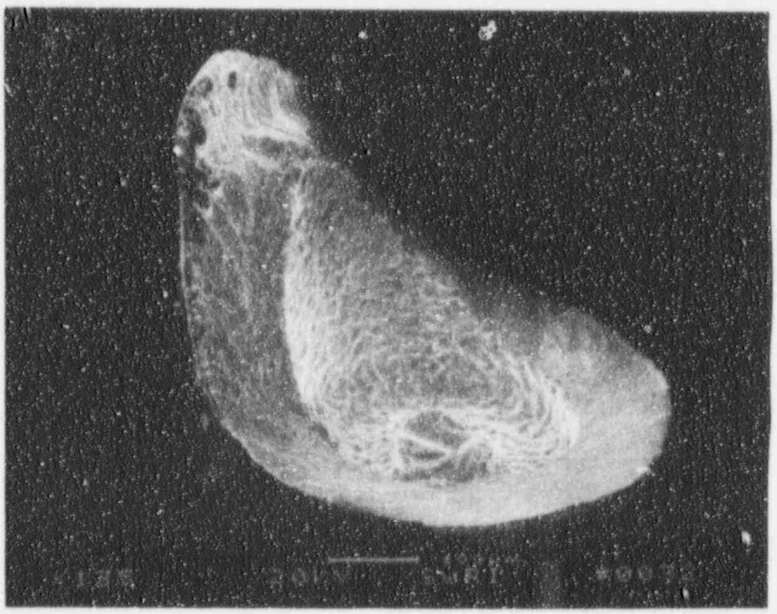

61373 135X

b) View Looking from the Side

Figure 5-18. SEM Fractographs of SwRI Wire No. 429-1

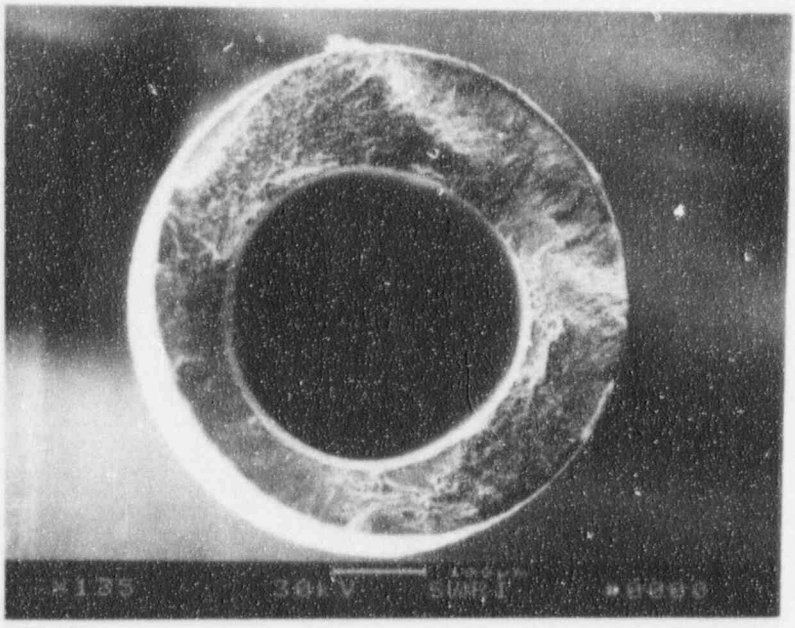

61263 135X

a)

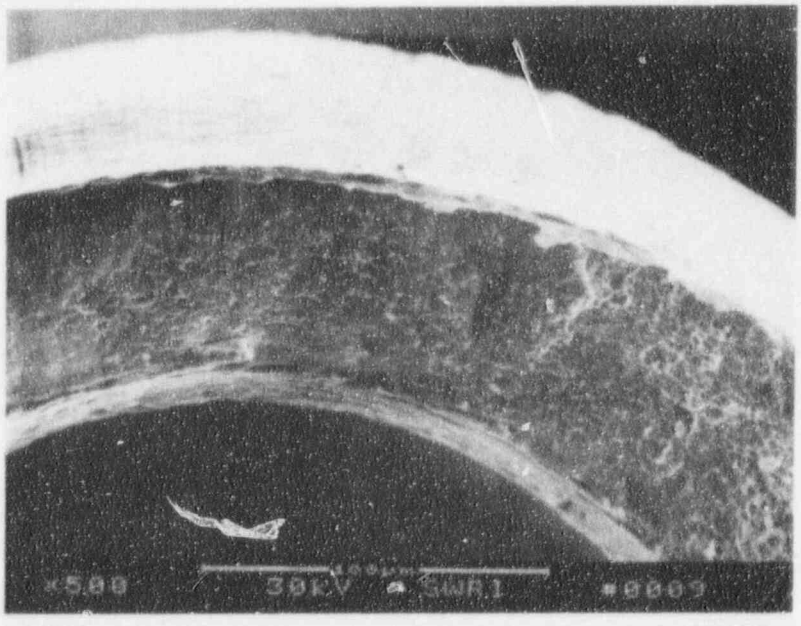

61266 500X

b)

Figure 5-19. SEM Fractograph of SwRI Wire No. 426-1

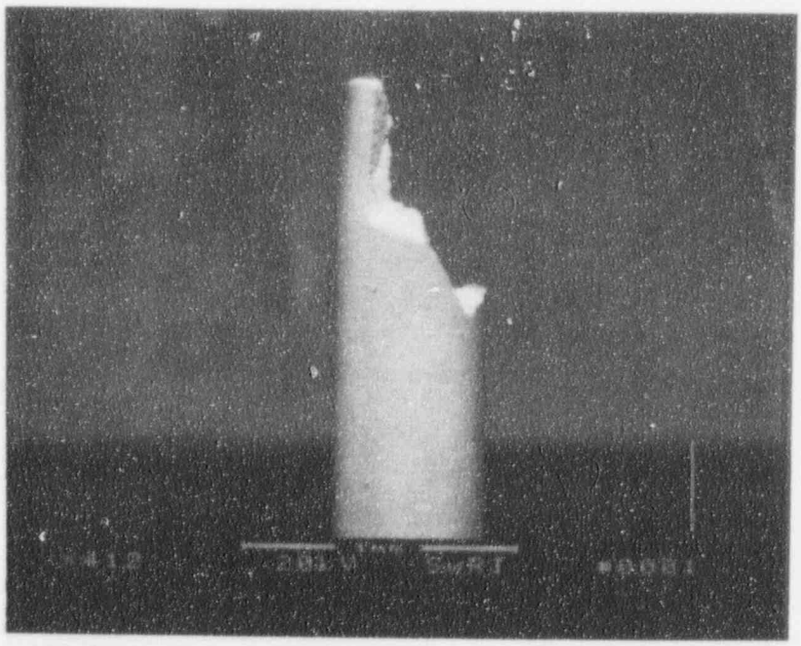

62538 41X

Figure 5-20. SEM Macrophotograph of SwRI Wire No. 442-1

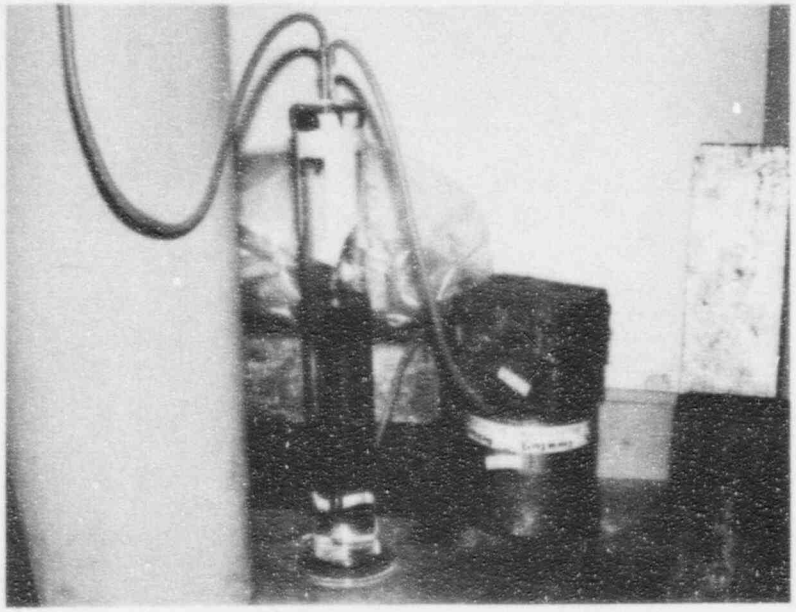

a) Moisture Set-Up

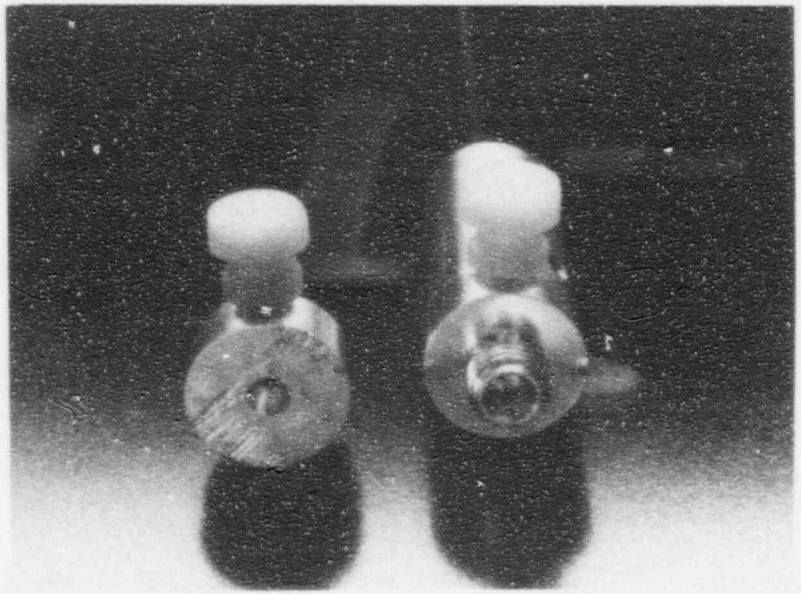

b) The Inverted Clamp

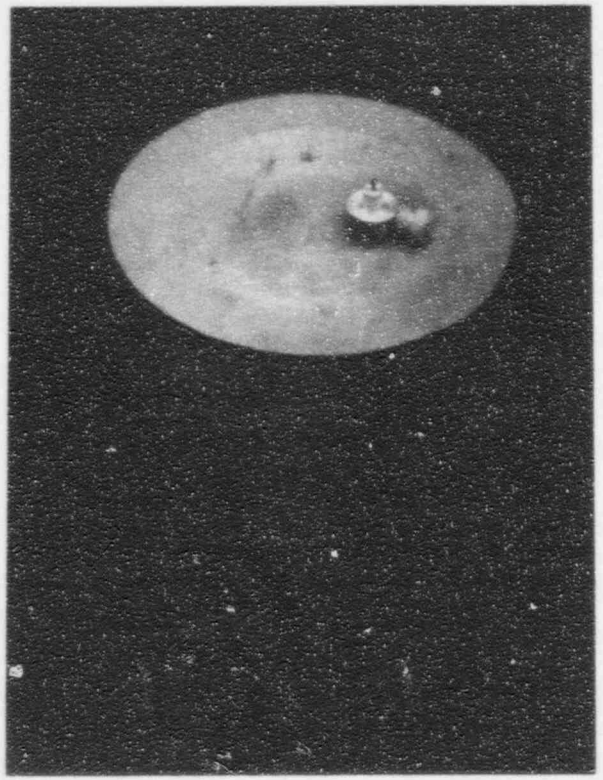

Figure 5-21. Photograph of the Moisture Chamber

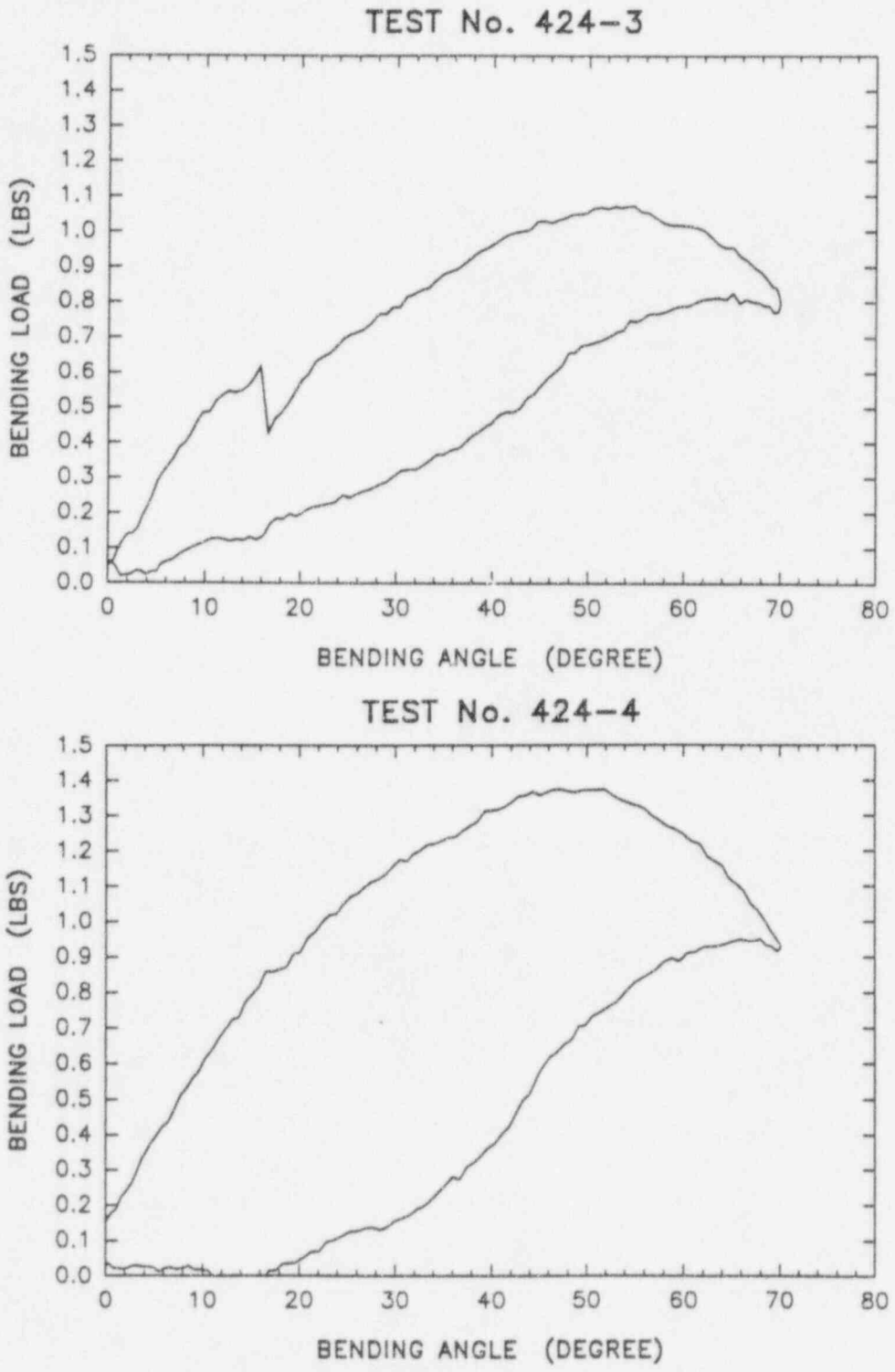

Figure 5-22. Bend Test Plots of Load vs. Angle of Deflection for SwRI Wires, Nos. 424-3 and 424-4

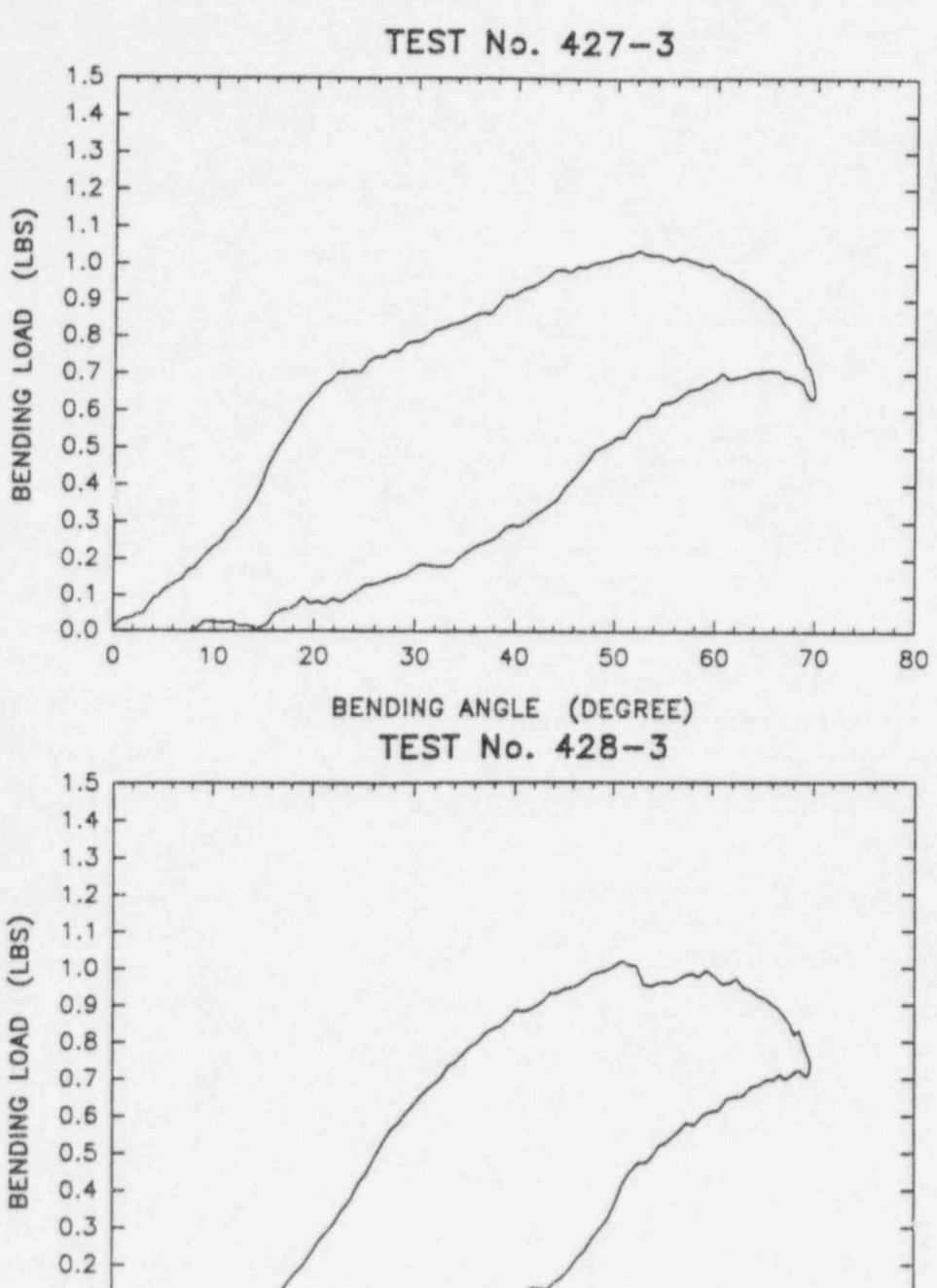

Figure 5-23. Bend Test Plots of Load vs. Angle of Deflection for SwRI Wires, Nos. 427-3 and 428-3

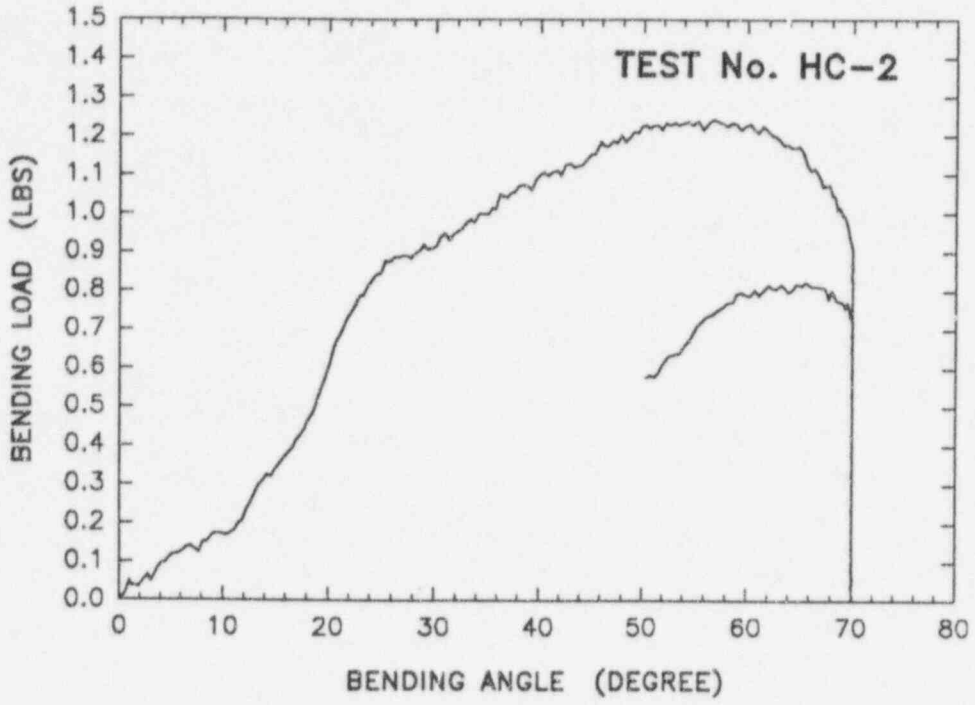

(a) Charging conditions: -0.5v, 120 min.

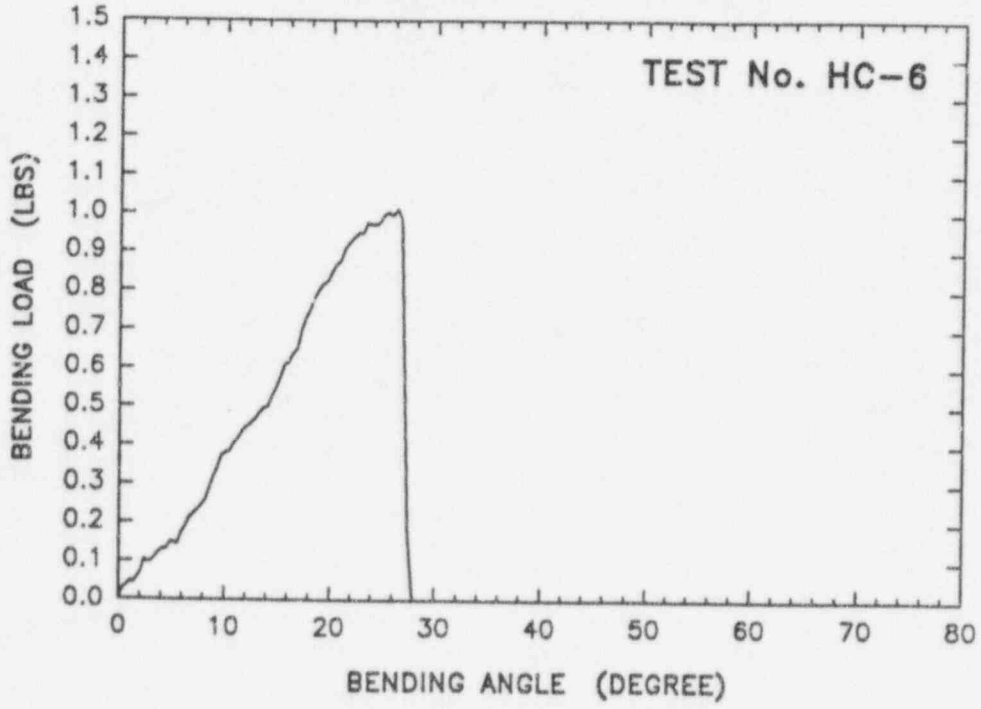

(b) Charging conditions: -1.0v, 120 min.

Figure 5-24. Load/Deflection Curves for Hydrogen-Charged Specimens

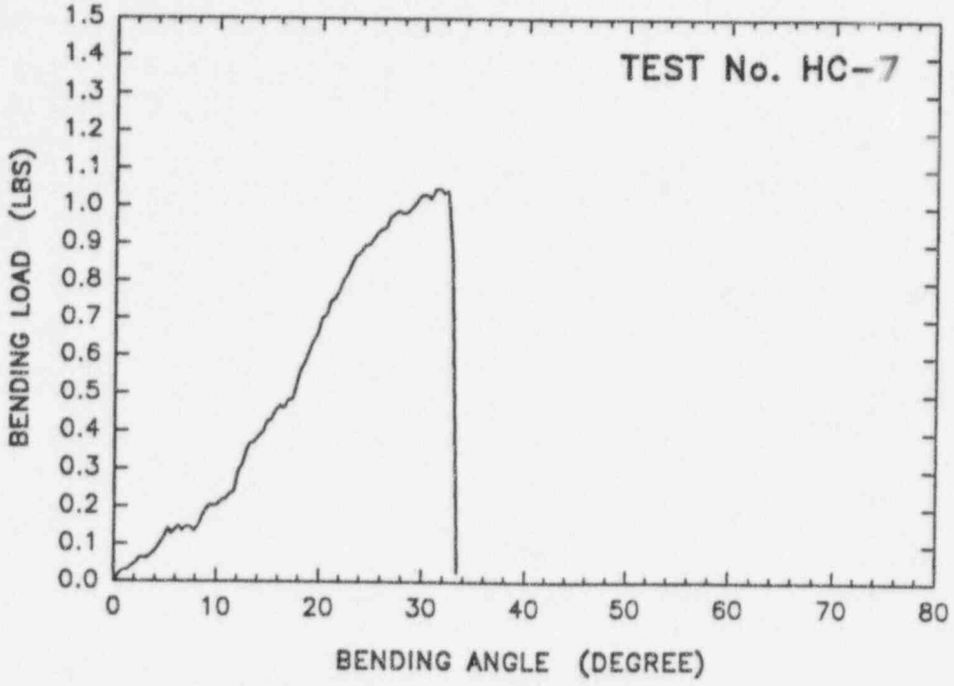

(a) Charging conditions: -1.0v, 100 min.

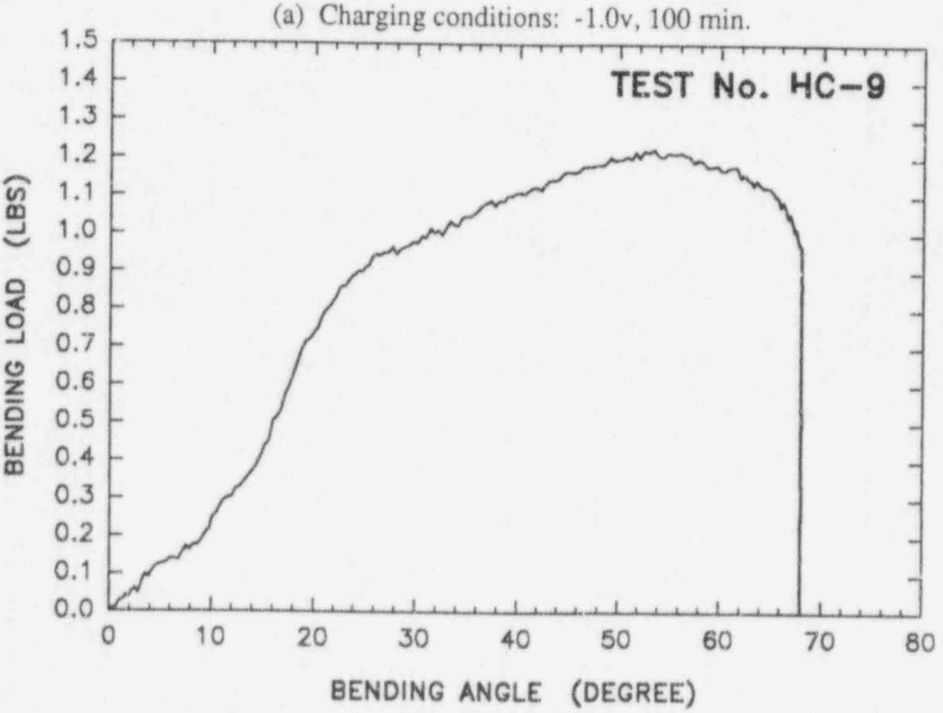

(b) Charging conditions: -1.0v, 60 min.

Figure 5-25. Load/Deflection Curves for Hydrogen-Charged Specimens

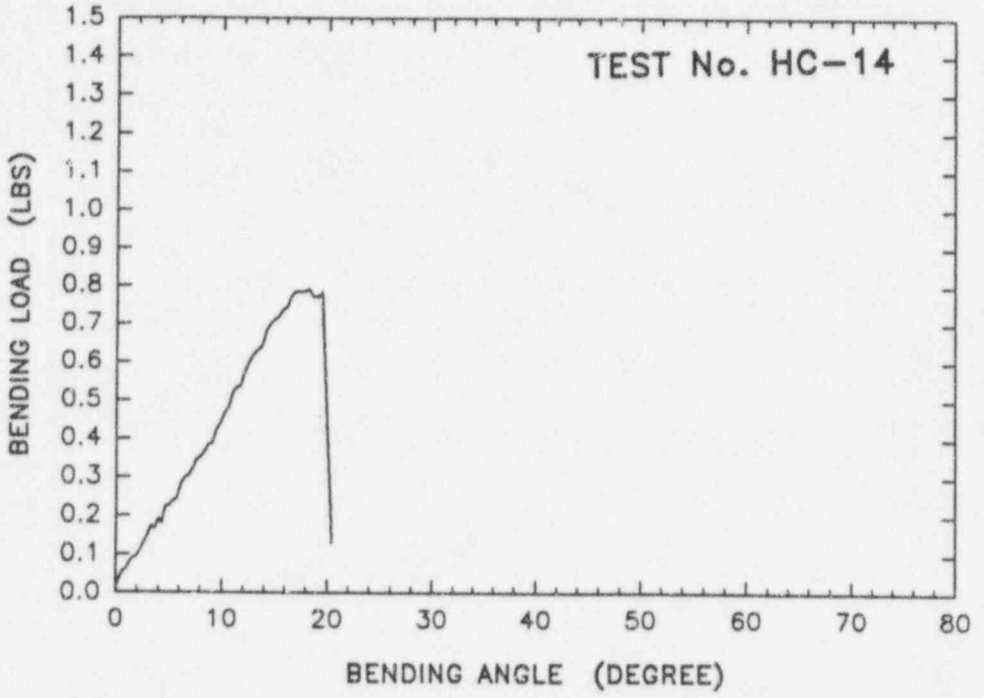

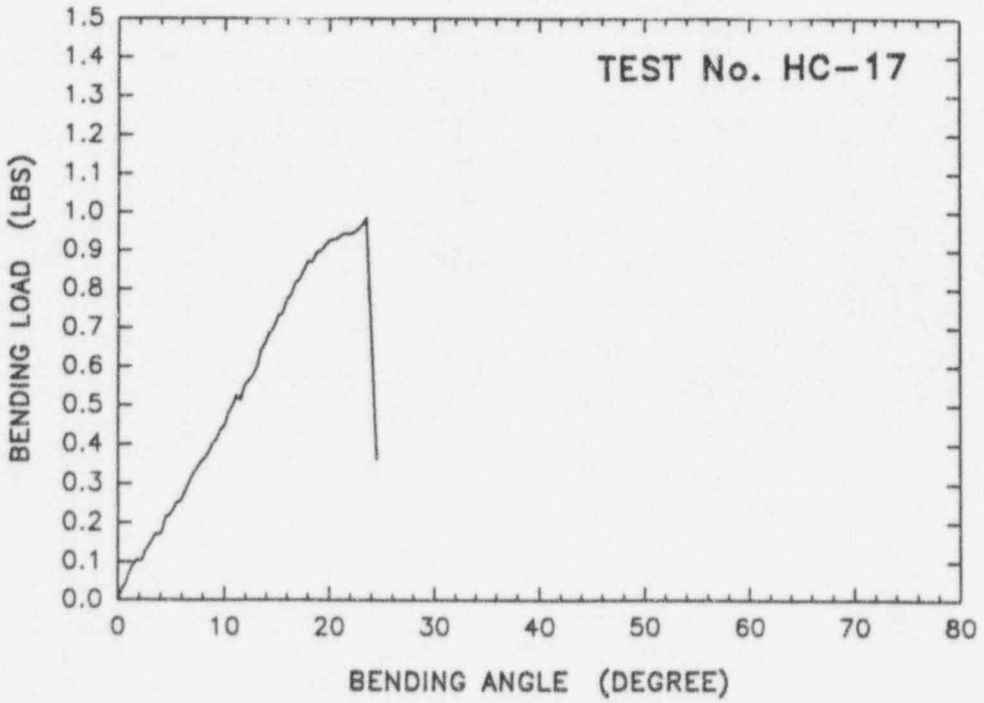

(b) 16-hr. delay.

Figure 5-26. Load/Deflection Curves for Hydrogen-Charged Specimens. Charged at -f1.0v for 120 min.

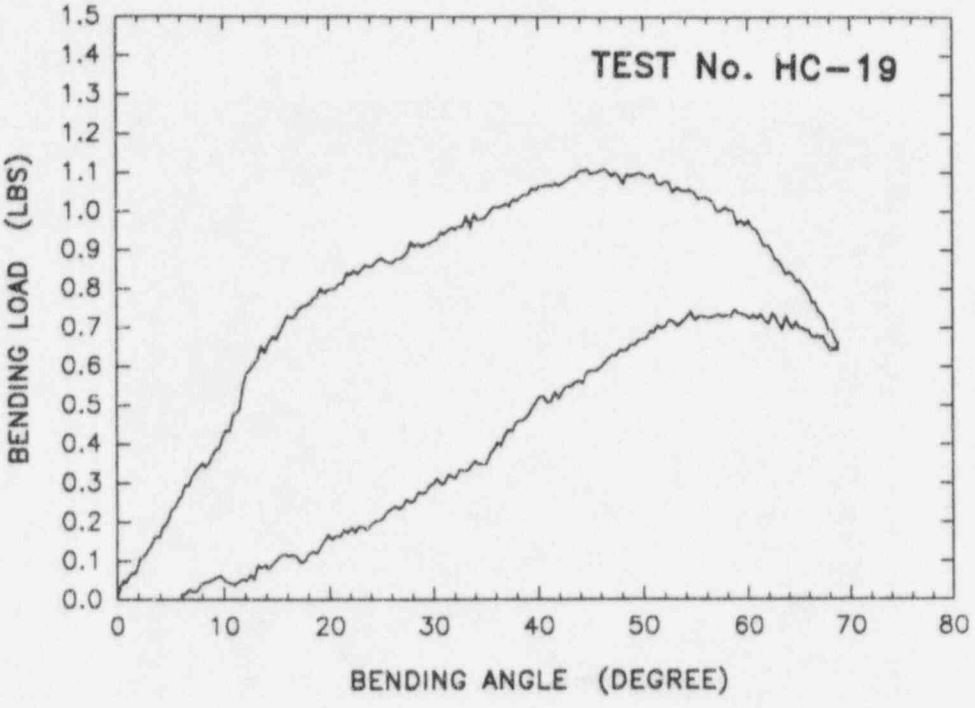

(a) 52-hr. delay.

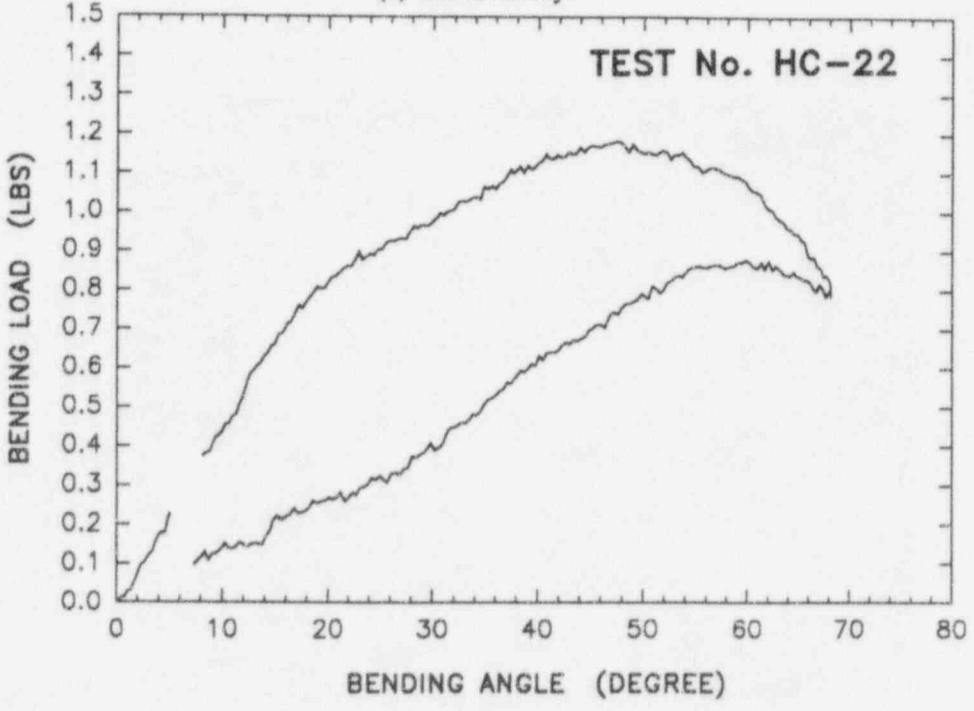

(b) After 2 hours at 450°F.

Figure 5-27. Load/Deflection Curves for Hydrogen-Charged Specimens. Charged at -1.0v for 120min.

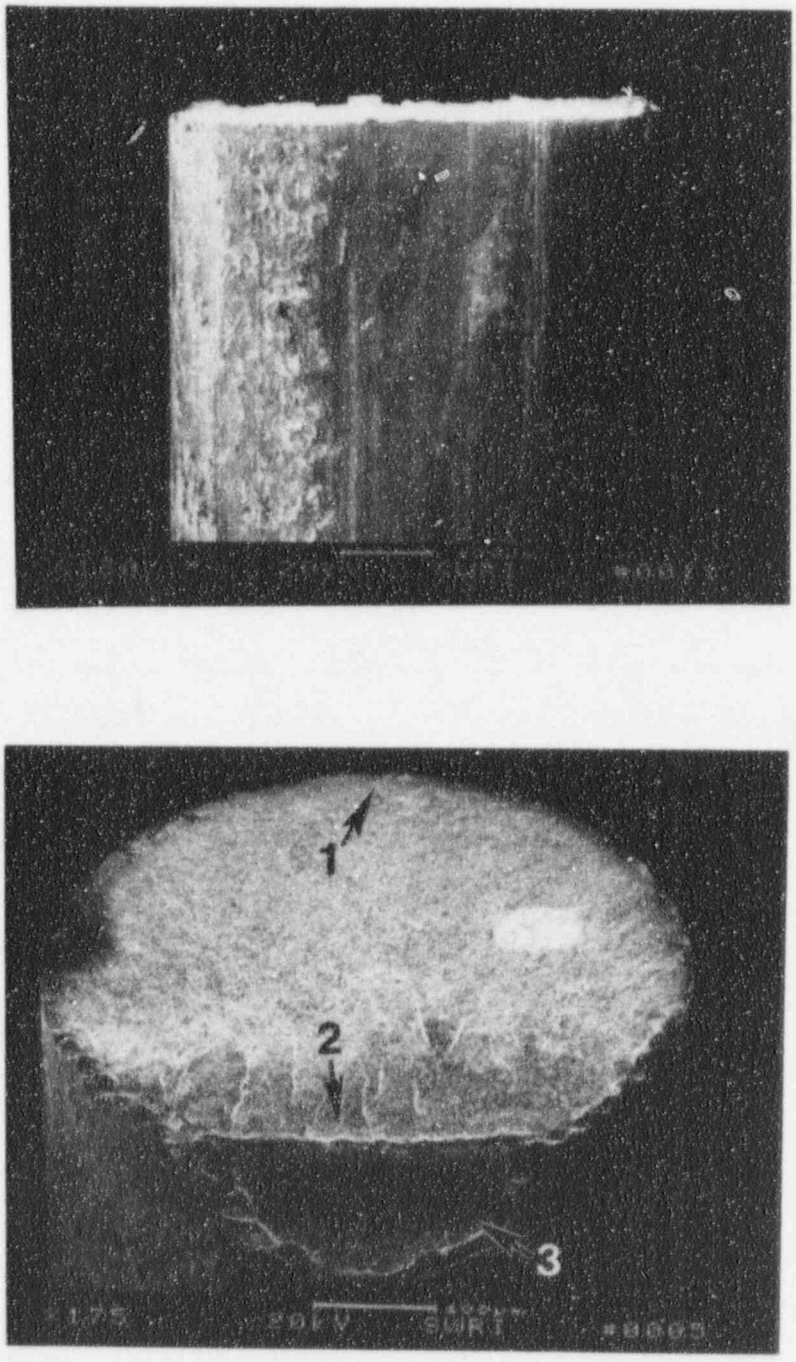

Figure 5-28. SEM Photomicrographs of Fracture in Hydrogen-Charged Specimen.
Test No. HC-6

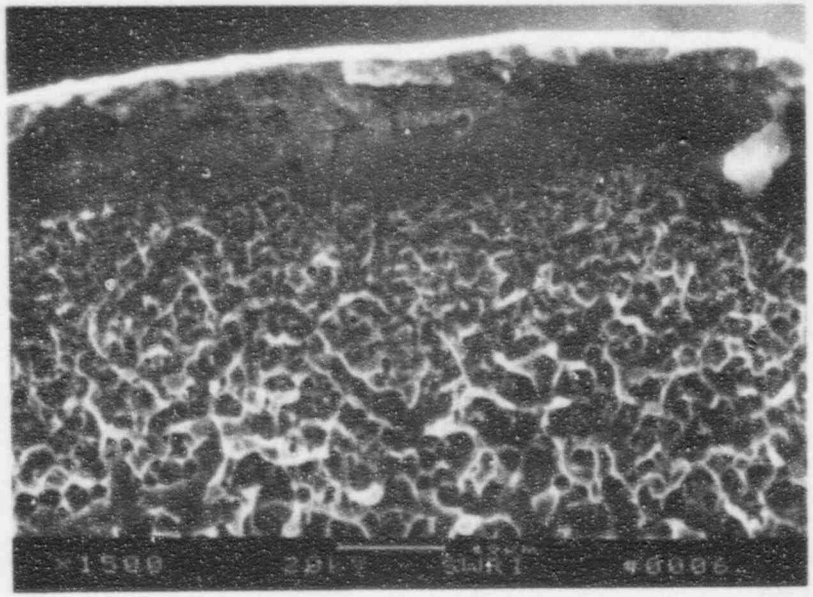

61795 (a) Location 1

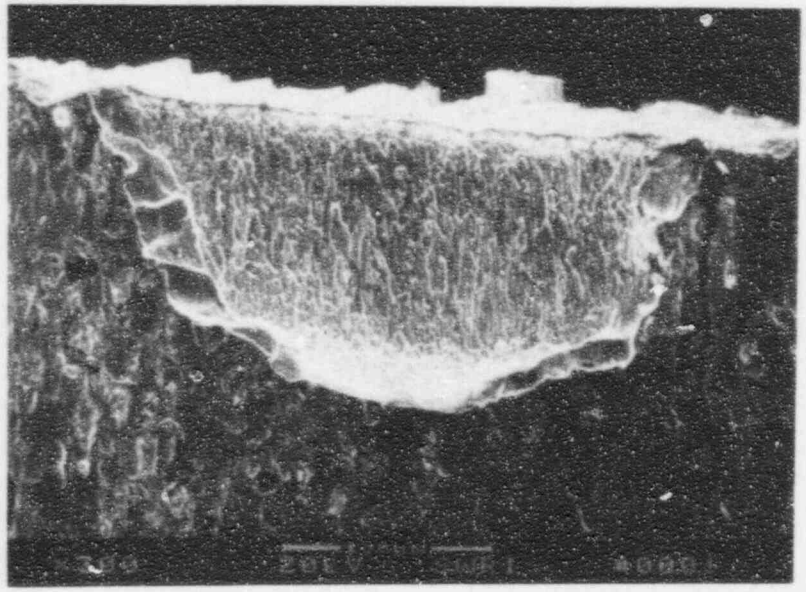

61791 (c) Location 3

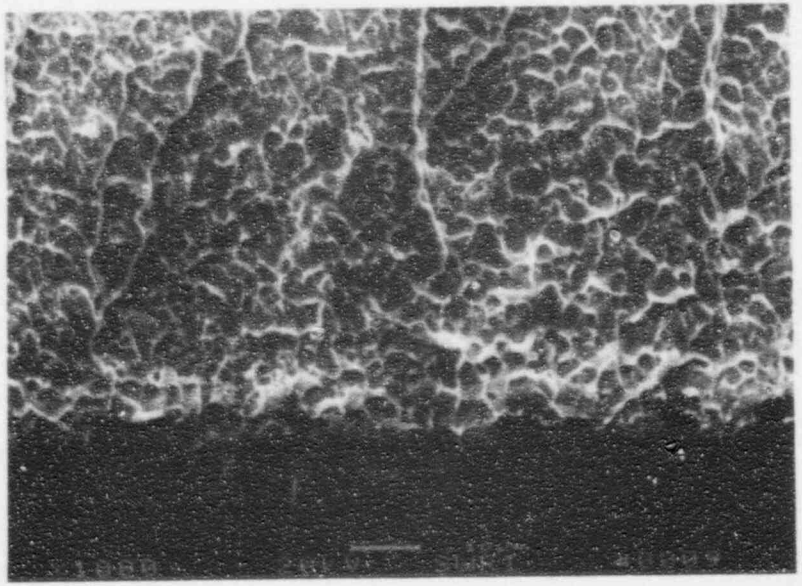

61796 (b) Location 2

Figure 5-29. SEM Fractographs from Hydrogen-Charged Specimen. Test No. HC-6. See Figure 5-28 for locations.

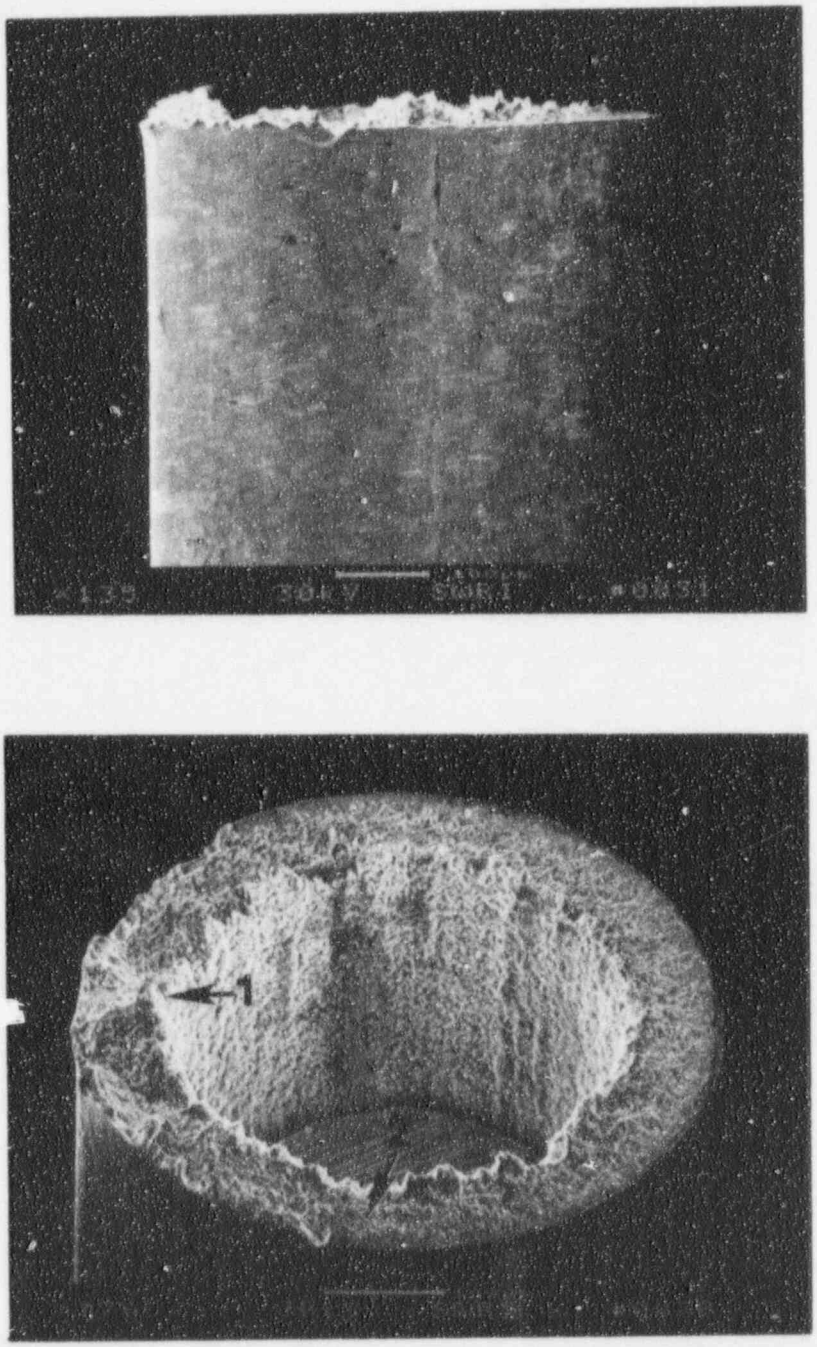

Figure 5-30. **SEM Photomicrographs of Fracture in Hydrogen-Charged Specimen.** Test No. HC-10, simulated sourcewire. Inside of bend is at LHS in (a) and (b).

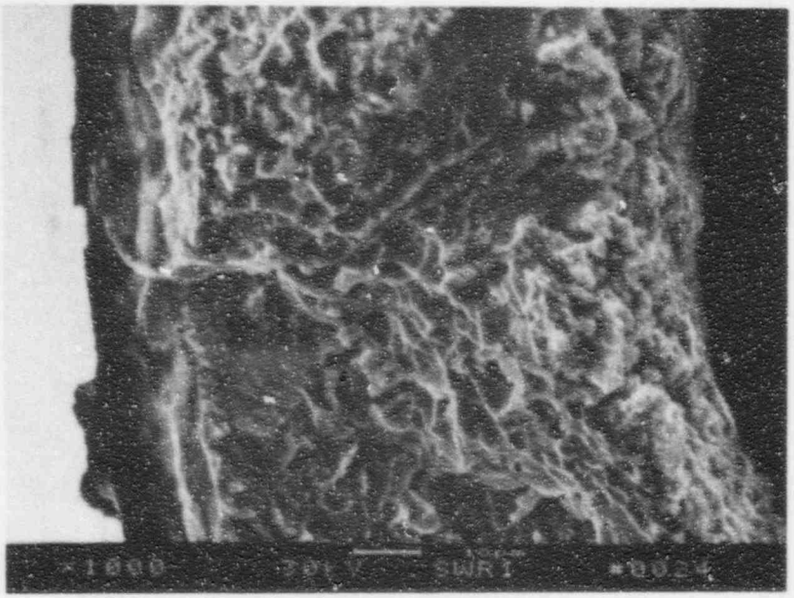

62098 (a) Location 1

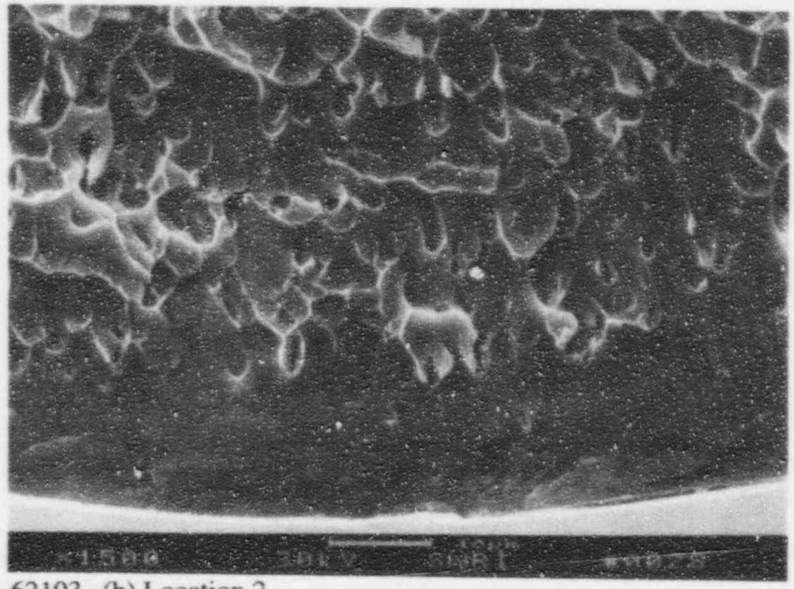

62103 (b) Location 2

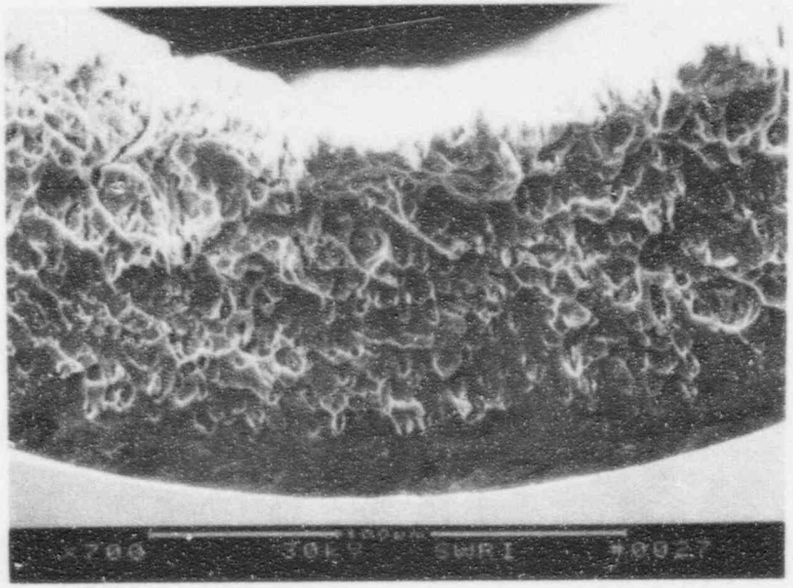

62102

Figure 5-31. SEM Fractographs from Hydrogen-Charged Specimen. Test No. HC-10, simulated sourcewire. See Figure 5-30 for locations.

6. SUMMARY, DISCUSSION AND CONCLUSIONS

The observations made and data obtained in this investigation which are pertinent to the determination of the root cause of the in-service failures of the sourcewires are summarized as follows.

6.1 Service Failures

1) Both in-service failures occurred by brittle fracture in contrast to the usual ductile behavior of Nitinol in overload fracture.

2) Solid specimens from the failed sourcewire underwent extensive deformation in a bend test without fracture or cracking.

3) The microstructure and hardness level of both sourcewires was normal for 55-Nitinol. Small crack-like defects were present in the thin resolidified layer at the cavity wall.

4) Both of the failed sourcewires had been shipped and stored in PTFE sleeves.

5) Considerable debris was present on the fracture surfaces and within the cavity of the failed sourcewires and, in one case, fluorine was consistently detected in analyses of the debris.

6.2 Laboratory Test Program

6) The chemical composition of duplicate samples from the lot of Nitinol wire used in fabrication of the failed sourcewires was normal for 55-Nitinol. Thermal analyses also indicated a satisfactory transformation temperature.

7) Dummy sourcewires, fabricated with inactive iridium pellets, underwent extensive deformation in bend tests without cracking or fracture.

8) Finite-element stress analyses verified that, for sourcewires loaded in bending, the peak stress values occur at the bottom of the cavity.

9) Three cases of deterioration and disintegration of PTFE sleeves in the presence of the high radiation field, accompanied by degradation of the sourcewire, were documented.

10) All sourcewires which had been shipped and stored with the PTFE sleeve in place and subsequently tested or examined in this program, either failed prior to removal from the cask or failed in a brittle fashion in the bend test.

11) Sourcewires stored in stainless steel needles for periods of up to 210 days, with the high radiation field of the encapsulated Iridium-192 sources, survived the bend tests without brittle fracture.

12) Bend tests of sourcewire samples at temperatures below the martensitic transformation temperature did not result in brittle fracture.

13) Introduction of moisture into the environment for sourcewires stored in stainless steel needles did not induce brittle fracture in bend tests.

14) Electrolytic charging of solid Nitinol wires and simulated sourcewires resulted in marked embrittlement as evidenced by brittle fracture at low bend angles.

An important point in the consideration of possible causes of the in-service failures of the two sourcewires is that both failures were brittle in nature and brittle fracture in 55-Nitinol is abnormal. On the basis of the typical properties of Nitinol, the sourcewires would be expected to behave in a ductile manner. In addition, when subjected to a bend test, specimens of solid wire from the failed samples underwent extensive deformation without cracking or fracture. When forced to fracture in bending, the failed wires exhibited high ductility with significant plastic deformation in the region of fracture.

These factors, together with the normal microstructure, hardness level and martensite transition temperature, indicate that the failures were not associated with any inherent materials flaw or abnormal materials properties. Small defects were noted in the surface of the cavity wall. Apparently, these developed in the electric discharge machining (EDM) process employed in fabrication. However, there was no evidence to indicate that these features were a direct cause of the failures. Certain portions of the fractures occurred with crack initiation at the surface of the cavity but there was no fractographic evidence that the defect-like features were the basic fracture initiation site. It was also noted that the cavity on one of the failed sourcewires was not exactly aligned with the wire axis. However, there was no evidence to indicate that this was a causitive factor in the failure. In addition, multiple bend tests of other sourcewire samples, fabricated by the same process, did not result in any brittle fracture.

Since sourcewires are subjected to repeated bending in service due to extension and retraction through irregular paths, the question of failure by low-cycle fatigue must be addressed. In general, the fractographic features of the failures are not consistent with fatigue crack initiation. First, fatigue cracking would be expected to exhibit clear evidence of unique origins of cracking and no such origins were evident in the fractographic examination. Secondly, the equiaxed dimples which characterized the flat zones of fracture and the absence of any zones representing subcritical cracks are not consistent with either high-cycle or low-cycle fatigue.

All features of the in-service failures, together with the known properties and characteristics of Nitinol in general, demonstrate that the failures were abnormal but there was no indication that the failures were associated with any inherent materials deficiency, fabrication flaw, induced mechanical damage or with in-service cyclic loading. This factor suggests that some form of environmentally-induced degradation of both sourcewires occurred during shipping, service or storage. One factor, common to both failed wires was that, like all other previously manufactured Nitinol sourcewires, they had been shipped and stored in PTFE sleeves in the shipping cask.

There are a number of possible environmental effects to be considered. High-level radiation exposure is known to embrittle certain materials and although radiation embrittlement does not occur in the austenitic stainless steels, little data is available concerning its effects on Nitinol. The chemical environment can also contribute to embrittlement of some metals and alloys, especially if certain corrosive species are involved. Nitinol is generally corrosion resistant and at first thought the sourcewire would be expected to encounter relatively benign environments. However, in light of the failures, chemical environment factors, such as atmospheric moisture, possible breakdown of or reactions with the PTFE sleeves and the possibility of introduction of extraneous corrosive species must be evaluated as possible causes of failure. One additional factor to be considered is the possible effect of the temperature-dependent austenite-to-martensite transformation. The laboratory test program carried out as part of this investigation, and described in the earlier section of this report, was organized to address all of the above issues.

The ductile behavior of 55-Nitinol at temperature above the martensitic transformation temperature is well established. Typically, this alloy exhibits a fracture ductility on the order of 12%. Specifically, the normally ductile behavior of the sourcewire at the location of the service failures was demonstrated in the bend test program. Two dummy sourcewire samples, fabricated by the same process as actual sources but with inactive iridium pellets, survived bend tests to strains well in excess of 10%.

Considering the possibility of radiation embrittlement of the sourcewires due to the encapsulated Iridium-192 source pellets, it must be noted that no brittle fractures occurred in any of the bend tests of actual sourcewire samples stored in stainless steel for periods of up to 210 days. Sourcewire service life is based on the decay of the radioactivity of the iridium source pellets. These sources rapidly decay beyond a useful level and are routinely removed from service and destroyed after a service period of approximately 90 days. The test program included exposure times up to twice that period and the lack of brittle failures demonstrates that radiation embrittlement is not a factor within the useful service life of the sourcewires.

The question of possible effects of the martensite transformation on the fracture characteristics of the sourcewire was addressed by the low-temperature tests. Duplicate bend tests conducted at temperatures <10°C did not result in cracking or fracture. The martensite transformation temperature for the sourcewires is 15±5°C so the test results show that the sourcewires are not susceptible to brittle fracture in the martensitic condition. Thus, temperature excursions in shipment, service or storage would not have an adverse effect on the fracture characteristics of the wires.

It is conceivable that in the course of temperature changes during shipment and storage that moisture might collect within the stainless steel tube of the shipping cask and influence the environment surrounding an active sourcewire. Bend tests of sourcewire samples which were exposed to moist environments in stainless steel sleeves were performed in the program. Exposure periods were up to 108 days, matching typical service periods, and no fractures or cracking resulted in any of the tests. These results demonstrate that neither the presence of moisture alone nor moisture in conjunction with the high-radiation field results in embrittlement of the Nitinol sourcewires.

Analyses of the deposit material on one service failure consistently detected fluorine. Evidently, the presence of this element is associated with debris from deterioration of the PTFE sleeve. Small quantities of sulfur and chlorine were also detected in both failure cases. These are potentially corrosive species but their source is unknown and there is insufficient evidence to evaluate their significance. A number of other extraneous elements were also detected in both cases, but these were all of a nature not likely to contribute to corrosive attack or embrittlement.

Considering that all tests gave negative results concerning the influence of the environmental factors discussed, attention must be directed toward the possible role of the PTFE sleeves in the failure process. In this regard, it is important to note that all test samples stored in PTFE sleeves failed in an abnormal manner. Deterioration and disintegration of the PTFE sleeves was observed in several cases and considerable amounts of nonmetallic debris, some containing fluorine, was present in the case of the in-service failures. General consideration of the possible effects of high-level radiation on PTFE also leads to the conclusion that significant deterioration may be expected. Details of possible mechanisms of radiation-induced deterioration of PTFE are presented in Appendix G. Furthermore, the deterioration of PTFE can also produce by-products which could conceivably embrittle Nitinol alloy. Possible mechanisms for this process are also discussed in Appendix G. The possible by-products are capable of producing reactive environments which could induce corrosive attack and related embrittlement.

In summary, all factors indicate that the two service failures involved some type of environmentally-induced embrittlement. The results of bend tests of selected sourcewire samples eliminated all conceivable environmental factors except the presence of the PTFE sleeves. That factor coupled with the observed in-service deterioration of PTFE accompanied by obvious degradation of the sourcewires leads to the conclusion that the presence of the PTFE sleeves played a key role in the in-service failures. Finally, it can be noted that the test program demonstrated that 55-Nitinol is markedly susceptible to classic hydrogen embrittlement. Also, the known hydrogen-induced failures exhibited several fractographic features which were common to the service failure.

On the basis of the factors discussed above, it is concluded that the root cause of the in-service failures of the sourcewires was environmentally-induced embrittlement due to the breakdown of the PTFE protective sleeves in the presence of the high-radiation field and subsequent reaction or interaction of the breakdown products with the Nitinol alloy. It is likely that the embrittlement occurred by a classic hydrogen-embrittlement process or by a process with very similar characteristics.

APPENDIX A. FINITE-ELEMENT ANALYSIS OF THE WIRE

1. SCOPE

A finite-element analysis was performed to determine strains and stresses in the wire as it was bent over the die by the roller in the test fixture. An understanding of the strains and stresses produced by the test was needed in order to set test parameters. Because the test produced large displacements and strains in the wire, a nonlinear analysis was required to treat the geometric and material nonlinearities.

2. GEOMETRY OF THE TEST FIXTURE

A schematic of the test fixture is shown in Figure A-1. A roller is moved from left to right, contacting the wire specimen and bending it over the 0.10 in. radius die. Once contact has been made with the wire, a motion of the roller 0.5 inches to the right, bends the wire through about 90 degrees. A slot around the outer circumference of the roller permits the roller to maintain contact with the top surface of the support block and die without compressing the wire cross-section. The roller outer radius (to the rolling surface) is 0.400 in., and to the point of contact with the wire the radius is 0.375 in.

3. GEOMETRY OF THE WIRE

A drawing of the wire is shown in Figure A-2. The drawing gives overall dimensions of the wire, dimensions of the cavity and seed, and shows the point along the wire which corresponds to the bottom of the die radius in the test fixture. The wire and seed are assumed to be fixed at this point in the finite-element mode. An enlargement of a portion of the wire, given in Figure A-3, shows nodal positions along the wire and seed. Node 1 is at the fixed point in the model. All displacements of the wire and seed are zero in the finite-element model at this location. A small cavity exists in the wire past the end of the seed. For this analysis, the cavity is assumed to extend 0.005 in. beyond the tip of the seed. This gives a distance of 0.0117 in. from the last point of contact between the wire and seed (proceeding along the wire toward its tip) and the end of the cavity. This is the distance between Nodes 5 and 6 in the model.

Section properties of the wire were calculated for an outer diameter of 0.025 inch and the maximum diameter of the internal cavity. Because the true wire diameter is less (0.0231-0.0235 in. per the drawing and 0.0231-0.0240 in. as-received), the stresses calculated in the model will be overestimated. The overestimate will depend upon the wire diameter and will be about 6.4% for a 0.0235 in. diameter. Lateral motions of the wire and seed will be assumed equal in the finite-element model. This assumption ignores the fact that the diameter of the cavity in the wire is slightly greater than the diameter of the seed. Compatibility of rotations were not required between the wire and seed, but they will be approximately equal because of the requirement of equal lateral displacements.

4. MATERIALS PROPERTIES

Properties for the 55-Nitinol wire were obtained from References A.1 and A.2: properties for the iridium, IR-192 seed were obtained from Reference A.3. Room temperature properties were used in all cases. Stress and strain data for the Iridium were somewhat limited and included only the yield strength, ultimate strength, and elongation. A full stress-strain curve was available for the Nitinol.

Stress-strain curves derived from the data located are given in Figure A-4. The curve for the Nitinol is unusual in that it has a very long constant stress region, following what would normally be considered yielding, and before the stress starts to increase (strain hardening). In fact, the Nitinol will completely recover from strains as large as 8%, so much of the curve represents nonlinear elastic behavior. The iridium is considerably stiffer than the Nitinol alloy and has a higher yield stress; so, the seed adds considerable stiffness to the wire.

The stress-strain curve for iridium was represented as bilinear isotopic, and the stress-strain curve for Nitinol was represented as multilinear isotropic in the finite-element model. The iridium was found to have a modulus in tension that was 2.46 times larger than its modulus in compression. Thus, an average of the tension and compression modulii was used which gave E = 52.7E6 psi. The modulus for the 55-Nitinol alloy, E = 10.2E6 psi, was taken from Reference A.2 (only a single modulus was provided). Poisson's ratio was taken as 0.33 and 0.26 for the 55-Nitinol and iridium, respectively.

5. FINITE-ELEMENT GRID

Figure A-5 shows the finite-element grid for the wire. Node numbers are given on the left-hand side and element numbers on the right. Nodes and elements along the seed are not shown. They over-lie nodes and elements of the wire between Nodes 1 and 5 (refer to Figure A-3). The wire and the seed are represented by beam elements that lie along their respective centerlines, which coincide. No lateral dimensions are associated with the beam elements; thus, the model is referred to as a centerline model.

The roller and die are shown schematically by arcs that lie along the surfaces which contact the wire. In this case, the surfaces are set at the wire centerline; that is, the wire radius is added to the contact radius of both the roller and die, giving the values shown in Figure A-5. The roller and die are represented in the model by a series of contact elements that lie between the wire nodes and the surfaces that the wire may contact.

6. CALCULATED RESULTS

An analysis was performed that treated large displacements and material nonlinearity. It required an iterative process with automatic time stepping during the solution and convergence iterations at each time step. The problem was solved using the ANSYS computer code, Version 5.0. Even though the model was small, in terms of the number of nodes and elements, the solution time was quite long on the HP9000 work station.

Displacements -- A typical displaced position of the wire (without exaggeration) is shown in Figure A-6. It corresponds to a lateral motion of the roller, 0.3 in. to the right after it contacts the wire. The angle of the wire computed for this position is 50.2° from the vertical, its initial position, or 39.8° from the horizontal. Comparison with measurements from the tests revealed that the angles calculated (from the vertical) were smaller than those measured. To examine the causes for the differences, a graphic, kinematic study was performed using a CAD program. Results for a roller lateral displacement of 0.36 in. are given in Figures A-7 and A-8. Figure A-7 corresponds to test conditions, where the lateral dimensions of the wire are represented in the geometric model, and Figure A-8 corresponds to the centerline model used in the analysis. The angles determined from the study differed by 8.08 degrees, with calculated angles being smaller than measured angles, when measured from the vertical. These calculations were based on simple geometric considerations and assumed that the deformed wire lay in perfect contact with the die and that no deformation occurred in the wire between its last contact point with the die and its contact point with the roller. There is evidence in the calculated results that the wire does not maintain contact with the die. This is shown in Figure A-9, which gives lateral displacements at Nodes 5 through 8. It shows that each node reaches a maximum displacement and then "rebounds" slightly, that is, the wire appears to spring back from its contact with the die.

To further examine the differences between measured and calculated results, they were plotted together in Figure A-10. Tabulated data, given in Table A-1, show that to make the angles agree, the calculated results must be shifted about 0.048 in. (the average scale shift) to the left. The effect is to give higher calculated rotations of the wire at smaller displacements of the roller. Because stresses and strains are strongly dependent upon rotations, rather than, for example, roller lateral displacement, this adjustment was made for the presentation of strains and stresses.

Stresses and Strains -- Strains calculated at nodal positions along the wire are given in Figure A-11. The abscissa gives roller displacement, after its contact with the wire, over a range of about 0.15 in. to 0.45 in. Labels on the curves denote element and nodal position, *e.g.*, eax_66 denotes axial strain in element 6 at node 6. The strains are computed on the outer surface of the wire on the tension side and correspond to maximum principal strain. As noted previously, the calculated strain and stresses correspond to a wire with an outer diameter of 0.025 in. and are somewhat higher than would be

calculated for a wire of smaller diameter. We estimate that the strains and stresses are 6% higher than what would be calculated for a wire with 0.0235 in. outer diameter. High strains in the wire occur as it is forced to conform to the die radius. Thus, the strains increase first in elements near the bottom of the die, *i.e.*, element 1, and increase last in elements further up the wire. For example, the strain in element 7, eax_77, is low until the roller displacement reaches 0.34 inch. It then starts to increase rapidly and is the highest strain calculated out to a roller displacement of 0.45 in.

The strain first reaches 10% in element 6 at node 6, corresponding to a roller displacement between 0.35 in. and 0.36 in. This is the point in the wire just above the end of the seed. Here the wire is no longer stiffened by the seed and apparently flexes more. The flexing is probably enhanced by the spring back of the wire that was indicated by the displacements in Figure A-9.

Stresses corresponding to the strains in Figure A-11 are given in Figure A-12. The labels follow the convention used for strain, that is, sax_55 is the stress in element 5 at node 5. A rapid increase in stress occurs when the strain reaches about 7%, as evident from the stress-strain curve for Nitinol in Figure A-4. This behavior is evident when one examines the stresses labeled sax_66 and sax_77 in Figure A-12 and their corresponding strains in Figure A-11.

7. CONCLUSIONS

The calculated behavior of the Nitinol wire as it was bent over the die in the test fixture by motion of the roller, produced both useful and interesting results. Stiffening of wire by the seed concentrated stresses in the region of the wire just above the seed. Maximum wire flexure occurred here for two reasons: (1) the wire is slightly weaker because of the unfilled cavity that exists beyond the end of the seed, and (2) partial spring-back of the wire from the die, due in part to the stiffening effect of the seed. These calculations, along with the adjustments required to match measured and calculated rotations, permitted test limits to be set that achieved the desired objectives. It was shown that a displacement of 0.36 inch, which is equivalent to 70° angle of deflection, resulted in a strain greater than 10%.

8. REFERENCES

A.1. 55-Nitinol - The Alloy with a Memory: It's Physical Metallurgy, Properties, and Applications, NASA, SP. 5110.

A.2. High Technology Handbook, Volume II, Chapter 11, 1993. Prepared by SwRI for SA-ALC under Contract No. F41608-87-A237.

A.3. Publication giving properties for Iridium (Ir) on p. 740/Pure Metals.

Table A-1 Rotation vs. Displacement: Calculations and Measurements

Table A1. Rotation vs Displacement: Calculations and Measurements							
ANSYS run					*Measrements*		Scale Shift
Time	Displ.	Rotation		Adj Displ	Displ.	Rotation	Delta Disp
	(in)	(rad)	(deg)	(in)	(in)	(deg)	(in)
					0.15	28.16667	
					0.175	33.16667	
					0.2	38.41667	
21	0.21	0.57698	33.05852	0.174459			
22	0.22	0.607818	34.82541	0.182899			
			35.61827	0.186674	0.225	43.58333	-0.038326
23	0.23	0.635494	36.41112	0.19045			
24	0.24	0.670032	38.39001	0.199873			
25	0.25	0.70773	40.54994	0.210322	0.25	49.91667	-0.039678
26	0.26	0.745047	42.68805	0.220668			
27	0.27	0.781838	44.79602	0.229787			
			45.62483	0.233059	0.275	53.75	-0.041941
28	0.28	0.810769	46.45364	0.23633			
29	0.29	0.843746	48.34308	0.243788			
30	0.3	0.876095	50.19655	0.251825	0.3	58.83333	-0.048175
31	0.31	0.907897	52.01867	0.263709			
32	0.32	0.941962	53.97045	0.276084			
			54.9001	0.280656	0.325	63.66667	-0.044344
33	0.33	0.974413	55.82975	0.285228			
34	0.34	1.00604	57.64185	0.29414			
35	0.35	1.03633	59.37734	0.302814	0.35	67.66667	-0.047186
36	0.36	1.06191	60.84296	0.310395			
			61.19625	0.312222	0.362	70.08333	-0.049778
37	0.37	1.09274	62.60939	0.319531			
			63.5267	0.324695	0.375	72	-0.050305
38	0.38	1.12476	64.444	0.329858			
39	0.39	1.15891	66.40065	0.342087			
			67.94076	0.351036	0.398	74.91667	-0.046964
40	0.4	1.19251	68.32579	0.353273			
41	0.41	1.22581	70.23374	0.36302		Average=	-0.047792
41.8175	0.418175	1.25514	71.91422	0.374418			
41.818	0.41818	1.25521	71.91824	0.374445			
41.8185	0.418185	1.25526	71.9211	0.374465			
41.8195	0.418195	1.25536	71.92683	0.374504			
41.8215	0.418215	1.25552	71.936	0.374566			
41.8235	0.418235	1.25563	71.9423	0.374609			
41.8275	0.418275	1.25577	71.95032	0.374663			
41.8315	0.418315	1.25587	71.95605	0.374702			
41.8355	0.418355	1.25599	71.96293	0.374749			
41.8435	0.418435	1.25627	71.97897	0.374857			
41.8515	0.418515	1.25659	71.9973	0.374982			
41.8595	0.418595	1.25691	72.01564	0.375123			
41.8615	0.418615	1.25699	72.02022	0.375159			

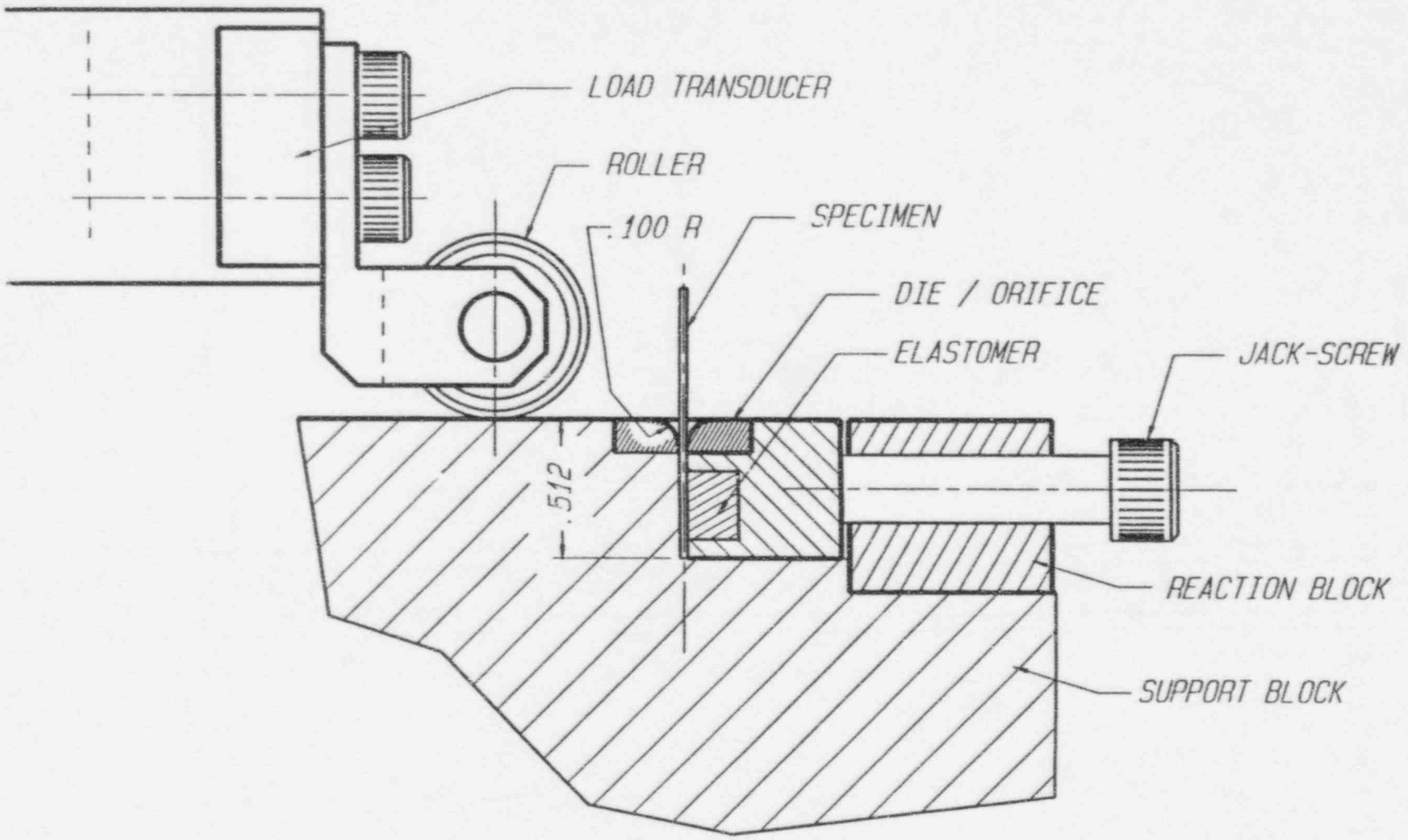

Figure A-1. The Test Fixture (about 2X Scale)

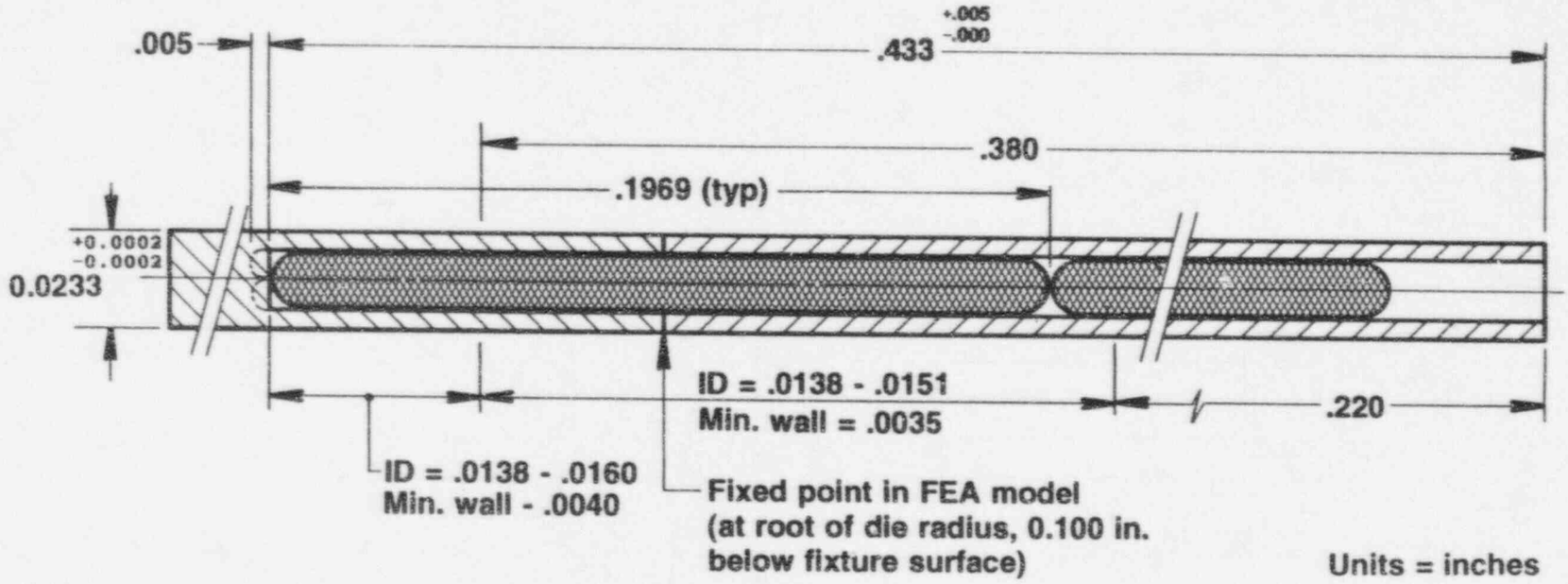

Figure A-2. Wire Geometry and Seed Placement

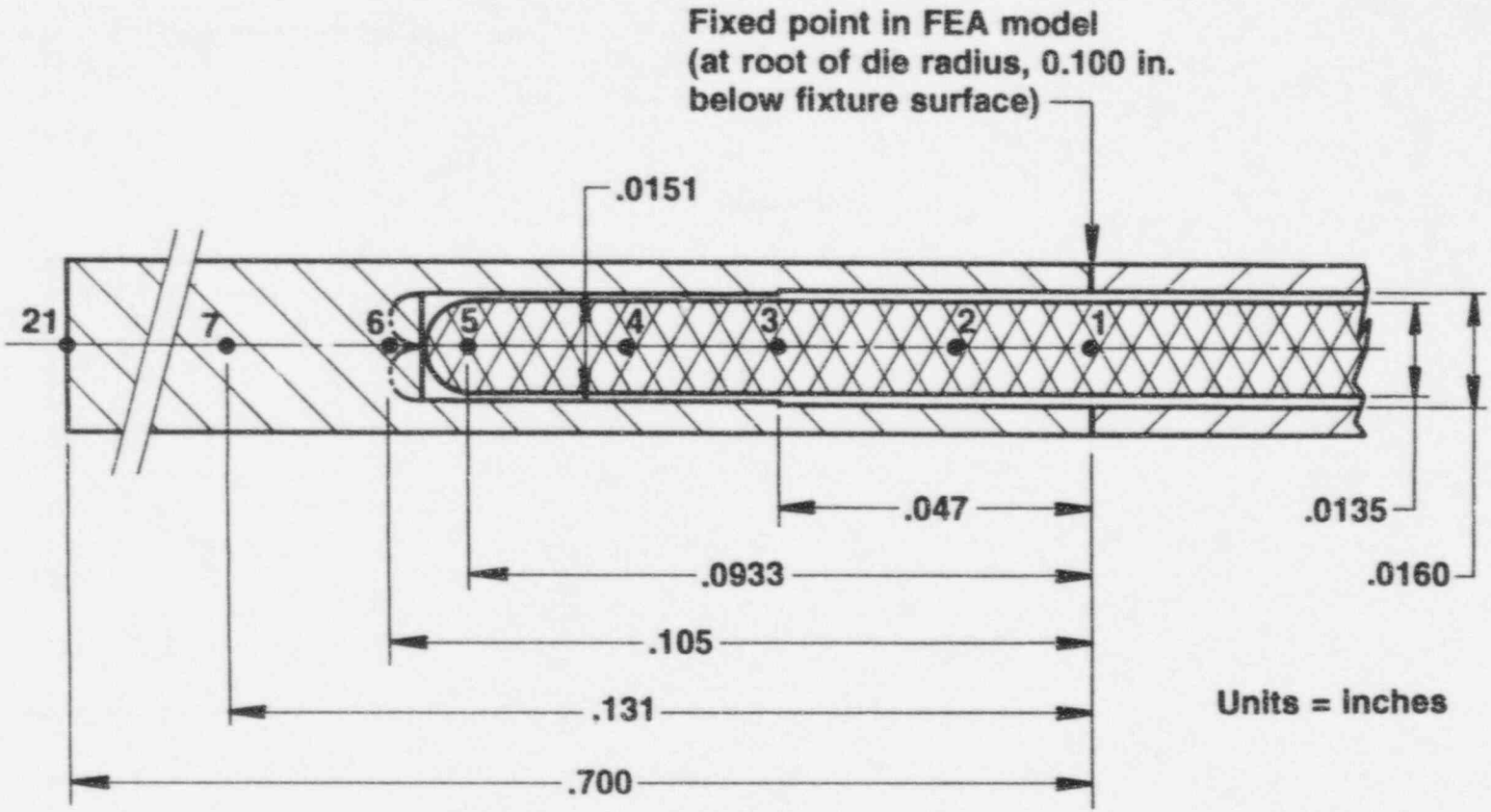

Figure A-3. Seed and Cavity Dimensions and Node Locations in the Finite Element Model

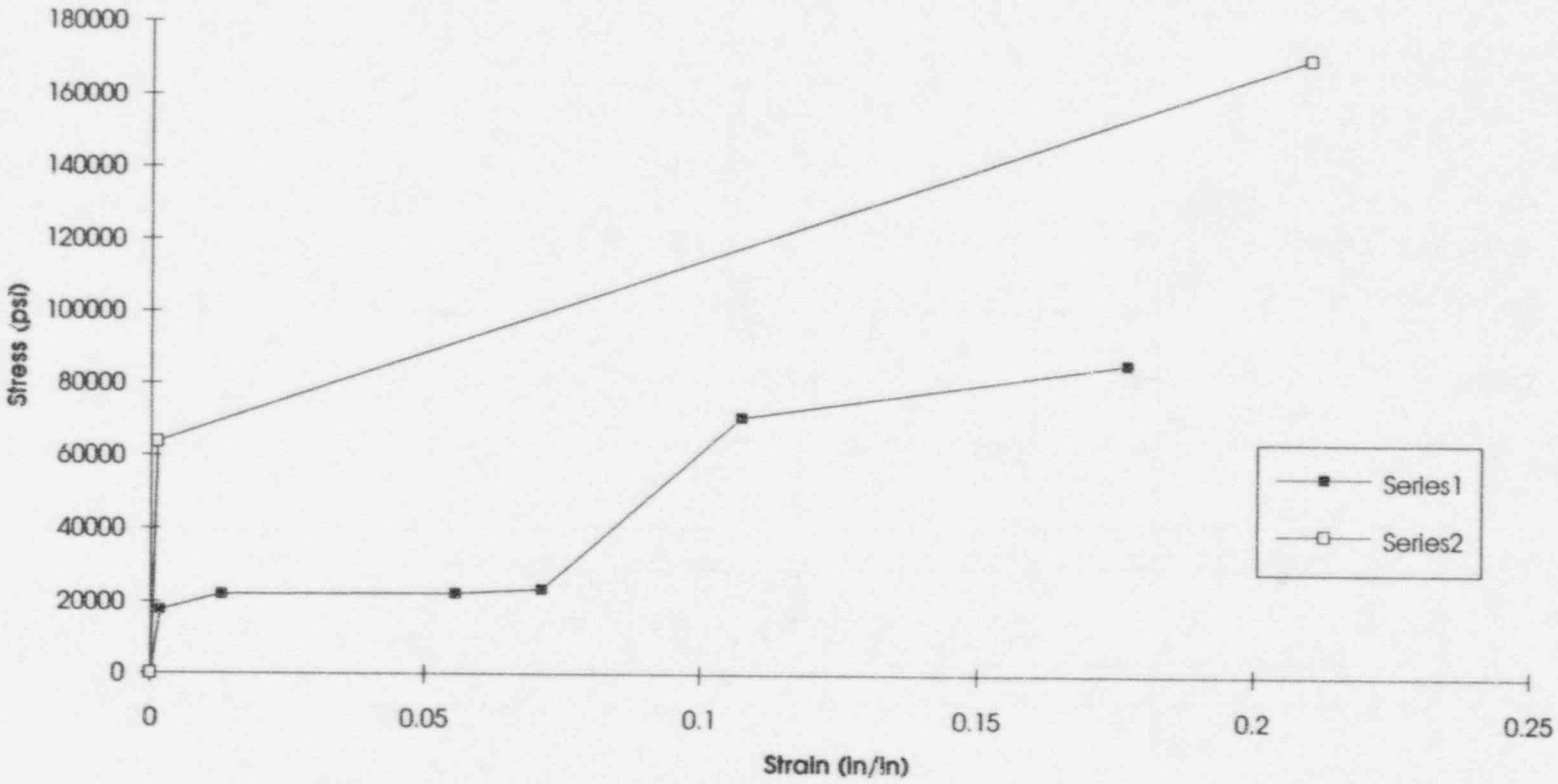

Figure A-4. Stress-Strain Properties of the Wire and Seed

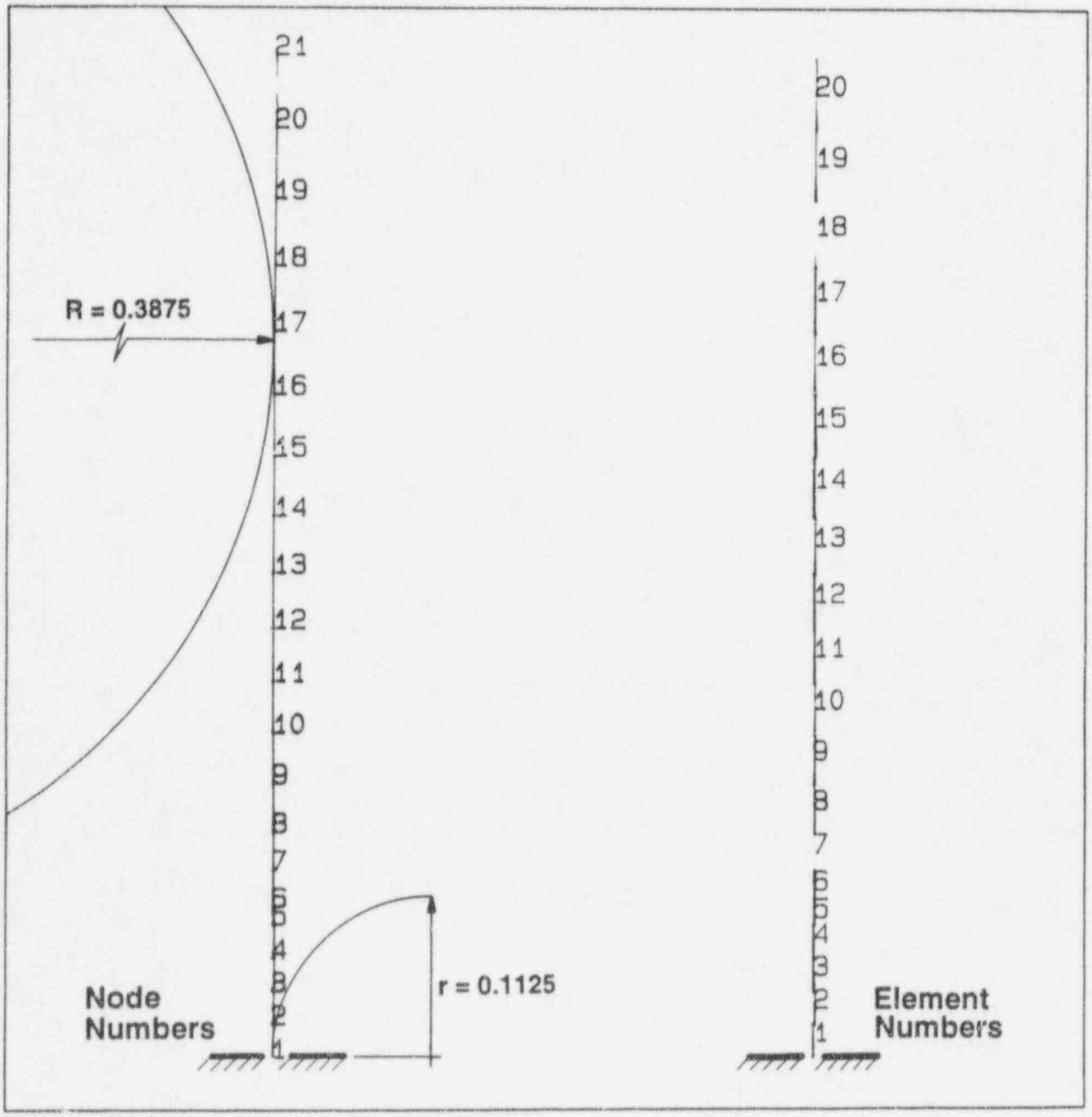

Figure A-5. Node and Element Numbers Along the Wire Model

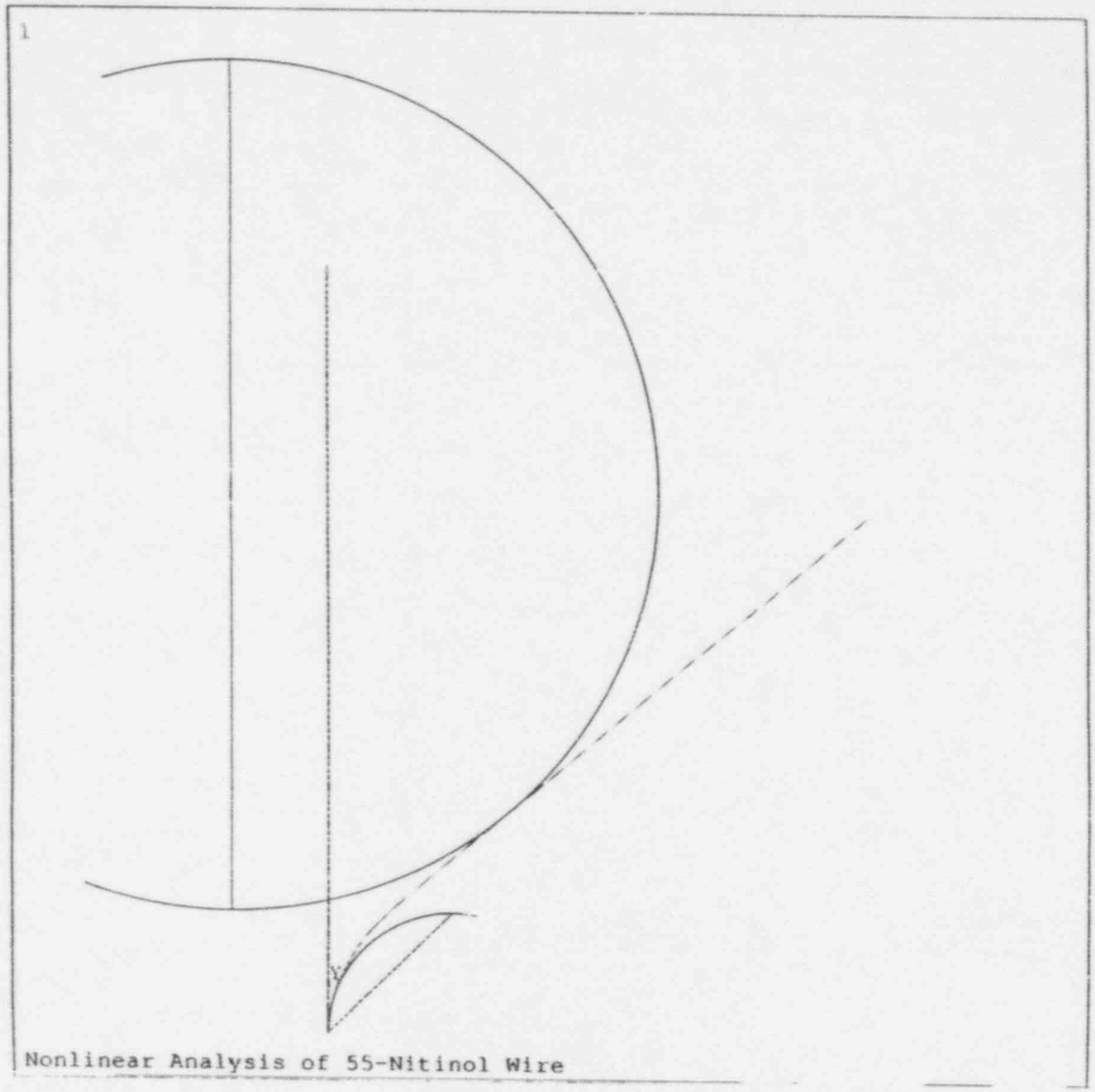

Figure A-6. Displaced Position of the Wire for Roller Displacement of 0.3 Inch

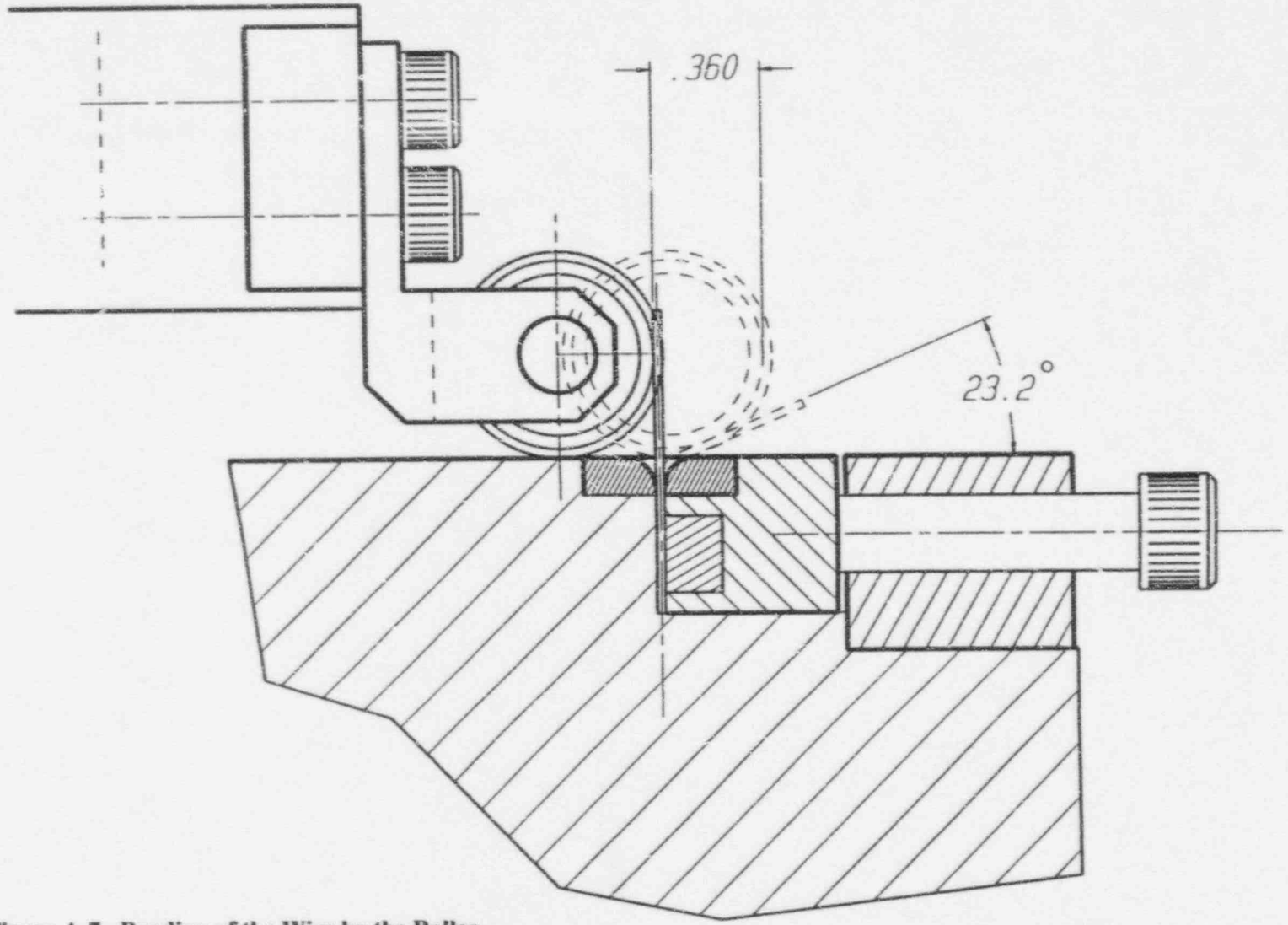

Figure A-7. Bending of the Wire by the Roller

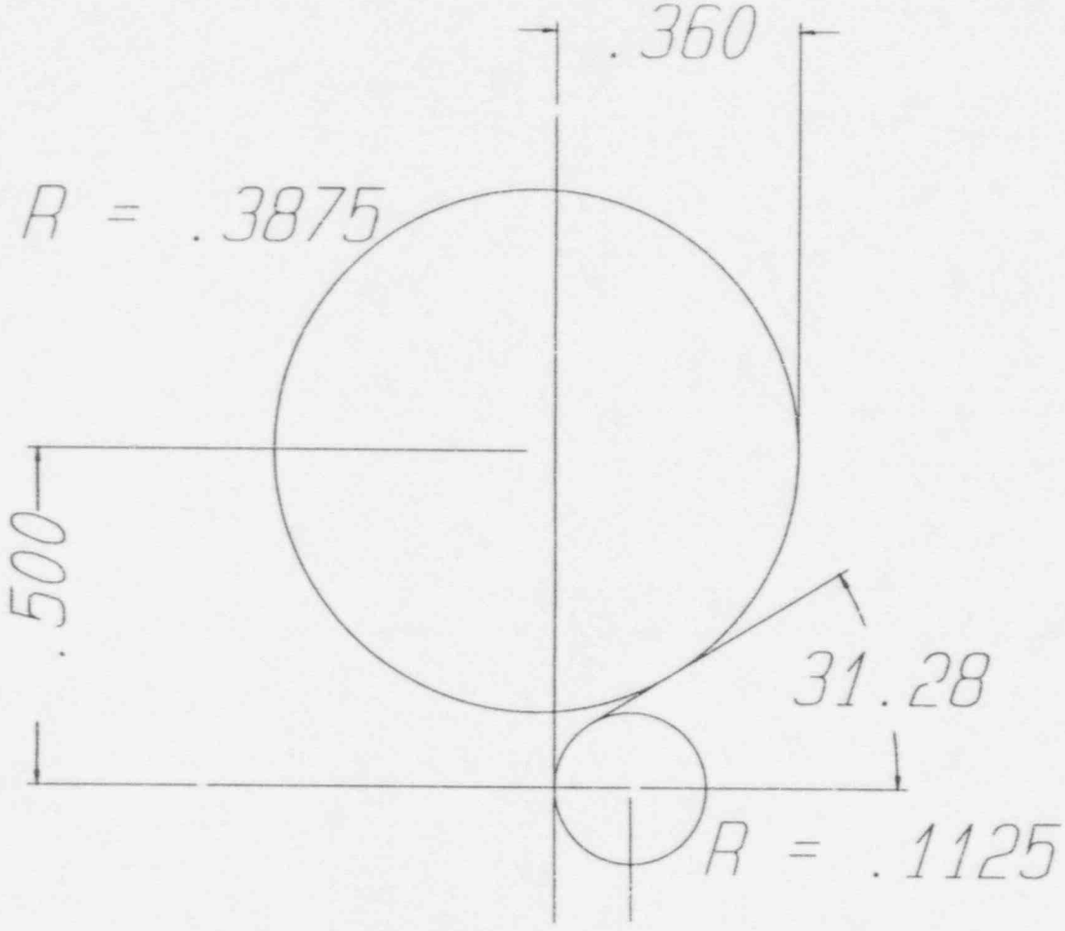

Figure A-8. Bending of the FEA Wire Centerline Model by the Roller

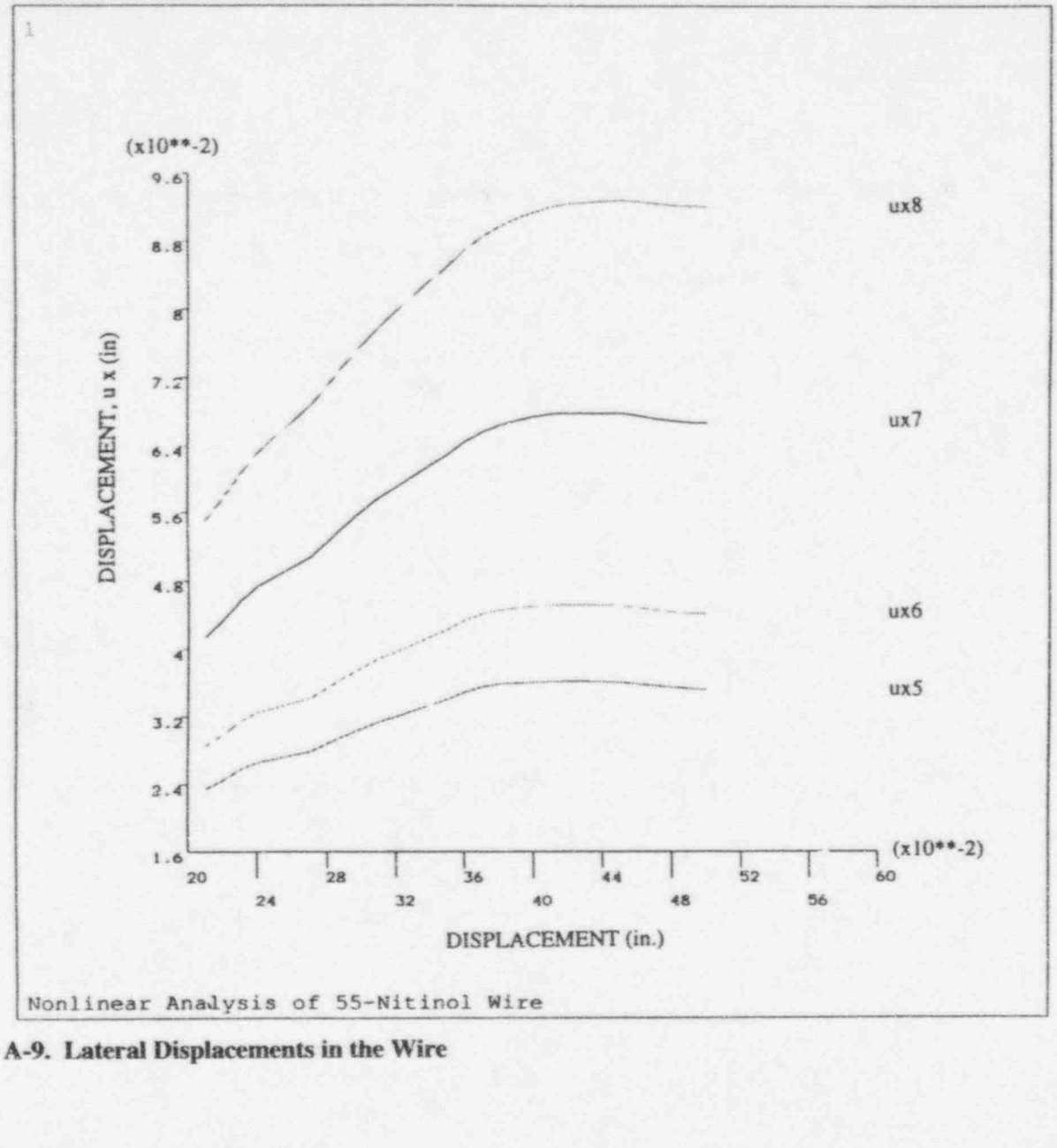

Figure A-9. Lateral Displacements in the Wire

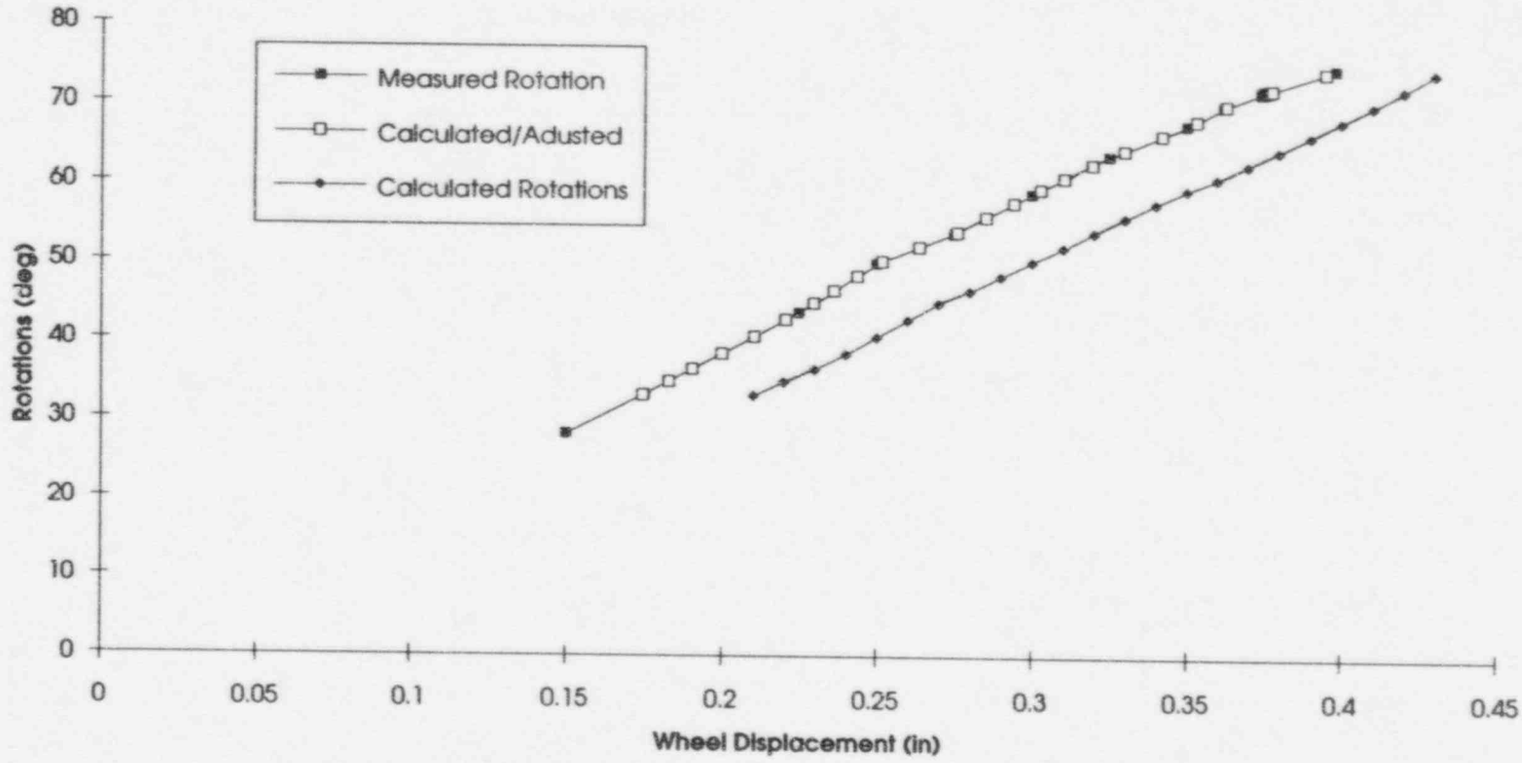

Figure A-10. Wire Rotations (Bend Angle): Measured, Calculated and Calculated/Adjusted

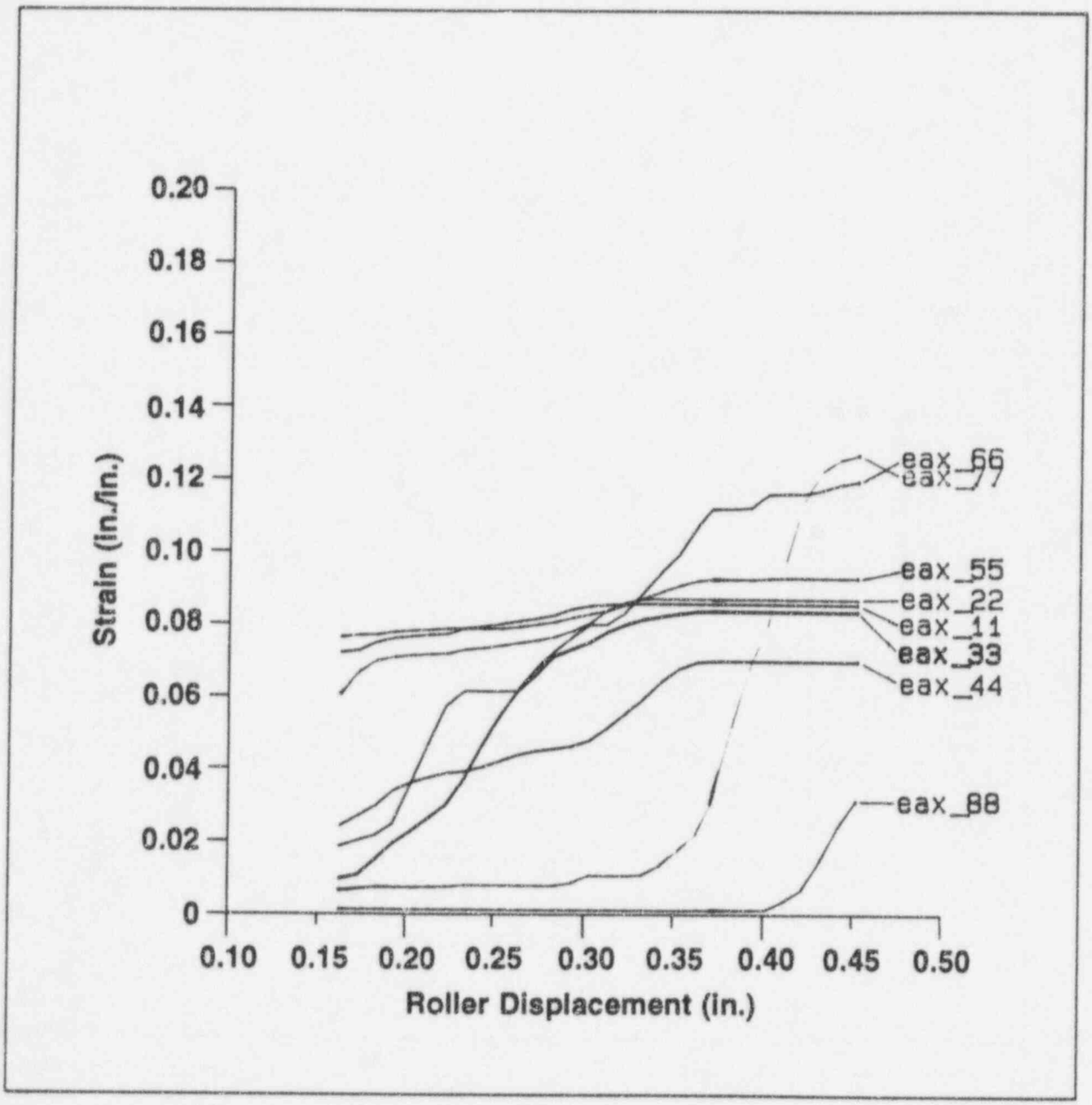

Figure A-11. Maximum Axial Strain on Wire Outer Surface.

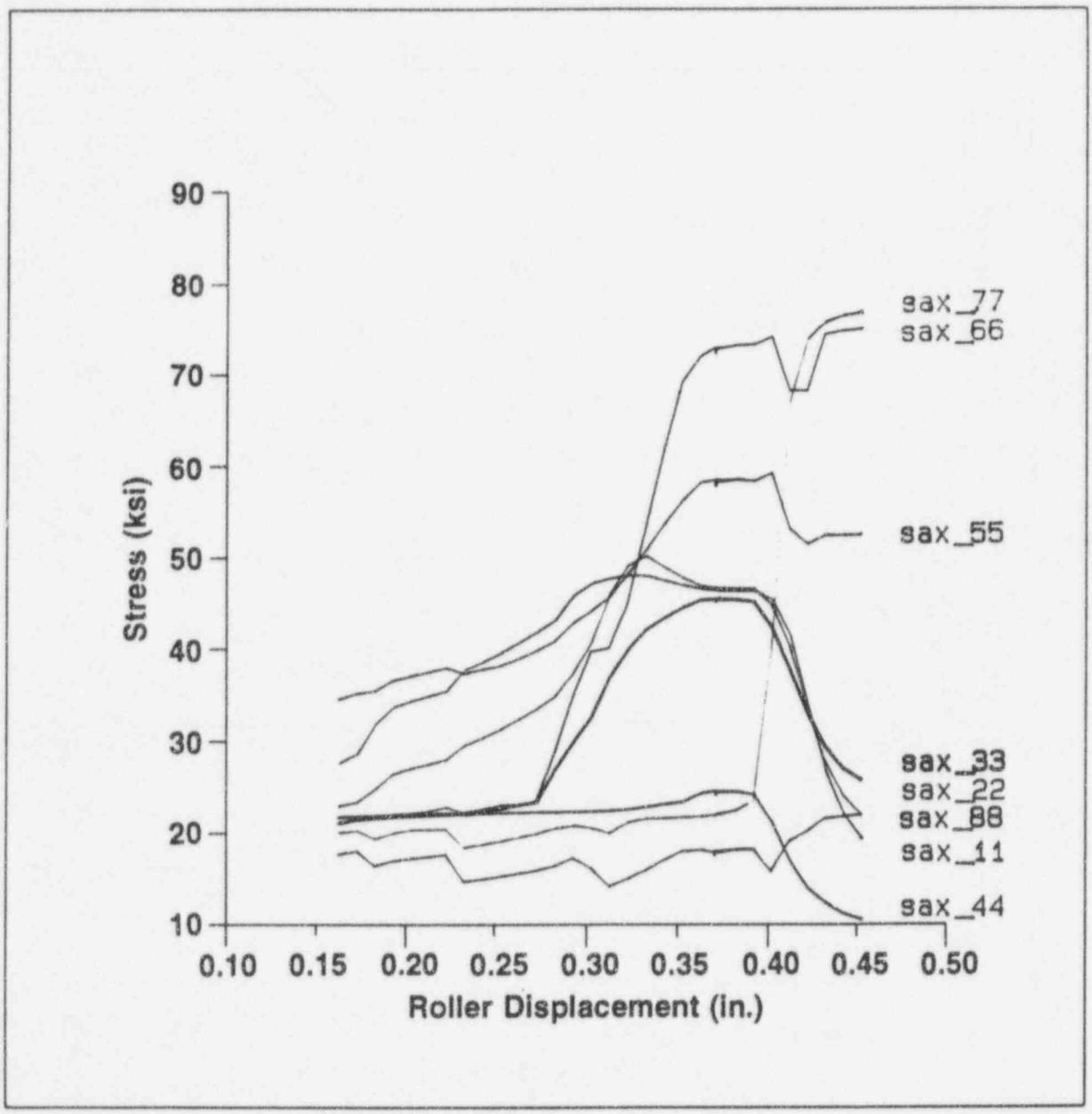

Figure A-12. Maximum Axial Stress on Wire Outer Surface.

APPENDIX B. FRACTOGRAPHIC EXAMINATION OF SOURCEWIRE BEND TEST SPECIMENS

1. SCOPE

As part of the bend test program, several of the sourcewires failed prior to extraction from the lead cask or during the bend test. This Appendix is the detailed fractographic examination of those failed wires. The Appendix includes SEM fractographs, observations on the failed wire, and discussion of fracture features. In this Appendix, included are discussions on dummy wires, SwRI Wire Nos. 435 and 436; the teflon exposed wires, SwRI Wire Nos. 421, 422, 423, and 429; the tensile overloaded wire, SwRI Wire No. 426, and a sourcewire, SwRI No. 442, which failed during the pretest.

2. METHODOLOGY

Wires that failed or required surface evaluation were examined using an Amray Scanning Electron Microscope (SEM) equipped with a Kevex Energy Dispersive X-ray (EDS) detector, and the Tracor Northern Computer System, shown in Figure B-1. Since the wire diameter was small, it was necessary to resolve fracture and surface features using the SEM. The EDS system enabled the wire to be examined for corrosion products or contamination. EDS is able to determine elements present on the surface and about 1 micron below the surface. Two types of detector windows were utilized, one was an ultra-thin window (UTW) which identifies lighter elements like fluorine and oxygen. The other window was a beryllium window which determines elements with a higher atomic weight than sodium.

3. FRACTOGRAPHIC EVALUATION

3.1 Dummy Wires

Both dummy wires, Nos. 435 and 436, were examined after bend testing using the SEM. Figures B-2, B-3, and B-4 show the OD surface at the inside bend radius, the outside bend radius and a location remote from the bend for Sample No. 435-2, which was the solid portion of the wire, after being deflected two times. The OD surface indicated transverse microcracks and surface blemishes. The surface blemishes were likely due to the grinding operation which removed the oxide film. After extreme bending to 90°, these blemishes likely resulted in microcracks. Since these blemishes were present at locations remote from the bend radius, it would indicate that the blemishes were inherent of the wire.

Figures B-5, B-6, and B-7 show similar SEM photographs of the inside bend radius, the outside bend radius and a location remote from the bend for Sample No. 436-1. The surface had similar blemishes, but more pronounced longitudinal scratches or gouges. There were no pronounced microcracks in the bend radius.

For purposes of comparison, the OD surface of a new wire with the oxide not removed is shown in Figure B-8. The current design of the wire does not call for removal of the protective oxide.

3.2 Teflon Lined Wires

SwRI Wire No. 421

SwRI Sample No. 421 was stored in PTPE for 222 days. After extraction from the lead storage cask, it was noticed that the wire had failed. The wire was broken into at least two sections, the other end containing the source stayed in the cask. The source remaining in the cask was not examined because it was excessively radioactive. Therefore, the end with minimum radioactivity was examined.

Figure B-9 shows that the wire failed in the solid section of the wire which was beyond cavity. Overall the fracture was smooth with some relief. There was no distinct flat zone. Figure B-10 shows that the OD of the wire had a dirty, layered appearance causing the sample to charge in the SEM. Figure B-11 shows a longitudinal crack through the center of the fracture. The fracture surface, even after ultrasonic cleaning in acetone, was covered with debris. Figures B-12 and B-13 show a close-up of some of the debris and fracture surface which was brittle in nature.

Energy dispersive X-ray spectra, shown in Figures B-14, B-15, B-16, and B-17, were generated on the OD of the wire and the fracture surface. The typical elements for Nitinol, titanium and nickel were identified. Additional elements identified included fluorine and oxygen. The fluorine obviously was a by-product of the teflon degradation. Figure B-51 shows that fluorine and carbon are the main elements for teflon. Even the fracture surface had significant amounts of fluorine present after cleaning the surface.

SwRI Wire No. 422

Wire sample No. 422 was stored in teflon 142 days. The wire was still intact and was not severed or deteriorated after extraction from the storage cask. The wire was bend tested and failed. Figure B-18 shows that the break occurred in the solid section of the wire. The fracture plane was angled at 30° from the axis of the wire. The diameter of the wire was uniform and measured 0.021 inch. The fracture surface was smeared and had shear marks on the surface. Figures B-19 and B-20 show that shear dimples were present in several locations. Microfracture features of the dimples indicate a shear, tearing failure occurred. The direction of the dimples and the elongated fracture flow lines indicated the fracture progressed along the slant fracture. Figure B-21 shows the OD surface had some evidence of contamination or debris build-up. EDS spectra, shown in Figure B-22, determined typical elements of titanium, and nickel about 3/8 of an inch away. Adjacent to the fracture, fluorine, oxygen, sodium, potassium, and aluminum were all identified.

SwRI Wire No. 423

Wire Sample No. 423 was stored in PTFE for 103 days, after extracting from the lead storage cask the wire was noticed failed. No bend test was performed on this wire. SEM fractography, shown in Figures B-23 and B-24, shows that the fracture occurred at the base of the cavity. Figures B-25 and B-26 show the fracture was burnished. Figure B-27 shows the fracture surface was covered with a film, oxide, etc. The wire did not display a layered surface appearance as wire Sample No. 421, see Figure B-10. No distinct or definitive fracture features were evident.

The profile of the failed wire showed a slight slant from two opposite sides of about 20°. The radial flow lines may be indicative of initiation on the inside diameter. The OD surface of the wire in the vicinity of the fracture appeared to have some residual material on the surface. However, the material was not deteriorated. The wall thickness of the cavity was not thinned and was uniform throughout. The diameter of the wire measured 0.020 from the SEM photograph.

SwRI Wire No. 429

Wire Sample No. 429 was exposed to PTFE for six days during shipment to the clinic, put in service and subsequently stored in stainless steel for 199 days in a cask. Sample No. 429 was extracted from the storage rig. The wire was still intact and was not severed or deteriorated. Subsequently, the wire was bend tested. After the slotted wheel displaced 0.201 inches and the wire deflected 37°, failure occurred.

Figure B-28 and B-29 show that failure occurred at the base of the cavity. A flat region existed for 50% of the fracture surface, then a steep slant occurred which eventually failed through the OD. The tip of the slanted portion extended about 0.016 inches from the flat region. The OD measured 0.022 inches. Figure B-30 shows the OD surface with a darkened network that appeared to etch or attack the surface. A stereo pair, shown in Figure B-31, identified the network to be small cracks.

Crack initiation likely occurred on the ID in the flat zone. Figure B-32 shows ratchet marks adjacent to the ID surface. The EDM surface, shown in Figure B-33, had small microcracks but no flaw was present to initiate failure. This same location had unusual fine-scale equiaxed dimple-like microfeatures, shown in Figure B-34. A penny-shaped region existed with fine scale dimples. The length of this region was about 0.005 inch. As one progressed from the penny-shaped region in either direction on the fracture, the dimples became broader. Figures B-35 through B-39 are fractographs at various locations on the fracture. This dimple-like pattern progressed around the wire and up the slanted portion of the fracture. On the slanted portion, the dimples were elongated, typical of a shear or tear dimple.

Figure B-36 shows that a ridge, which was possibly a shear lip, was present around the outer circumference. There was also a flat feature on the edge. A unique feature found on the OD surface in the vicinity of the fracture was a network of surface attack. EDS analysis, shown in Figure B-40, identified nickel, titanium, oxygen, fluorine, and aluminum in this region.

3.3 Wires Stored in Stainless Steel Needles

SwRI Wire No. 426

SwRI No. 426 was stored in a stainless steel needle in a lead cask for 131 days. Afterwards, a pre-test was conducted to evaluate if the material was embrittled. The wire was deflected nearly 90° when the wire broke. An SEM examination was conducted to characterize the failure.

Figure B-41 shows that the failure occurred adjacent to the cavity bottom, about 0.024 inch from the bottom. Distinct necking and thinning occurred on one side of the wire where the failure initiated. The wall measured 0.0022 inch in the thinned section. Away from the thinned wall, the wall was about 0.0050 inch. The wall thinning is an indication that the wire was overloaded. Figure B-42 shows the thinned wall as viewed from the cavity. The thinned wall was slanted, typical of overload failure, shown in Figure B-43. Some microcracking of the ID scale on the cavity was also evident, see Figure B-44. The fracture surface was characterized at several locations along the fracture surface, shown in Figures B-45 through B-48. Figure B-45 shows flattened equiaxed dimples in the thinned location. At the locations shown in Figures B-46, B-47, and B-48, the dimples are more elongated and textured. In the thick zone, shown in Figure B-45, fracture flow lines from the ID of the wall proceeded outward. This location was the final failure area.

SwRI Wire No. 442

SwRI No. 442 was stored in a stainless steel needle in a cask. During the bend test, the wire unexpectedly failed. Figure B-49 shows the macroscopic features. A side view of the fracture plane, shown in Figure B-40, indicated that the wire had yielded at the fracture plane away from the cavity bottom. The fracture features were dimpled typical of an overload condition. In contrast, the brittle failures that had dimpling did not yield. A longitudinal fracture surface existed. Figure B-51 shows the microfracture features on each longitudinal split. The elongated and stretched dimples suggest failure proceeded from the yielded region along the longitudinal plane. The final fracture area, shown in Figure B-52, shows the fracture extending from the ID surface towards the OD surface. Because the wire yielded away from the cavity base, it can be concluded that the wire was inadvertently overloaded. The wire overloaded prematurely because the wire was not bottomed-out in the test fixture properly.

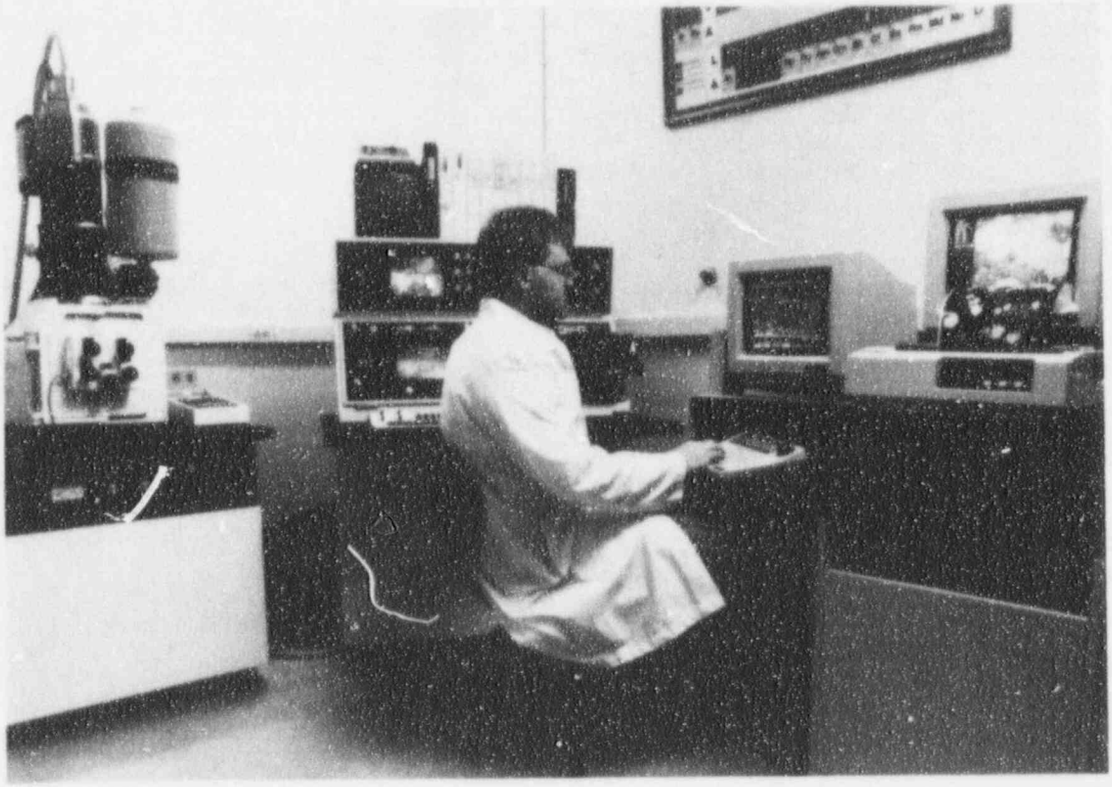

Figure B-1. Photograph of the Scanning Electron Microscope and Energy Dispersive X-Ray System

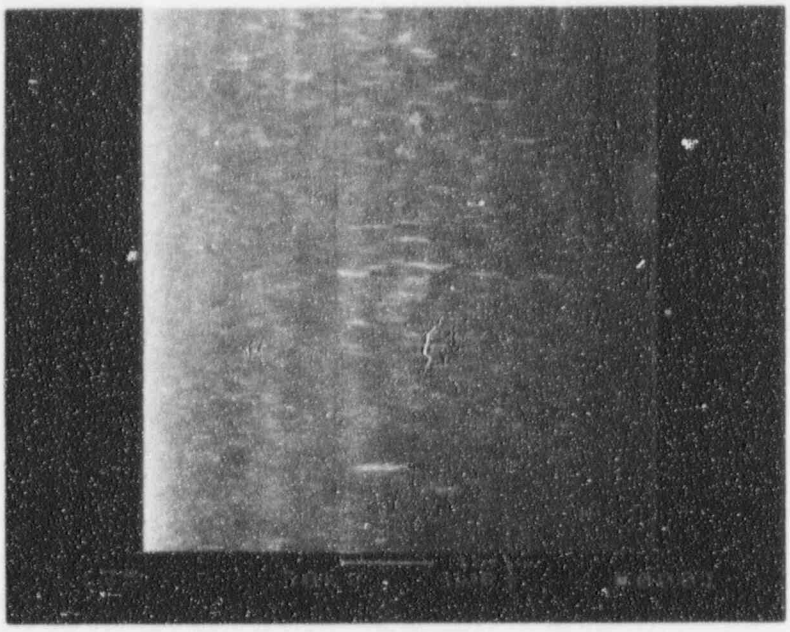

61935 135X

a)

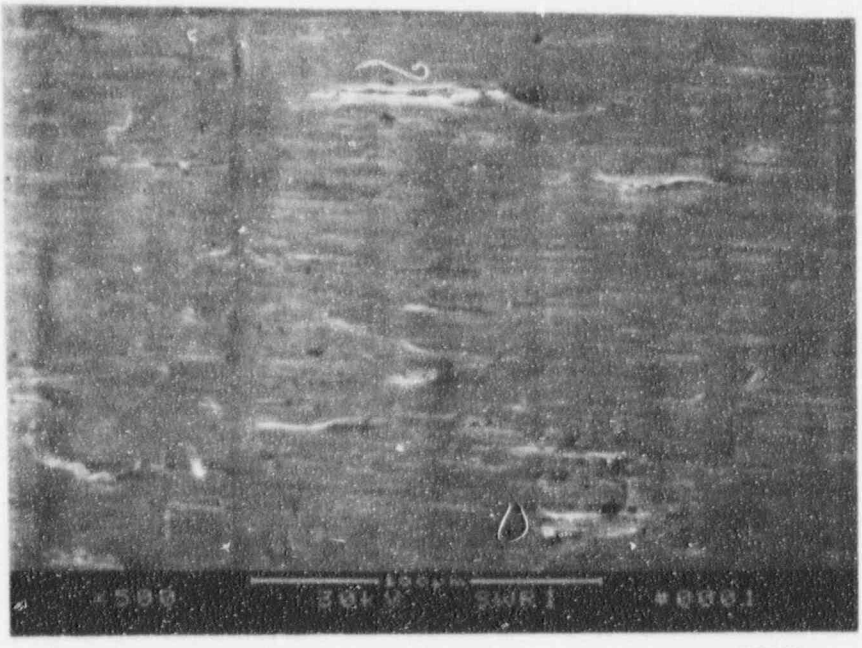

61936 500X

b)

Figure B-2. SEM Photographs of OD Surface at the Inside Bend for SwRI Wire No. 435-2

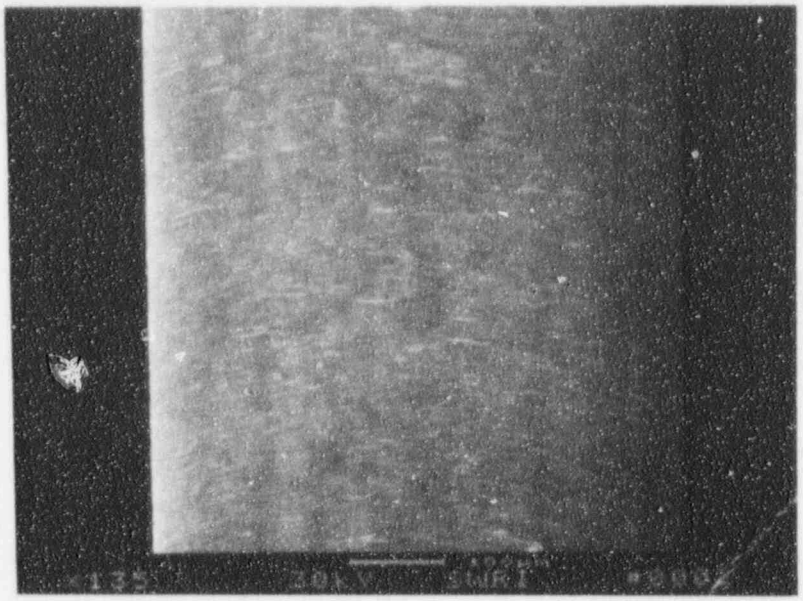

61937 135X

a)

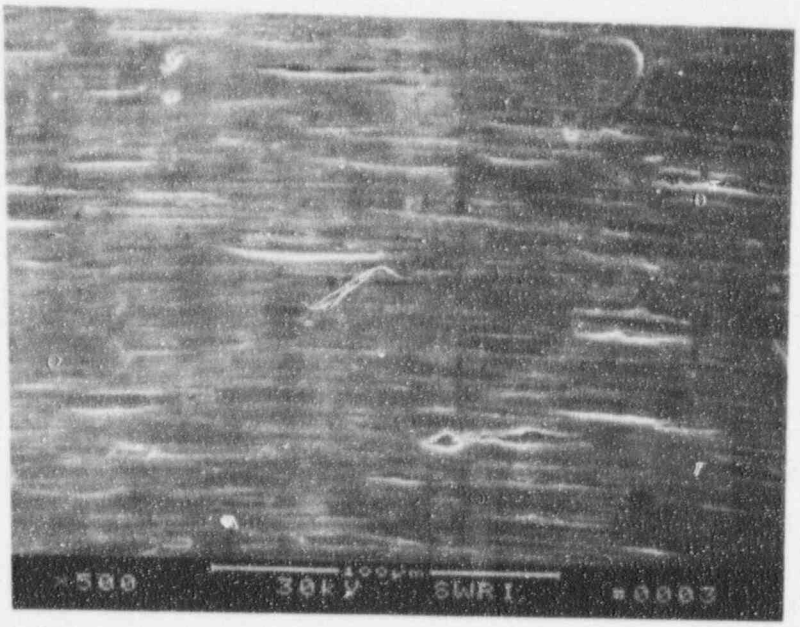

61938 500X

b)

Figure B-3. SEM Photographs of OD Surface at the Outside Bend for SwRI Wire No. 435-2

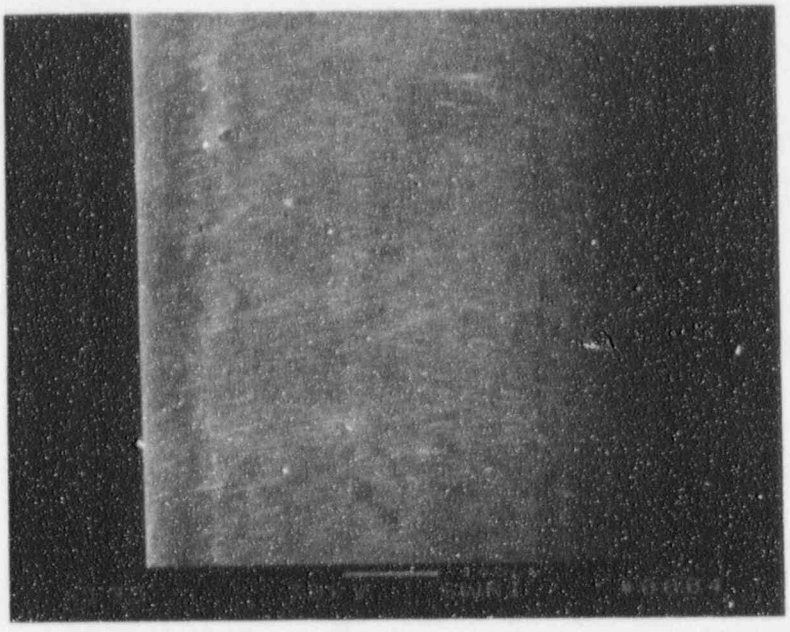

61939 135X

a)

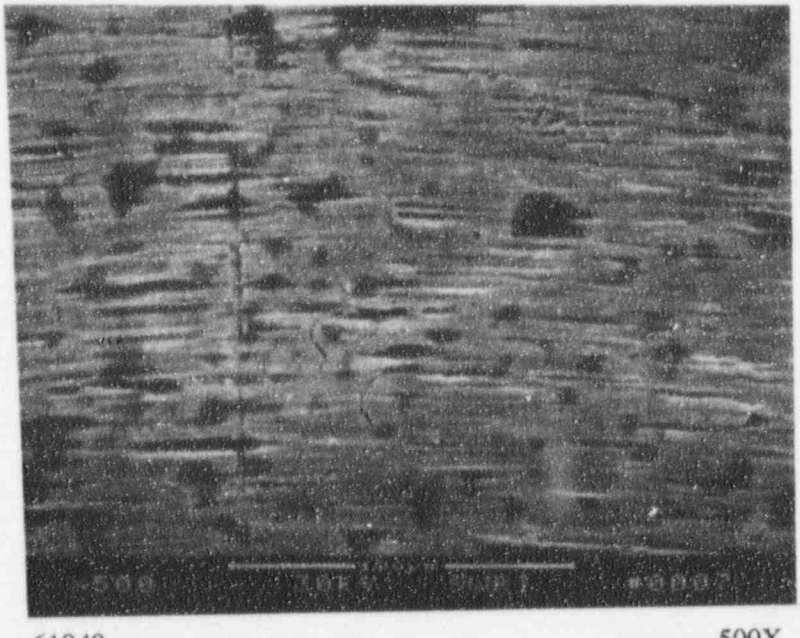

61940 500X

b)

Figure B-4. SEM Photographs of the OD Surface Away from the Bend Radius for SwRI Wire No. 435-2

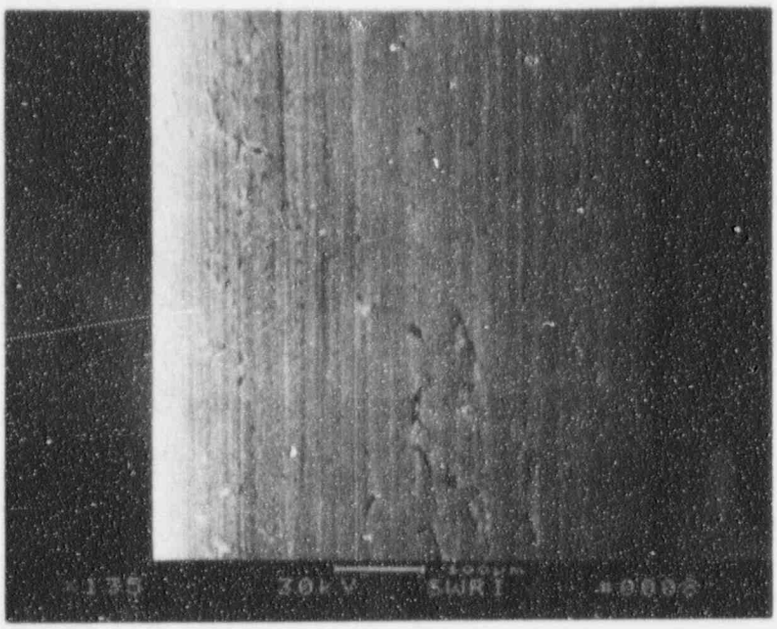

61920 135X

a)

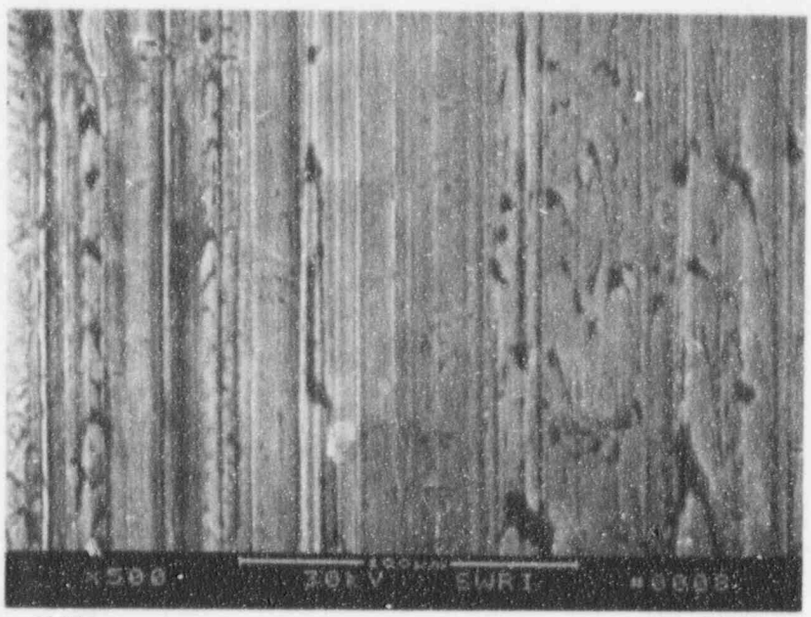

61921 500X

b)

Figure B-5. SEM Photographs of the OD Surface at the Inside Bend for SwRI Wire No. 436-1

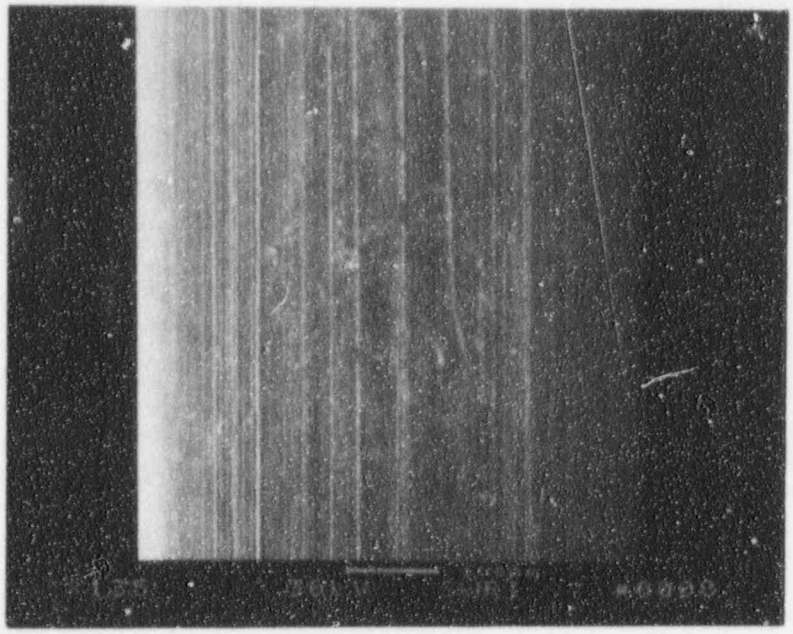

61922 135X

a)

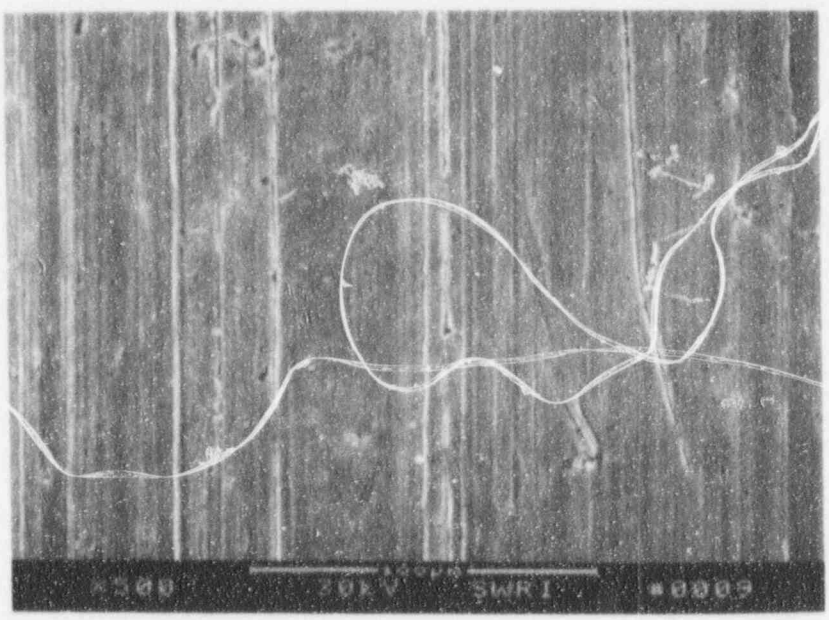

61923 500X

b)

Figure B-6. SEM Photographs of OD Surface at the Outside Bend for SwRI Wire No. 436-1

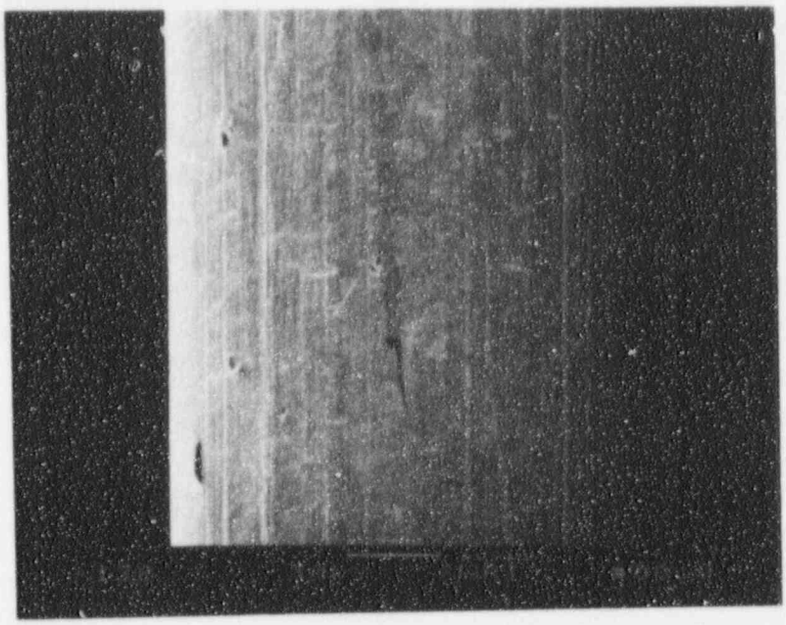

61924 138X

a)

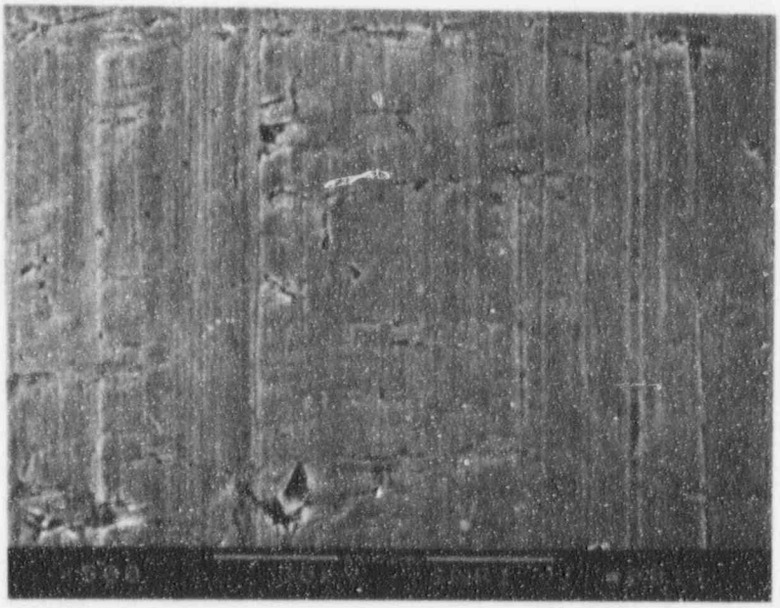

61925 500X

b)

Figure B-7. SEM Photographs of the OD Surface Away from the Bend Radius for SwRI Wire No. 436-1

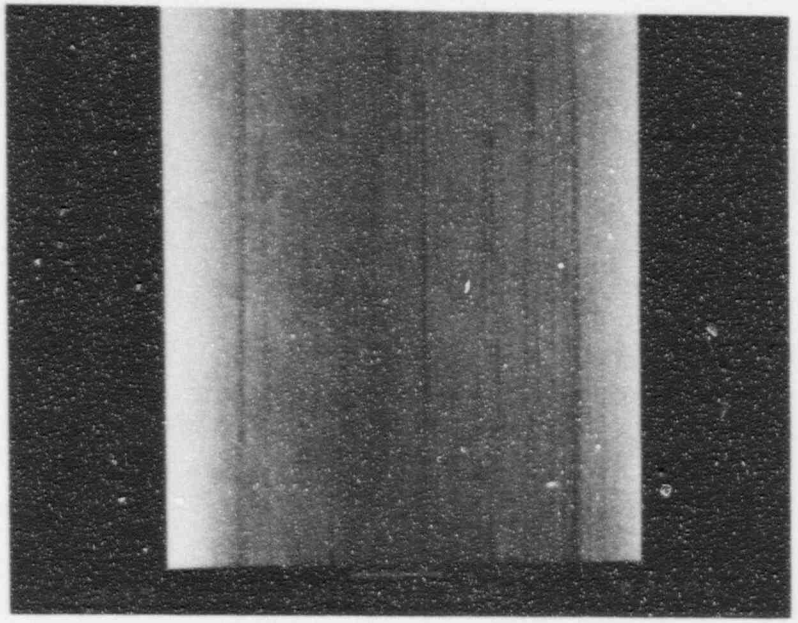

62925 135X

a)

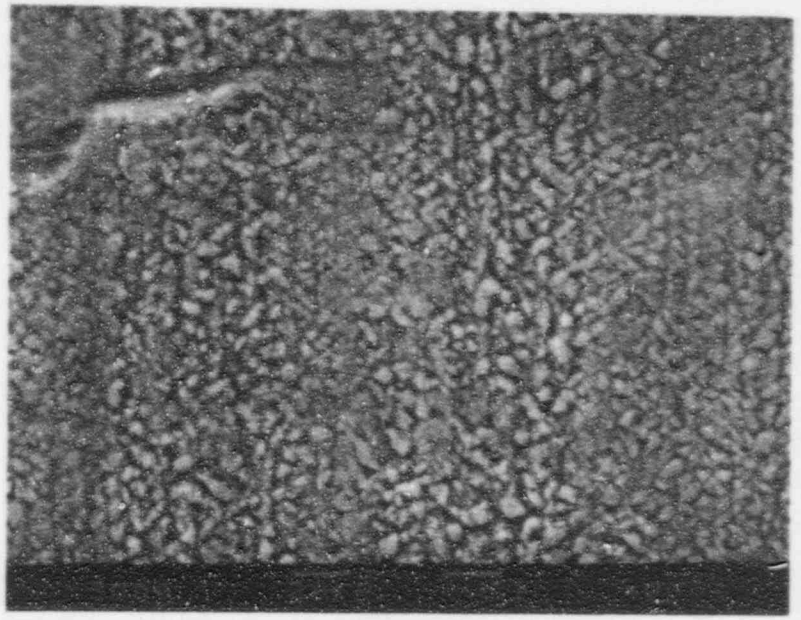

62927 3000X

c)

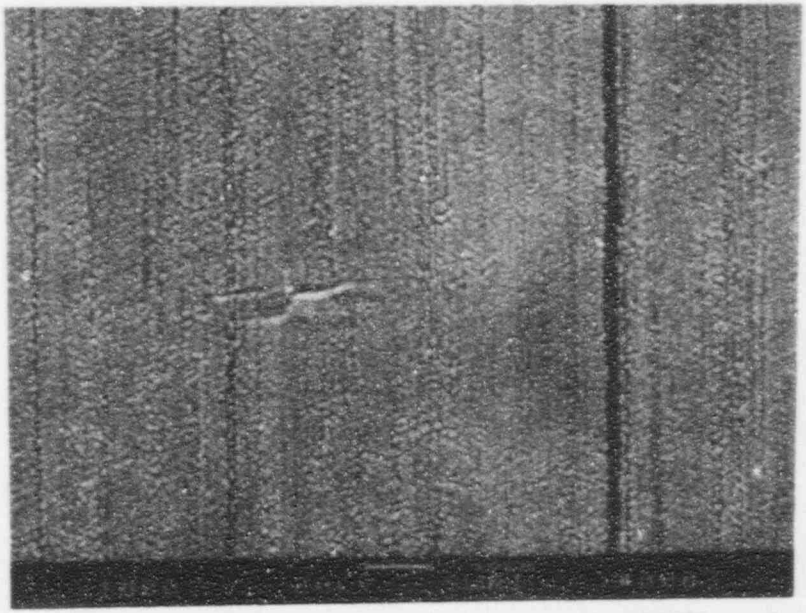

62926 1000X

b)

Figure B-8. SEM Photographs of the OD Wire with the Protective Coating Not Removed

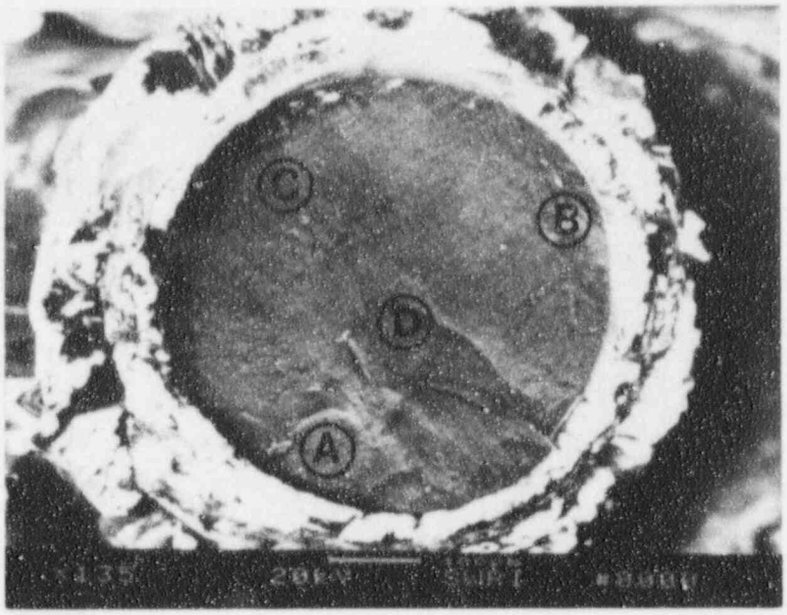

61943 135X

a) View Looking Down on Fracture

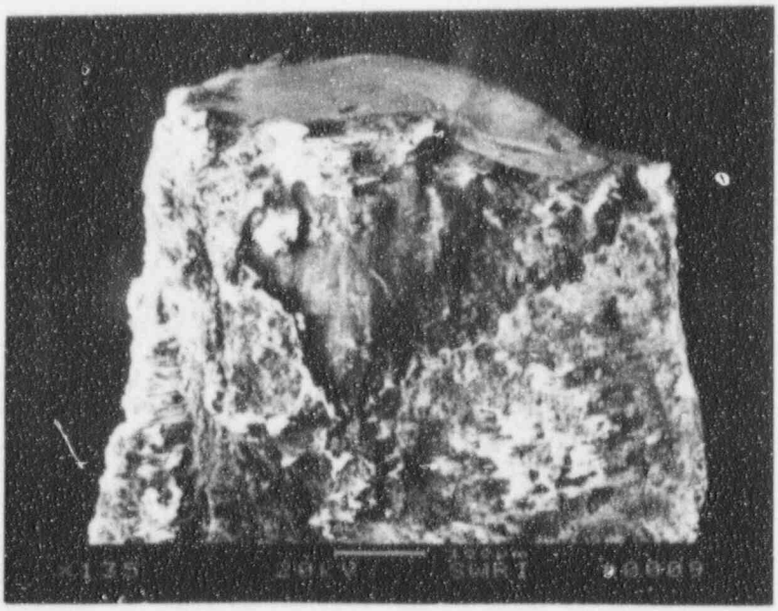

61951 135X

b) Side View

Figure B-9. SEM Fractographs of SwRI Wire No. 421-1

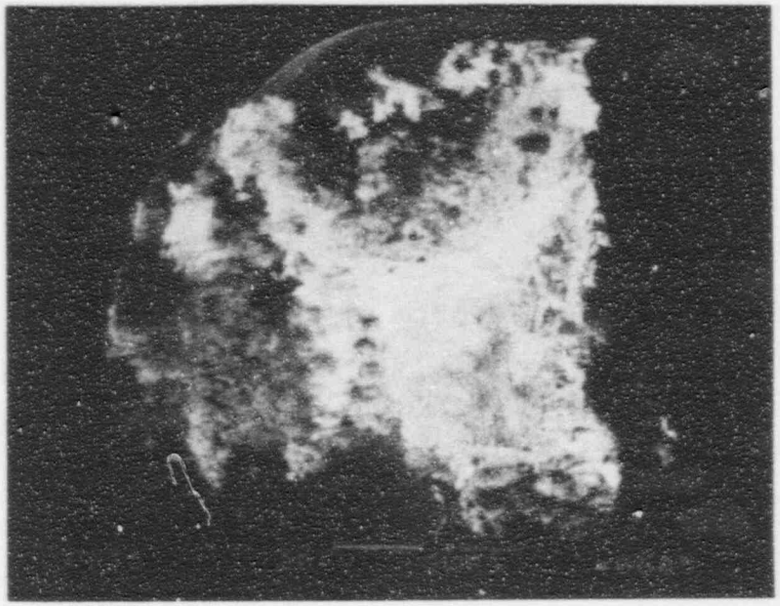

62905 135X

a) Location 1

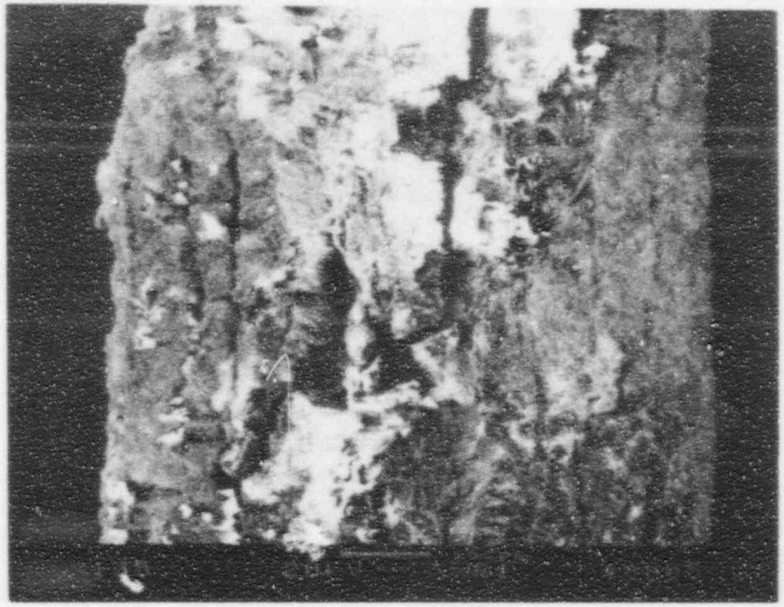

62904 135X

b) Location 2

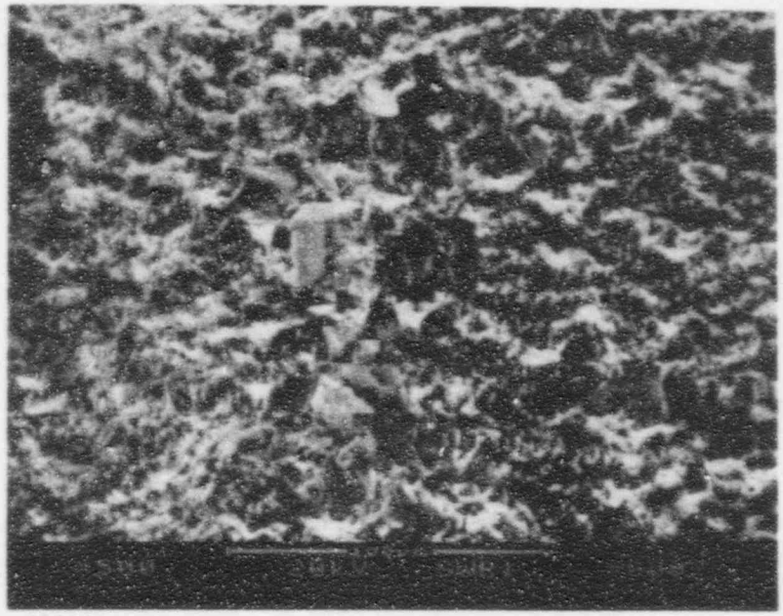

62903 500X

c) Location 3

Figure B-10. SEM Photographs of the OD Surface for SwRI Wire No. 421-1

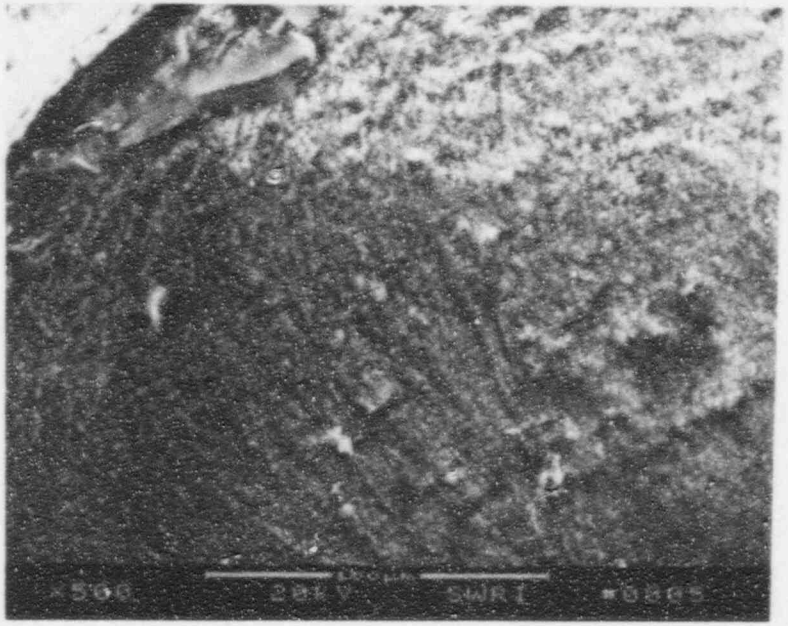

61946 500X

a) Location C

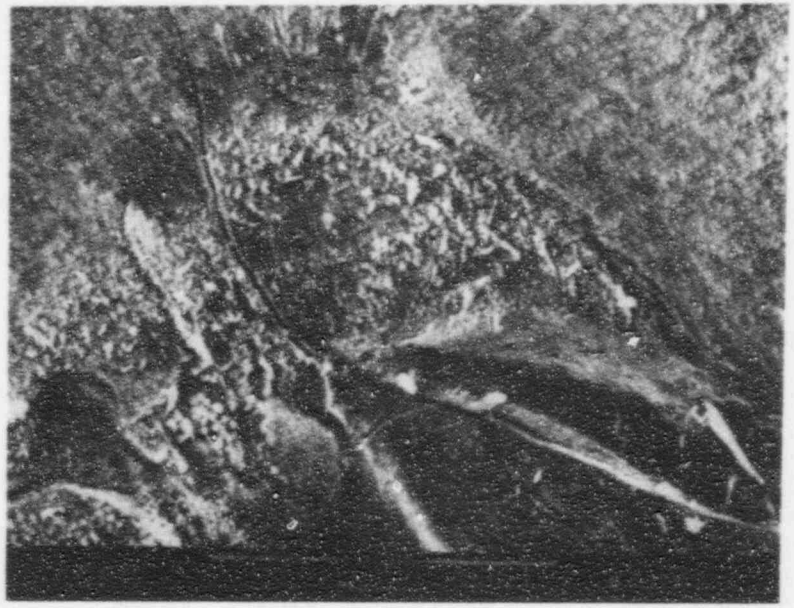

61947 500X

b) Location D

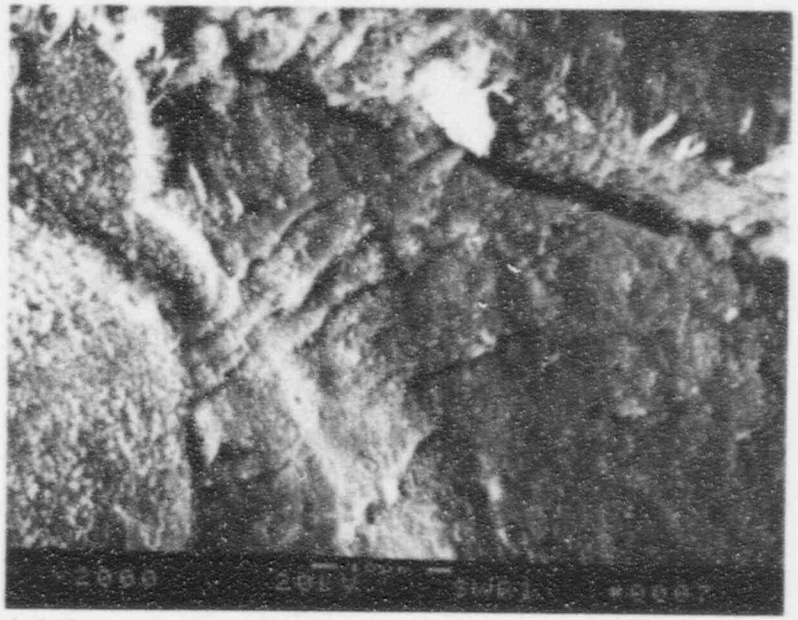

61948 2000X

c) Location D

Figure B-11. SEM Fractographs of Locations C and D on Wire Sample No. 421-1 in Uncleaned Condition

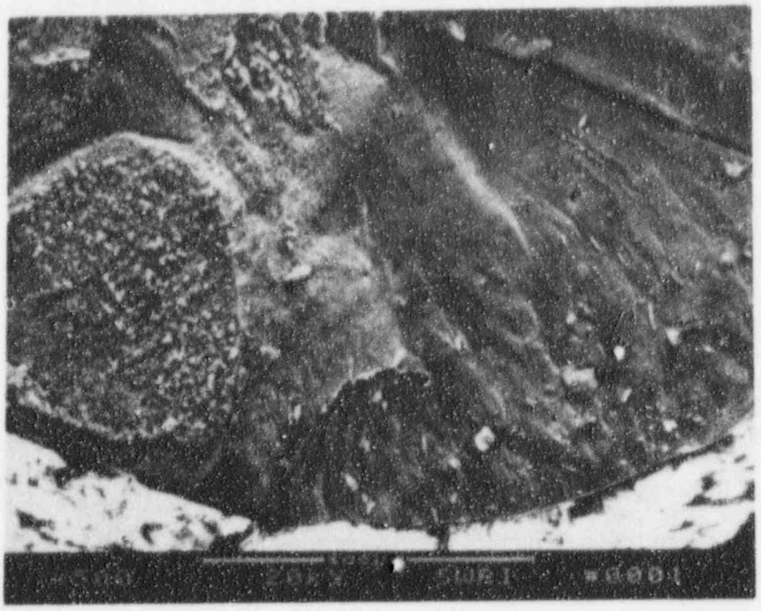

61944 500X

a)

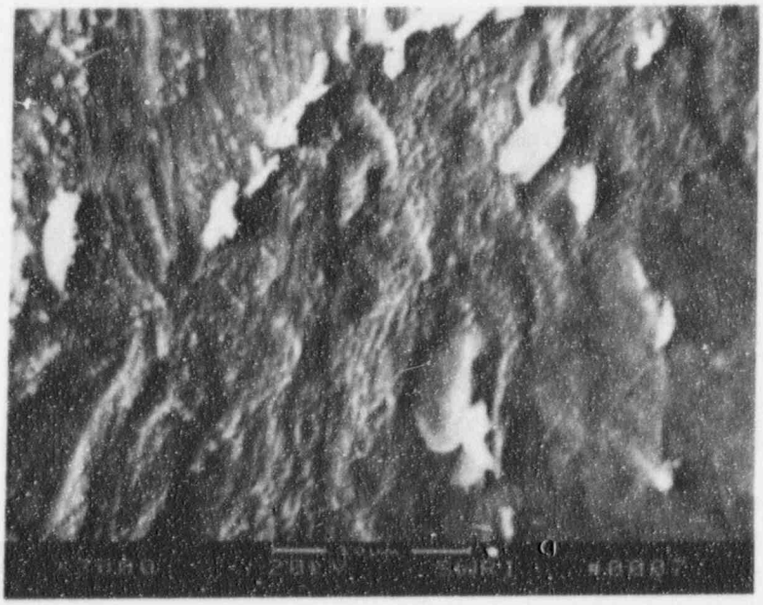

61949 3000X

b)

Figure B-12. SEM Fractographs of Location A on Wire Sample No. 421-1 in Uncleaned Condition

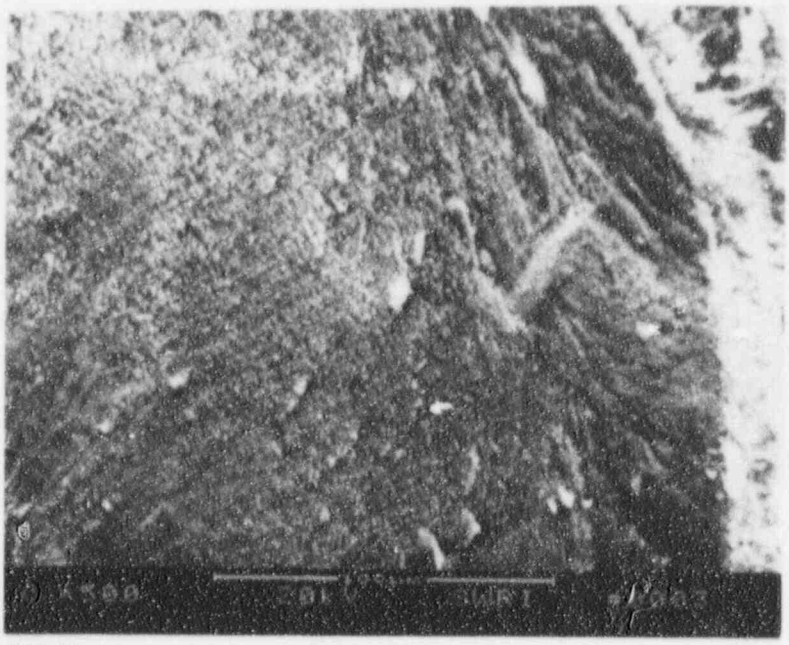

61945 500X

a)

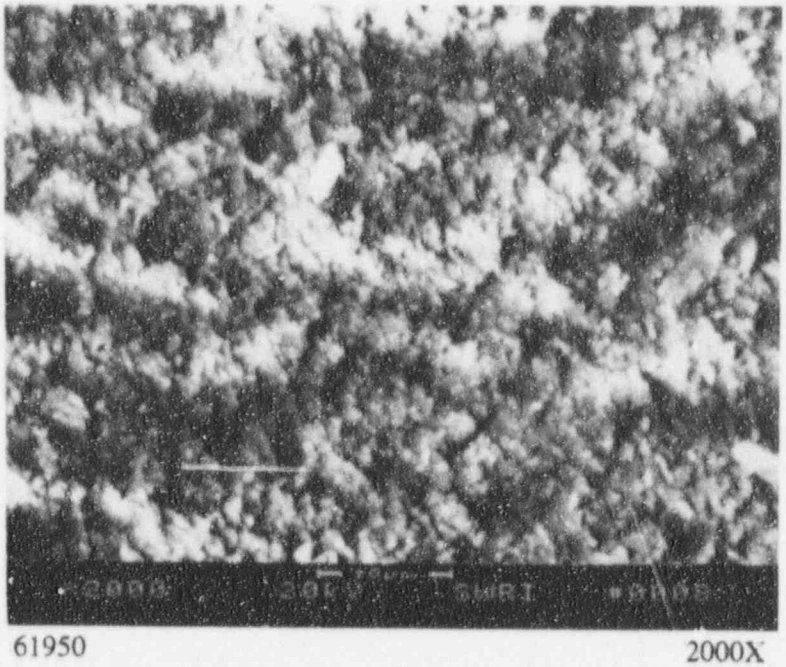

61950 2000X

b)

Figure B-13. SEM Fractographs of Location B on Wire Sample No. 421-1 in Uncleaned Condition

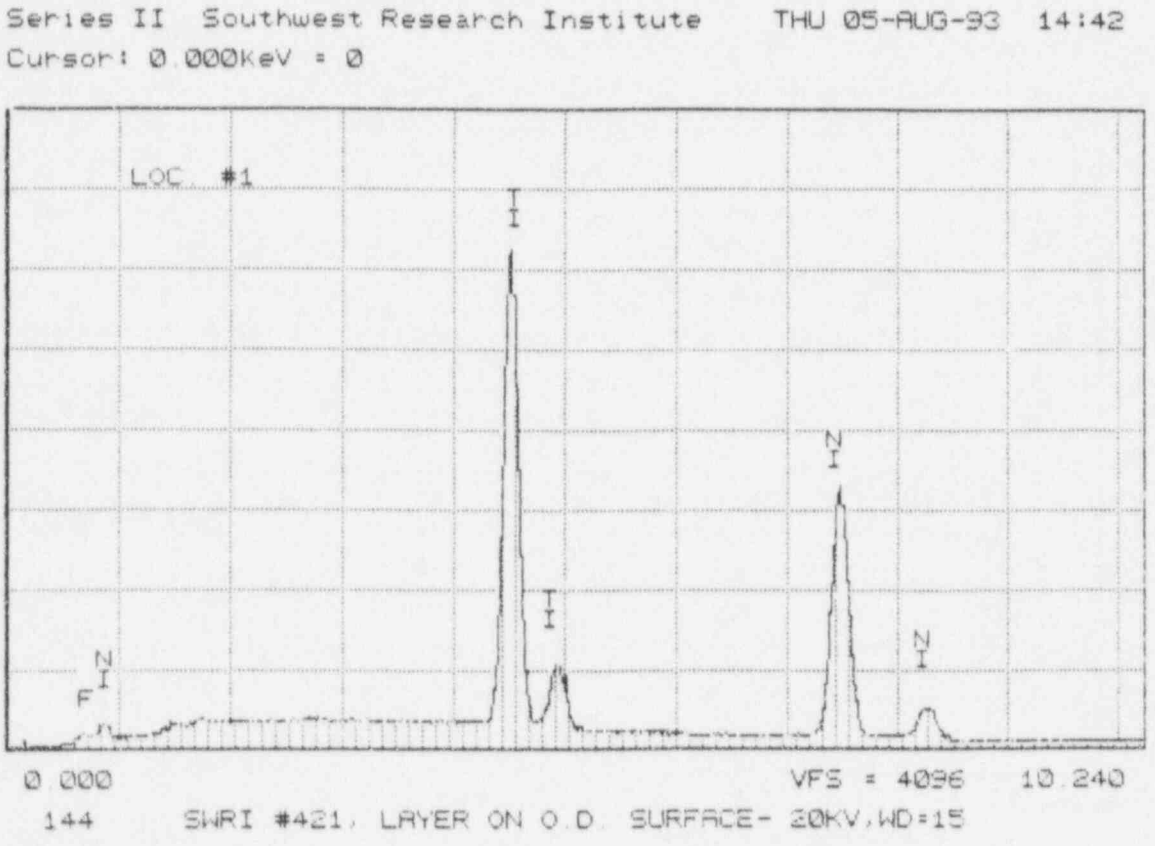

Figure B-14. Energy Dispersive X-Ray Spectra for the OD of SwRI Wire No. 421-1, Location 1

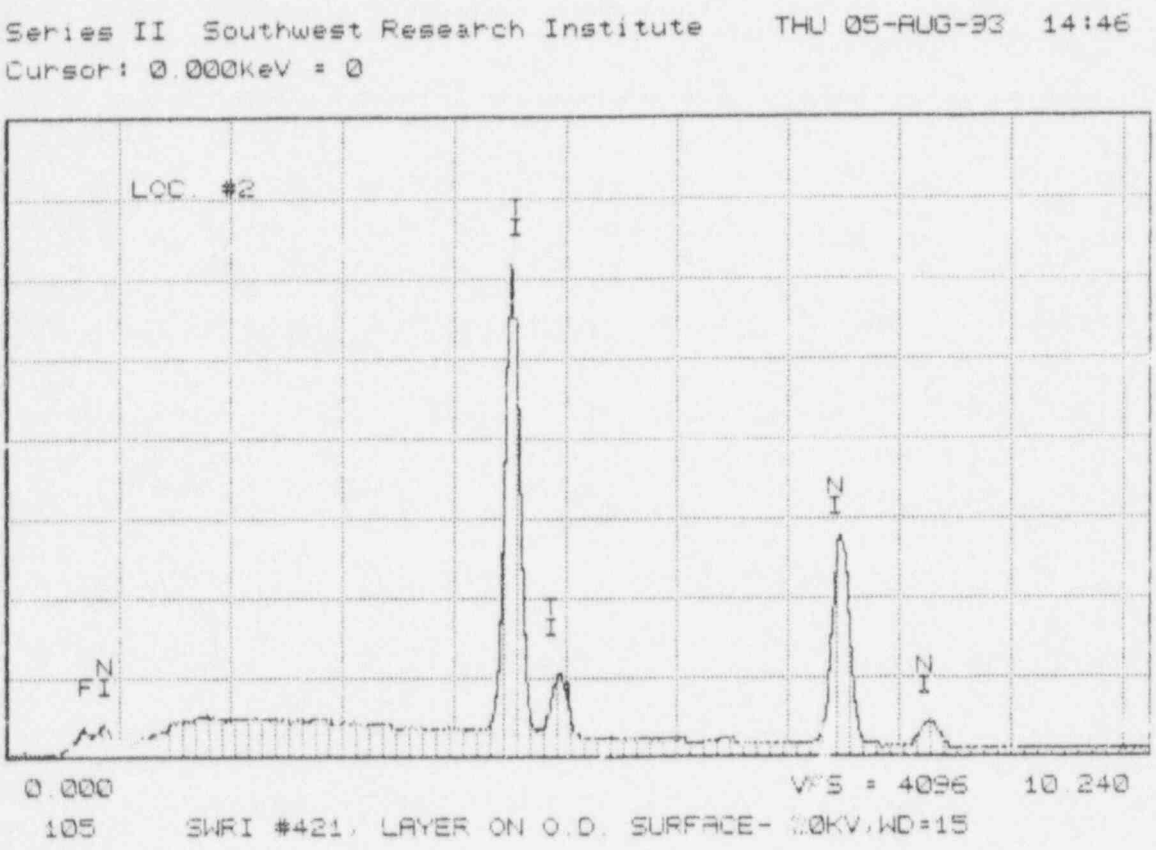

Figure B-15. Energy Dispersive X-Ray Spectra for the OD of SwRI Wire No. 421-1, Location 2

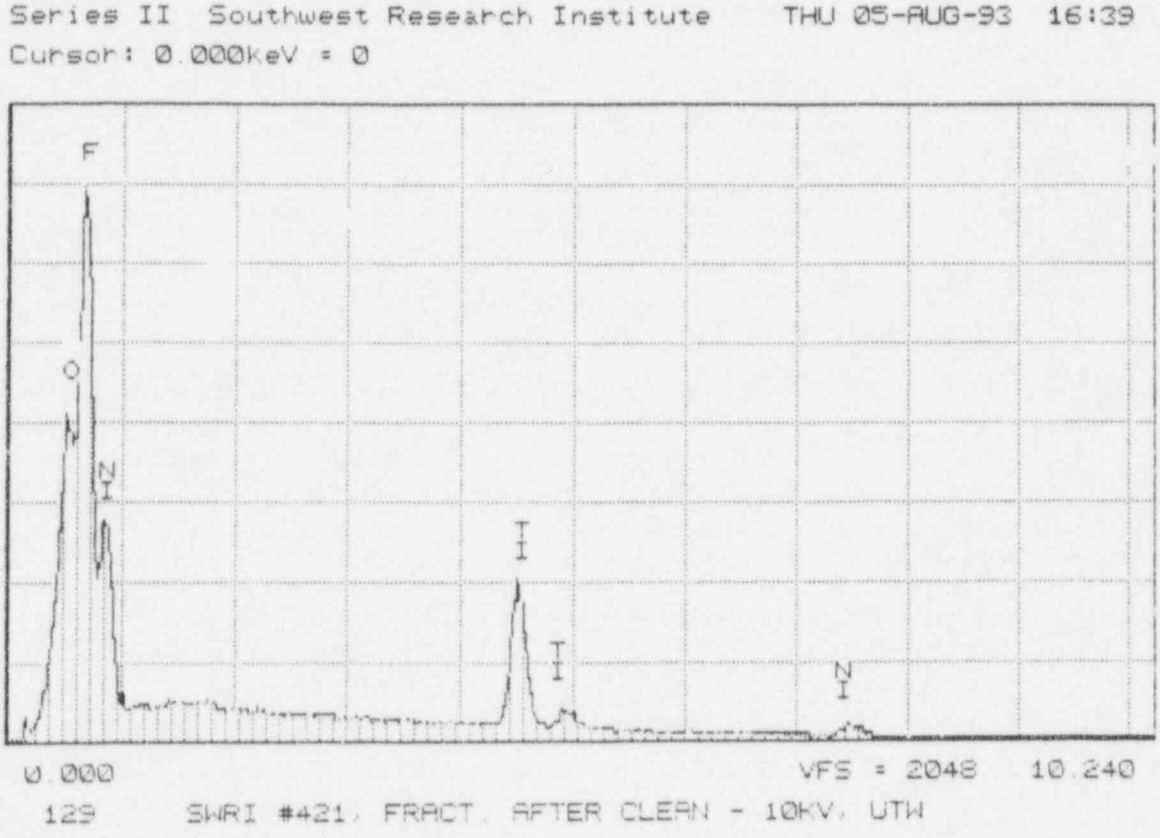

Figure B-16. Energy Dispersive X-Ray Spectra for the OD of SwRI Wire No. 421-1, Location 3

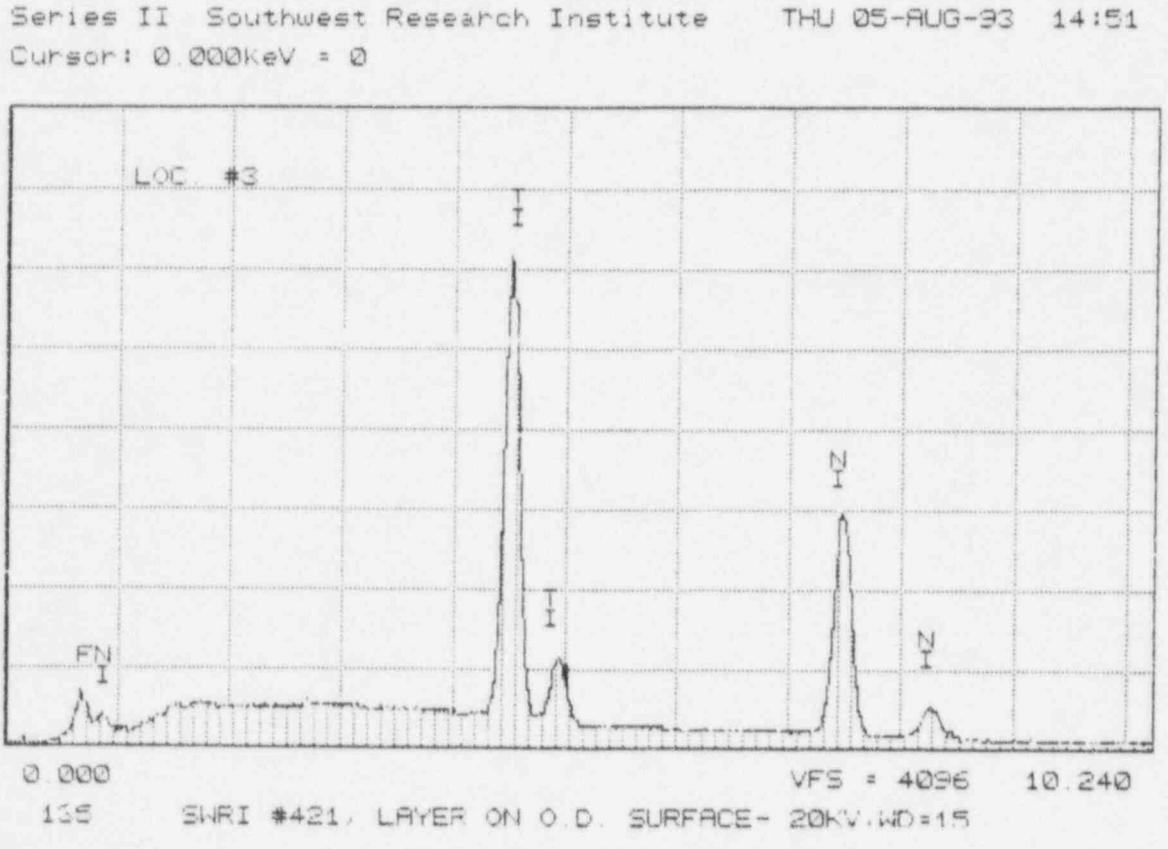

Figure B-17. Energy Dispersive X-Ray Spectra for the Fracture Surface for SwRI Wire No. 421-1

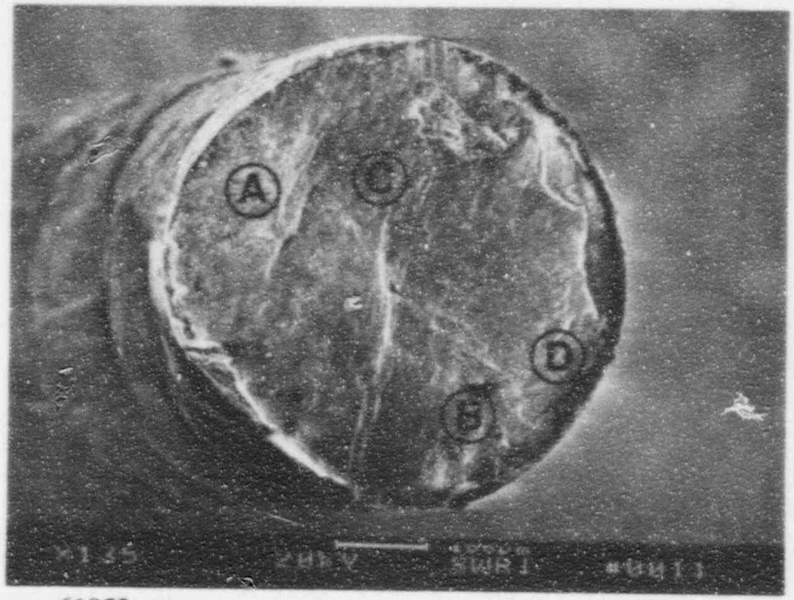

61952 135X

a) View Looking at Fracture Surface

61955 135X

c) Side View

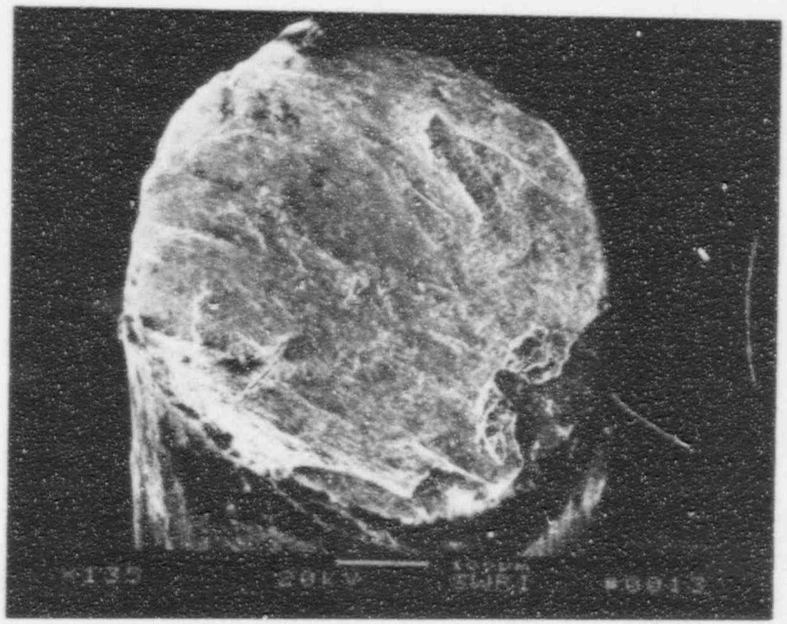

61956 135X

b) View Looking at Fracture Surface - Rotated 90° from (a)

Figure B-18. SEM Fractograph of SwRI Wire No. 422-1

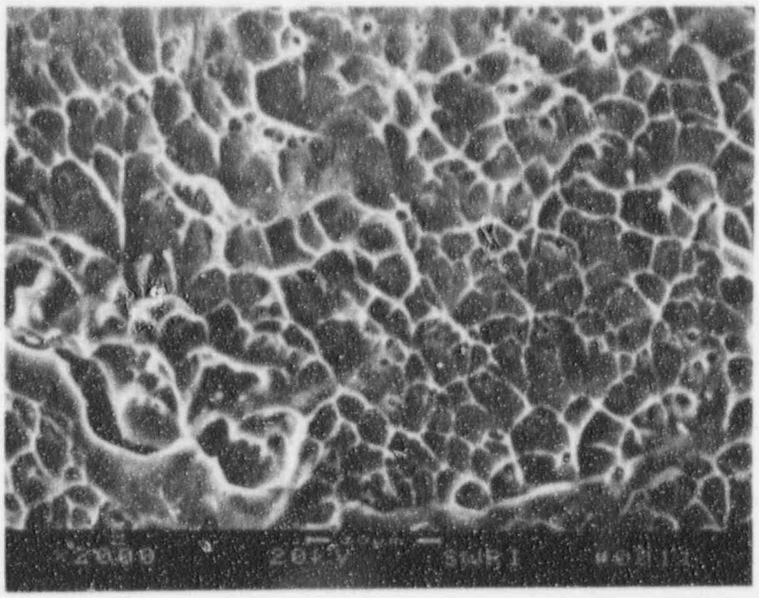

61933 2000X

a) Location A

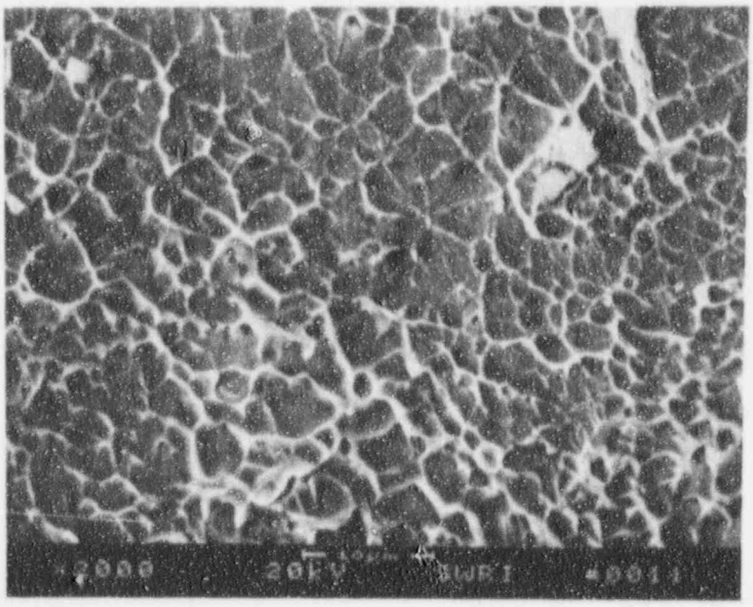

61954 2000X

b) Location B

Figure B-19. SEM Fractographs at Locations A and B for SwRI Wire No. 422-1

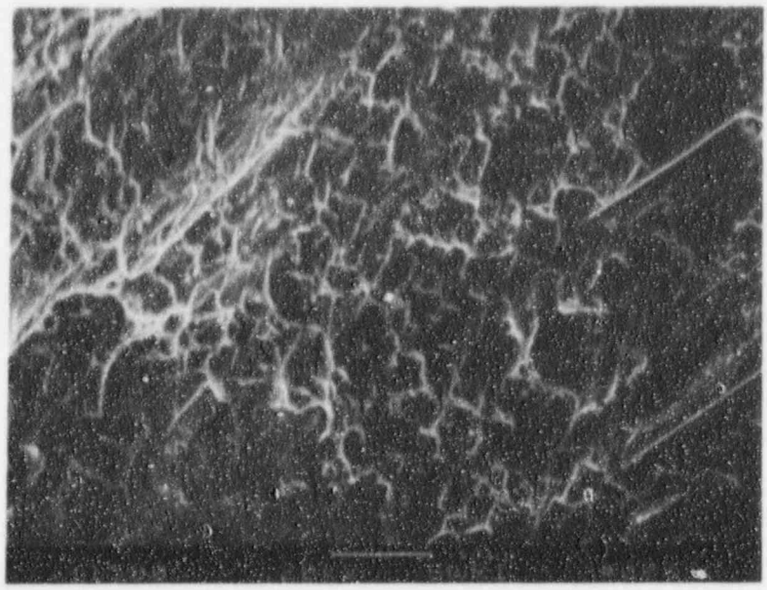

62915 1500X

a) Location C

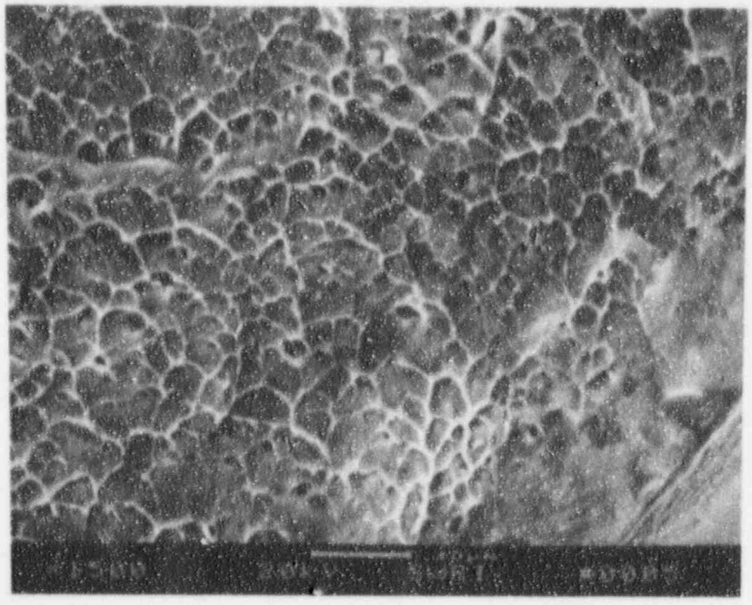

62916 1500X

b) Location D

Figure B-20. SEM Fractographs of Locations C and D on SwRI Wire No. 422-1.

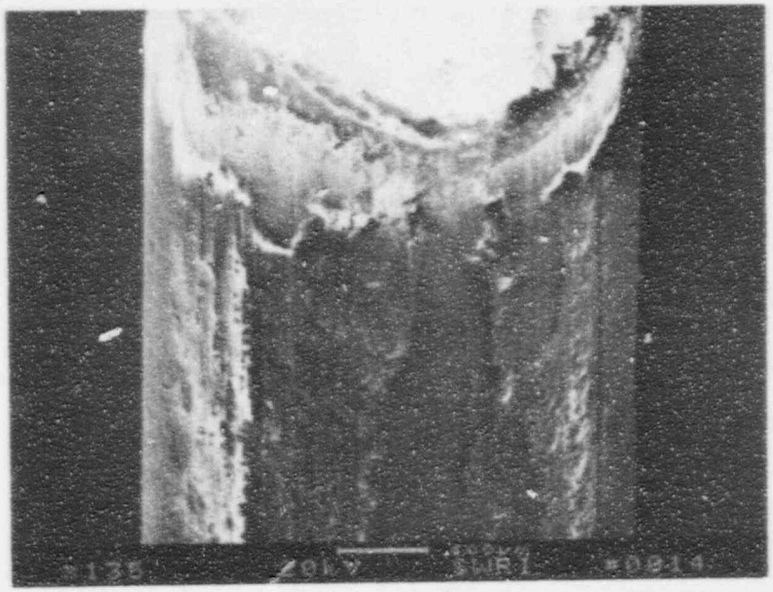

61957 135X

a)

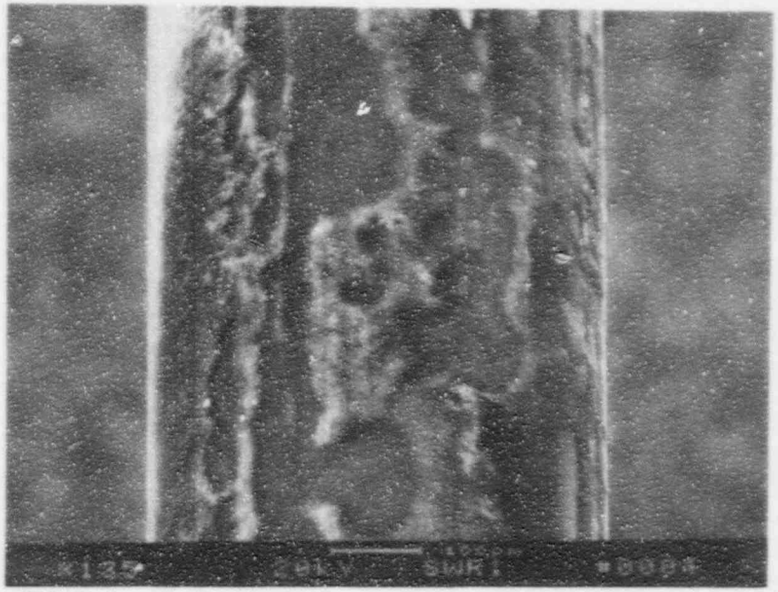

62917 135X

c)

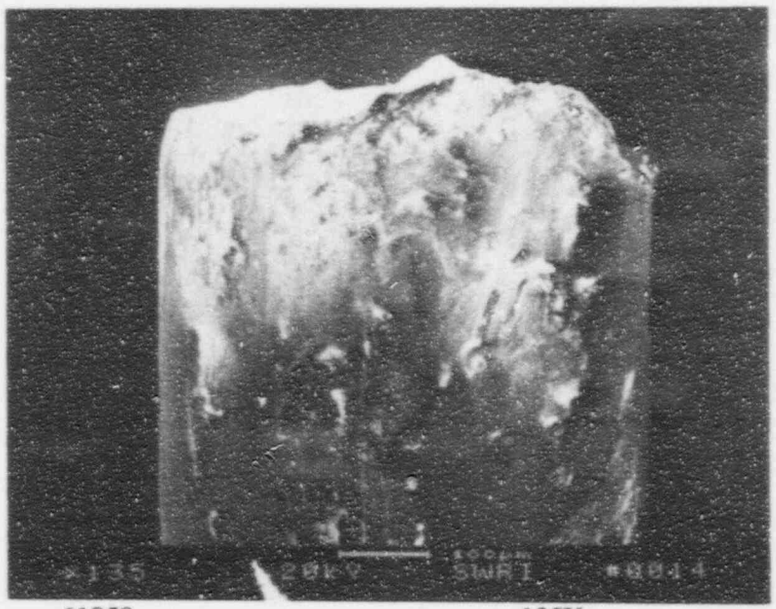

61958 135X

b)

Figure B-21. SEM Photographs of the OD Surface of SwRI Wire No. 422-1.

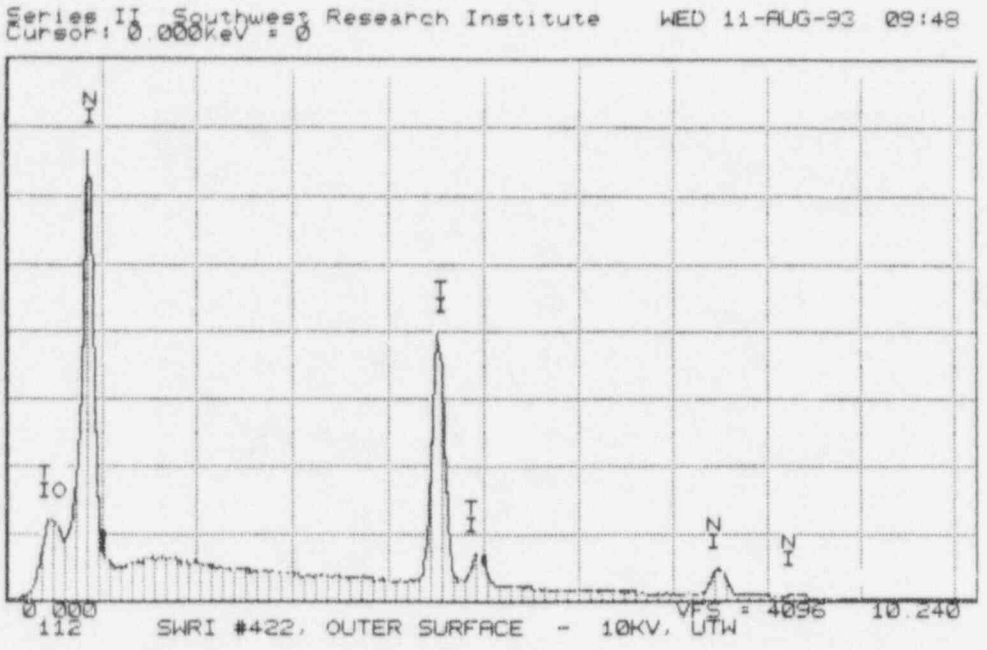

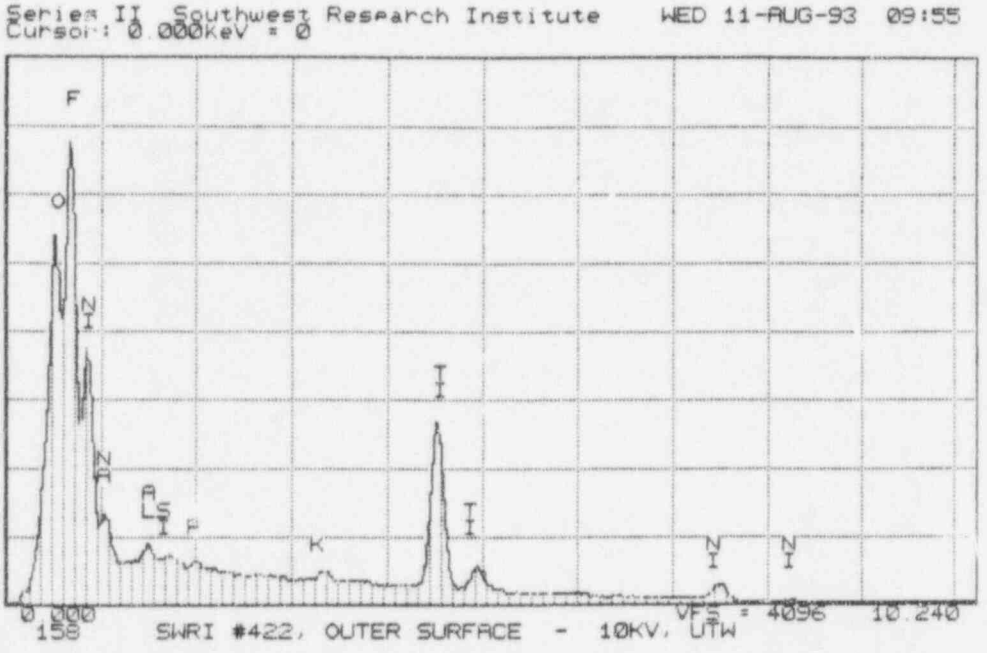

Figure B-22. Energy Dispersive Spectra of the OD Surface for SwRI Wire No. 422-1.

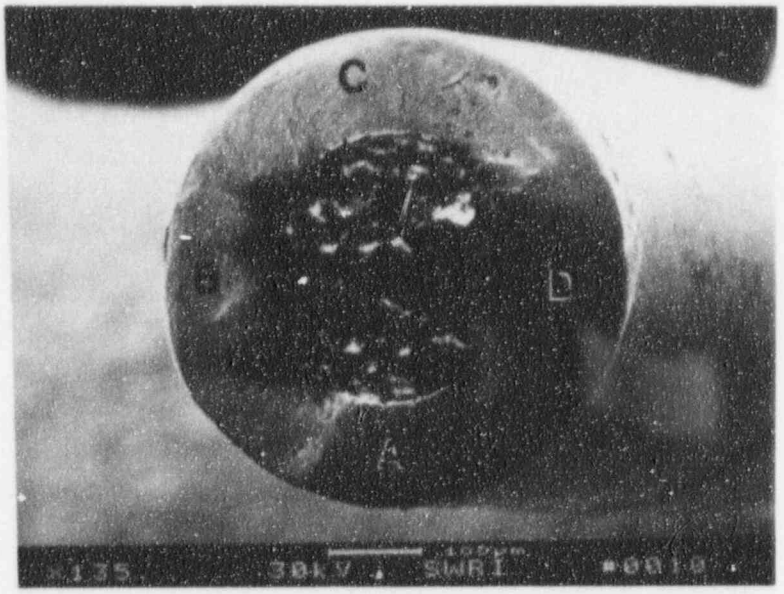

61926 135X

a)

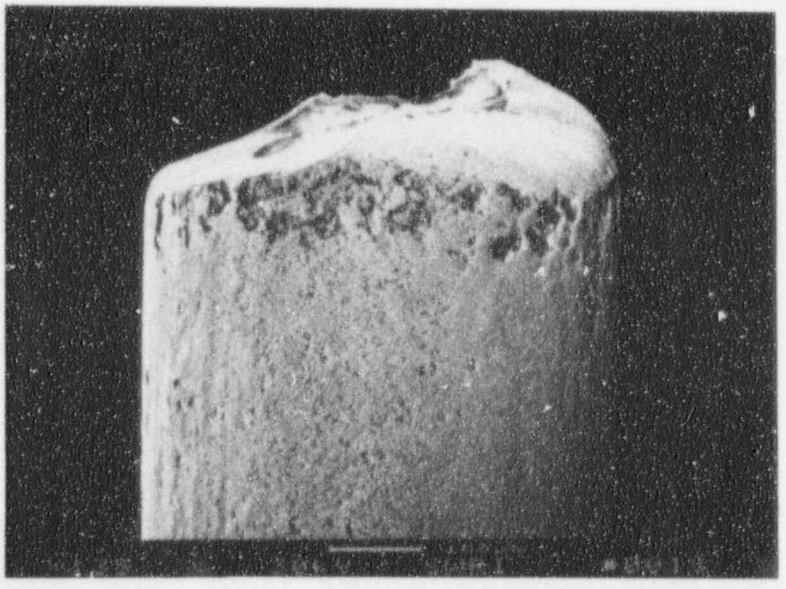

61932 135X

b)

Figure B-23. SEM Fra ·graphs of SwRI Wire No. 423-1.

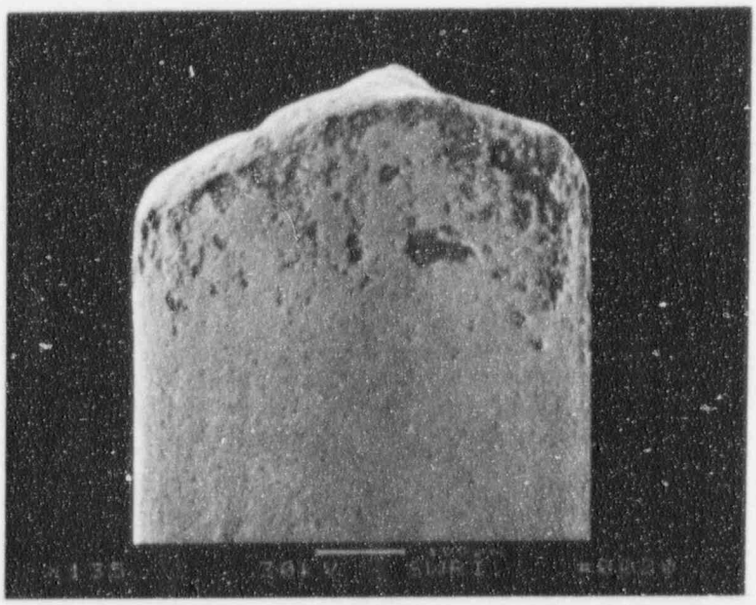

61934 135X

a)

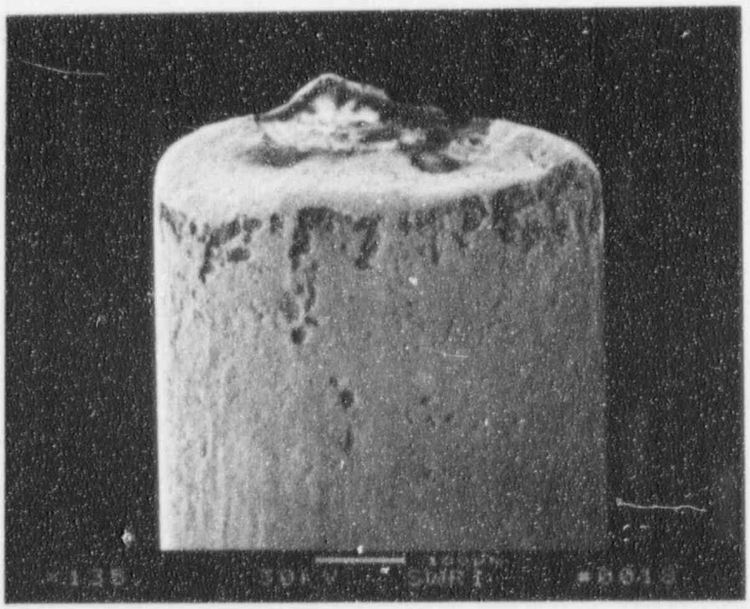

61933 135X

b)

Figure B-24. SEM Fractographs of SwRI Wire No. 423-1.

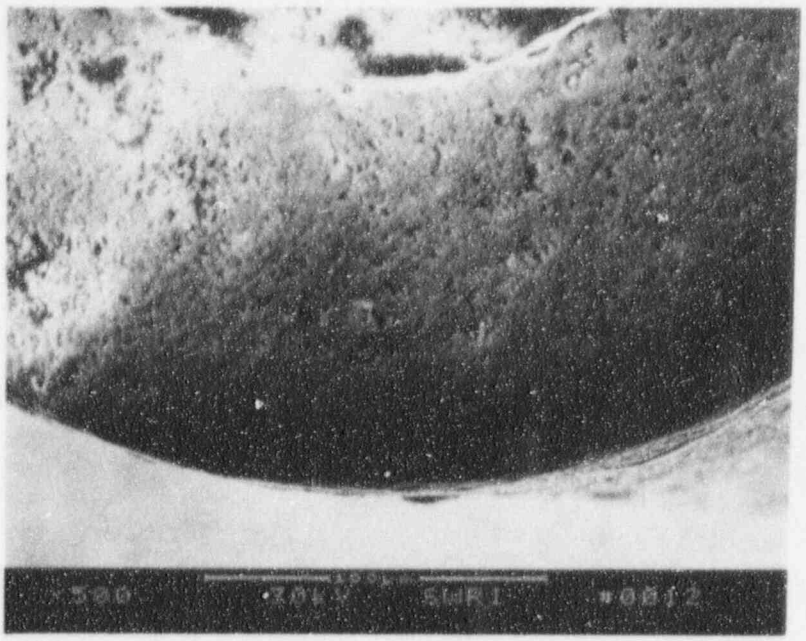

61928 500X

a) Location A

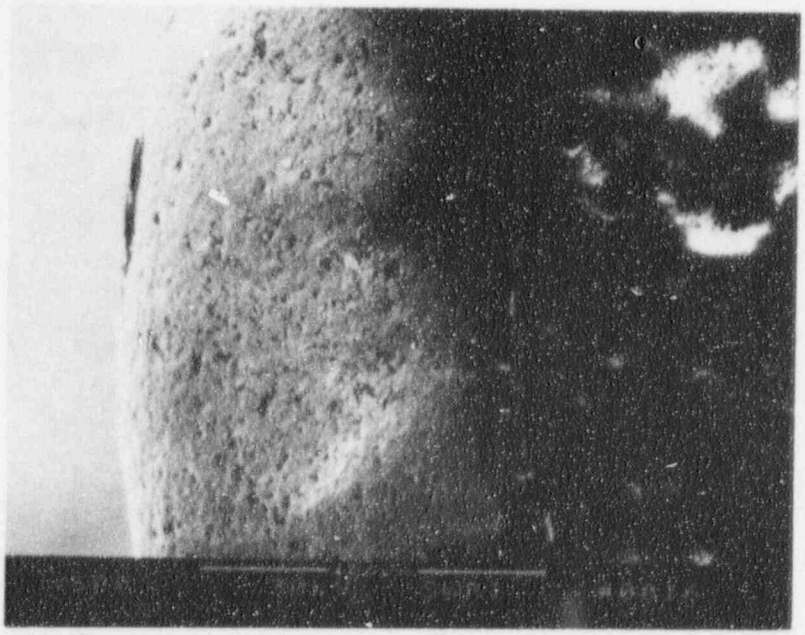

61930 500X

b) Location B

Figure B-25. SEM Fractographs at Locations A and B for SwRI Wire No. 423.

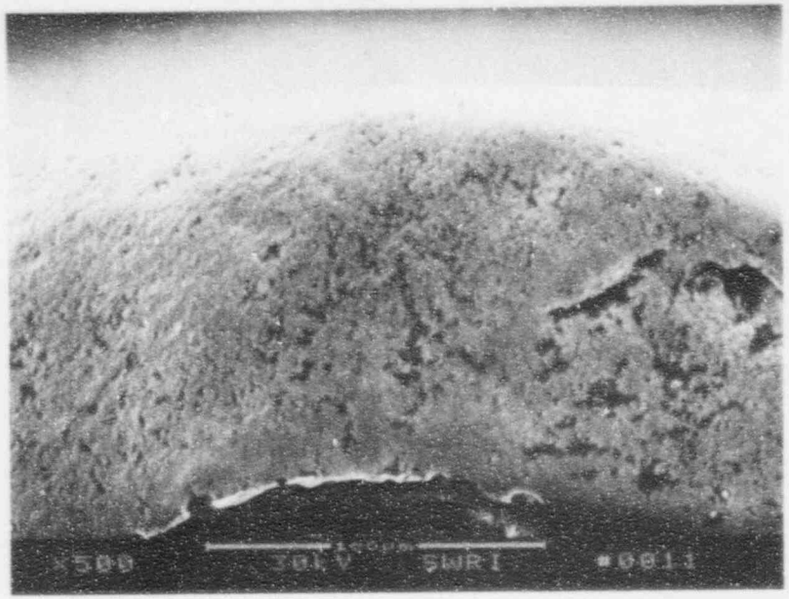

61297 500X

a) Location A

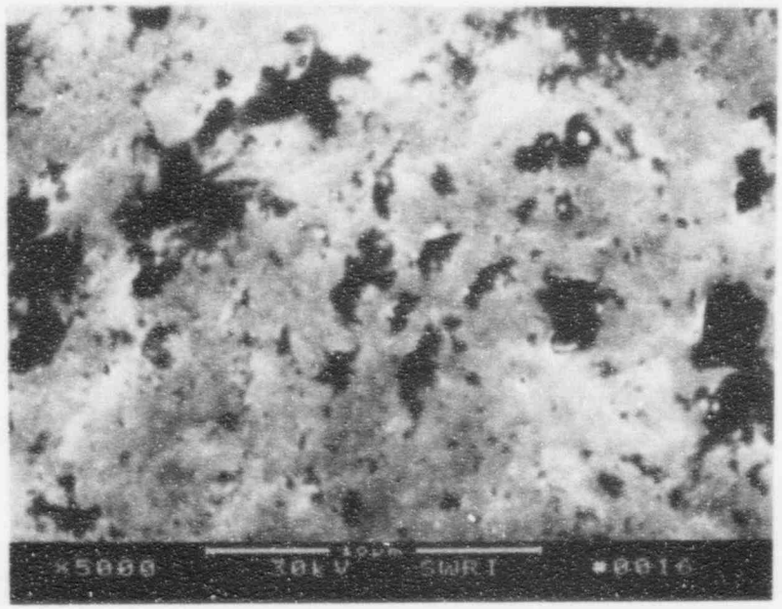

61931 5000X

b) Location C

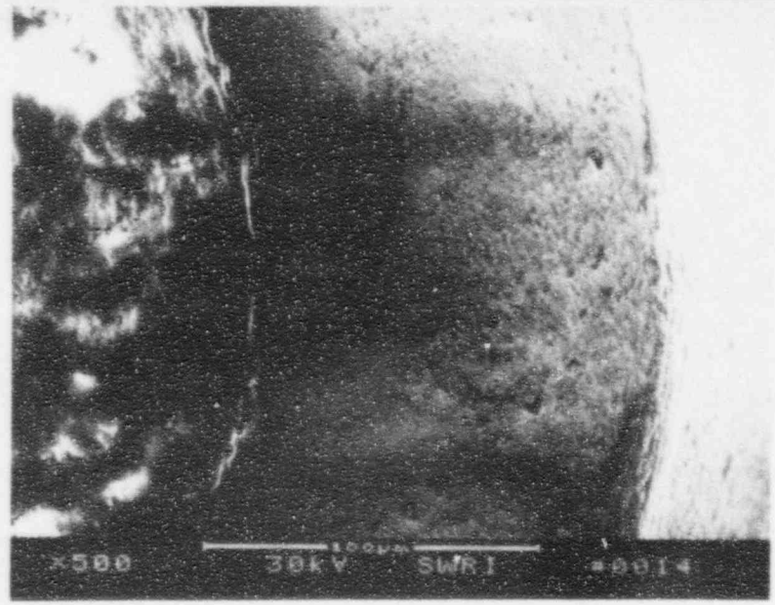

61929 500X

c) Location D

Figure B-26. SEM Fractographs at Locations C and D for SwRI Wire No. 423-1.

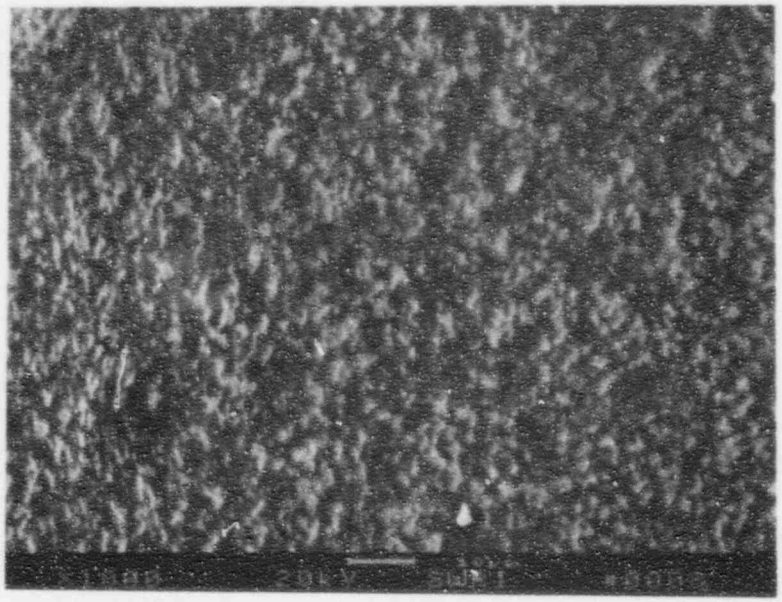

62918 1000X

a) OD Surface

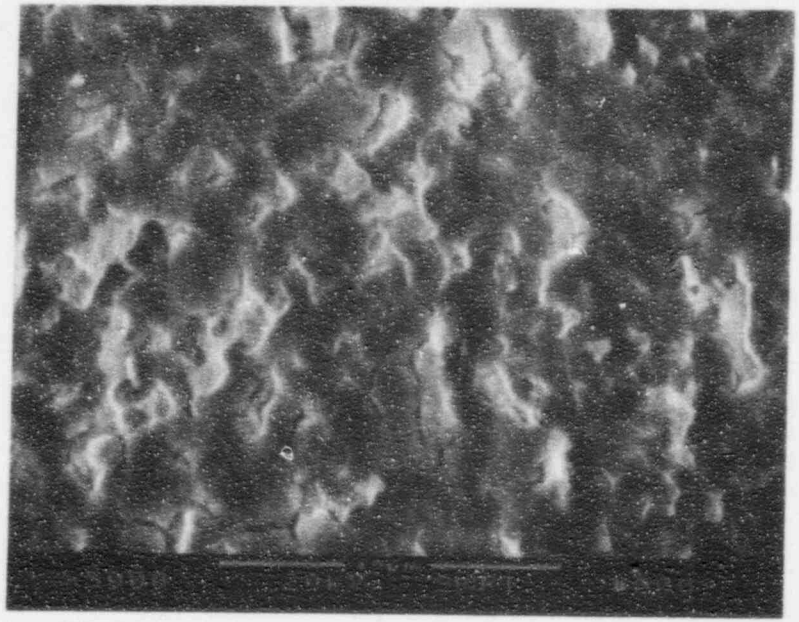

62919 5000X

b) OD Surface

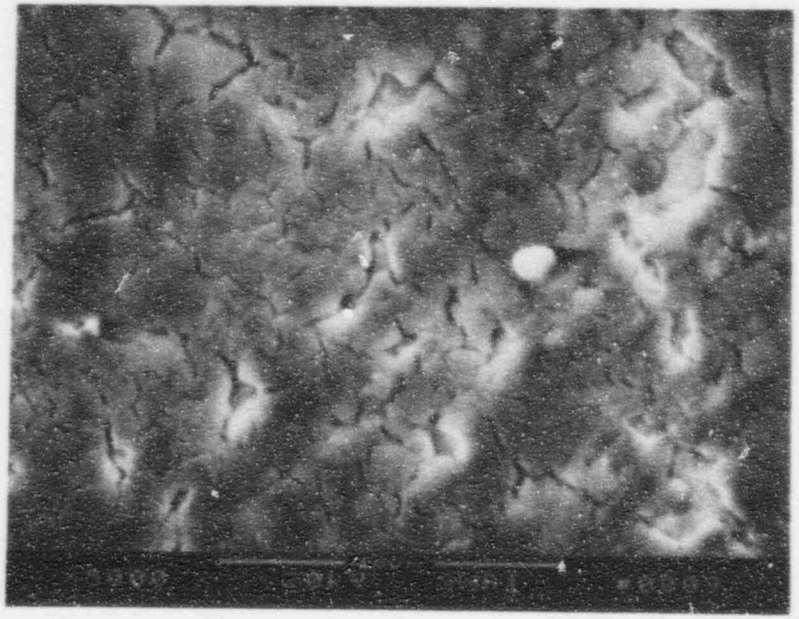

62920 5000X

c) Fracture Surface

Figure B-27. SEM Photographs of the OD and Fracture Surface for SwRI Wire No. 423.

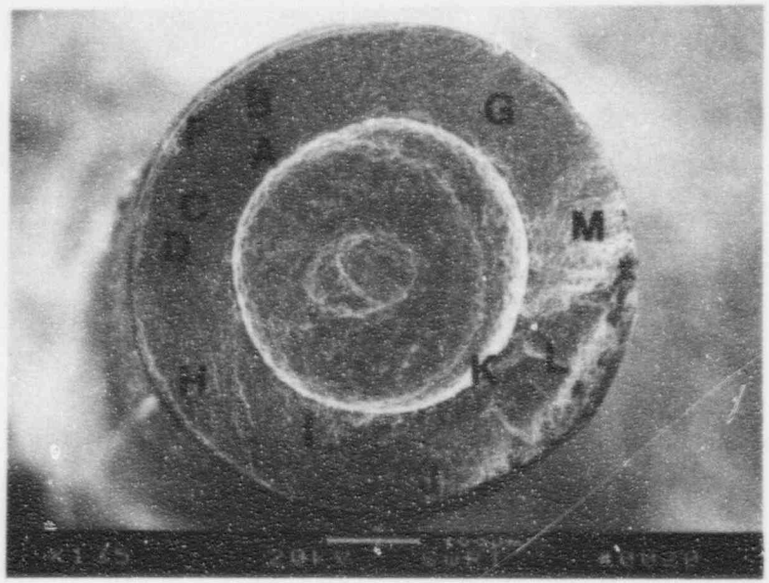

61365 135X

a) View Looking Down at the Wire

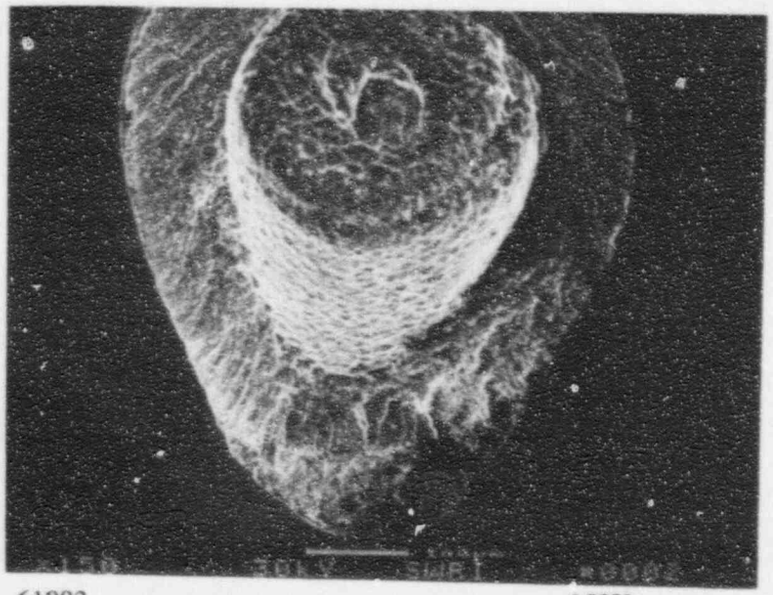

61883 150X

c) View Looking at Slant Fracture

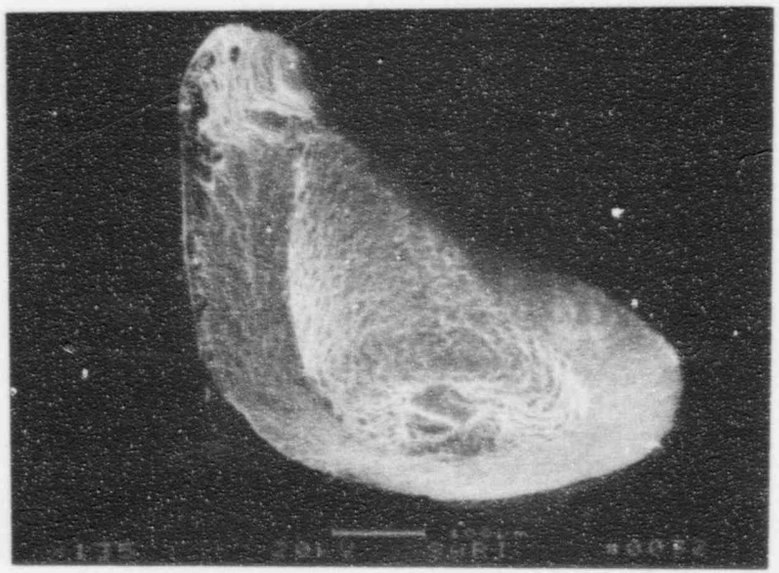

61373 135X

b) View Looking from the Side

Figure B-28. SEM Fractographs of SwRI Wire No. 429-1.

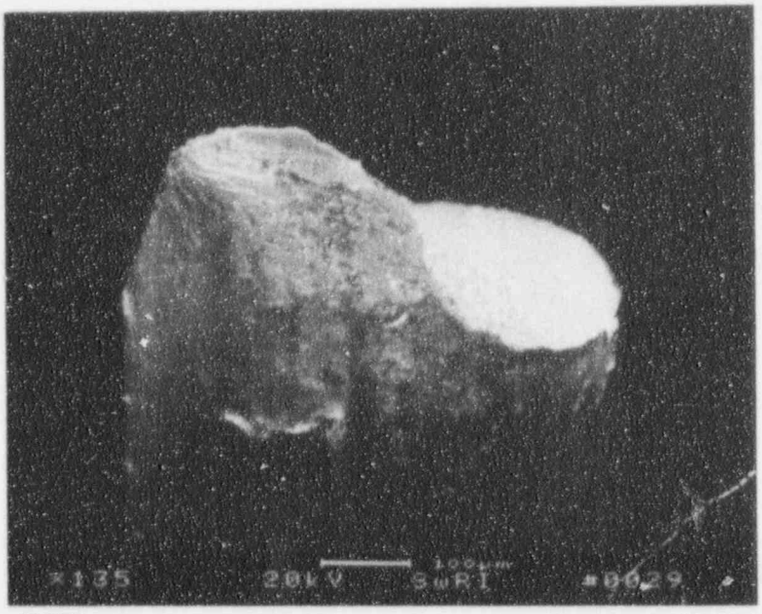

61372 135X

a)

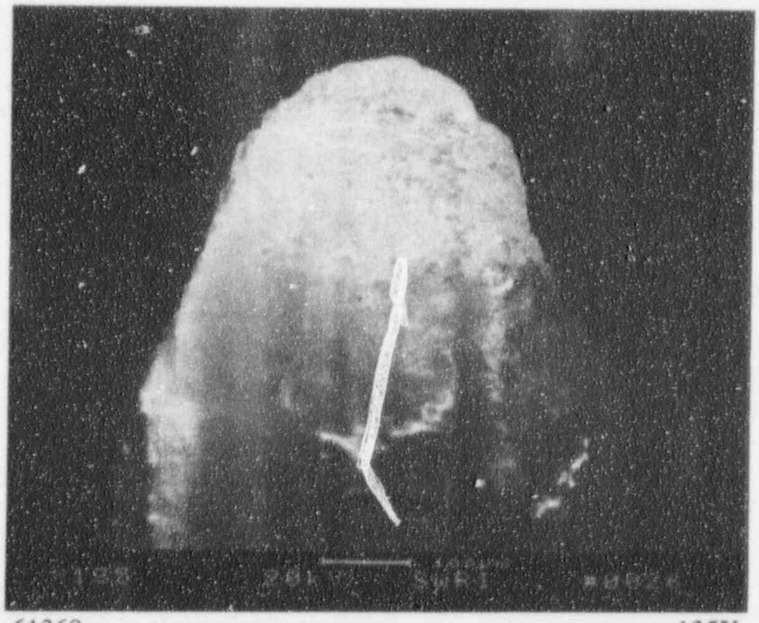

61369 135X

b)

Figure B-29. SEM Photographs of the OD Surface Adjacent to the Slant Region For SwRI Wire No. 429-1.

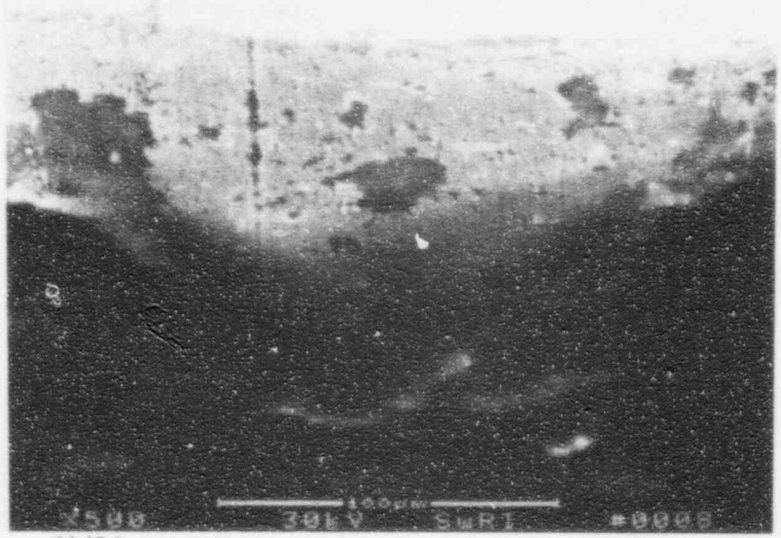

61404 500X

a)

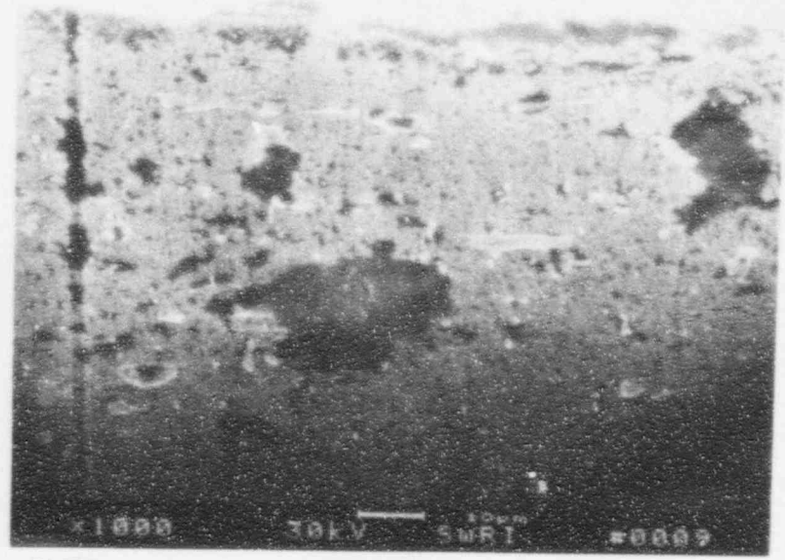

61405 1000X

c)

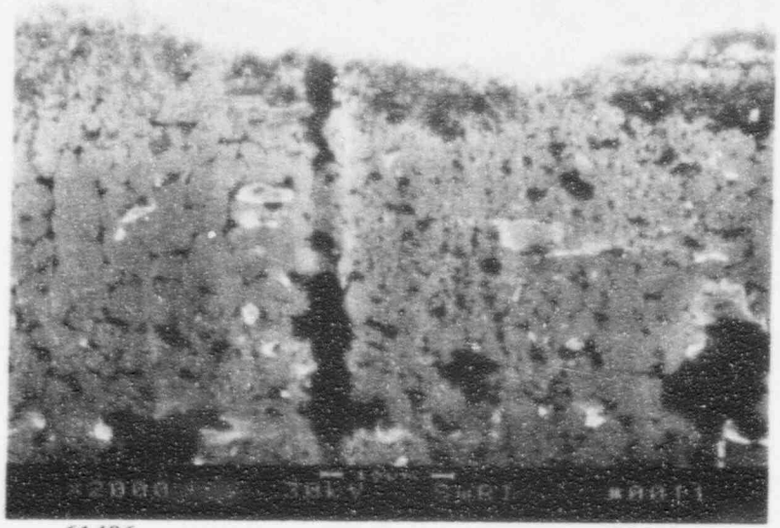

61406 2000X

b)

Figure B-30. SEM Photographs of the OD Surface Adjacent to the Flat Region for SwRI Wire No. 429-1.

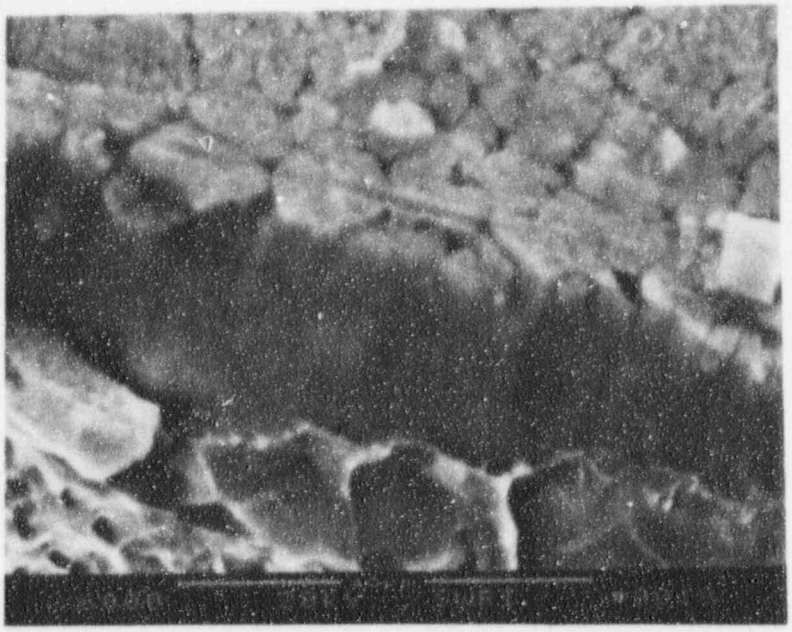

62922 6000X

a)

62921 6000X

b)

Figure B-31. SEM Fractograph Stereo Pair of the Attack Network on the OD Surface for SwRI Wire No. 429-1.

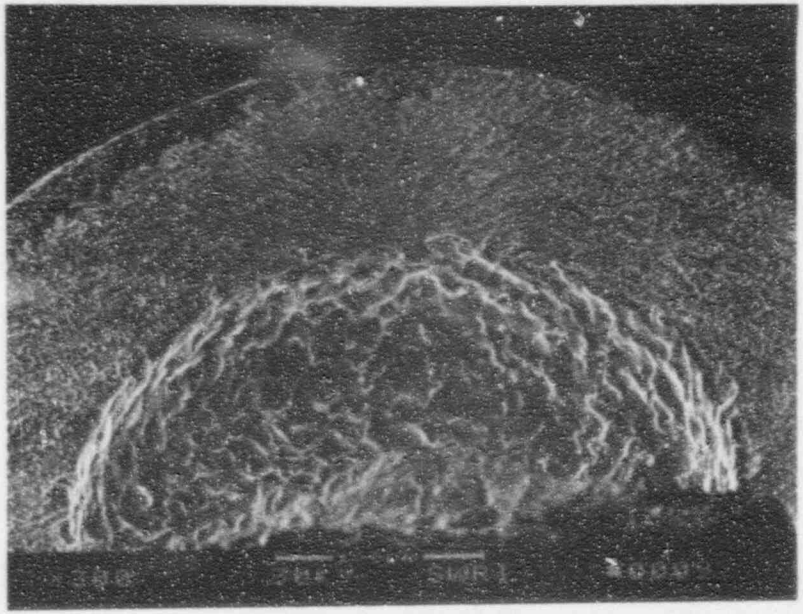

61889 300X

a)

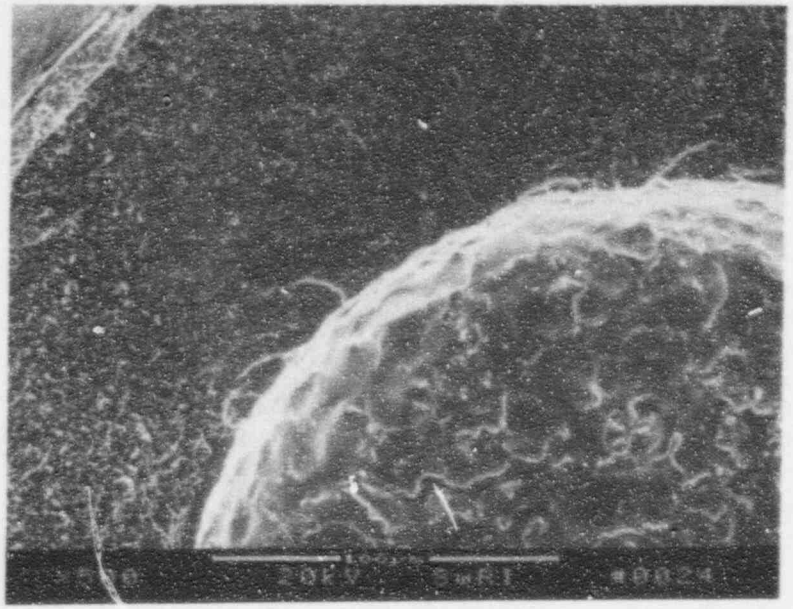

61368 500X

c)

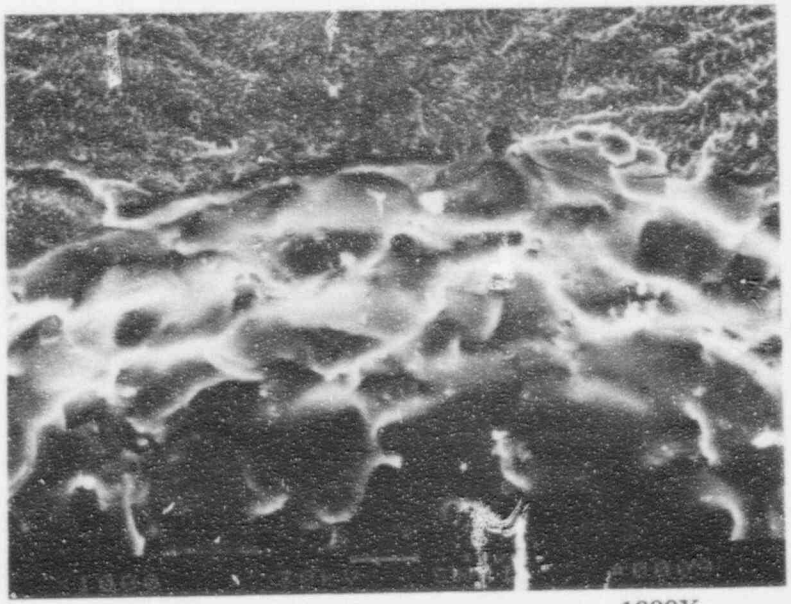

61890 1000X

b)

Figure B-32. SEM Fractographs of the Initiation Site at the Flat Region for SwRI Wire No. 429-1.

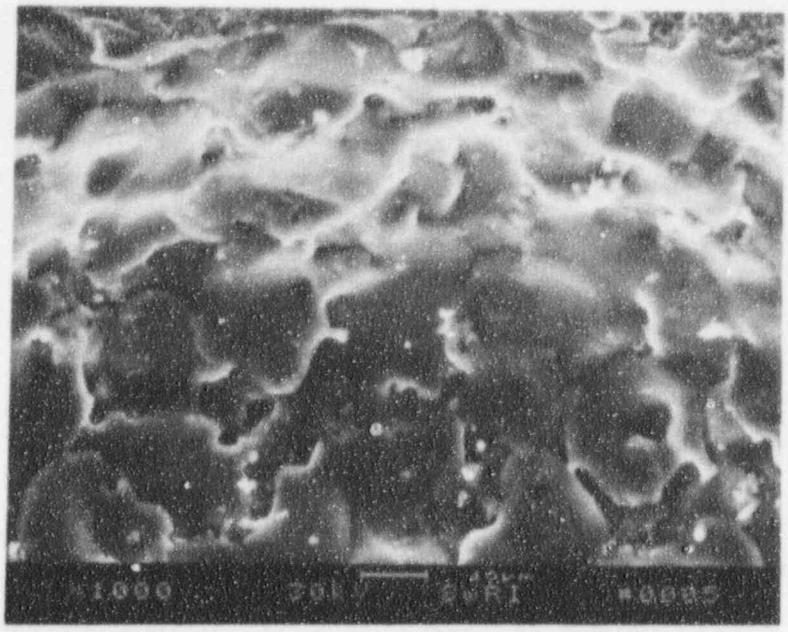

61402 1000X

a)

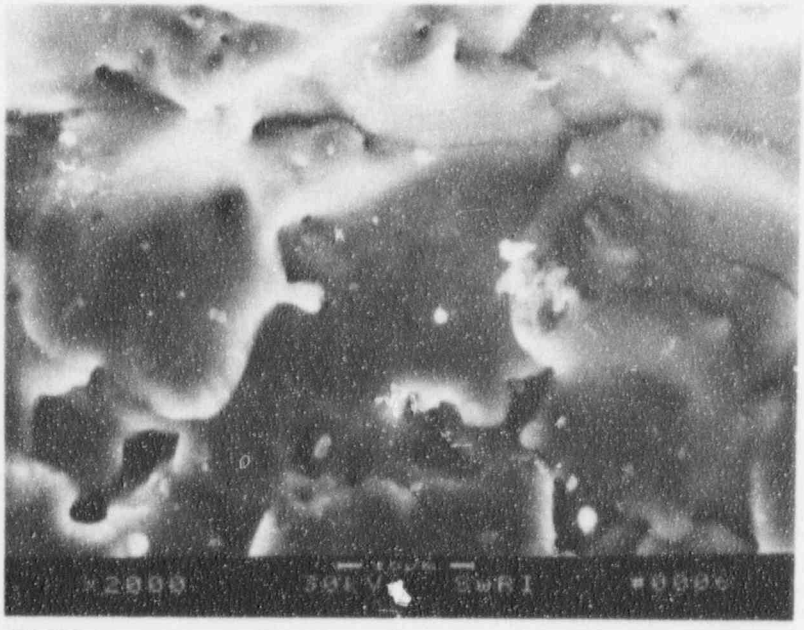

61403 2000X

b)

Figure B-33. SEM Fractographs of the Scale in the Cavity at the Flat Region for SwRI Wire No. 429-1.

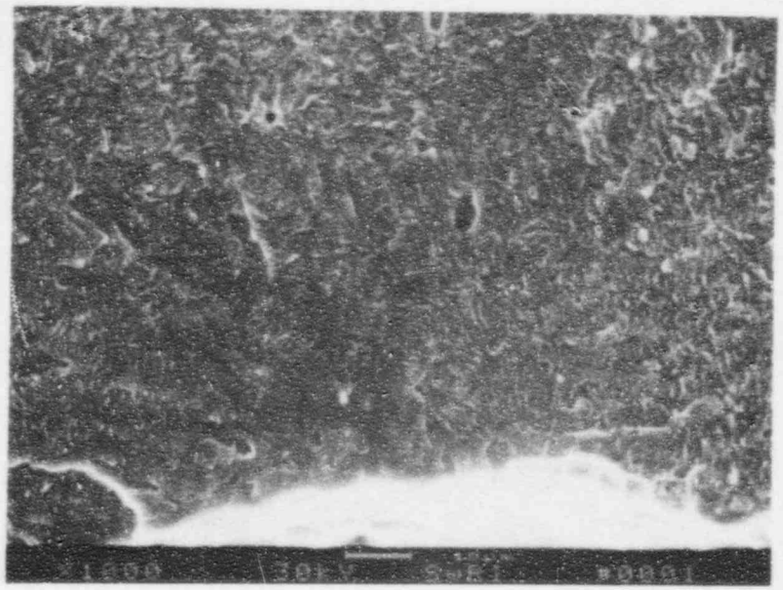

61399 1000X

a)

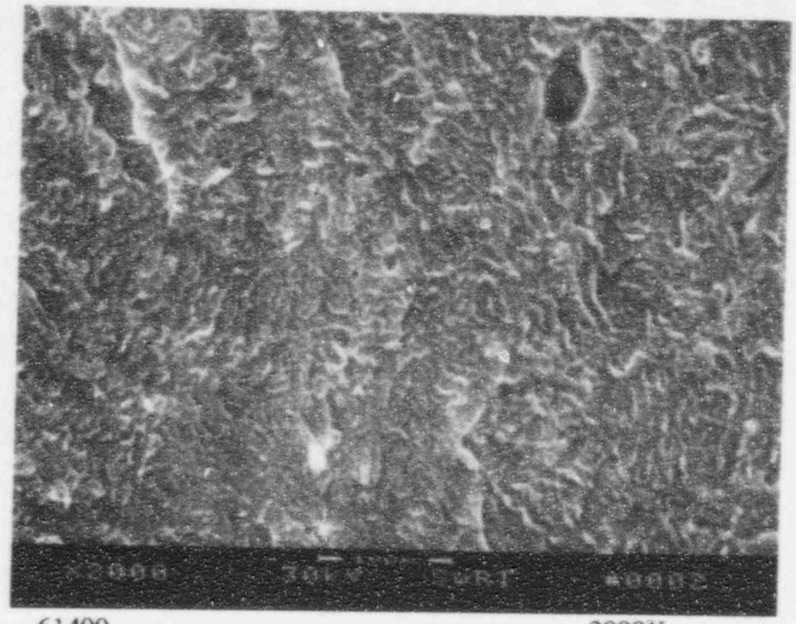

61400 2000X

c)

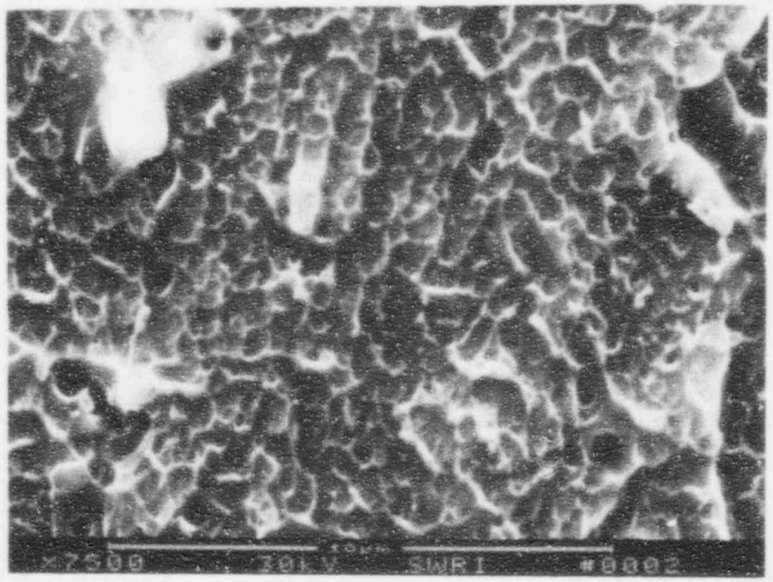

61875 7500X

b)

Figure B-34. SEM Fractographs at Location A for SwRI Wire No. 429-1.

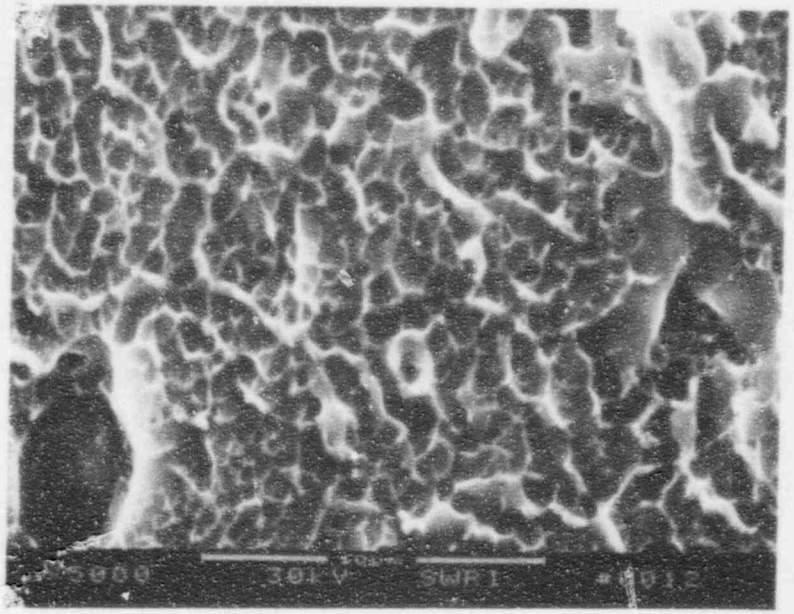

61876 5000X

Location B

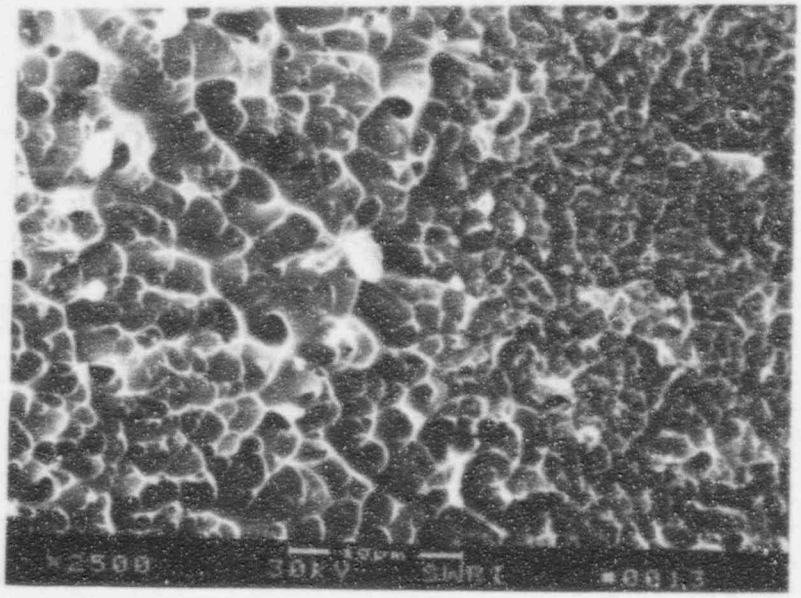

61878 2500X

Location D

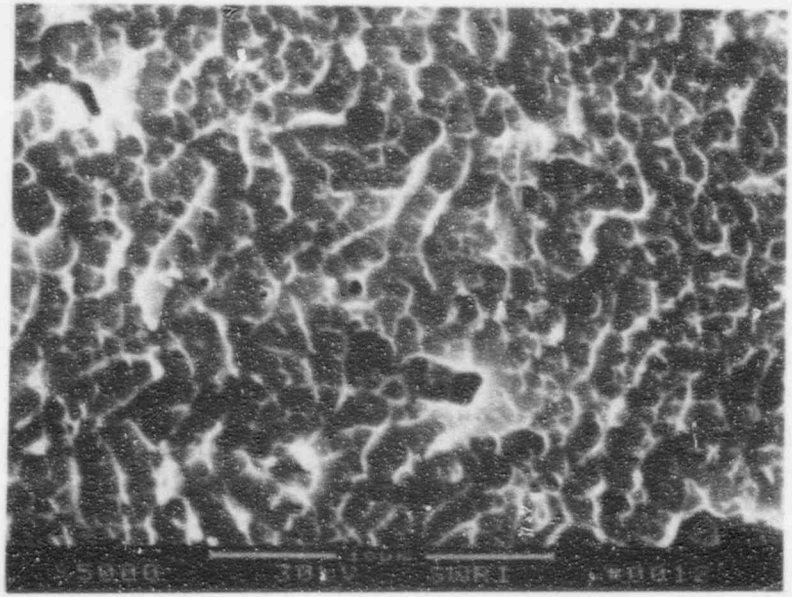

61877 5000X

Location C

Figure B-35. SEM Fractographs of Locations B, C and D for SwRI Wire No. 429-1.

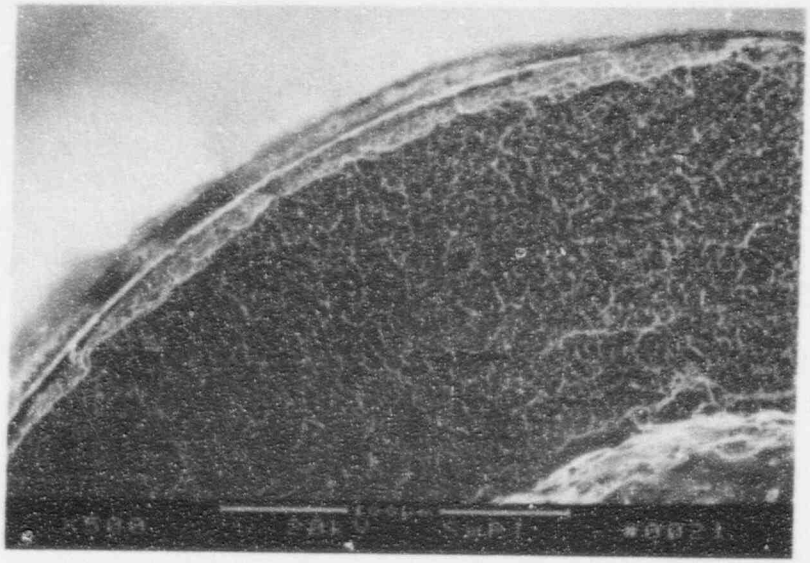

61366 500X

a)

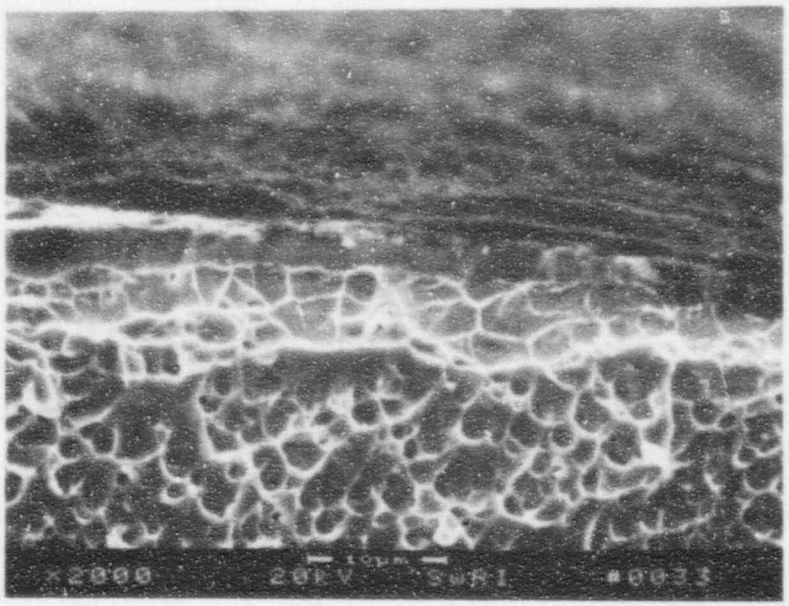

61374 2000X

b)

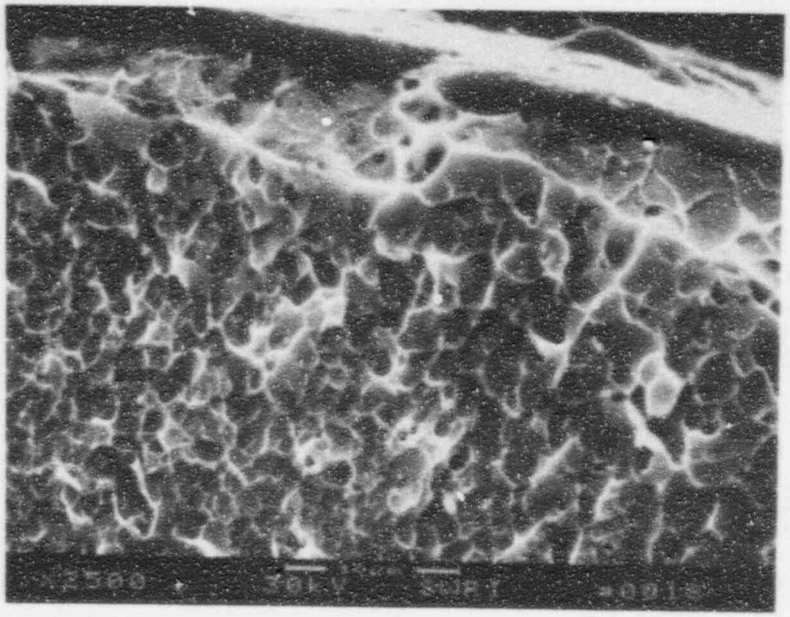

61880 2500X

c)

Figure B-36. SEM Fractograph of Location F, the OD Edge Adjacent to Flat Zone on SwRI Wire No. 429-1.

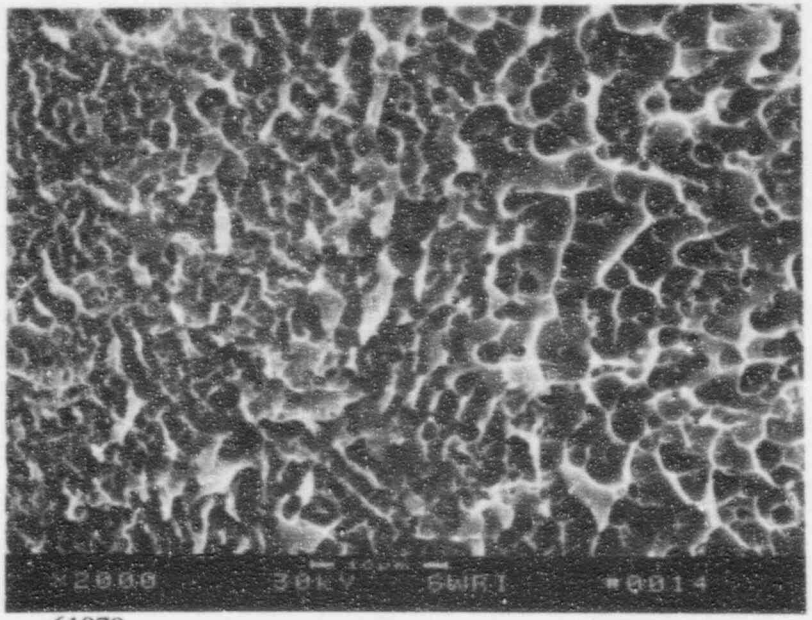

61879 2000X

Location E

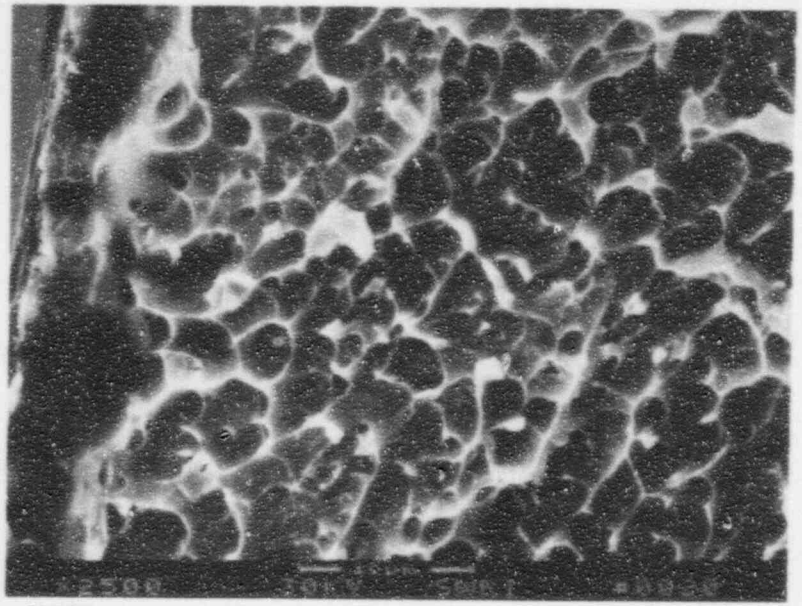

61882 2500X

Location H

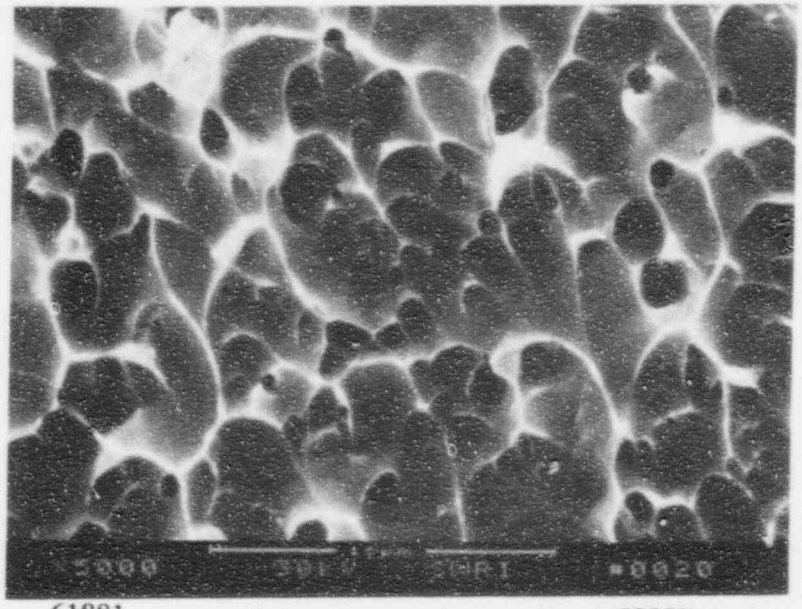

61881 5000X

Location G

Figure B-37. SEM Fractographs of Locations E, G and H for SwRI Wire No. 429-1.

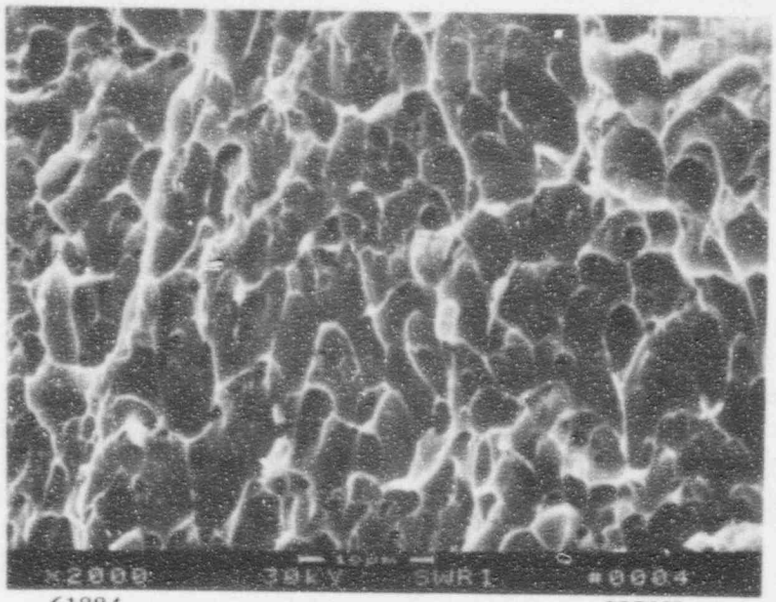

61884 2000X

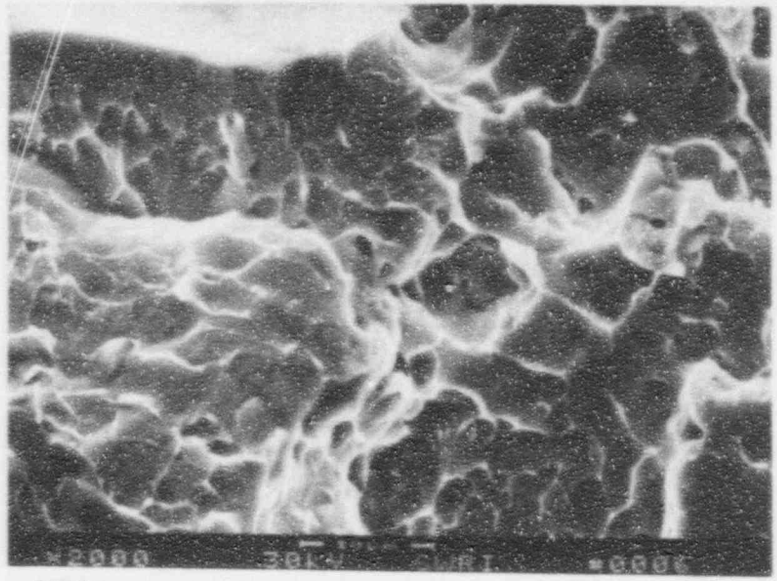

61886 2000X

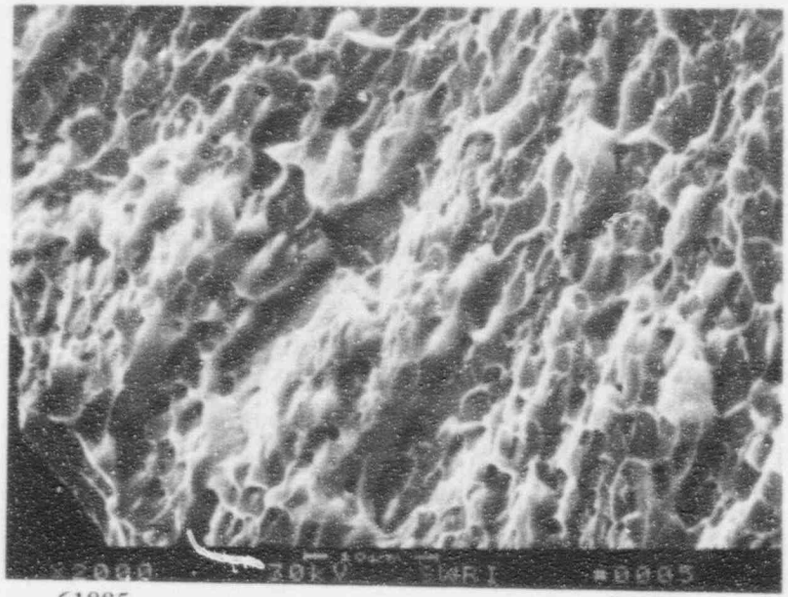

61885 2000X

Figure B-38. SEM Fractographs of Locations I, J and K for SwRI Wire No. 429-1.

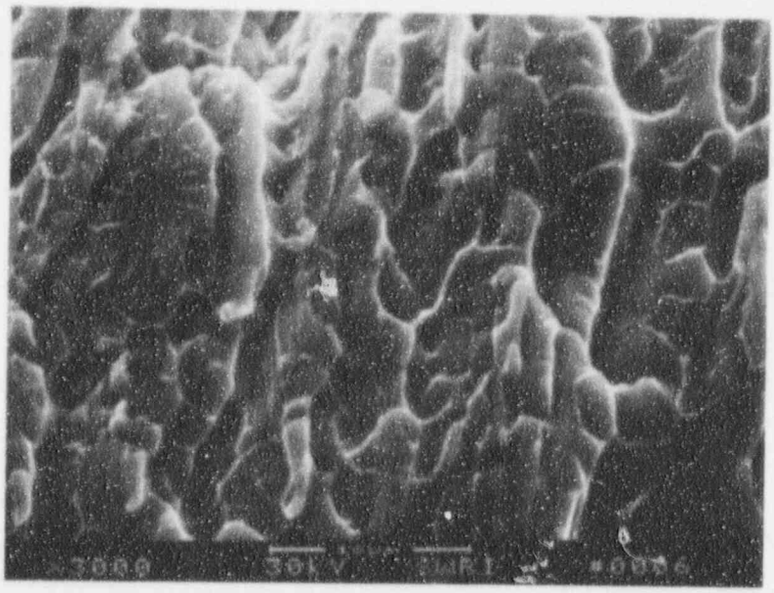

61887 3000X

a) Location L

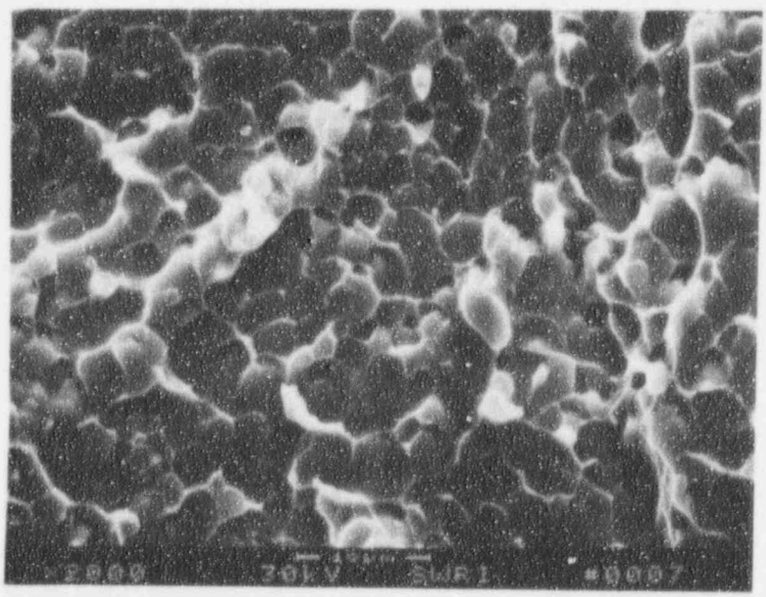

61888 2000X

b) Location M

Figure B-39. SEM Fractographs of Locations L and M for SwRI Wire No. 429-1.

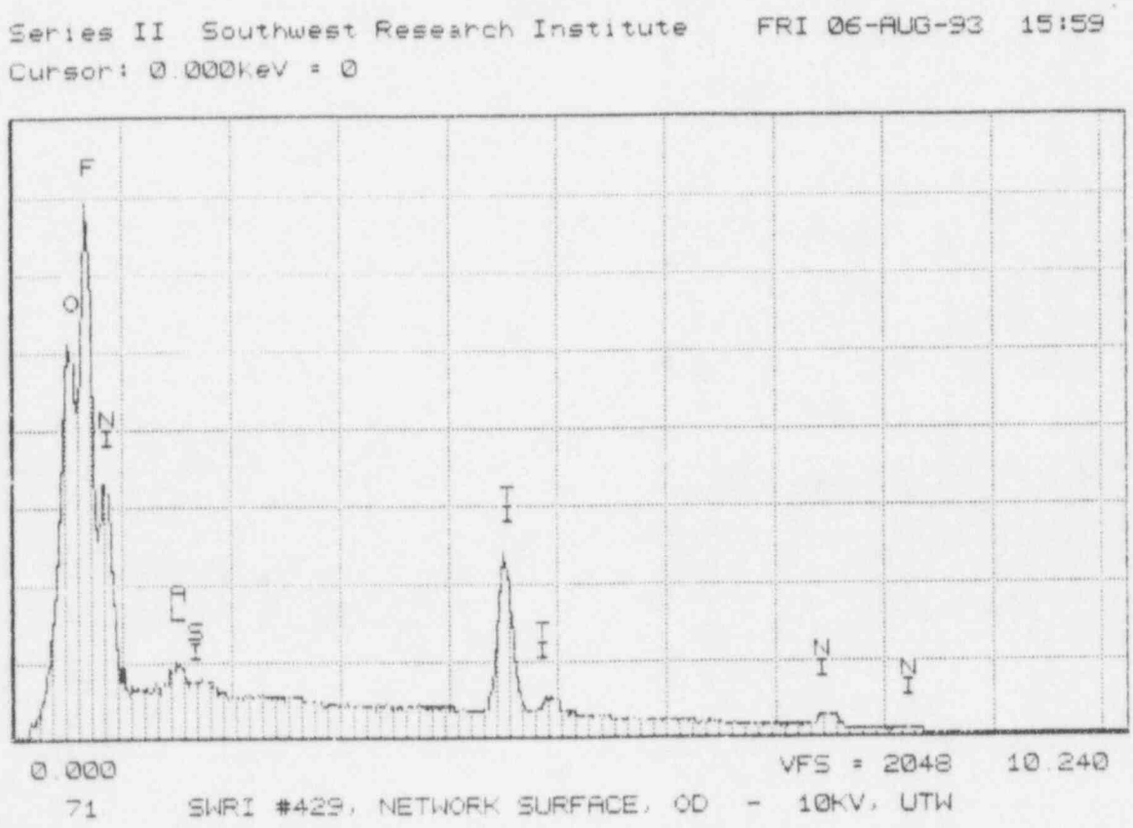

Figure B-40. Energy Dispersive X-Ray Spectra of the Network on the OD Surface for SwRI Wire No. 429-1.

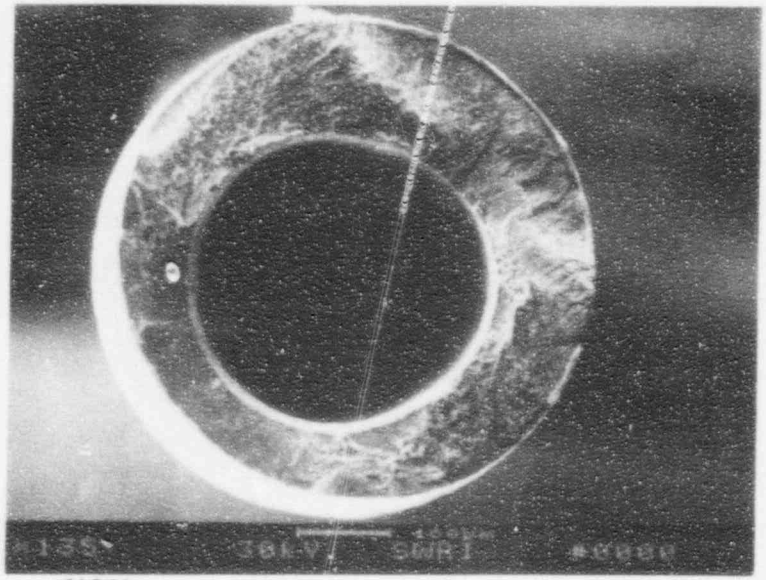

61263 135X

a)

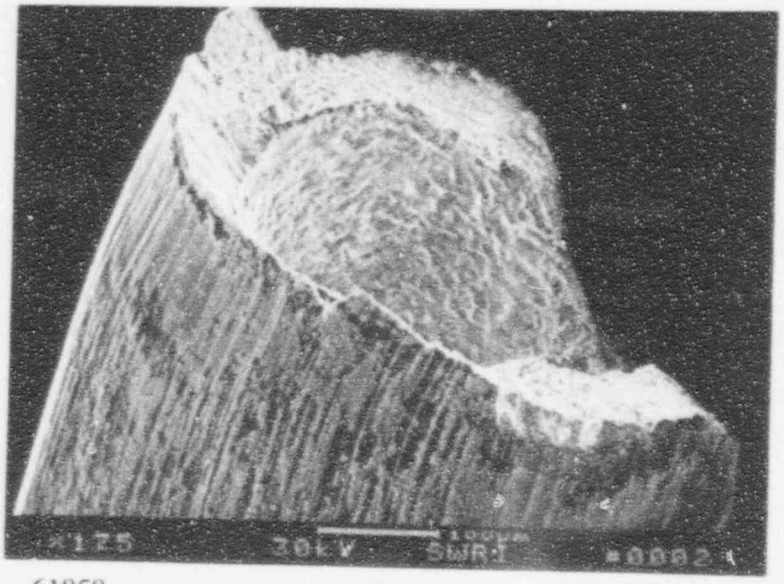

61858 175X

c)

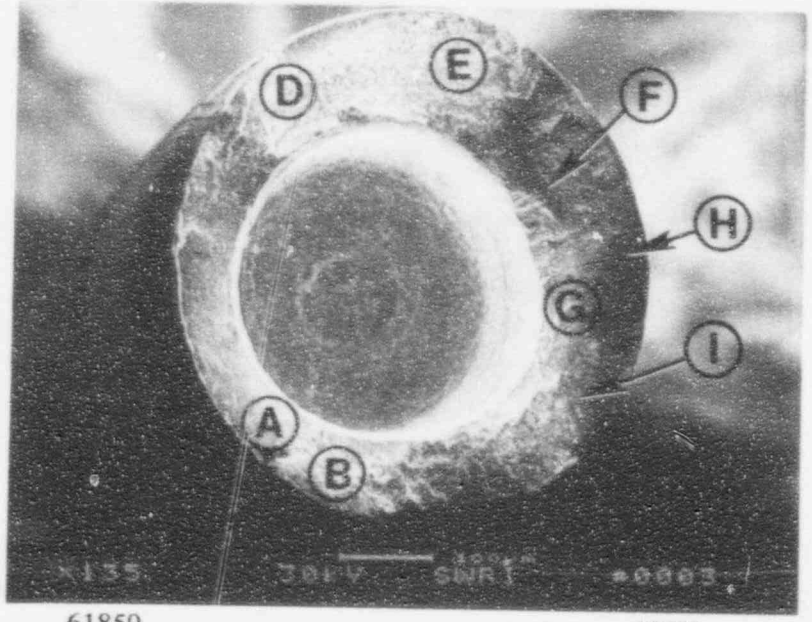

61859 135X

b)

Figure B-41. SEM Fractographs of the Overall Fracture for SwRI Wire No. 426-1.

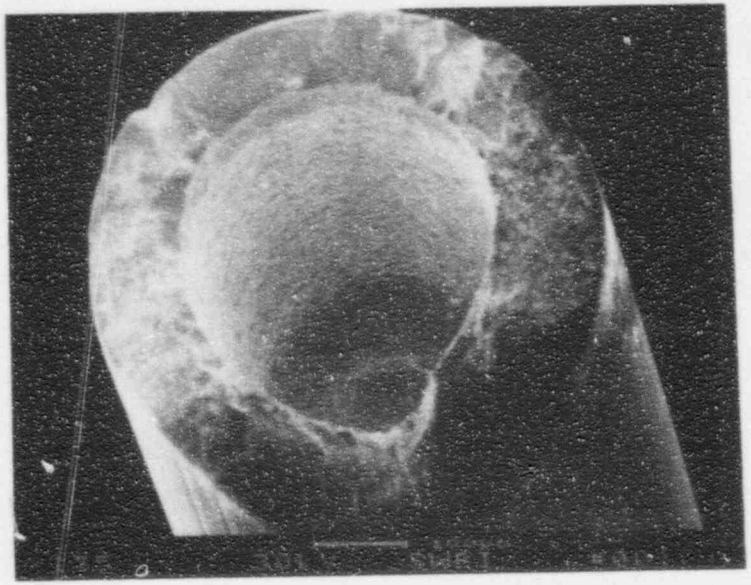

61273 135X

a)

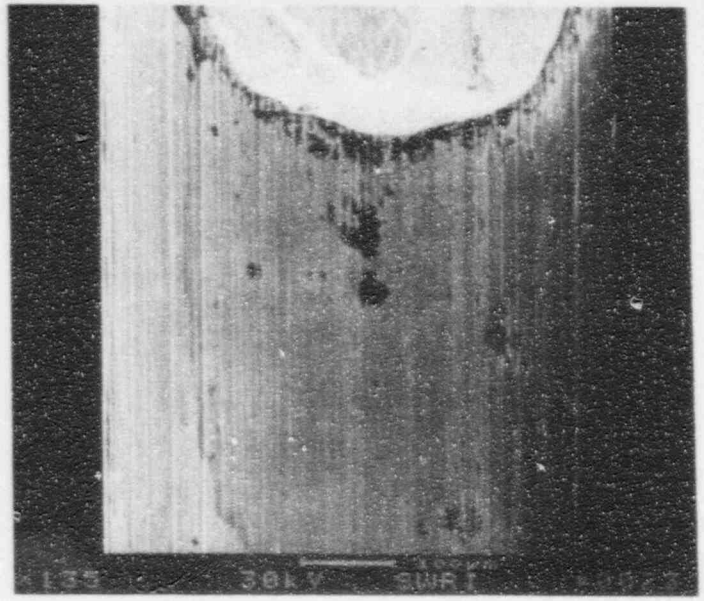

61872 135X

c)

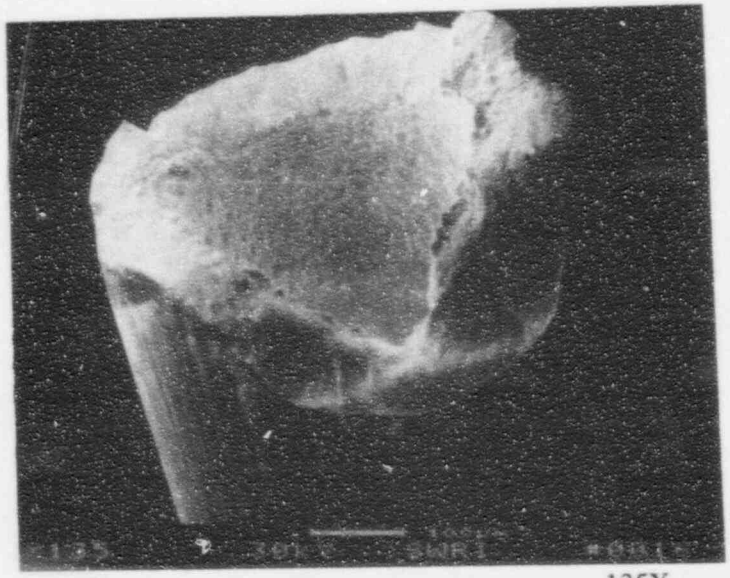

61271 135X

b)

Figure B-42. SEM Fractographs of SwRI Wire No. 426-1 Showing Slant Fracture.

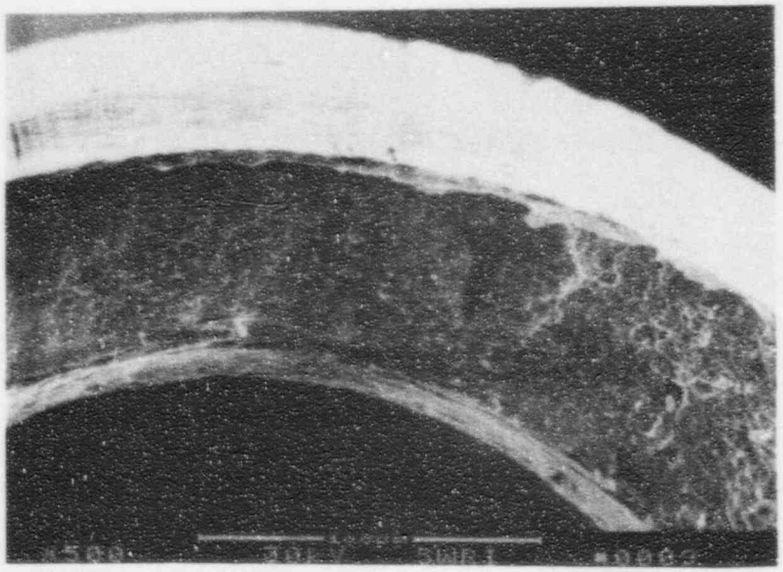

61266 500X

a)

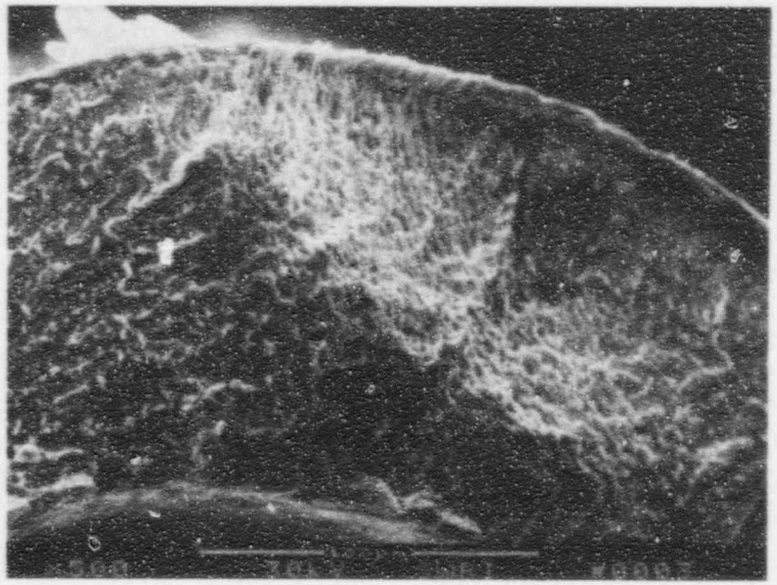

61265 500X

c)

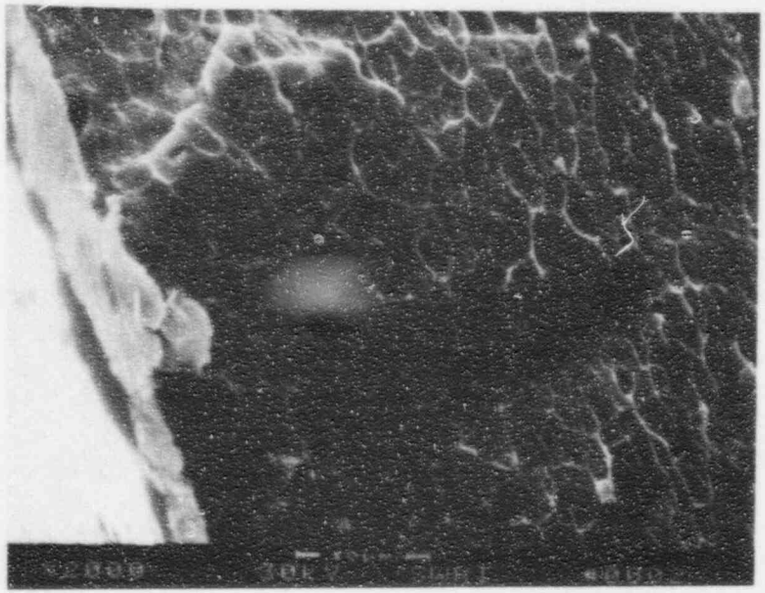

61264 2000X

b)

Figure B-43. SEM Fractographs Adjacent to the Thinned Section for SwRI Wire No. 426-1.

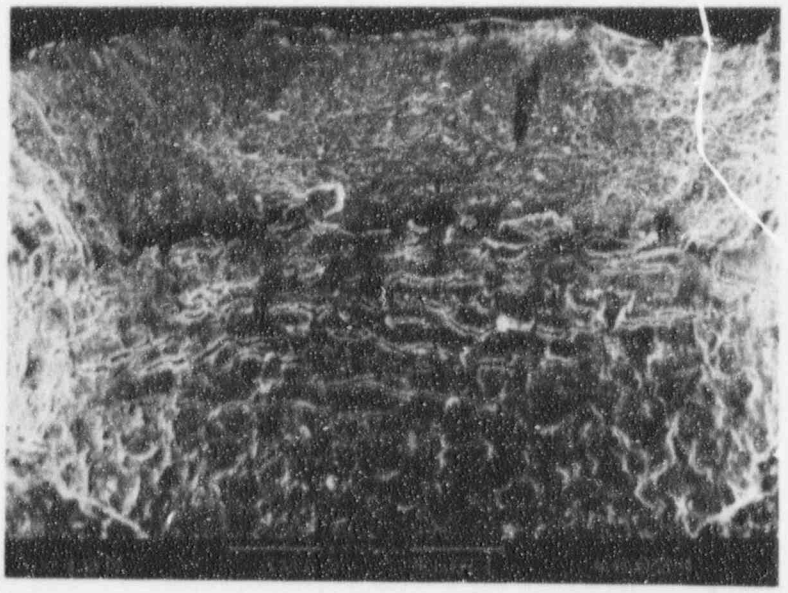

61873 400X

a)

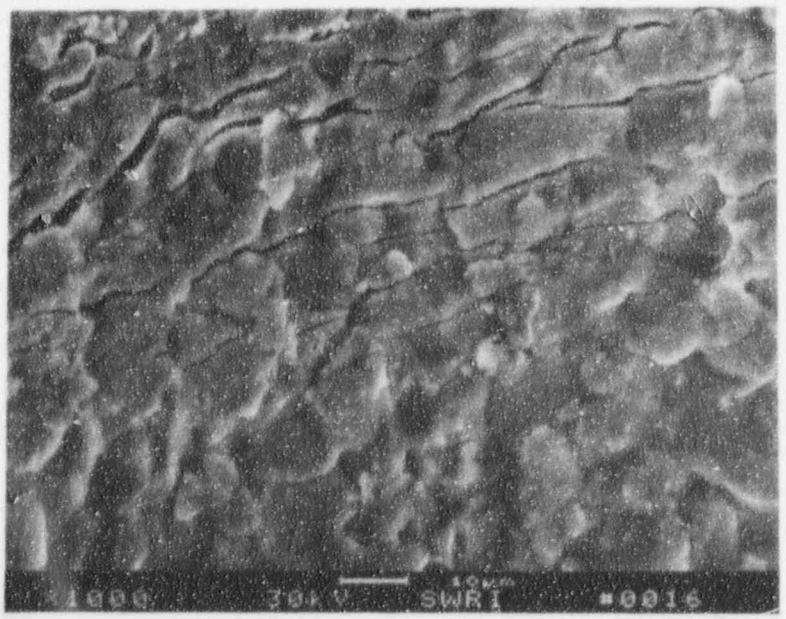

61272 1000X

b)

Figure B-44.SEM Photographs of the Cracked ID Scale at the Thinned Location for SwRI Wire No. 426-1.

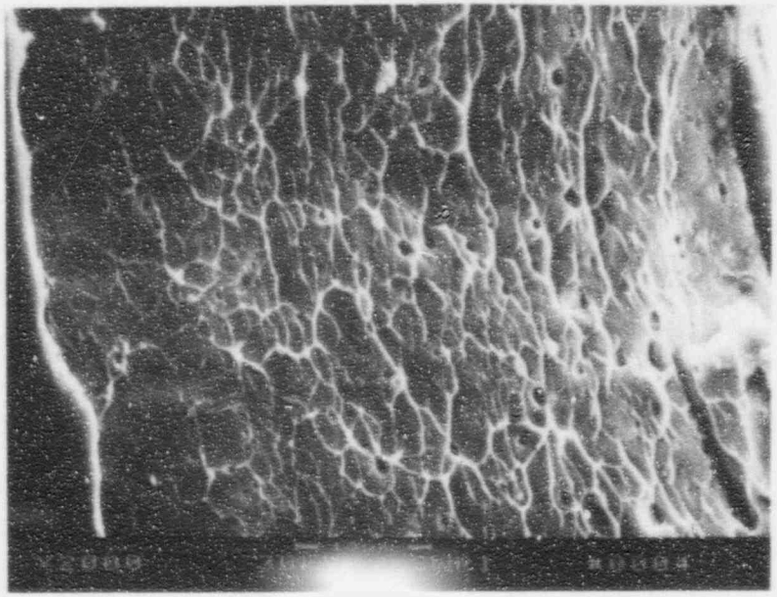

61860 2000X

a) Location A

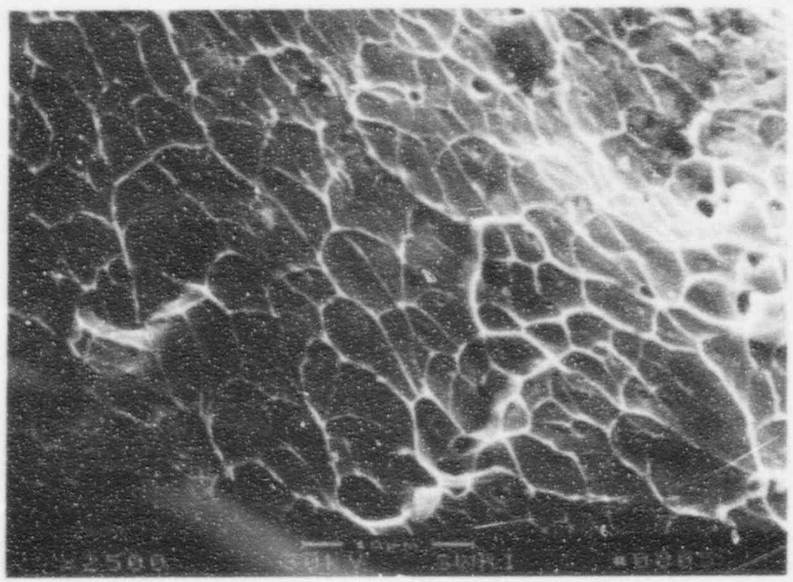

61861 2500X

b) Location B

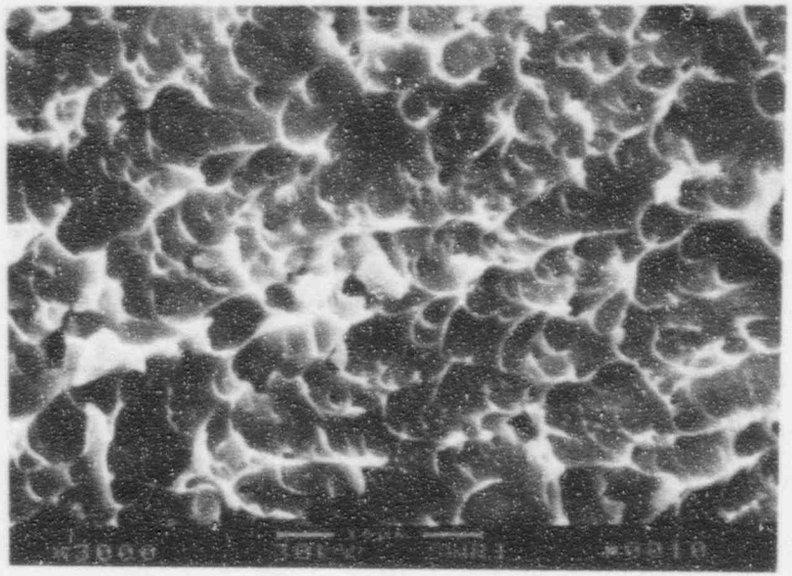

61862 3000X

c) Location C

Figure B-45. SEM Fractographs at Locations A, B and C for SwRI Wire No. 426-1.

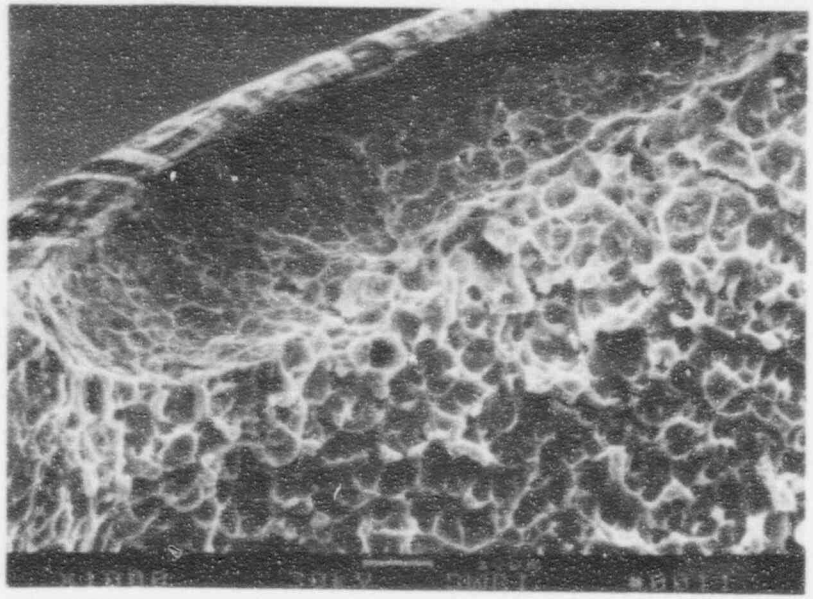

61863 1000X

a) Location D

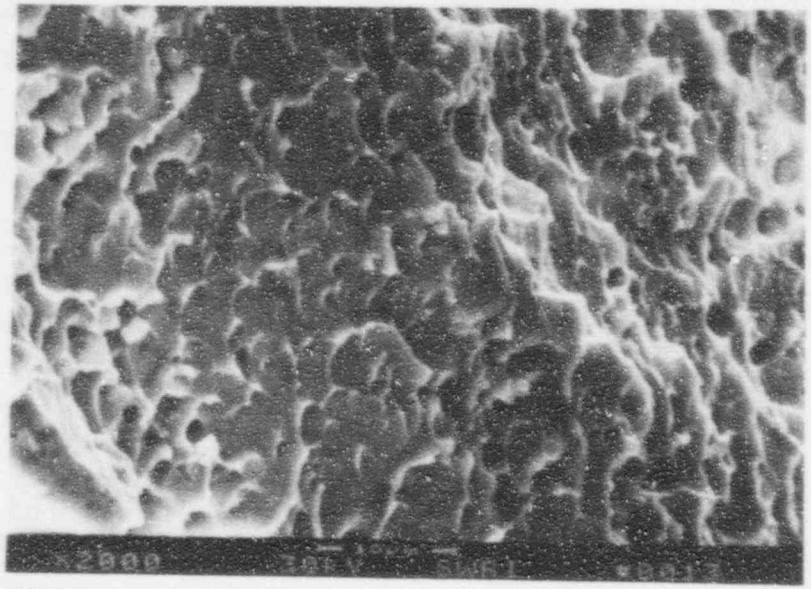

61865 2000X

c) Location F

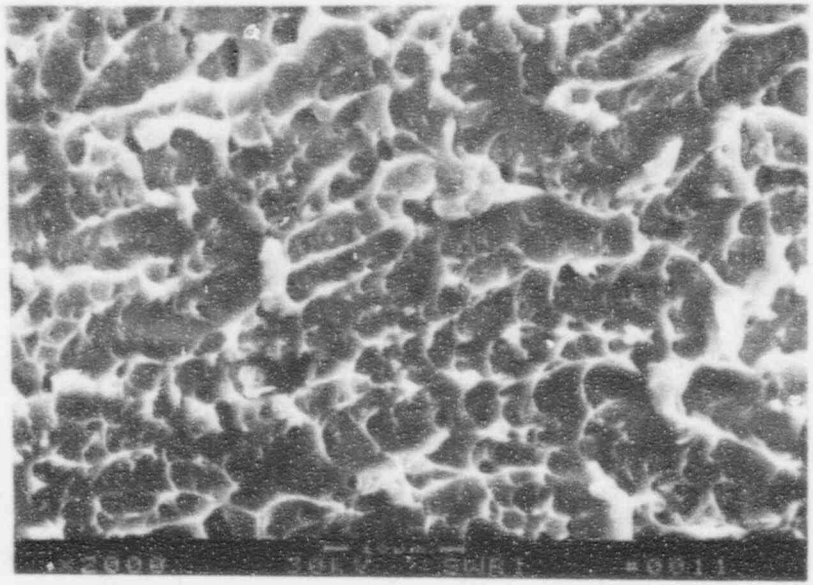

61864 2000X

b) Location E

Figure B-46. SEM Fractographs at Locations D, E and F for SwRI Wire No. 426-1.

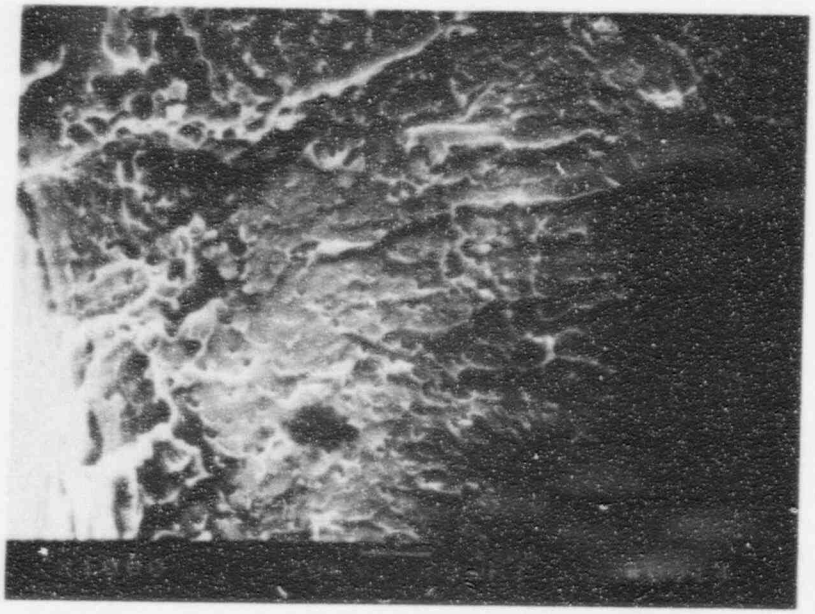

61866 1000X

a) Location G

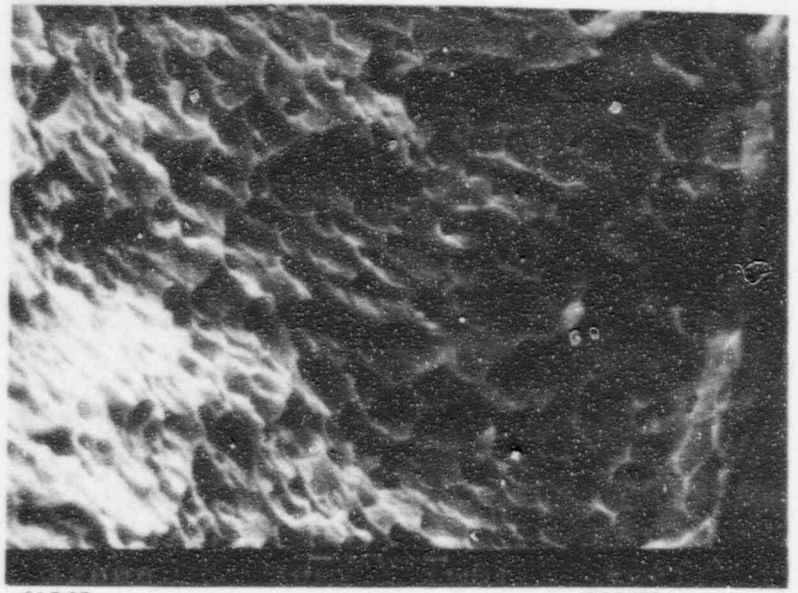

61868 2000X

c) Location I

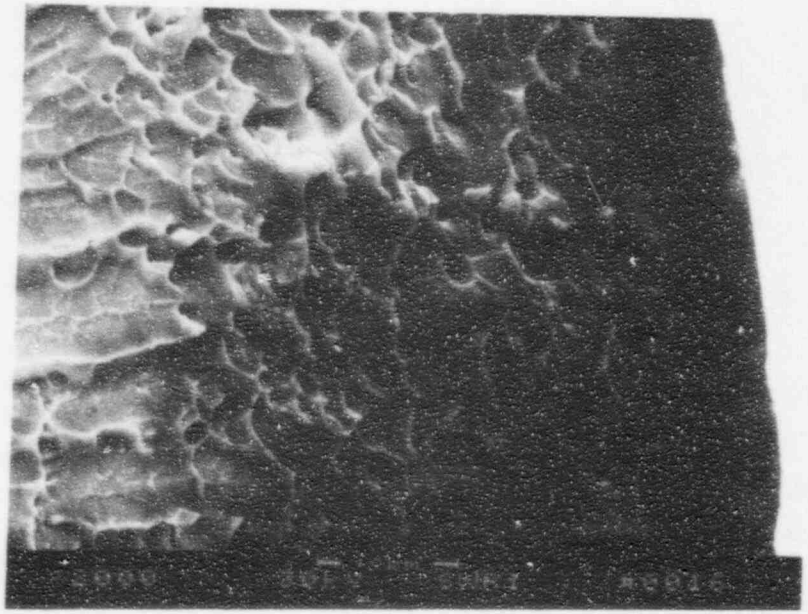

61867 2000X

b) Location H

Figure B-47. SEM Fractographs at Locations G, H and I for SwRI Wire No. 426-1.

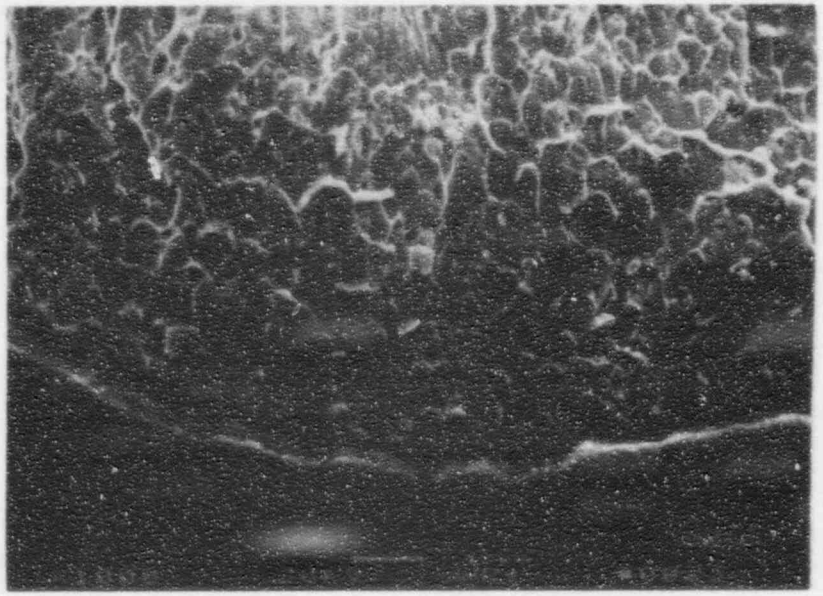

61870 1000X

a)

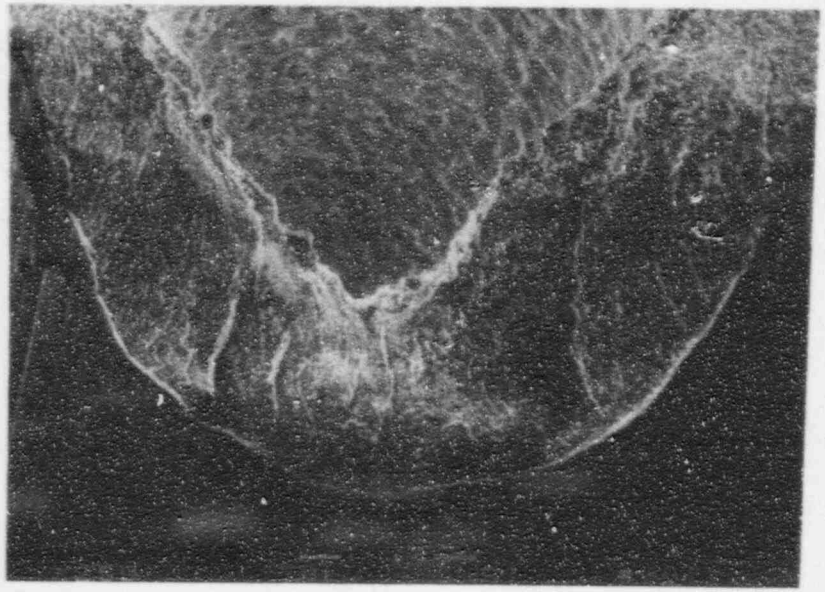

61869 250X

c)

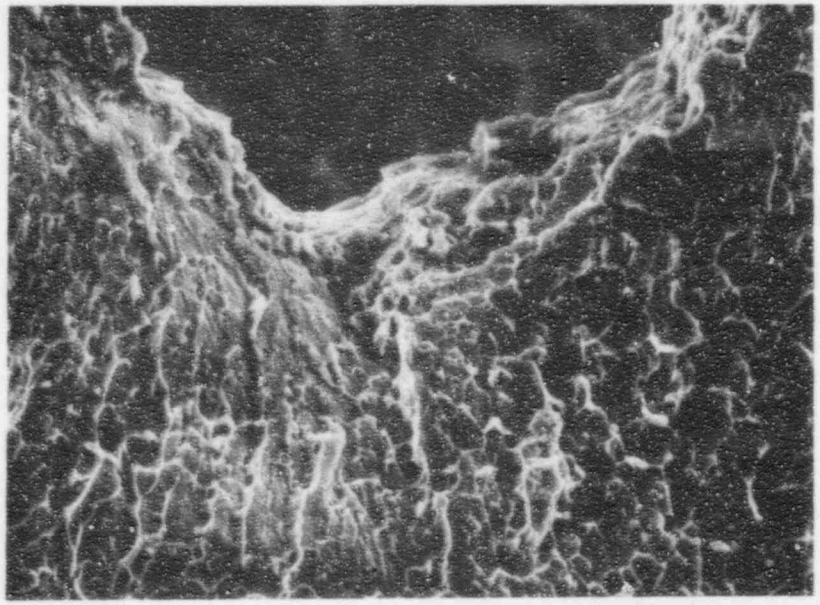

61871 1000X

b)

Figure B-48. SEM Fractographs of the Final Fracture on SwRI Wire No. 426-1.

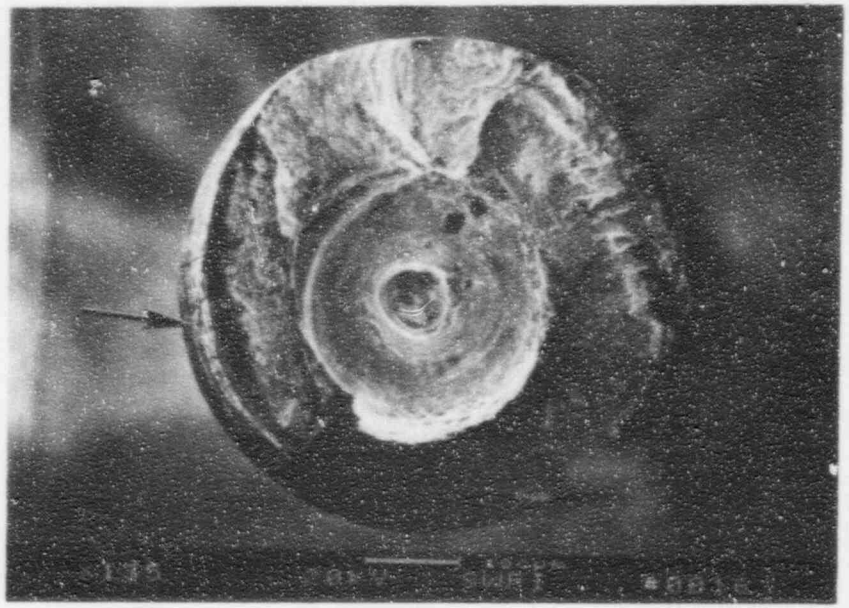

63320 135X

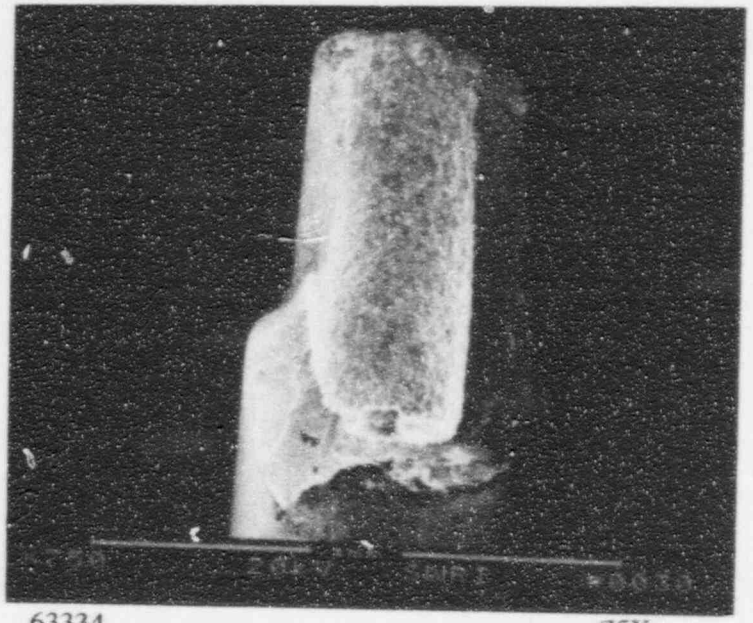

63334 75X

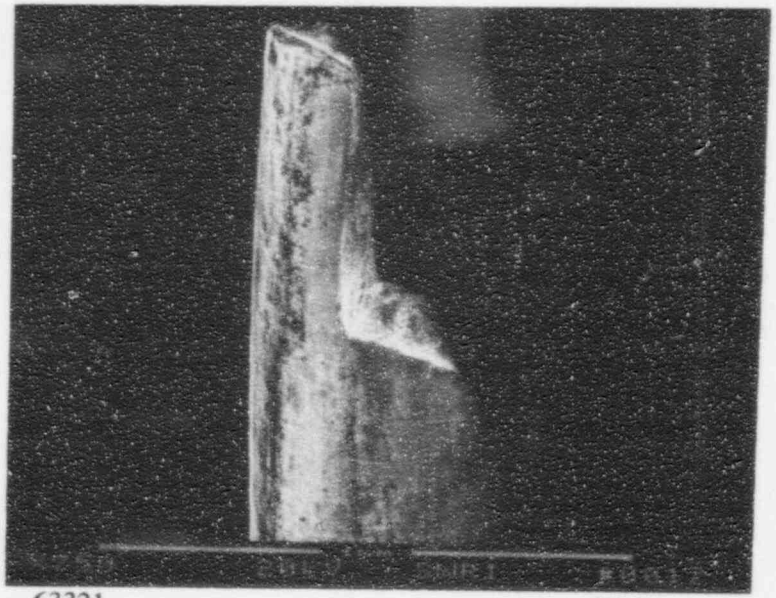

63321 75X

Figure B-49. SEM Fractographs for SwRI Wire No. 442.
Arrow shows yielded region.

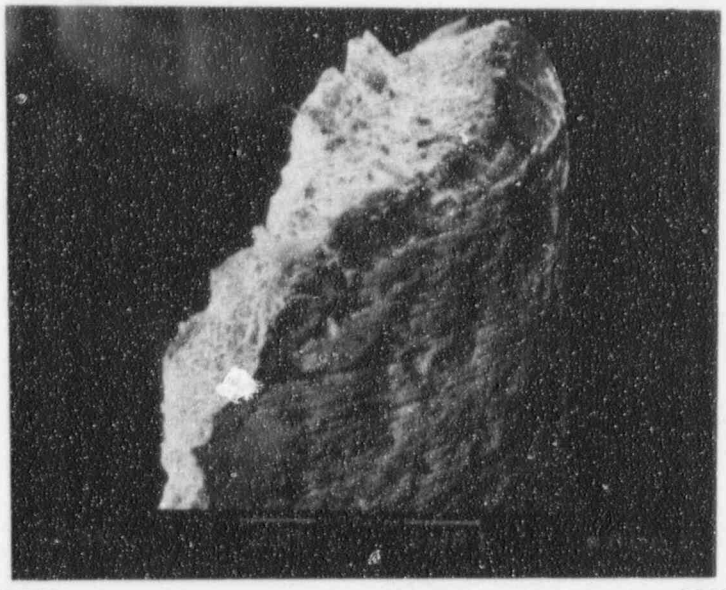

63341 350X

a)

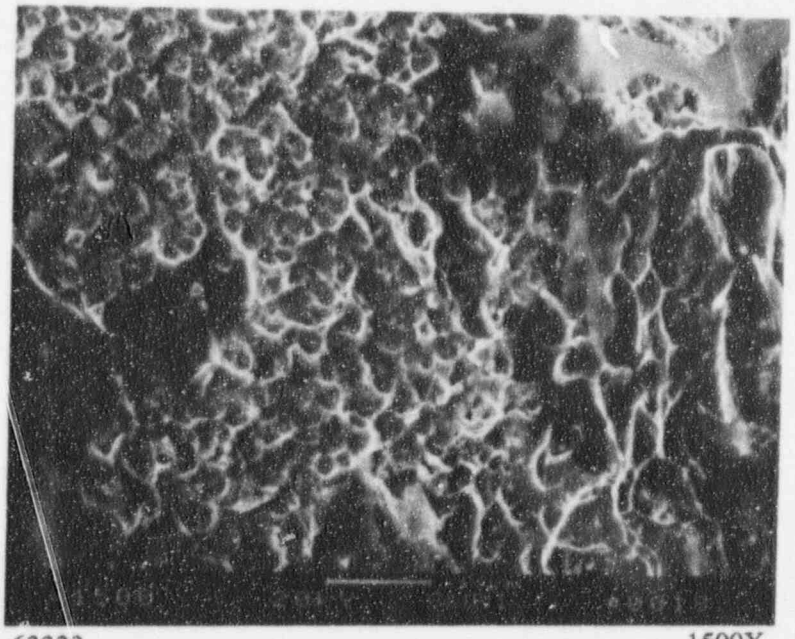

63322 1500X

b)

Figure B-50. SEM Photographs of the Yielded Region for SwRI Wire No. 442.

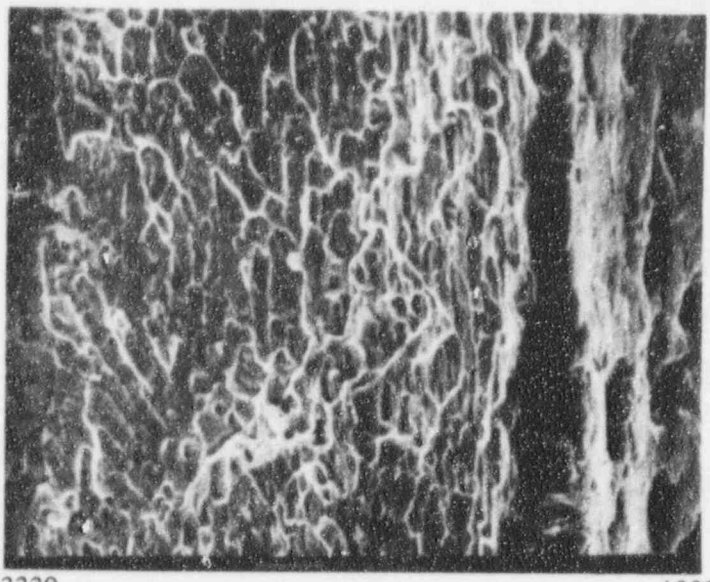

63339 1000X

a) Left Side

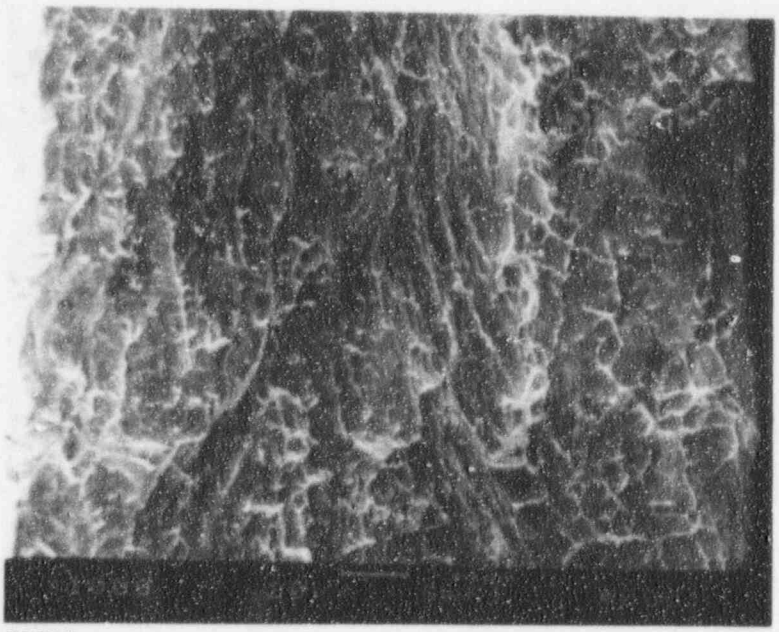

63337 1000X

b) Right Side

Figure B-51. SEM Fractographs of the Longitudinal Fracture Planes for SwRI Wire No. 442.

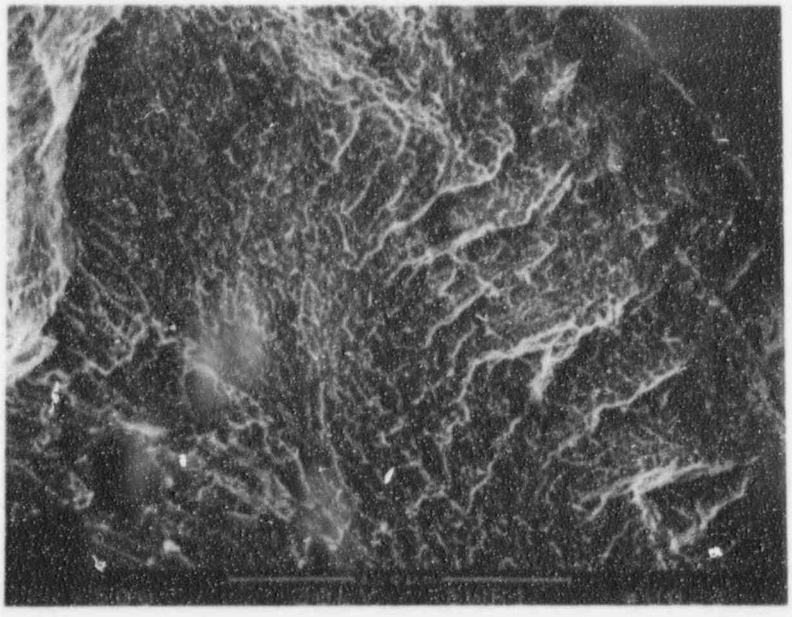

63328 500X

a)

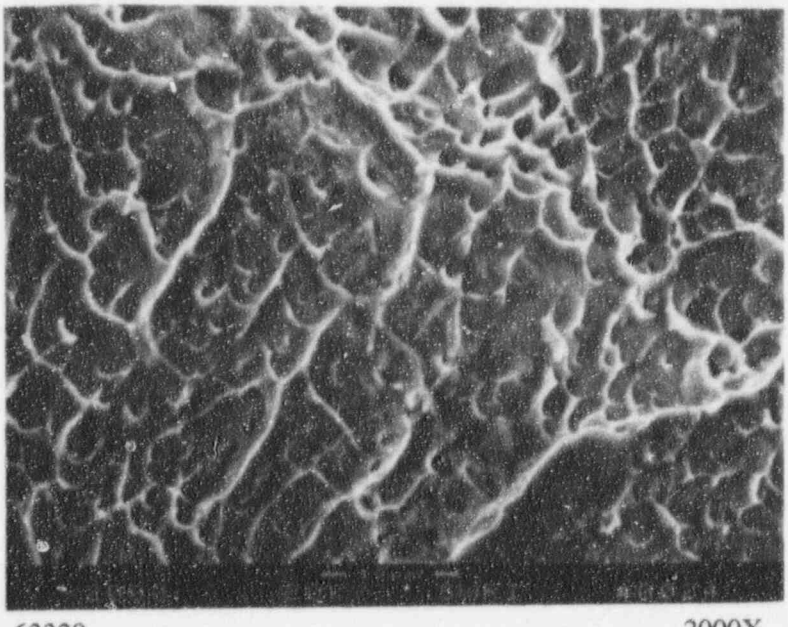

63329 2000X

b)

Figure B-52. SEM Fractographs of the Final Fracture Region for SwRI Wire No. 442.

APPENDIX C. BEND TEST PLOTS FOR SOURCEWIRES

1. BEND TEST PLOTS

This appendix has the bend test plots for each bend test performed on the sourcewires discussed in Section 5.0. There are three types of plots that resulted from the bend tests. One type occurred on the samples that were deflected nearly 90°, shown in Figure C-2. The plot shows the load dropping at 60°. This was caused as the slotted wheel rolled over the wire. As the slotted wheel returned, the wire was springing back, resulting in the load curve. A second type of curve, shown in Figure C-4, the wire was deflected to only 70°, then the test stopped. The load gradually reduced as the slotted wheel retracted. The third type of plot, shown in Figure C-1 was an embrittled condition. When the wire broke, a sharp drop-in load occurred at about 30° of deflection.

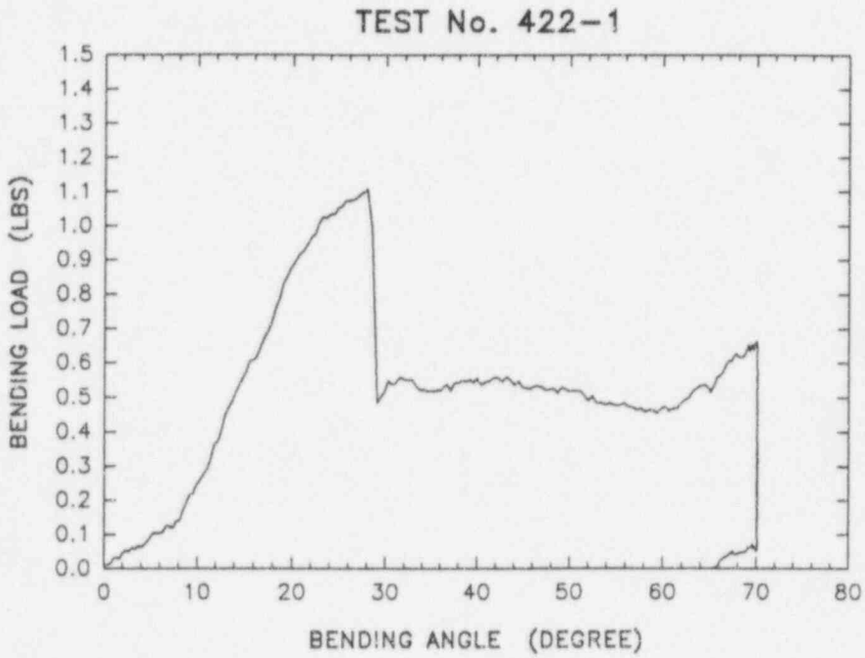

Figure C-1. Plot of Bending Load vs. Angle of SwRI Wire No. 422-1.

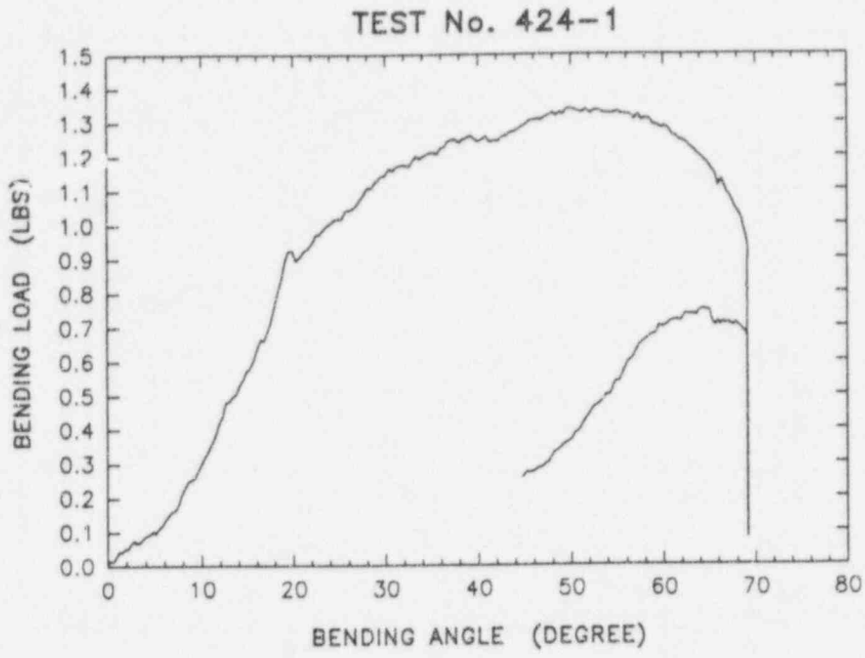

a)

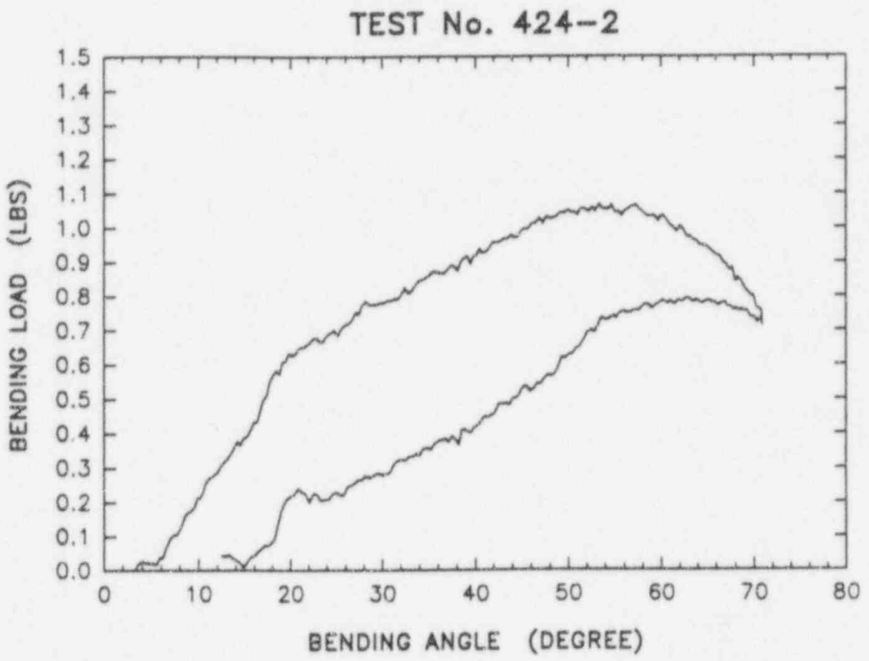

b)

Figure C-2. Plot of Bending Load vs. Angle for SwRI Figure C-2.Wires Nos. 424-1 and 424-2.

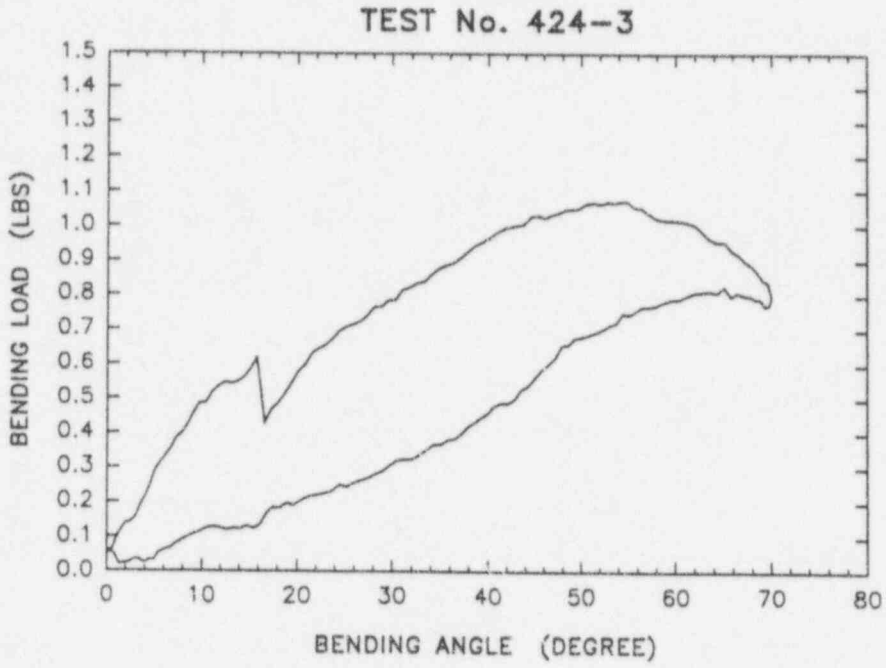

a)

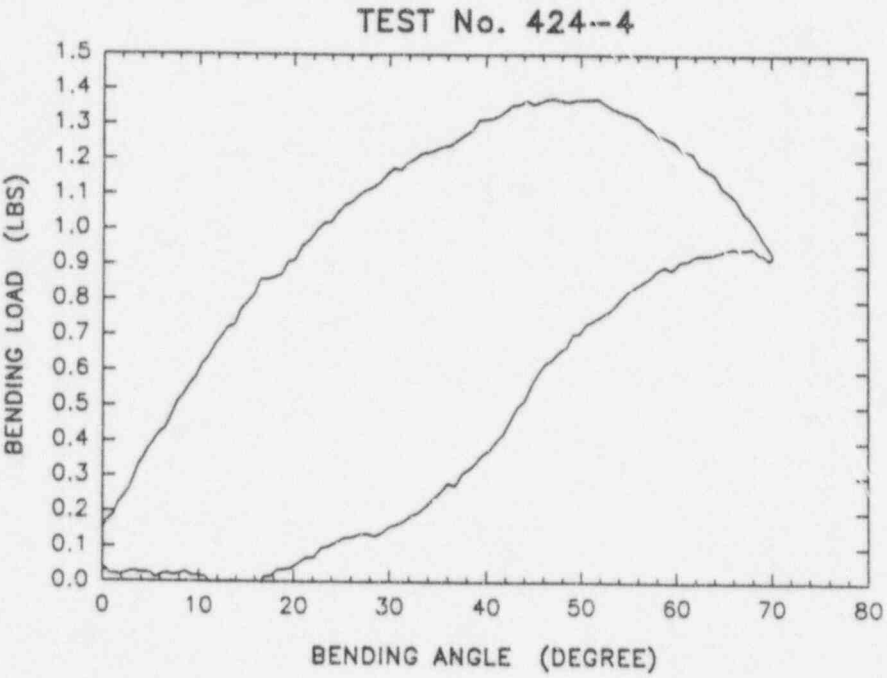

b)

Figure C-3. Plot of Bending Load vs. Angle for SwRI Wires Nos. 424-3 and 424-4.

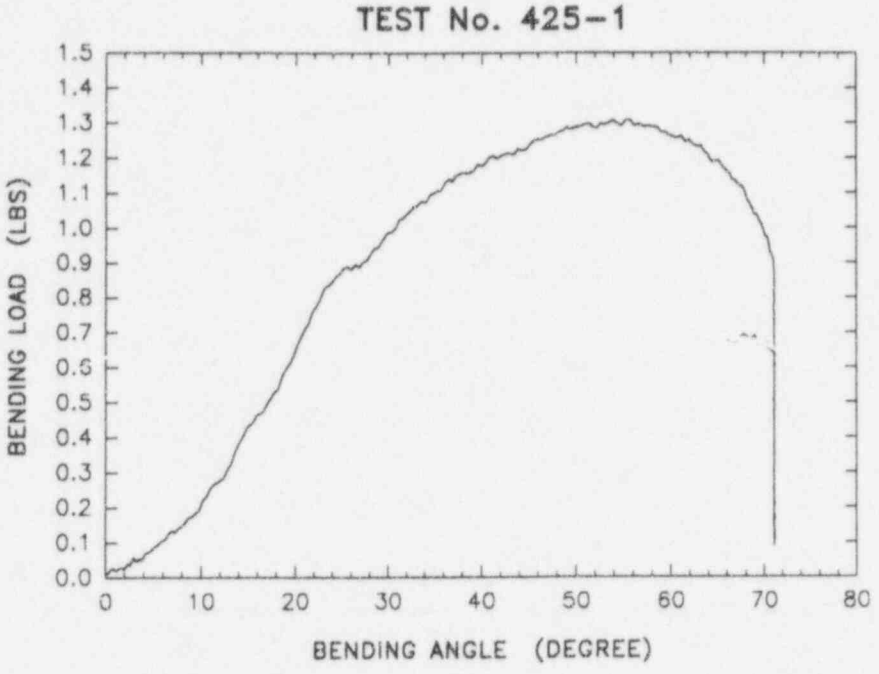

a)

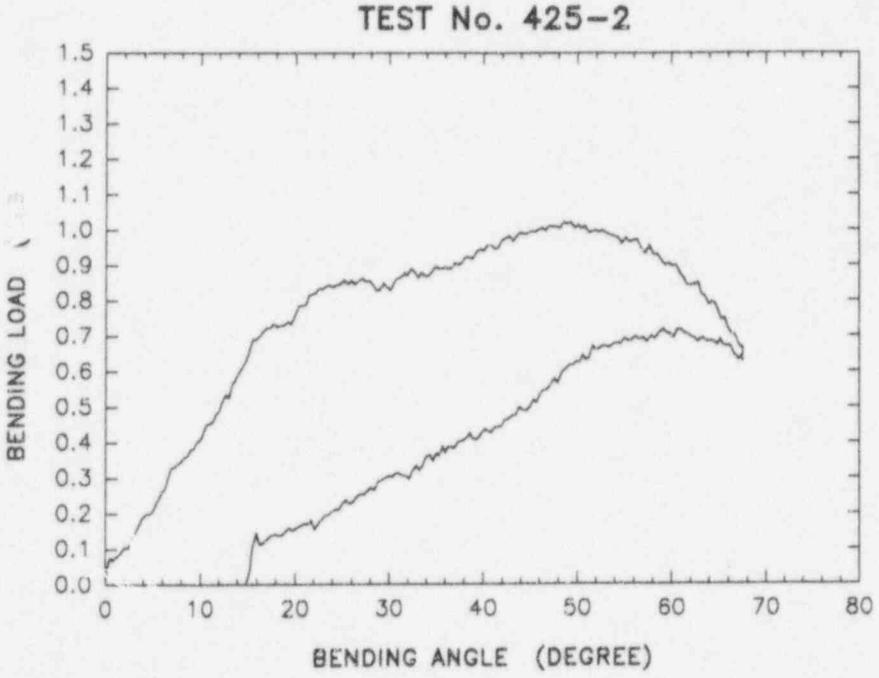

b)

Figure C-4. Plot of Bending Load vs. Angle for SwRI Wires Nos. 425-1 and 425-2.

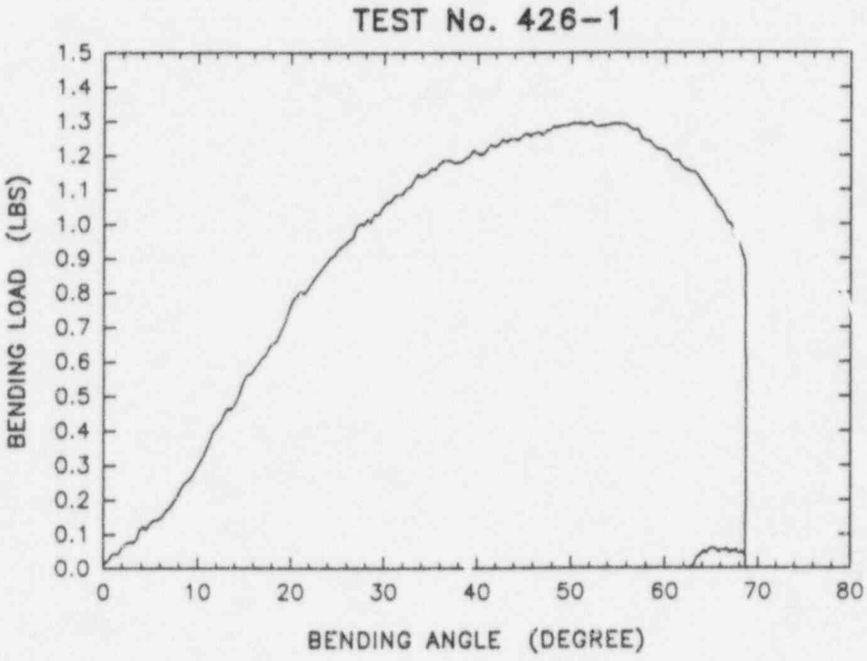

Figure C-5. Plot of Bending Load vs. Angle for SwRI Wire No. 426-1.

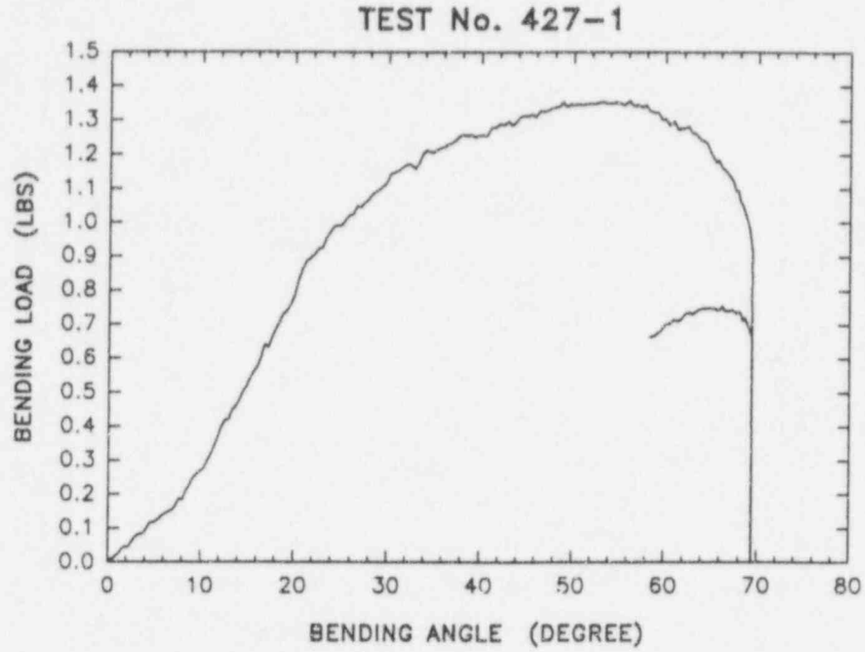

a)

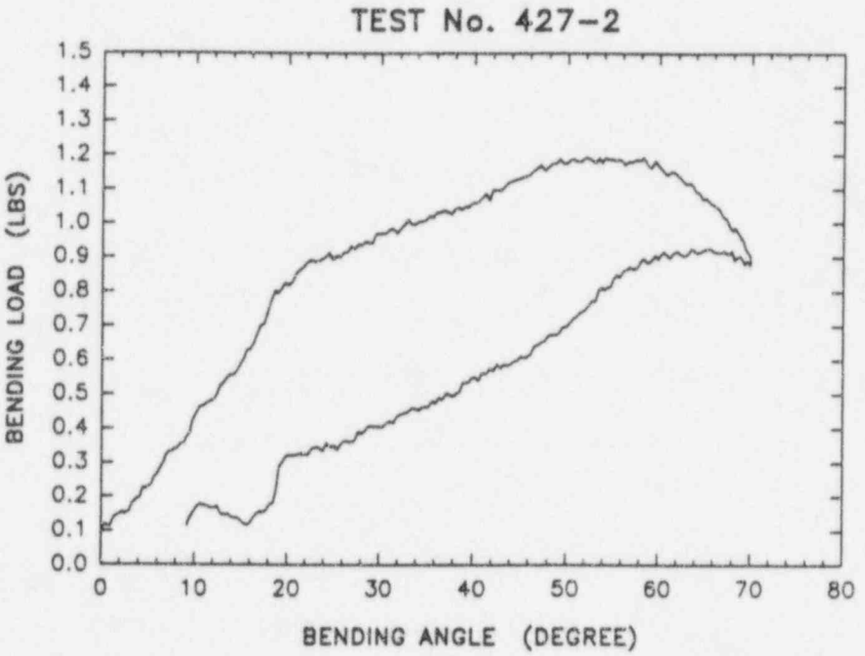

b)

Figure C-6. Plot of Bending Load vs. Angle for SwRI Wires Nos. 427-1 and 427-2.

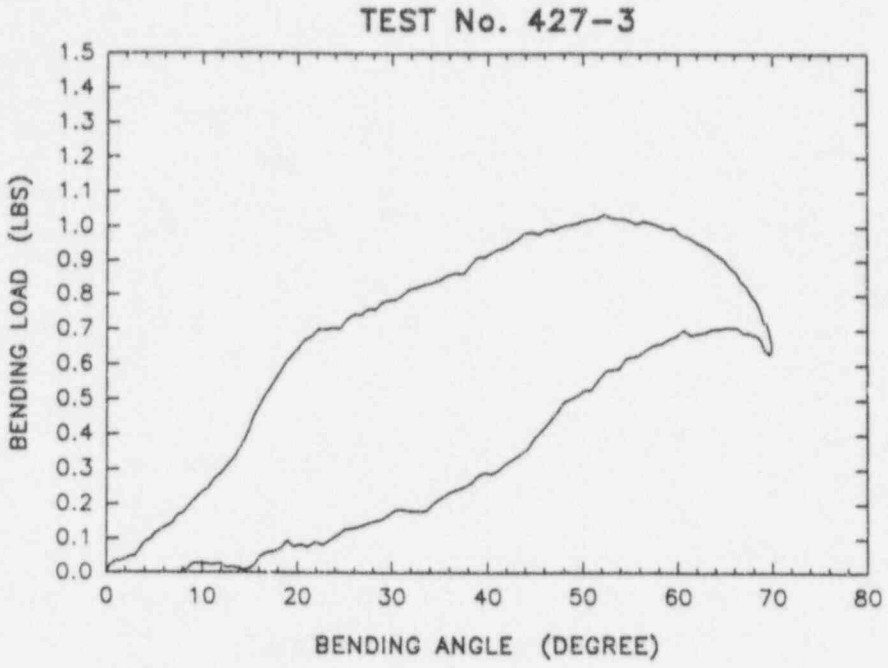

a)

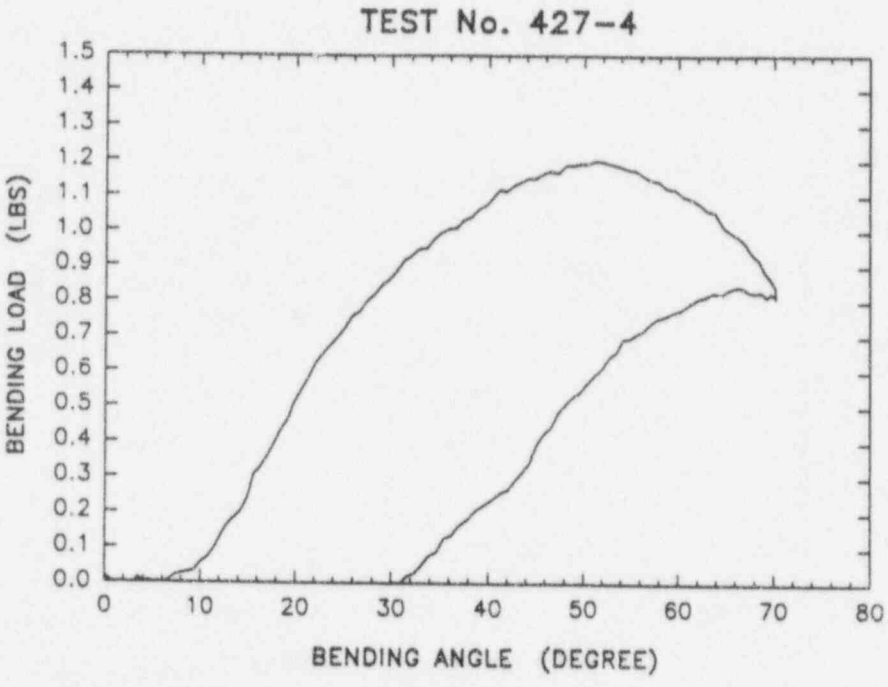

b)

Figure C-7. Plot of Bending Load vs. Angle for SwRI Wires Nos. 427-3 and 427-4.

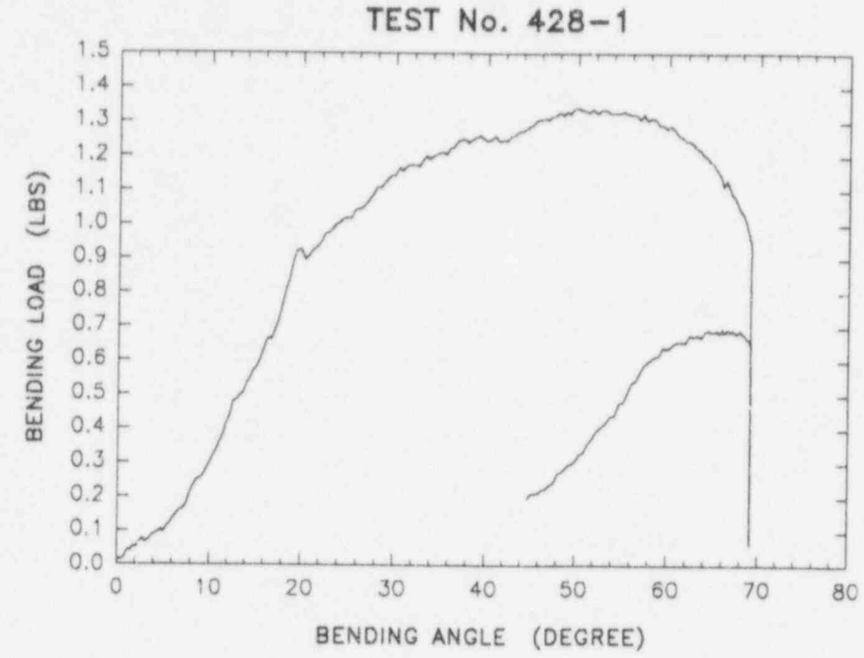

a)

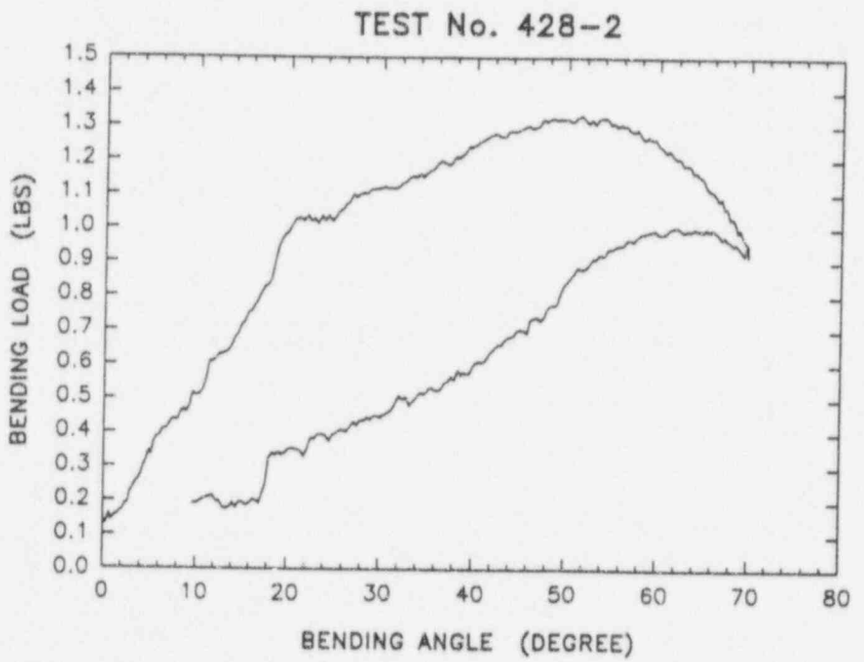

b)

Figure C-8. Plot of Bending Load vs. Angle for SwRI Wires Nos. 428-1 and 428-2.

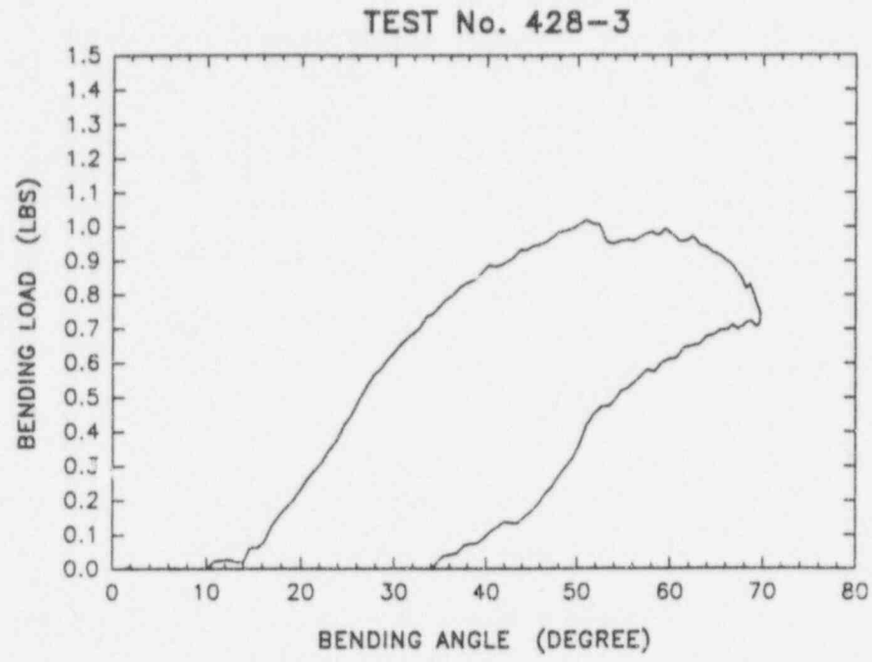

a)

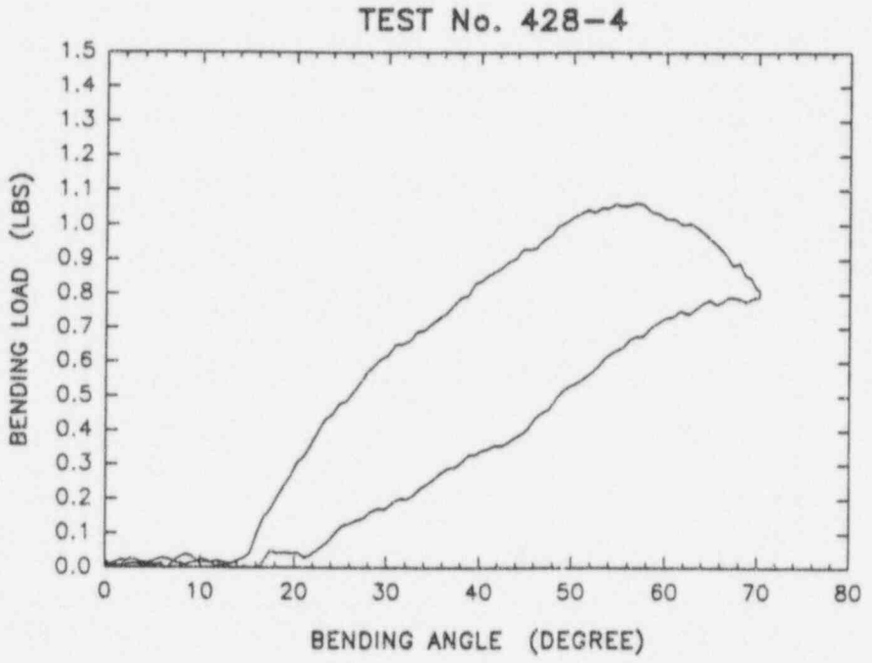

b)

Figure C-9. Plot of Bending Load vs. Angle for SwRI Wires Nos. 428-3 and 428-4.

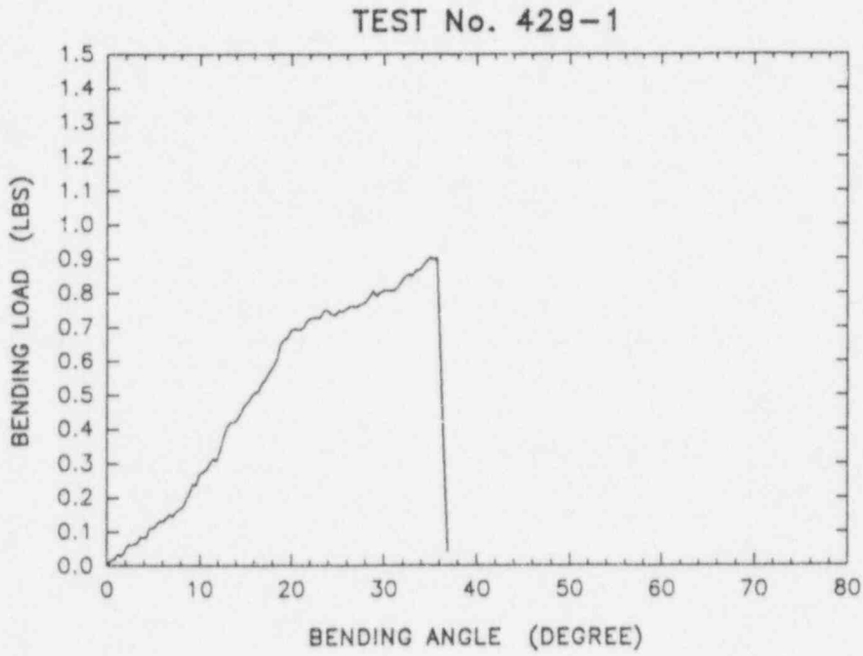

Figure C-10. Plot of Bending Load vs. Angle for SwRI Wire No. 429-1.

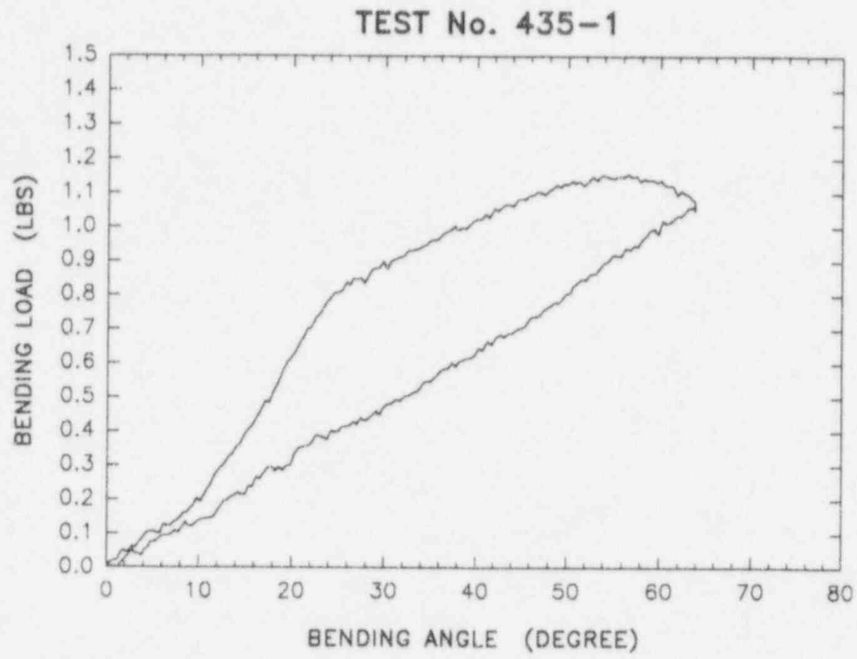

a)

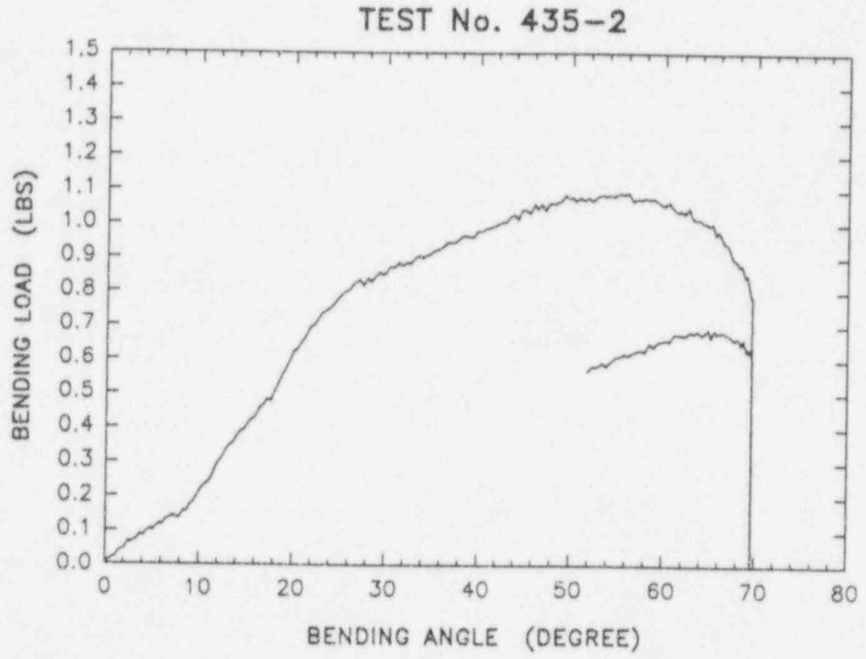

b)

Figure C-11. Plot of Bending Load vs. Angle for SwRI Wires Nos. 435-1 and 435-2.

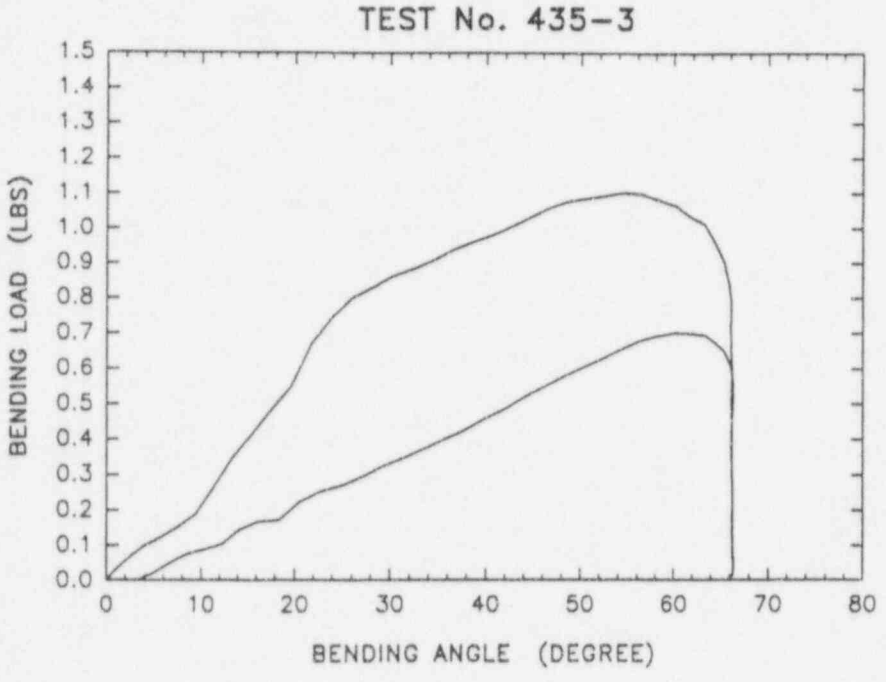

Figure C-12. Plot of Bending Load vs. Angle for SwRI Wire No. 435-3.

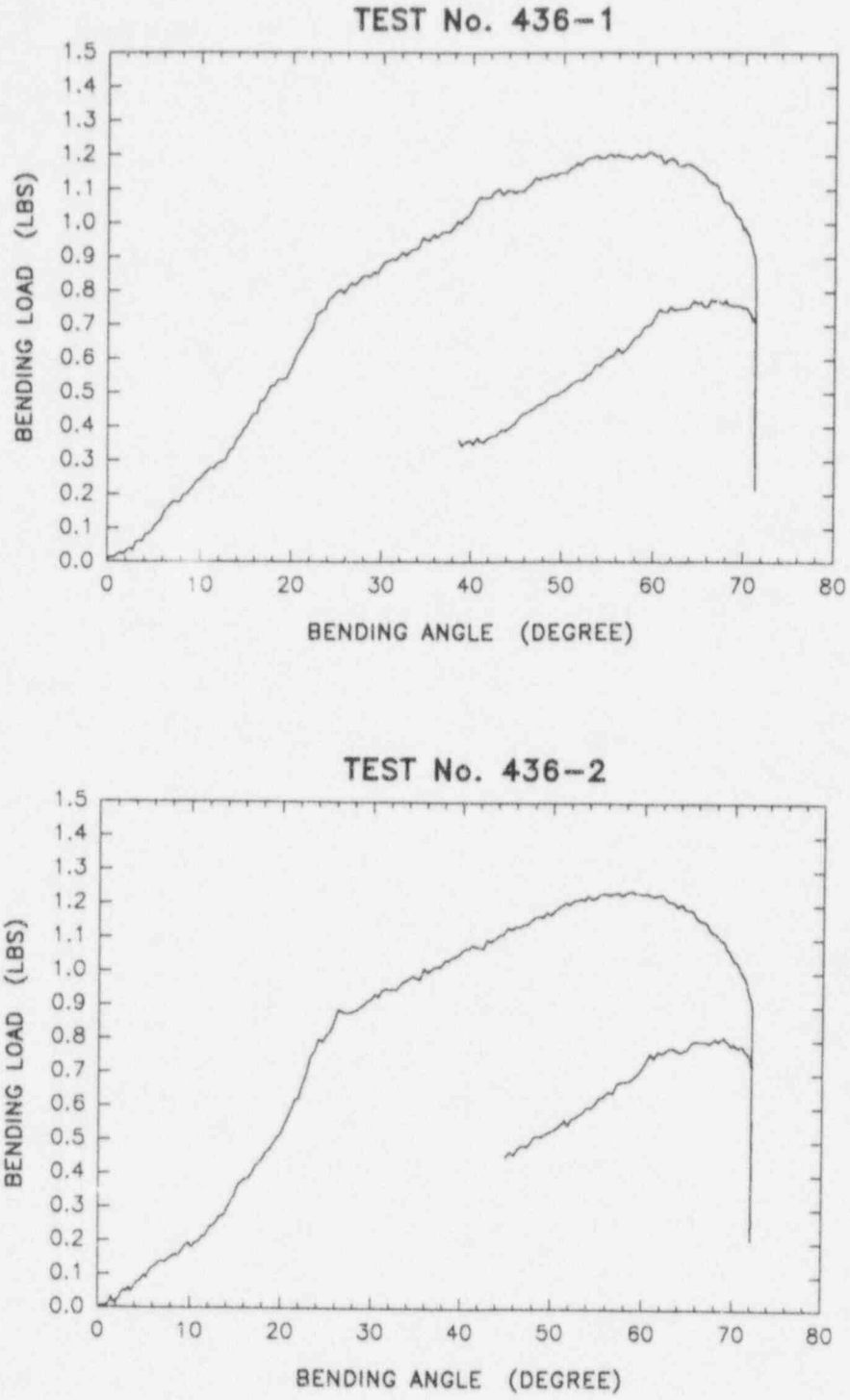

Figure C-13. Plot of Bending Load vs. Angle for SwRI Wires Nos. 436-1 and 436-2.

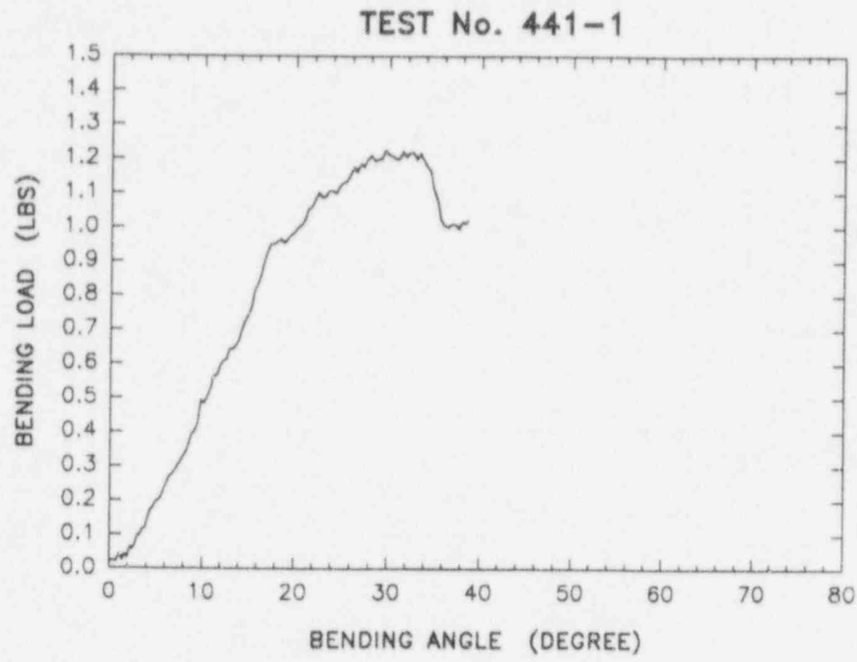

a)

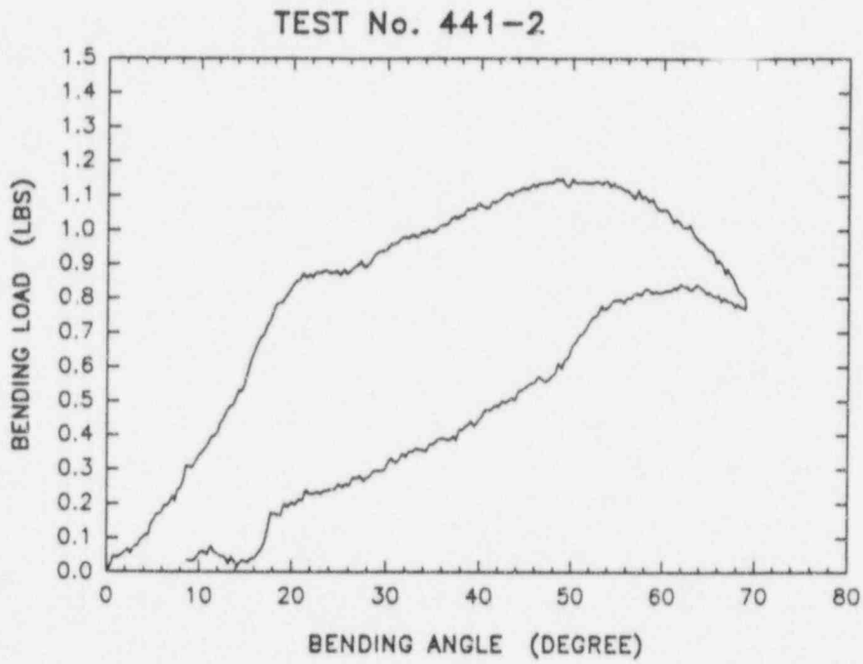

b)

Figure C-14. Plot of Bending Load vs. Angle for SwRI Wires Nos. 441-1 and 441-2.

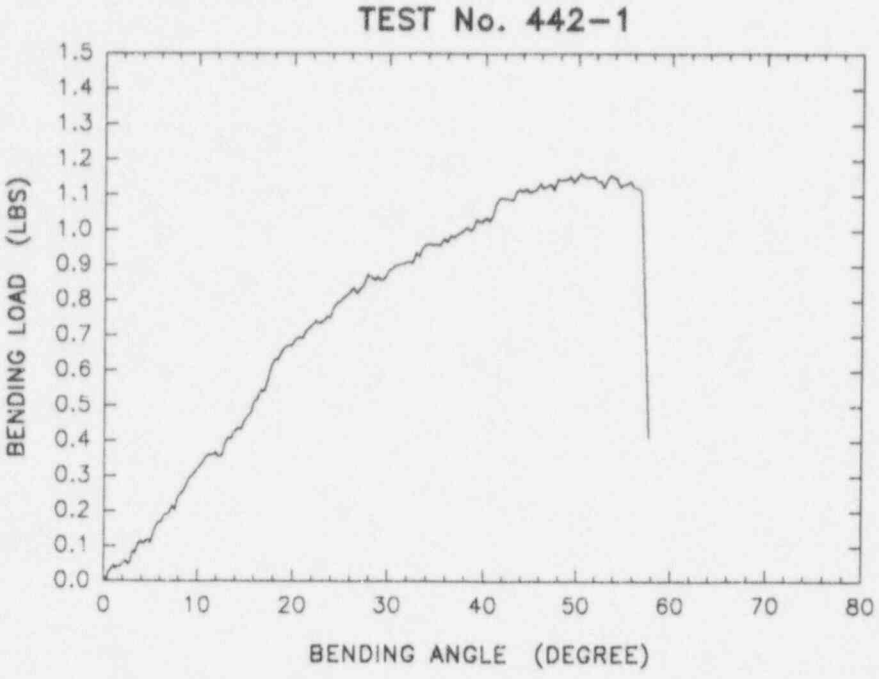

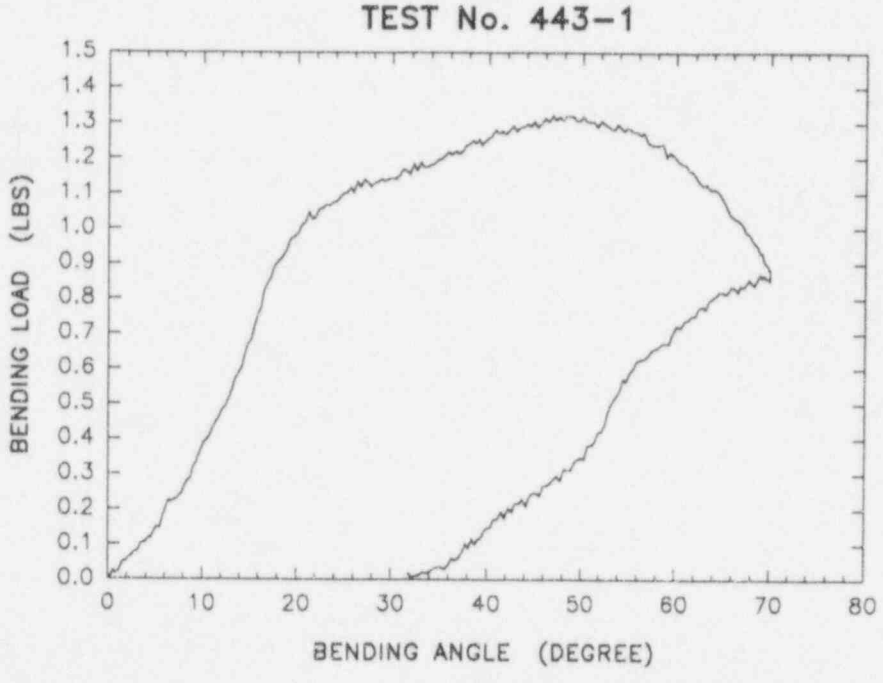

Figure C-15. Plot of Bending Load vs. Angle for SwRI Wires Nos. 442-1 and 443-1.

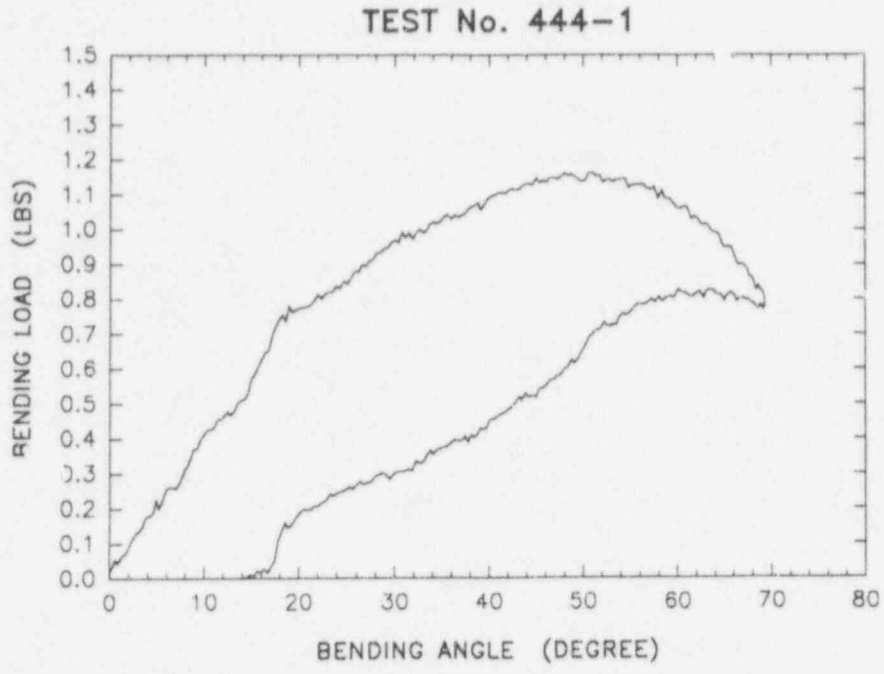

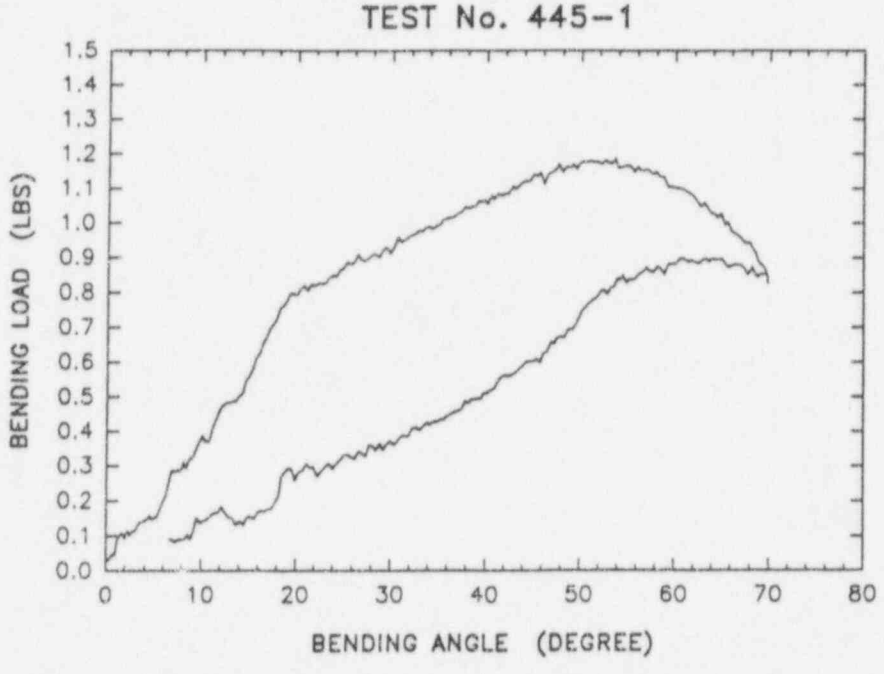

Figure C-16. Plot of Bending Load vs. Angle for SwRI Wires Nos. 444-1 and 445-1.

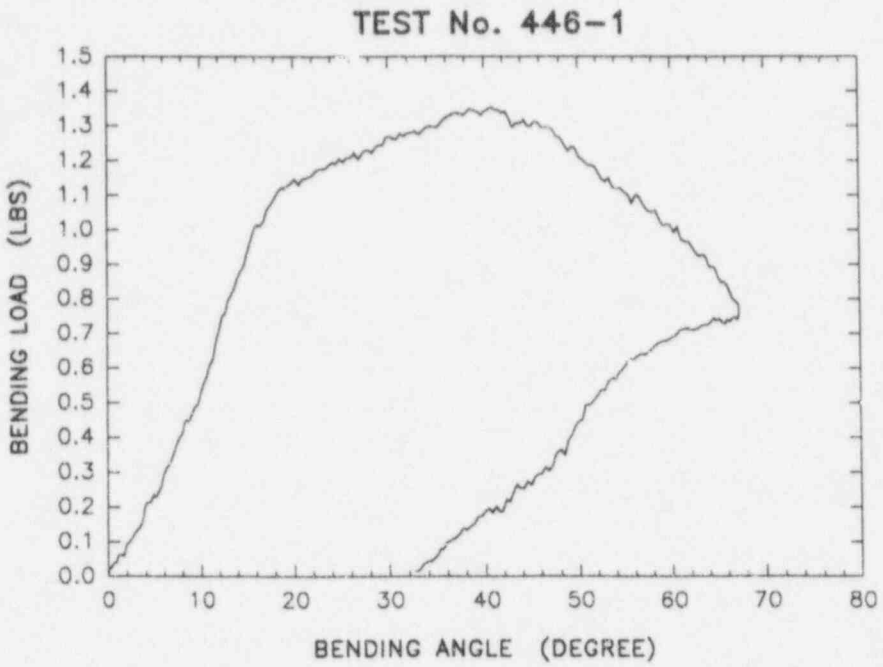

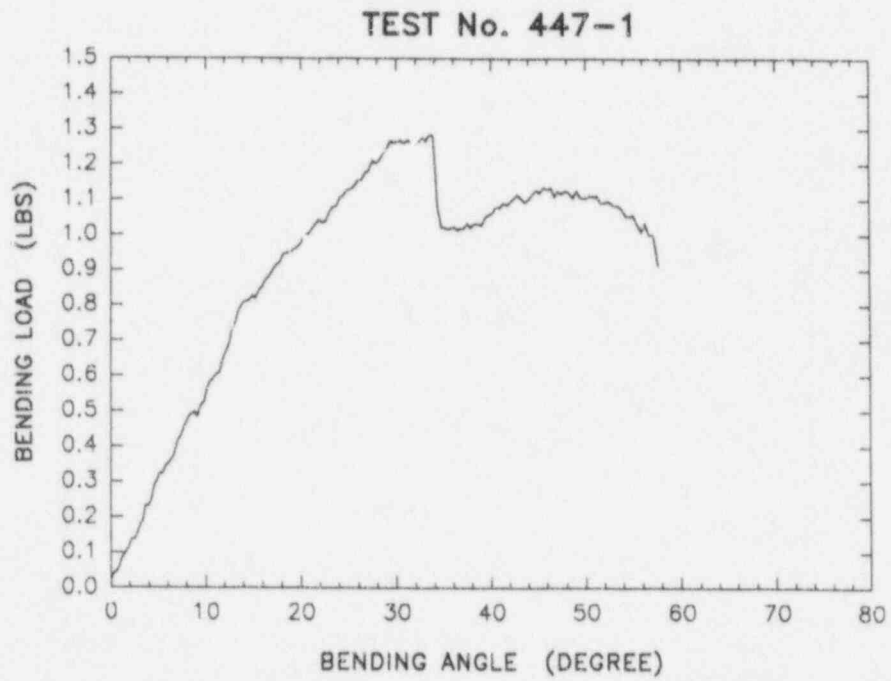

Figure C-17. Plot of Bending Load vs. Angle for SwRI Wires Nos. 446-1 and 444-7.

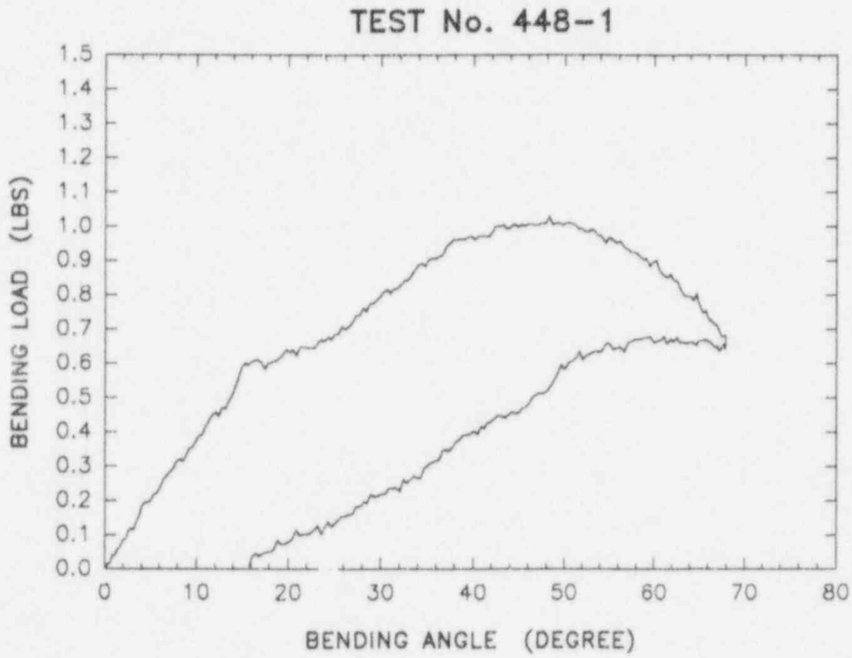

Figure C-18. Plot of Bending Load vs. Angle for SwRI Wire No. 448-1.

APPENDIX D. HYDROGEN CHARGING PROCEDURE AND FRACTOGRAPHIC DATA

1. HYDROGEN CHARGING PROCEDURE

The specimens for the hydrogen embrittlement tests were prepared by electrolytic charging in a 0.5% acetic and solution. Three Nitinol wire specimens, each approximately 1 1/2 inches long, were suspended in the acid solution equidistant from a graphite anode. Potentials were applied to the specimens by means of a commercial potentiostat utilizing a saturated calomel reference electrode.

2. TEST NOS. HC-2 AND HC-3

These two tests were performed in the optimization test series at the lowest charging potential. The specimens did not fracture but distinct microcracks developed, as shown in Figures D-1 and D-2. Cracks on the outside of the bends were relatively short and open [Figure D-1(a) and D-2(a)] while those on the inside were usually longer with 45° segments at the ends [Figures D-1(b) and D-2(b)]. It is evident that these charging conditions were insufficient to fully embrittle the specimens but that a degree of embrittlement did occur as evidenced by the cracking.

3. TEST NOS. HC-4 AND HC-7

These tests represent two cases where charging was sufficient to induce complete fracture in the bend test. Test HC-4 was one of the triplicate tests with charging conditions of -1.0v and 120 min. The fractographic features consist of a flat fracture surface with fine-scale dimples and a thin featureless rim at the outer periphery, see Figure D-3. These features are essentially identical to those of Test HC-6, see Section 5.5.

Test HC-7 was charged for a shorter period (100 min.) but still resulted in complete brittle fracture in the bend test. The fractographic features are shown in Figure D-4 and are essentially identical to those of Test Nos. HC-4 and HC-6.

Representative specimens from the other hydrogen charged tests which resulted in brittle fracture (Test Nos. HC-12 through HC-17) were also examined. In all cases, the fractographic features were essentially identical to those observed for Test Nos. HC-4, HC-6, and HC-7.

4. TEST NOS. HC-5 AND HC-8

Test Nos. HC-5 was one of the triplicate tests performed with the maximum charging condition but it did not result in fracture of the specimen. Post-test SEM examinations, did however, reveal significant cracking on the inside of the bend as shown in Figure D-5(b). The cracking which developed in the bend test demonstrates that some degree of embrittlement did occur. Apparently, the charging condition varied slightly among the three specimens (HC-4, HC-5, and HC-6) so that Test HC-5 did not represent as high a degree of embrittlement as the other two tests.

Reverse bending of the specimen after the initial test (Test No. HC-5R) resulted in complete brittle fracture. SEM fractographic from that fracture are shown in Figures D-6, D-7 and D-8. The specimen exhibited a flat fracture surface and uniform fine-scale dimples were evident throughout except for the initiation region [Figures D-6 and D-8]. The initiation zone exhibited a unique fine scale topography comprised of smooth features, ripples and very small tear dimples [Figure D-7].

5. TEST NO. HC-8

Test No. HC-8 involved a charging time of 80 min. and did not result in fracture. However, post-test SEM examinations showed subcritical cracking on the inside of the bend, as shown in Figure D-9(b). The cracking is less severe than that of Test HC-5. As in the case of Test No. HC-5, the cracking demonstrates partial embrittlement consistent with the less severe charging conditions.

Reverse bending after the initial test (Test No. HC-8R) resulted in complete brittle fracture. SEM fractographs are shown in Figures D-10, D-11, and D-12. The fractographic features are essentially identical to those of Test No. HC-5R. The flat fracture and fine scale dimples are shown in Figures D-10(b) and D-12. Figure D-12 shows the initiation zone with the unique ripples and fine-scale tear dimples similar to those observed in Test HC-5R. It should be noted that the reverse bends of Test Nos. HC-5R and HC-8R were performed several days after the initial bend tests so that initial embrittlement may have decayed. A possible explanation of the fractographic features is that the failures initiated by slow tearing from the surface cracks in the early stages of the bend and that the final dimpled rupture occurred when the tearing reaches the critical crack size for fast fracture of the remaining section.

6. TEST NOS. HC-18 THROUGH HC-23

These tests represent cases where the bend tests were performed either after a 52-hour delay (HC-18, HC-19, HC-20) or after a 2-hour 450°F bake-out procedure (HC-21, HC-22, HC-23). None of these bend tests resulted in fracture indicating that the hydrogen embrittlement process is reversible. However, post-test SEM examinations revealed subcritical cracking at the bend as shown in Figures D-13 and D-14.

A possible explanation of this behavior is that the embrittlement in the outer layer involves a non-reversible mechanism so that a thin brittle shell remains after a delay time or bake out. Then, during the bend test, the thin shell could develop cracks which are not of a critical size for fracture of the more ductile core. A second possibility is that surface microcracks form during the charging process and that these cracks are not critical to fracture of this full cross section after time delay or bake-out. Further detailed studies of the hydrogen embrittlement process in Nitinol would be necessary to resolve these questions. Such testing is not relevant to the identification of the root cause of the sourcewire failures and is beyond the scope of this investigation.

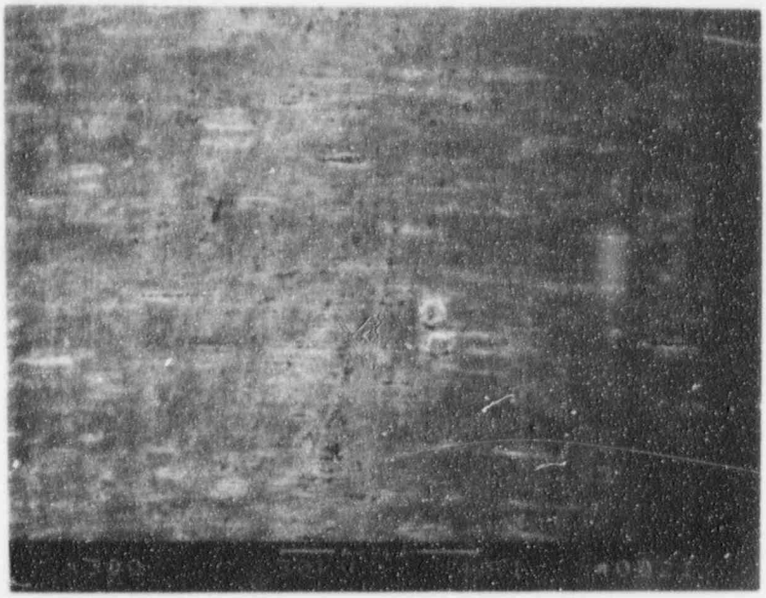

61707 300X

a) Outside of Bend

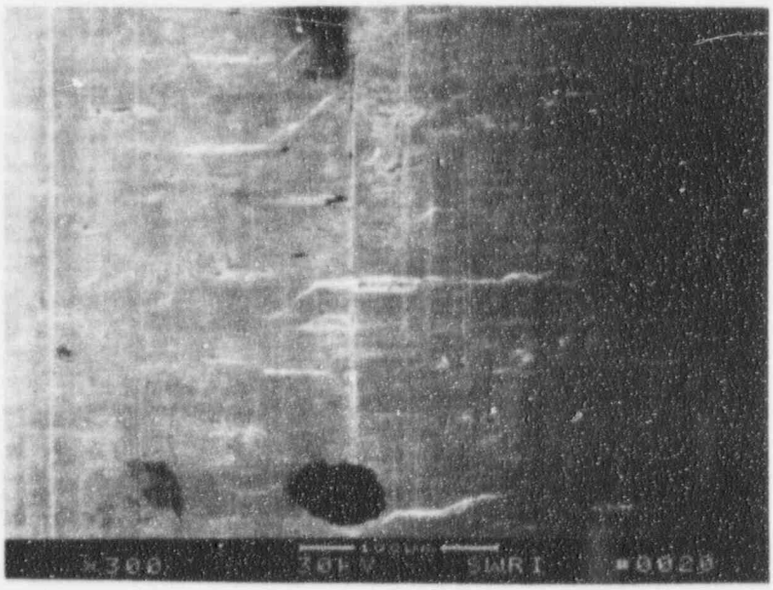

61706 300X

b) Inside of Bend

Figure D-1. SEM Photomicrographs from Surface of Hydrogen-Charged Bend Specimen. Test No. HC-2. Charging Conditions: -0.5V, 120 Min.

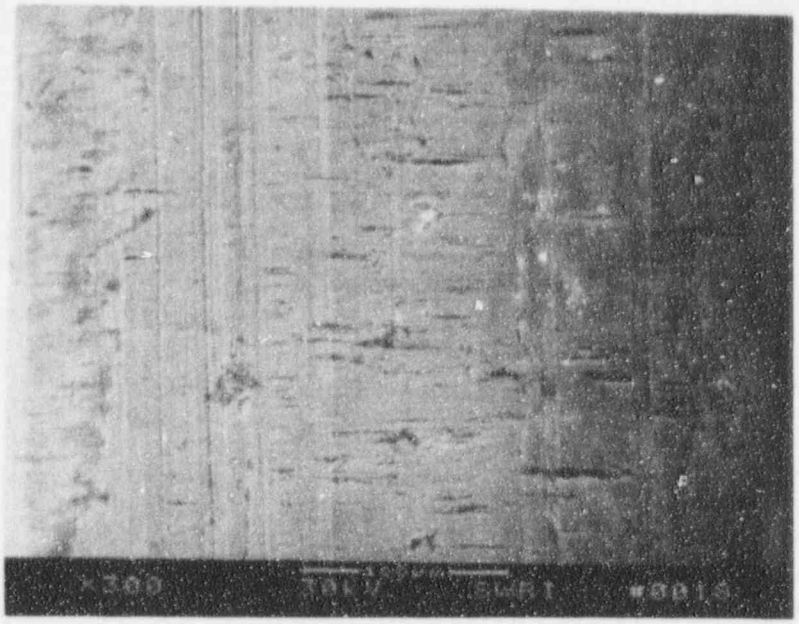

61710 300X

a) Outside of Bend

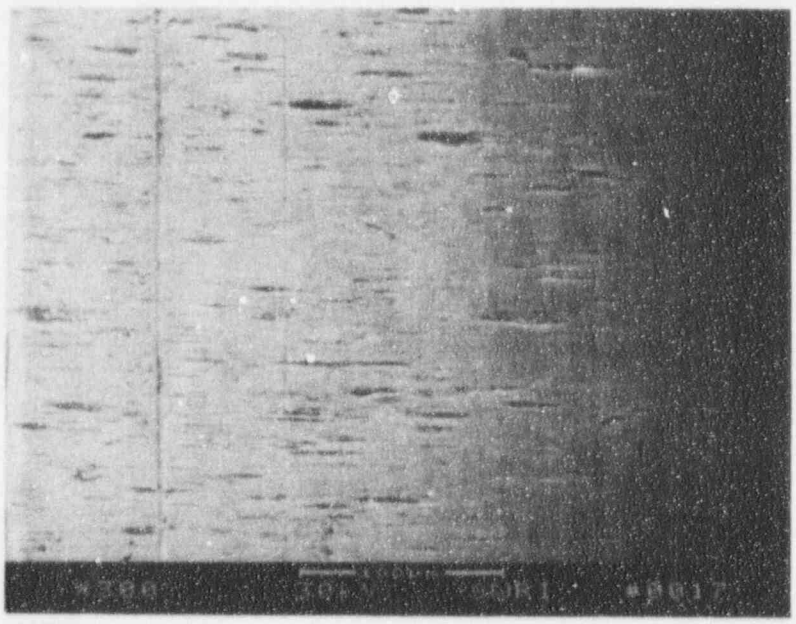

61709 300X

b) Inside of Bend

Figure D-2. SEM Photomicrographs from Surface of Hydrogen-Charged Bend Specimen. Test No. HC-3. Charging Conditions: -0.5V, 120 Min.

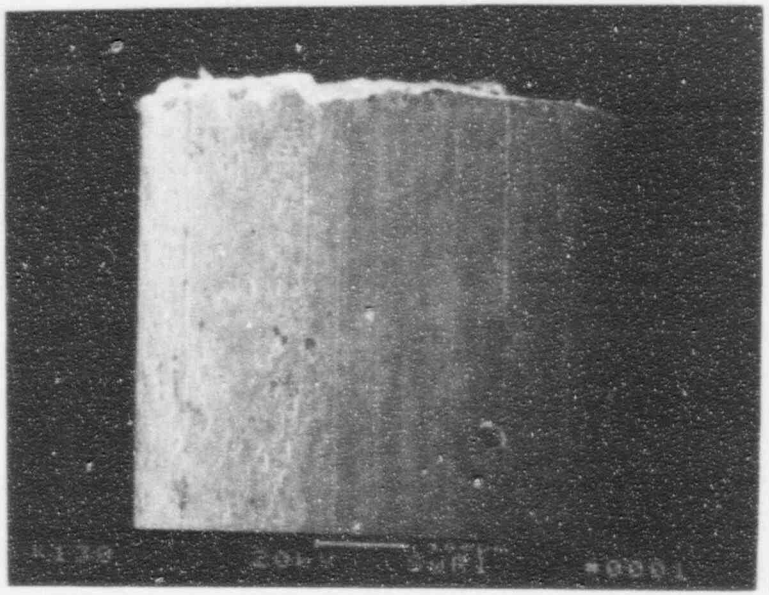

61813 130X

a) Side View

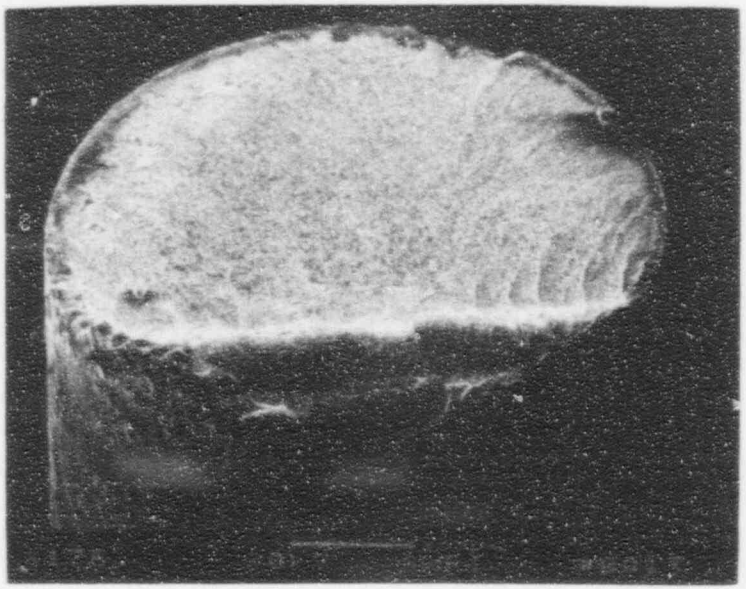

61800 176X

b) Fracture Surface

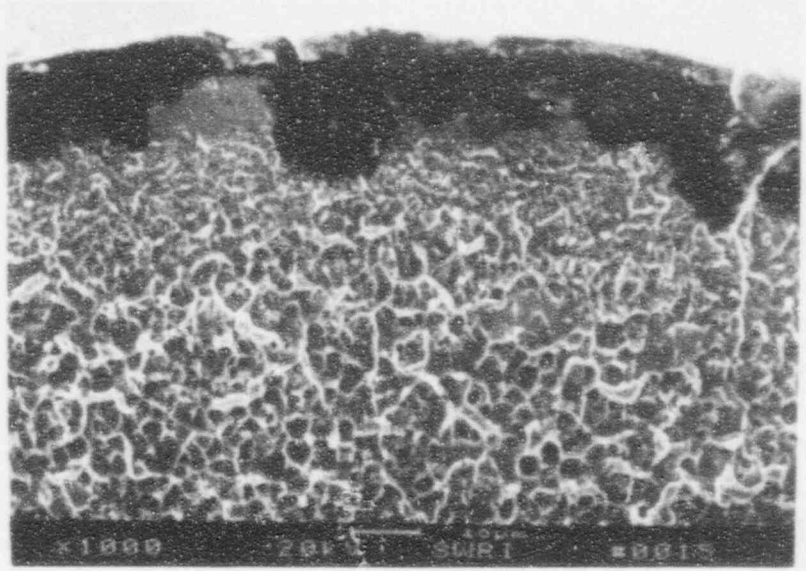

61802 1000X

c) At Edge Near Origin

Figure D-3. SEM Photomicrographs and Fractographs from Hydrogen-Charged Specimen. Test No. HC-4. Charging Conditions: -1.0V, 120 Min.

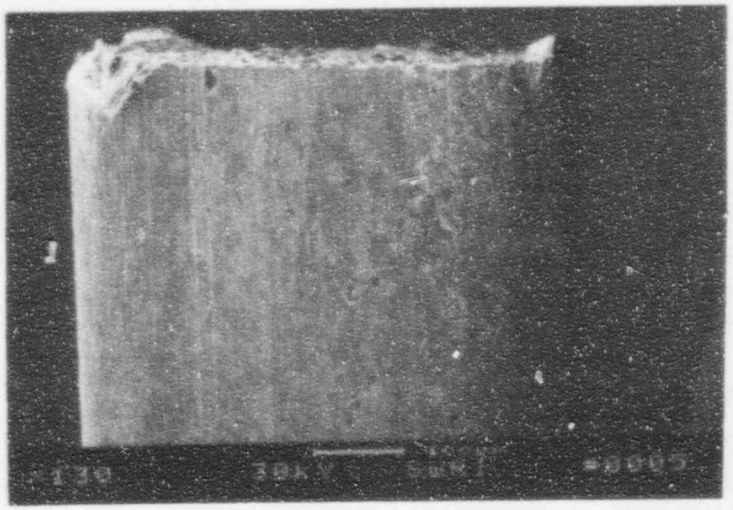

61808 130X

a) Side View

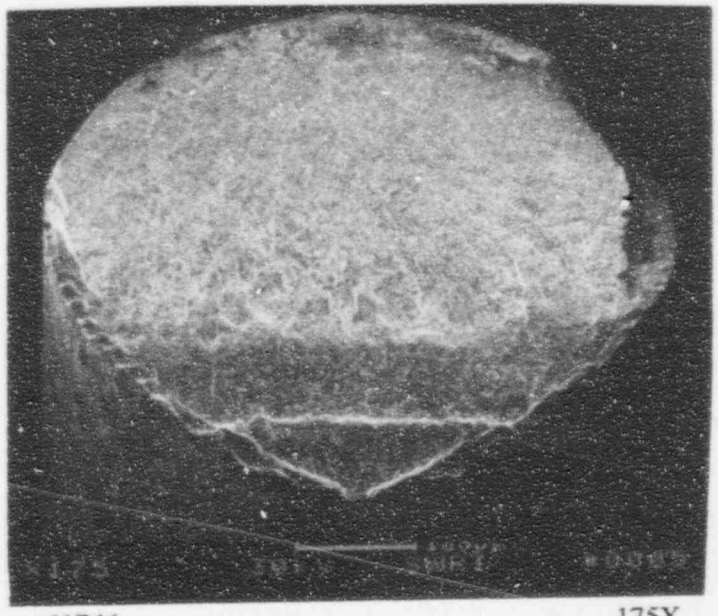

61746 175X

b) Fracture Surface

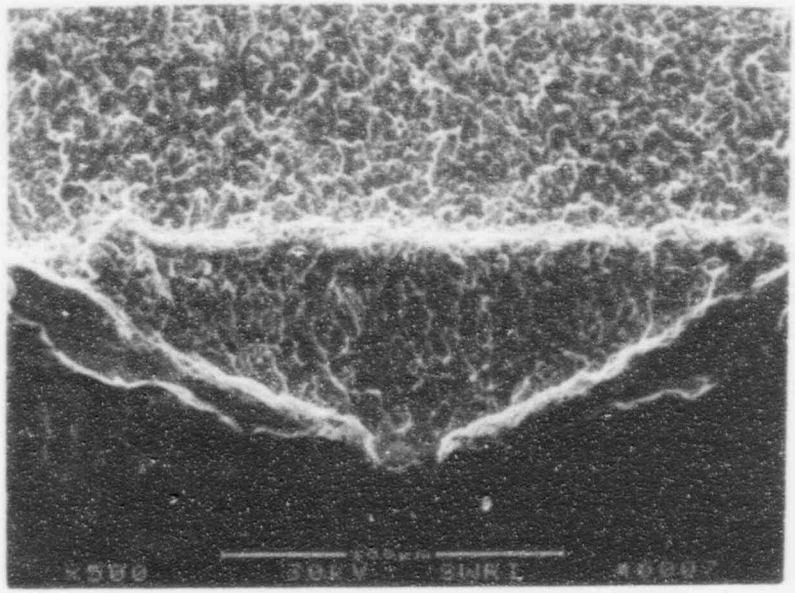

61748 500X

c) At Final Fracture

Figure D-4. SEM Photomicrographs and Fractographs from Hydrogen-Charged Specimen. Test No. HC-7. Charging Conditions: -1.0V, 100 Min.

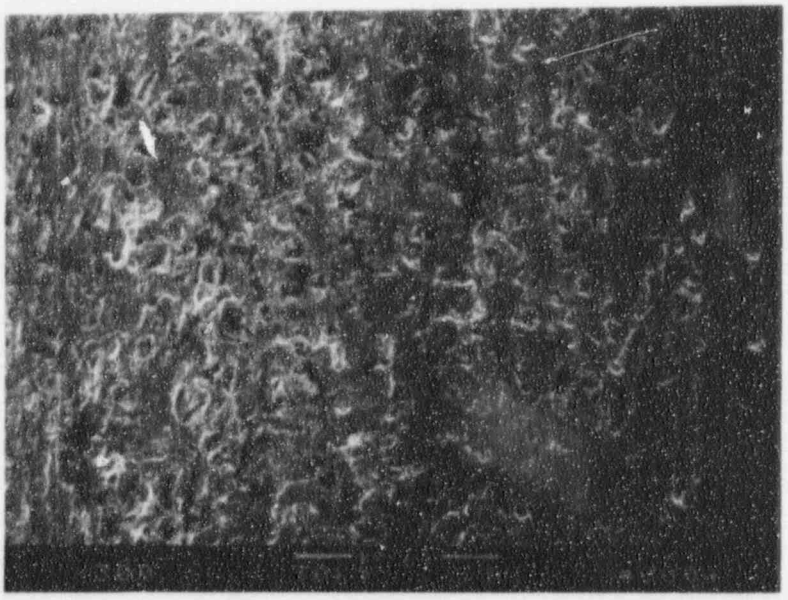

61744 300X

a) Outside of Bend

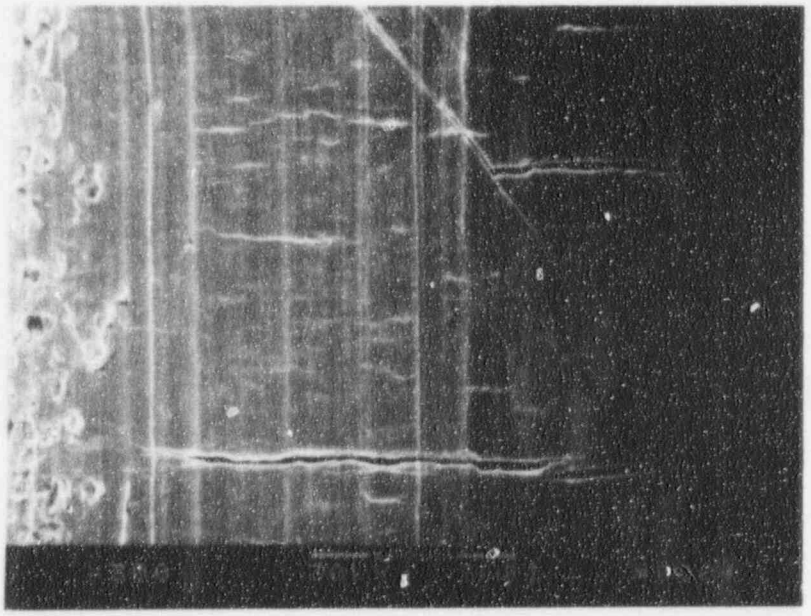

61743 300X

b) Inside of Bend

Figure D-5. SEM Photomicrographs from Surface of Hydrogen-Charged Bend Specimen. Test No. HC-5. Charging Conditions: 1.0V, 120 Min.

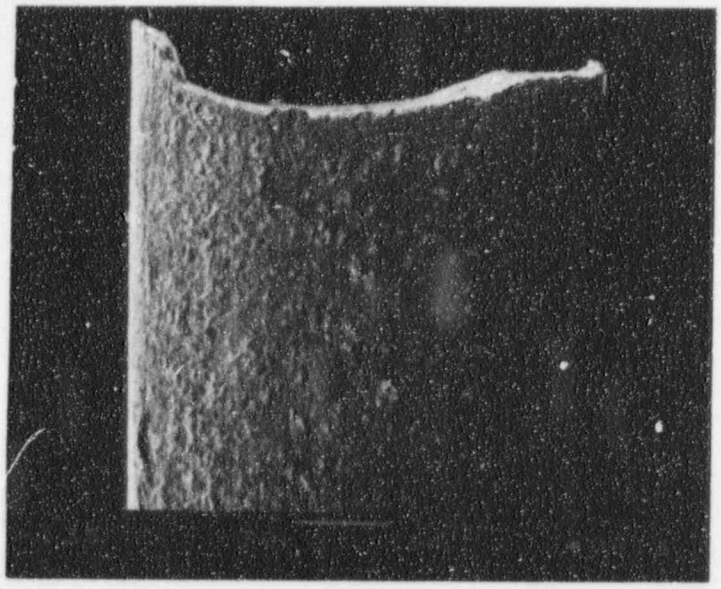

62065 135X

a) Side View

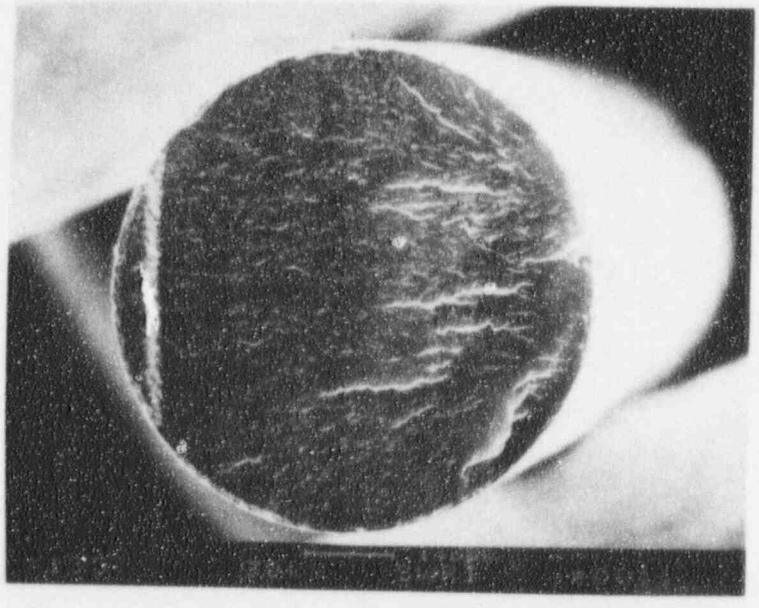

62060 135X

b)

Figure D-6. Fracture Surface of Hydrogen-Charged Bend Test Specimen. Test No. HC-5R. Charging Conditions: -1.0V, 120 Min. Reverse Bend After Initial test.

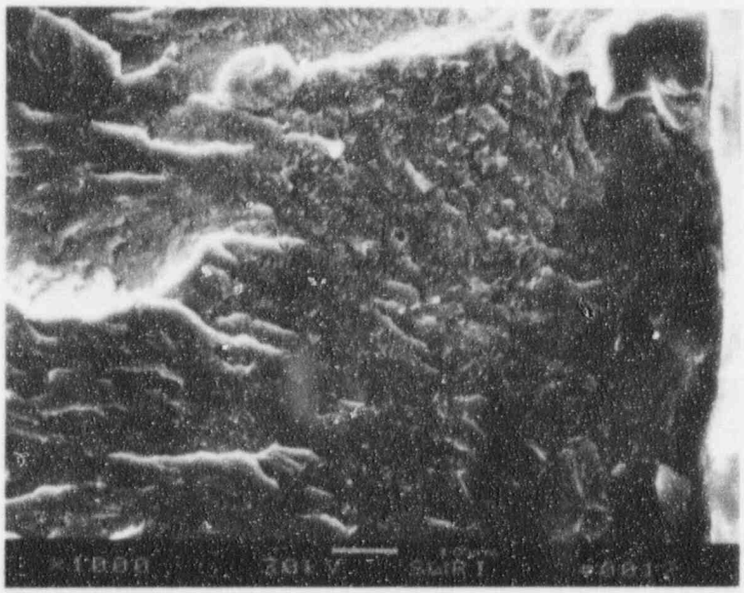

62061 1000X

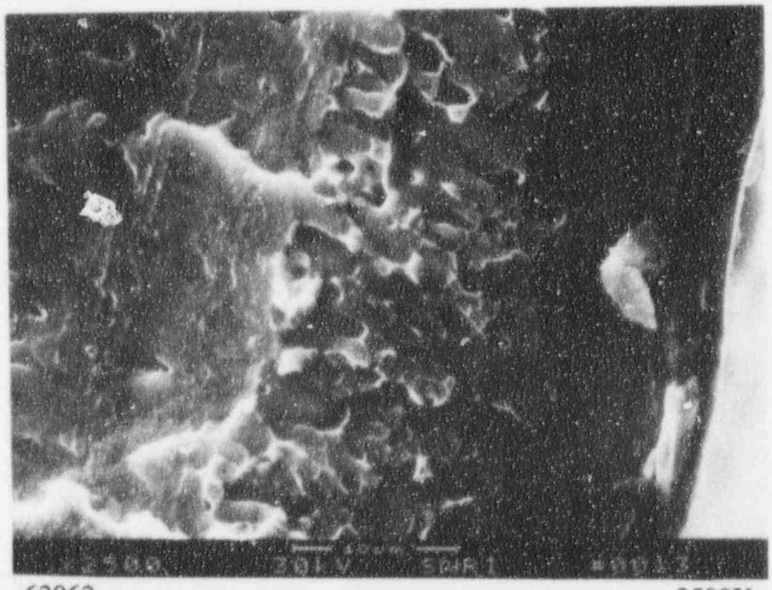

62062 2500X

b) Two Locations At Edge Near Origin

Figure D-7. SEM Fractographs from Hydrogen-Charged Bend Test Specimens. Test No. HC-5R.

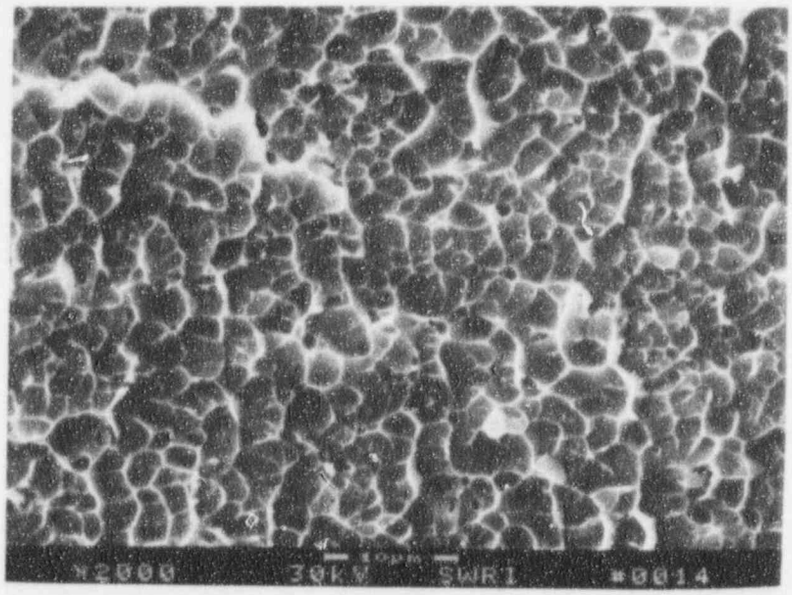

62063 2000X

a) Central Location

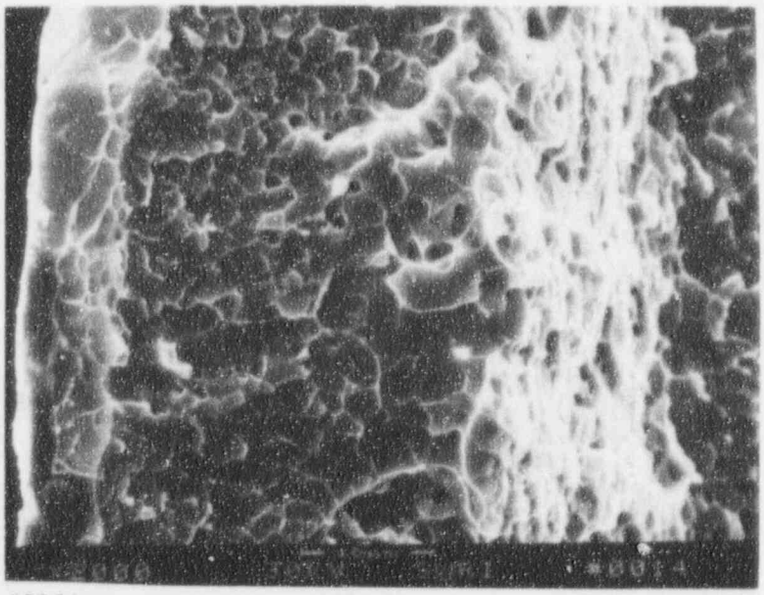

62064 2000X

b) At Edge Opposite Origin

Figure D-8. SEM Fractographs from Hydrogen-Charged Bend Test Specimens. Test No. HC-5R.

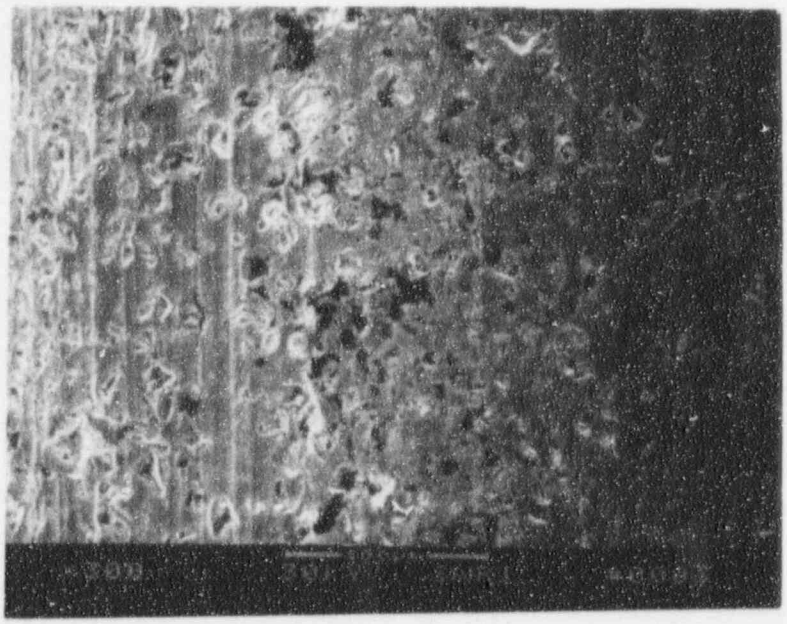

61741 300X

a) Outside of Bend

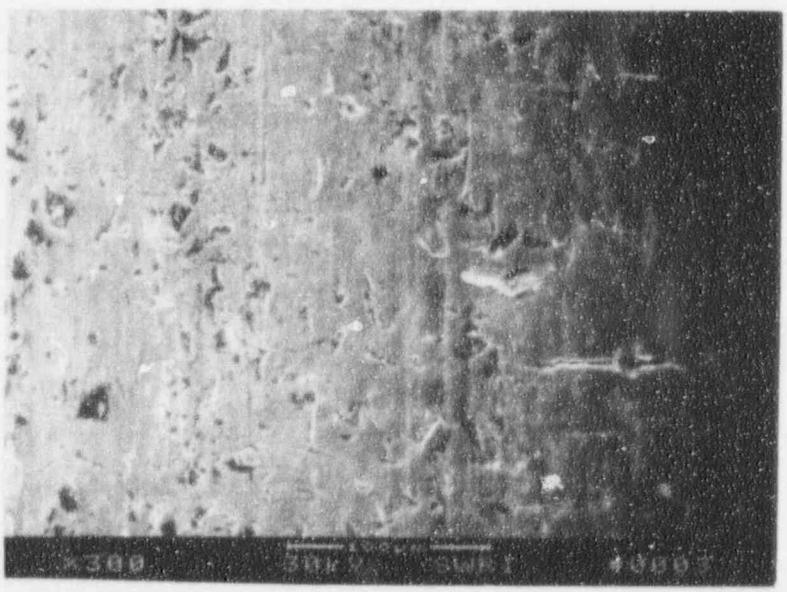

61740 300X

b) Inside of Bend

Figure D-9. SEM Photomicrographs from Surface of Hydrogen-Charged Bend Specimen. Test No. HC-8. Charging Conditions: -1.0V, 80 Min.

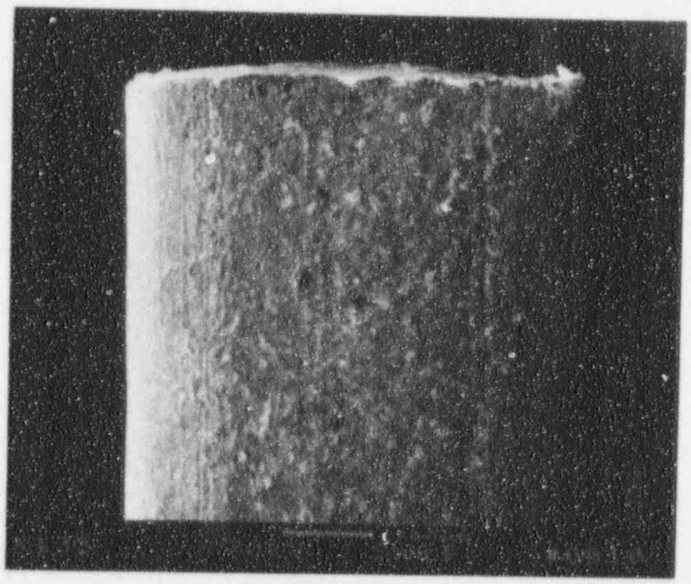

62059 135X

a) Side View

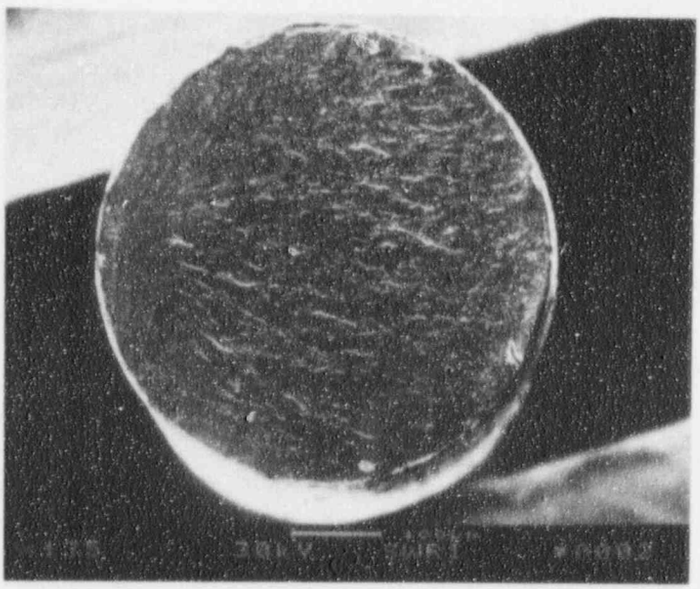

62052 135X

b) Fracture Surface

Figure D-10. Fracture Surface of Hydrogen-Charged Bend Test Specimen. Test No. HC-8R. Charging Conditions: -1.0V, 80 Min. Reverse Bend After Initial Tests.

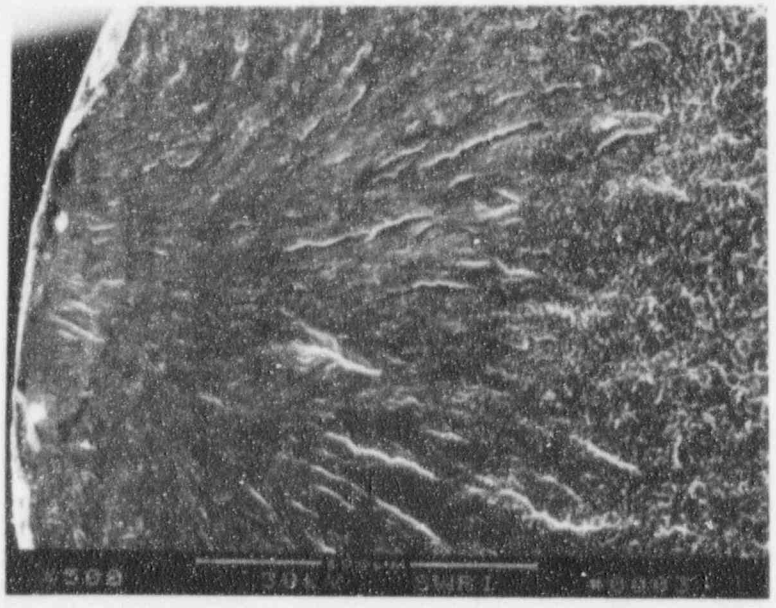

62053 500X

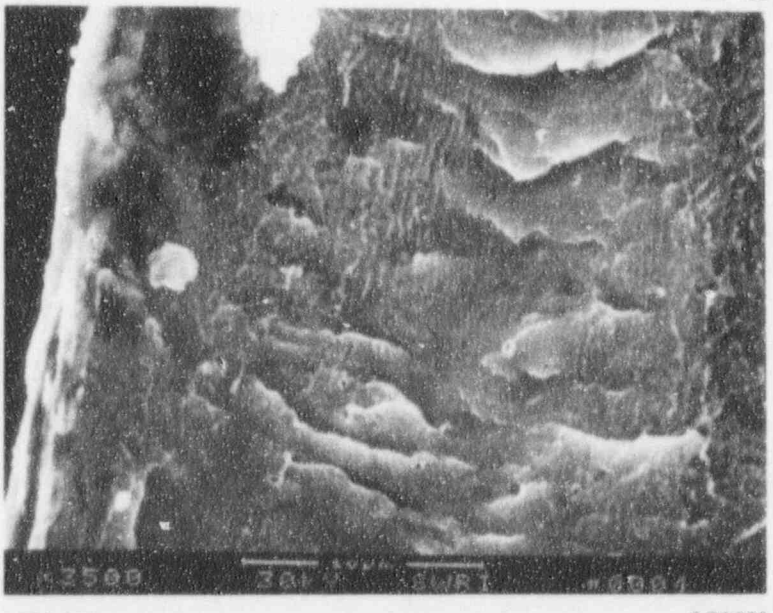

62054 3500X

At Origin

Figure D-11. SEM Fractographs from Hydrogen-Charged Bend Test Specimens. Test No. HC-8R.

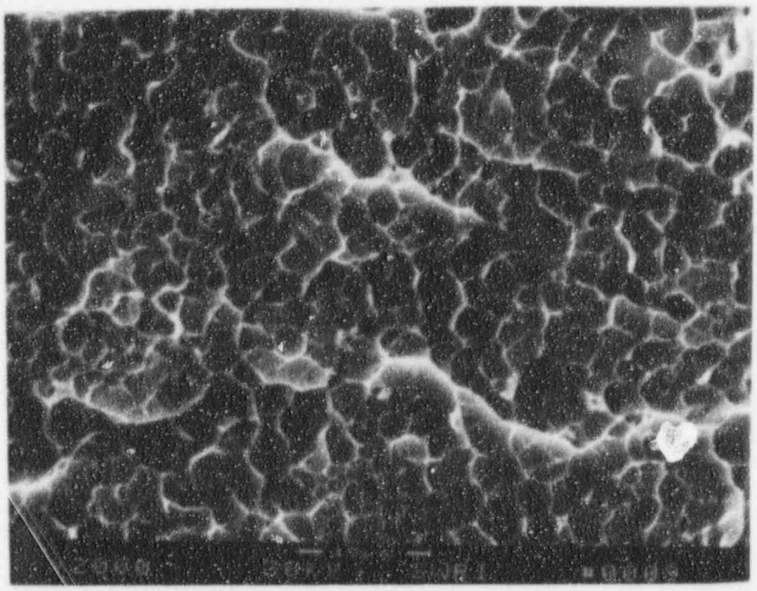

62057 2000X

a) Central Location

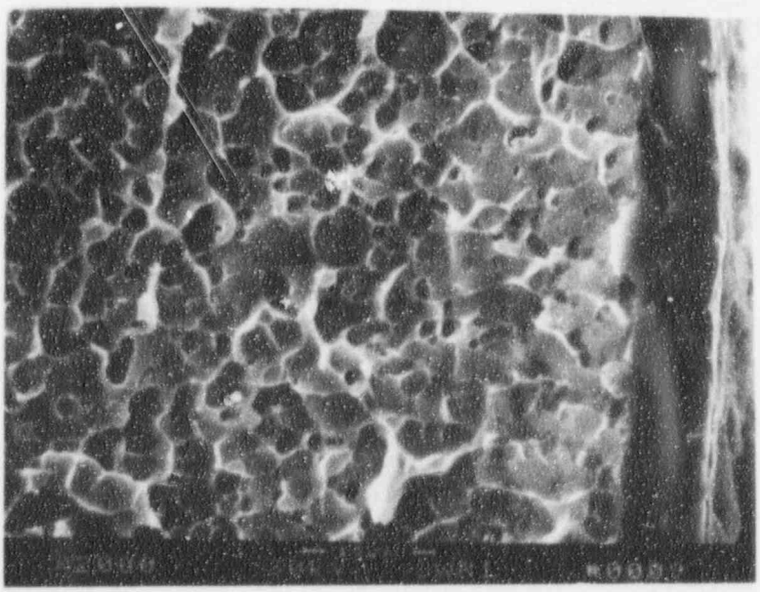

62058 2000X

b) At Edge Opposite Origin

Figure D-12. SEM Fractographs from Hydrogen-Charged Bend Test Specimens. Test No. HC-8R.

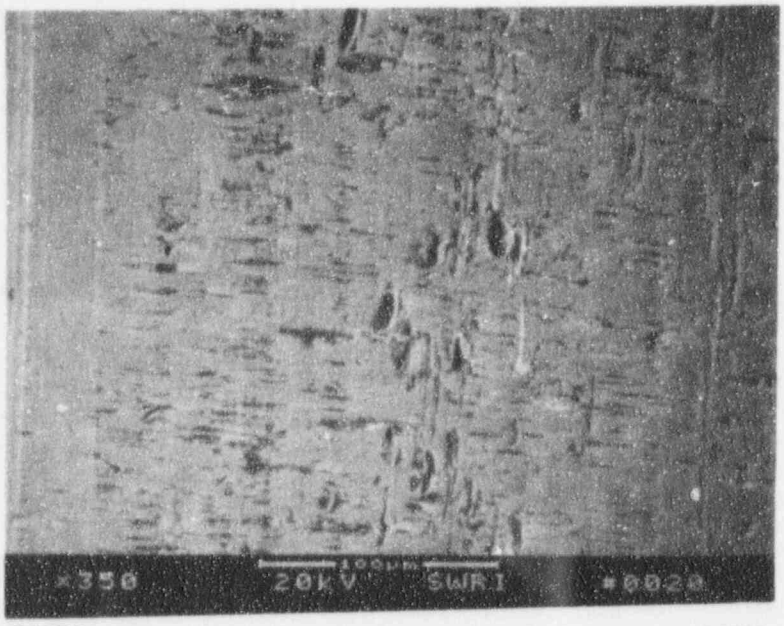

63376 350X

a) Outside of Bend

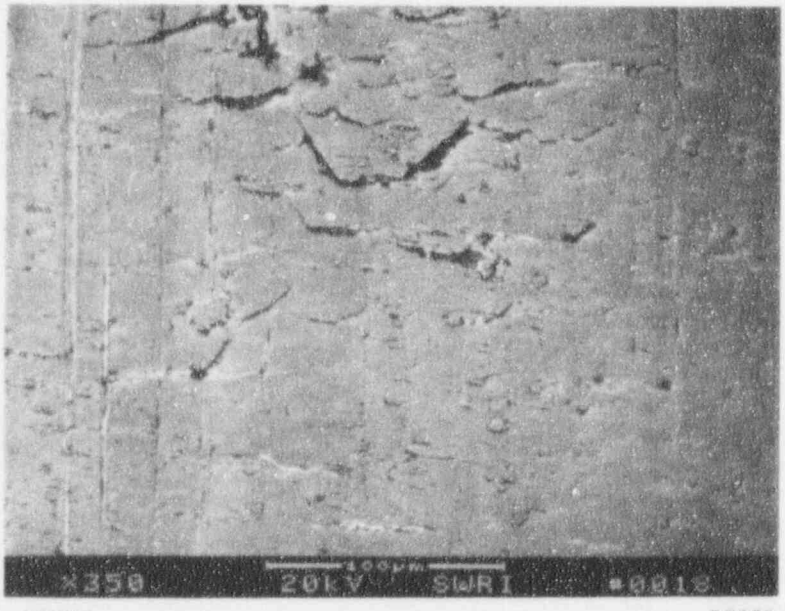

63375 350X

b) Inside of Bend

Figure D-13. SEM Photomicrographs of Surface of Hydrogen-Charged Bend Test Specimen. Test No. HC-19. Charging Conditions: -1.0V, 120 Min.; Tested After 52 Hrs. At Room Temperature.

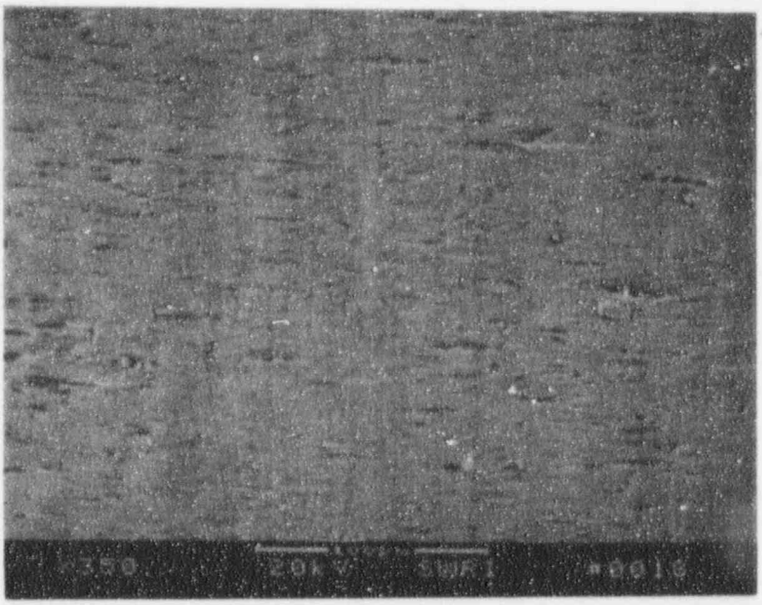

63374 350X

a) Outside of Bend

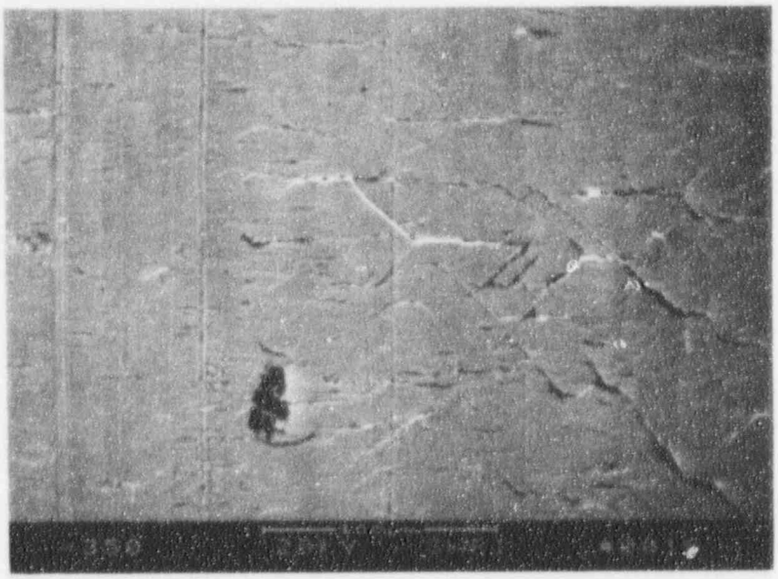

63373 350X

b) Inside of Bend

Figure D-14. SEM Photomicrographs of Surface of Hydrogen-Charged Bend Test Specimen. Test No. HC-21. Charging Conditions: -1.0V, 120 Min.; Tested After 2 Hrs. At 450°F.

APPENDIX E. LOAD DEFLECTION CURVE FOR HYDROGEN CHARGED SPECIMENS

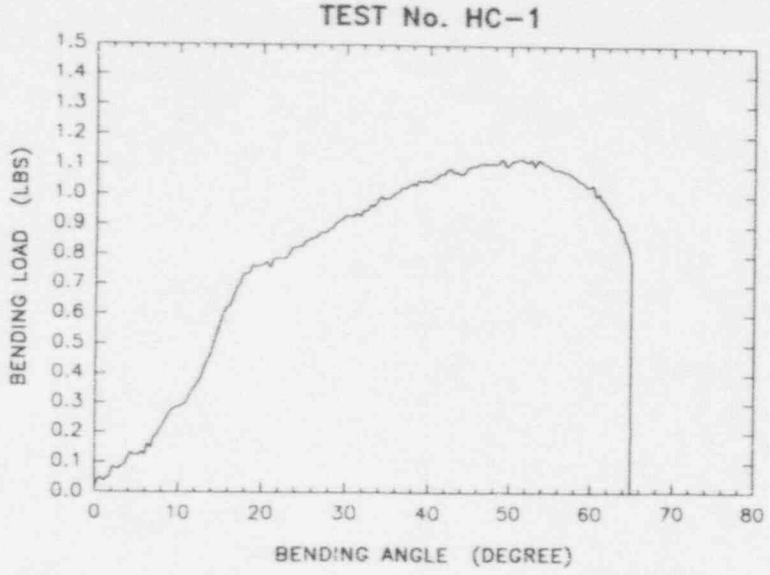

a)

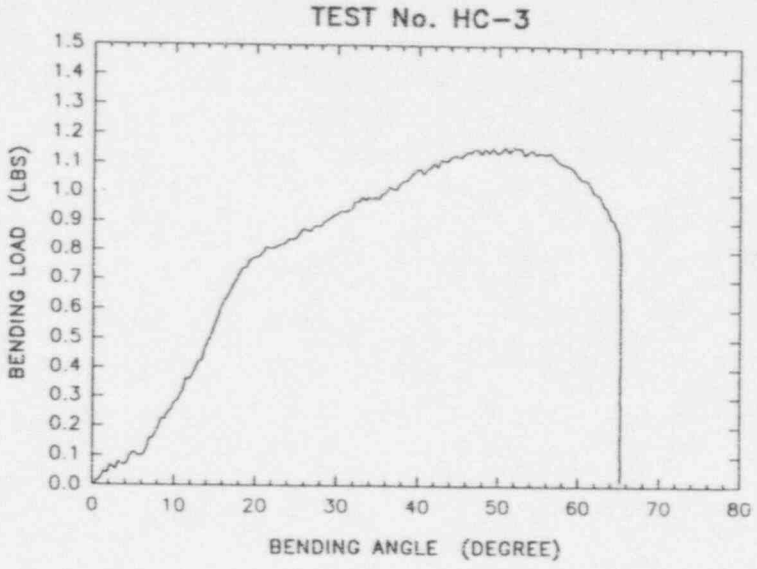

c)

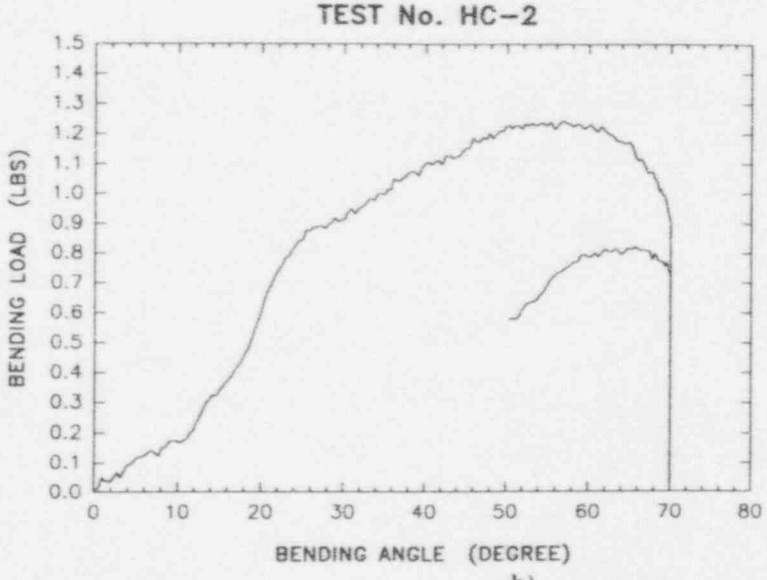

b)

Figure E-1. Plot of Bending Load vs. Angle for Test No. HC-1, HC-2, and HC-3.

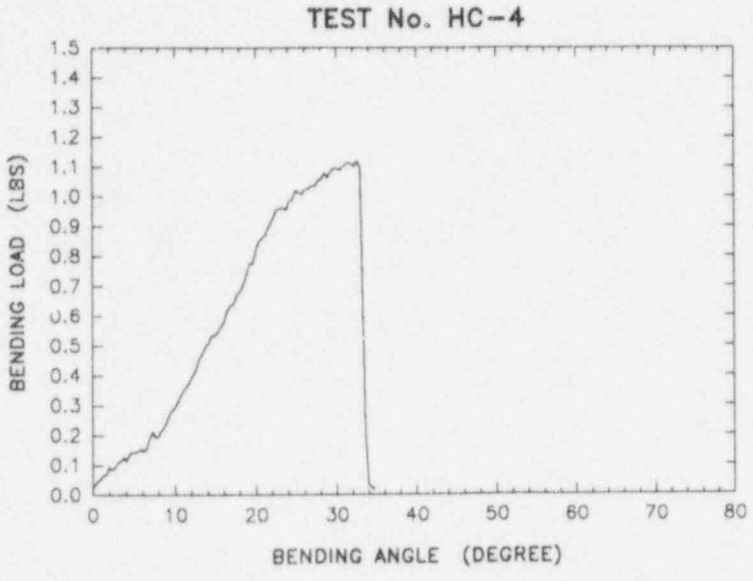

a)

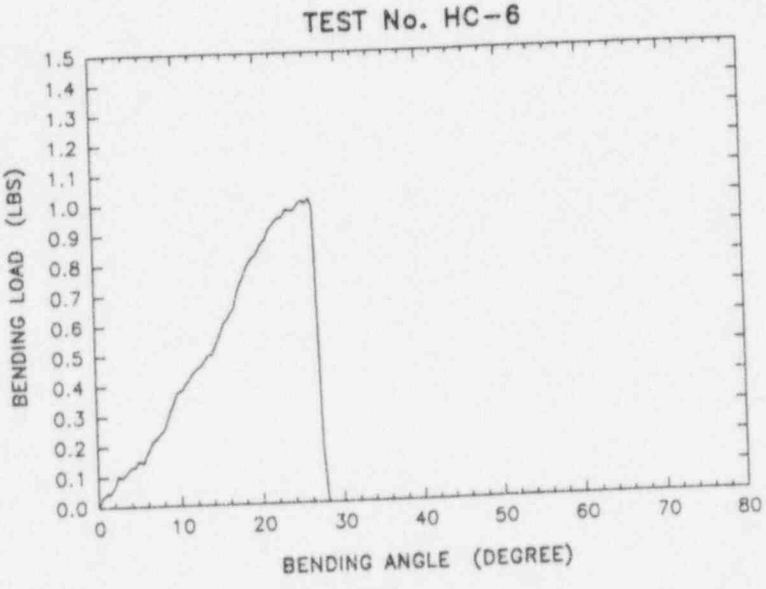

b)

Figure E-2. Plot of Bending Load vs. Angle for Test No. HC-4 and HC-6.

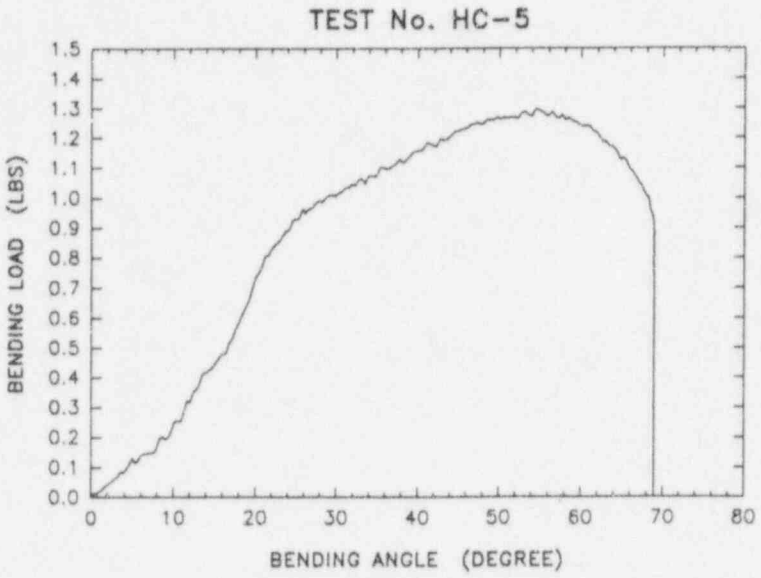

a)

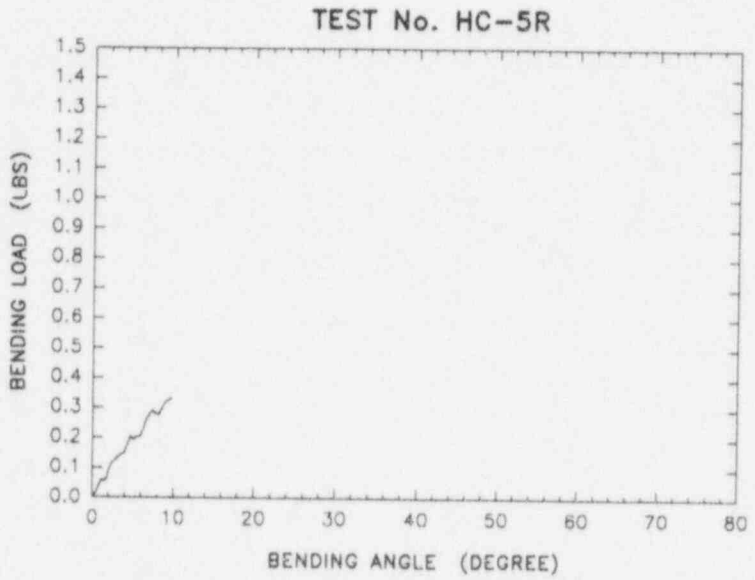

b)

Figure E-3. Plot of Bending Load vs. Angle for Test No. HC-5 and HC-5R.

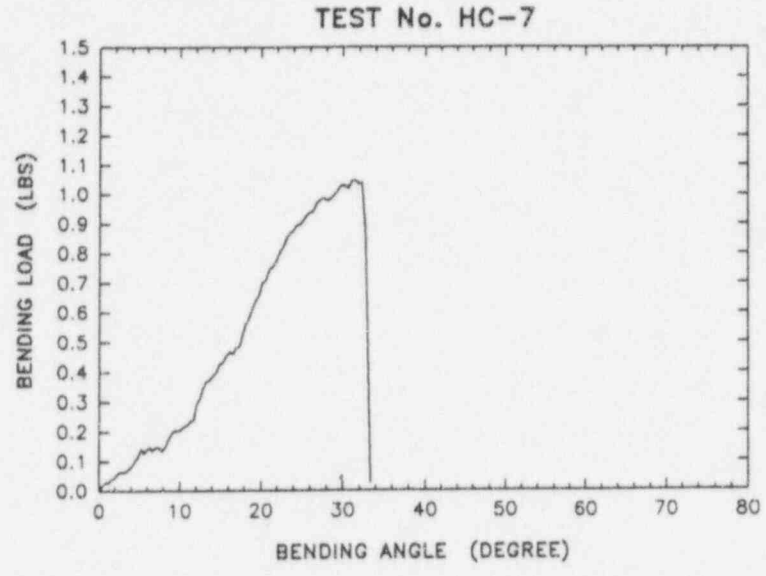

a)

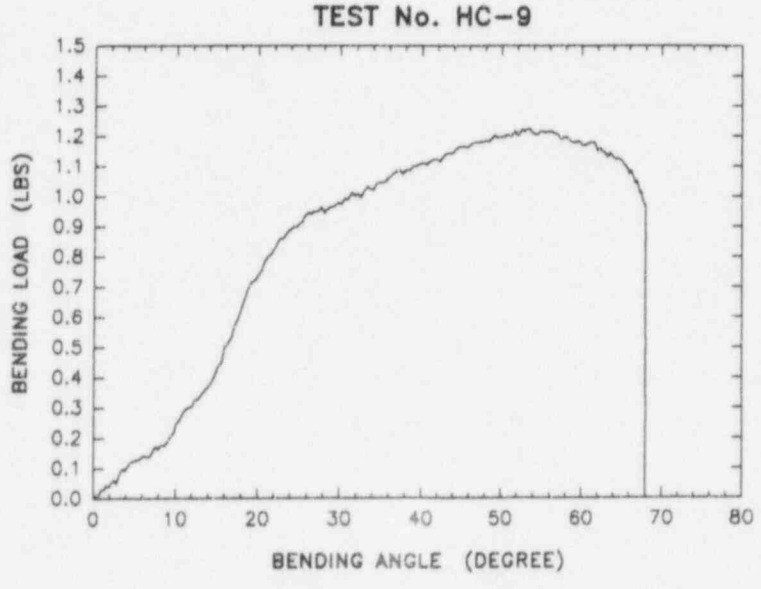

b)

Figure E-4. Piot of Bending Load vs. Angle for Test No. HC-7 and HC-9.

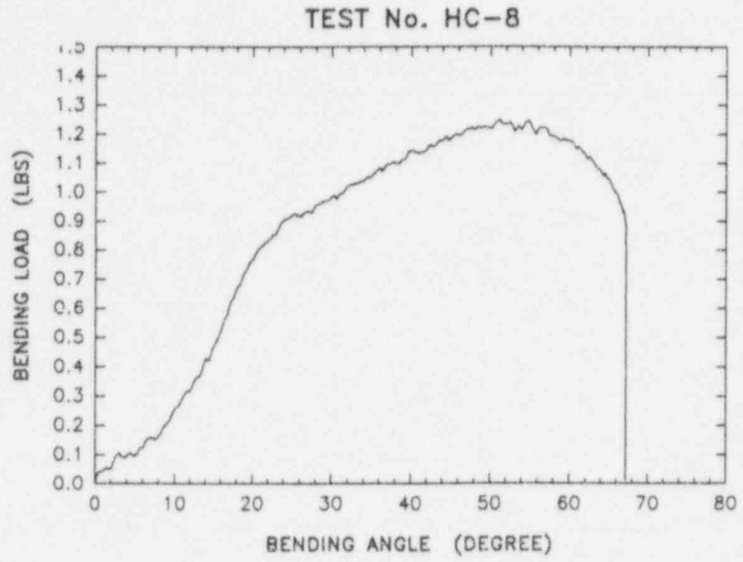

a)

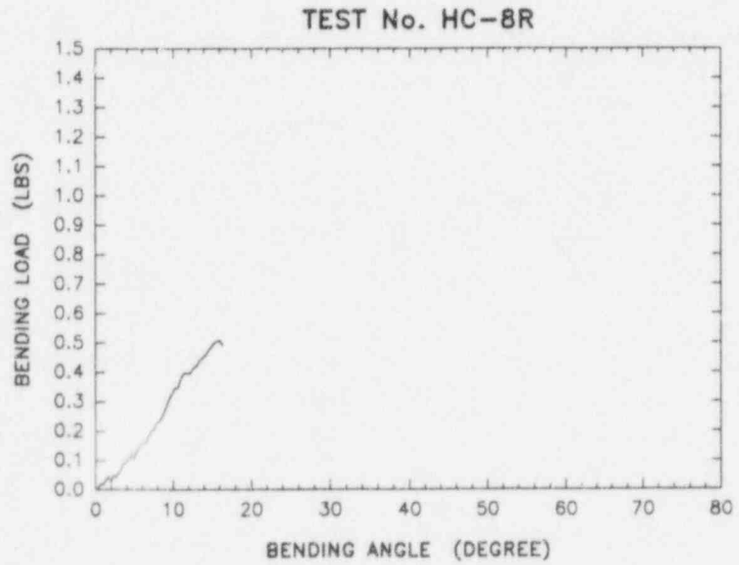

b)

Figure E-5. Plot of Bending Load vs. Angle for Test No. HC-8 and HC-8R.

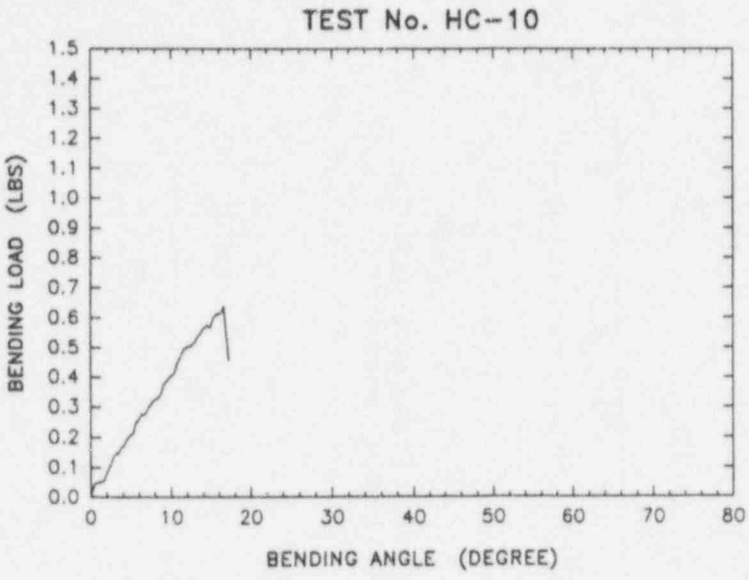

a)

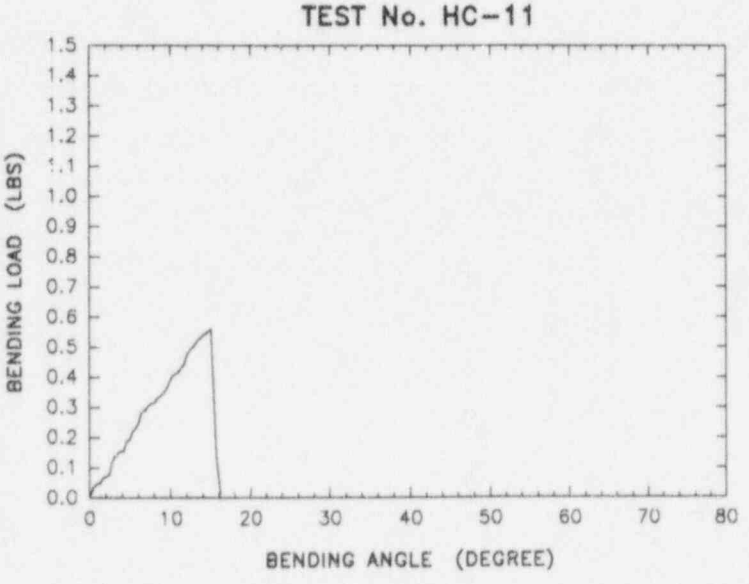

b)

Figure E-6. Plot of Bending Load vs. Angle for Test No. HC-10 and HC-11.

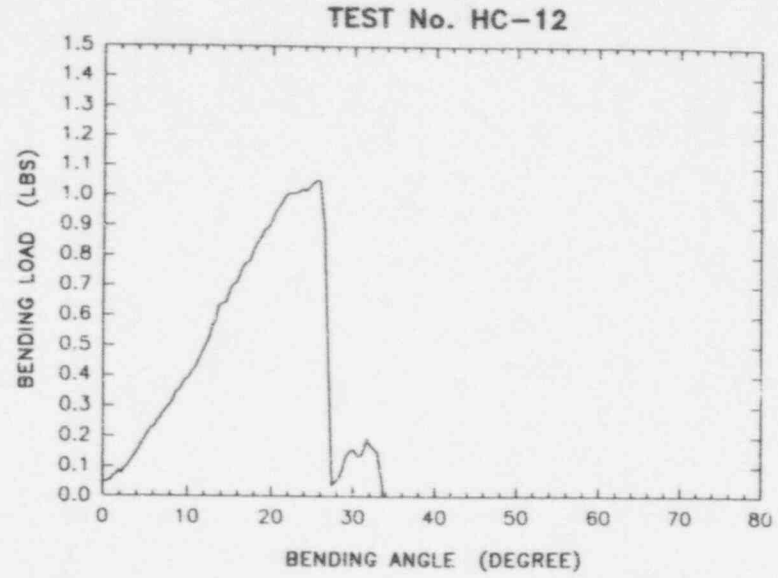

a)

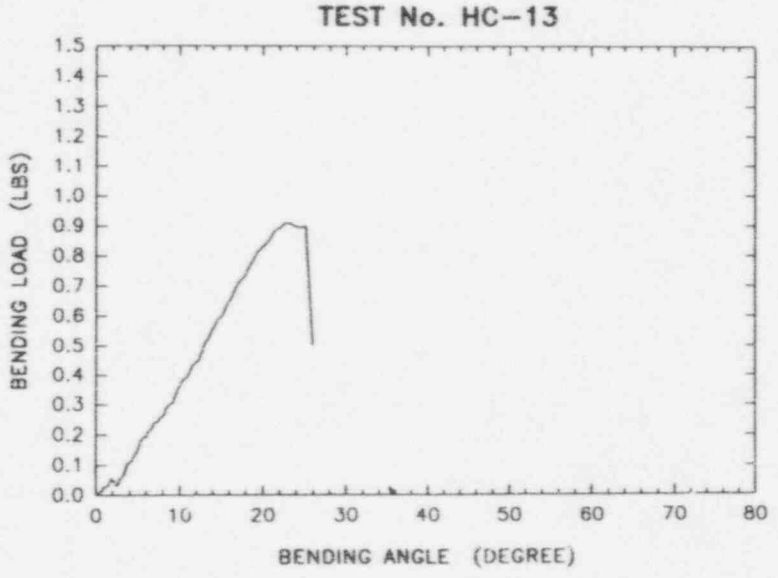

b)

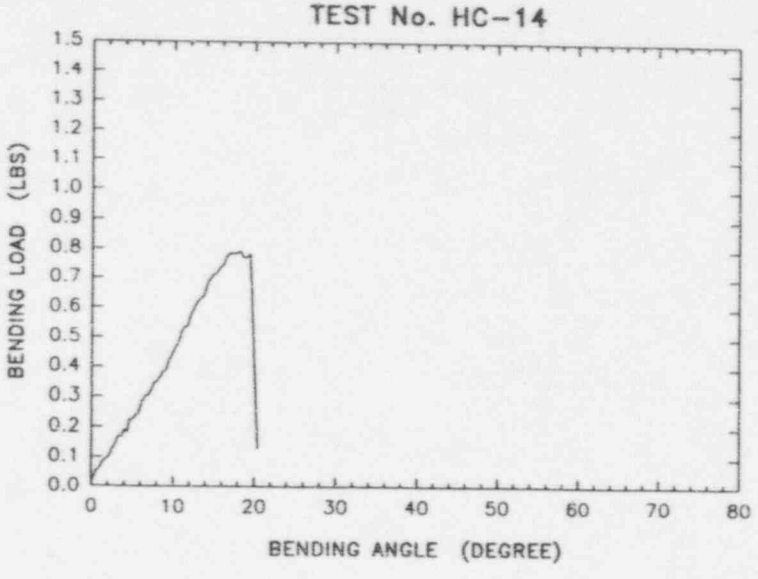

c)

Figure E-7. Plot of Bending Load vs. Angle for Test No. HC-12, HC-13, and HC-14.

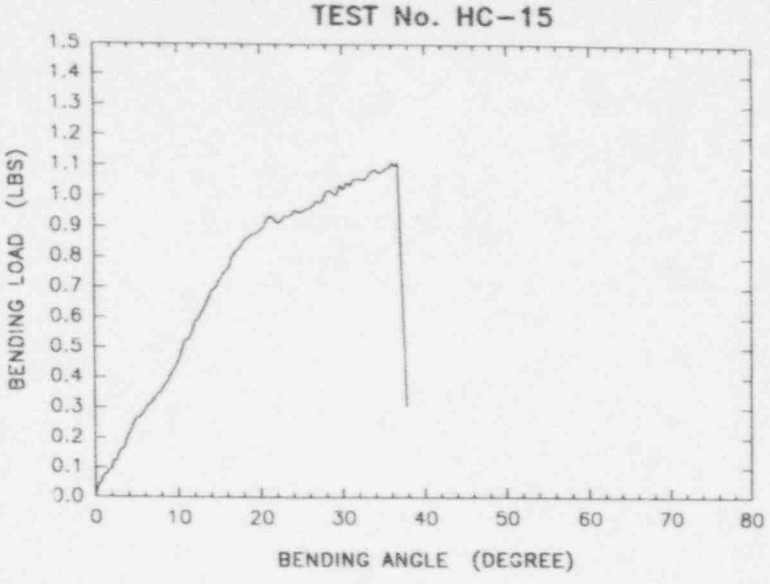

a)

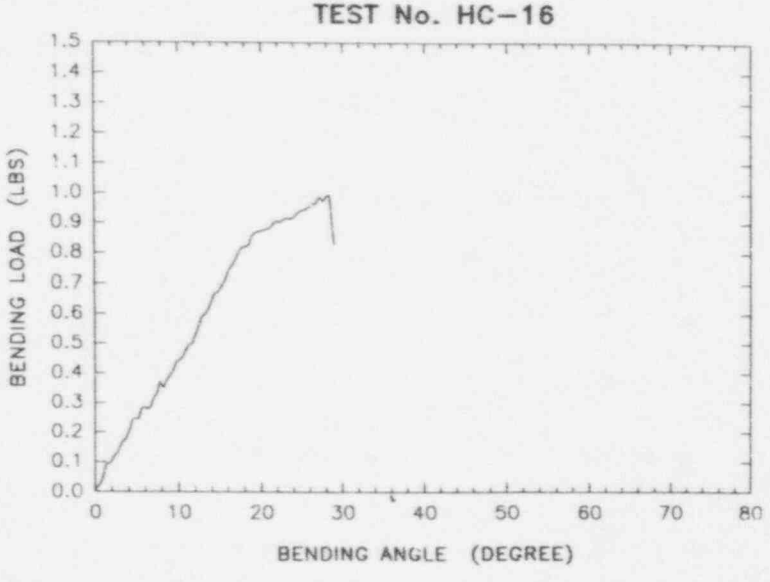

b)

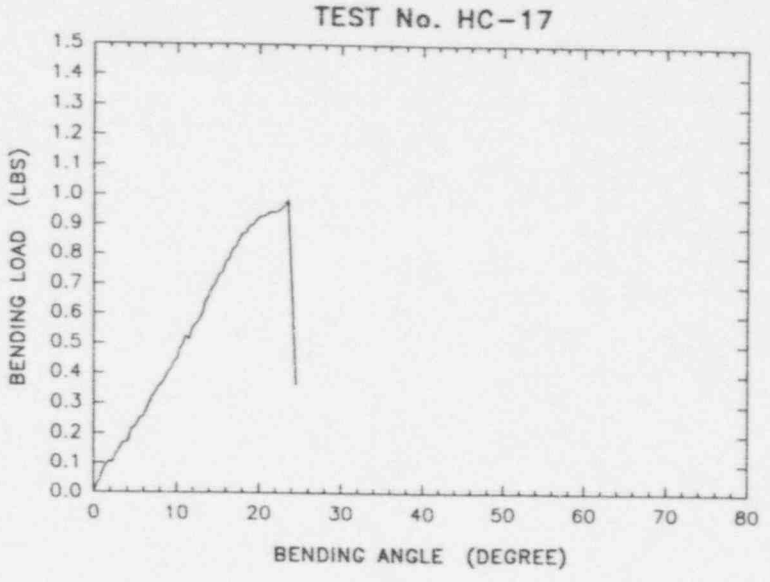

c)

Figure E-8. Plot of Bending Load vs. Angle for Test No. HC-15, HC-16, and HC-17.

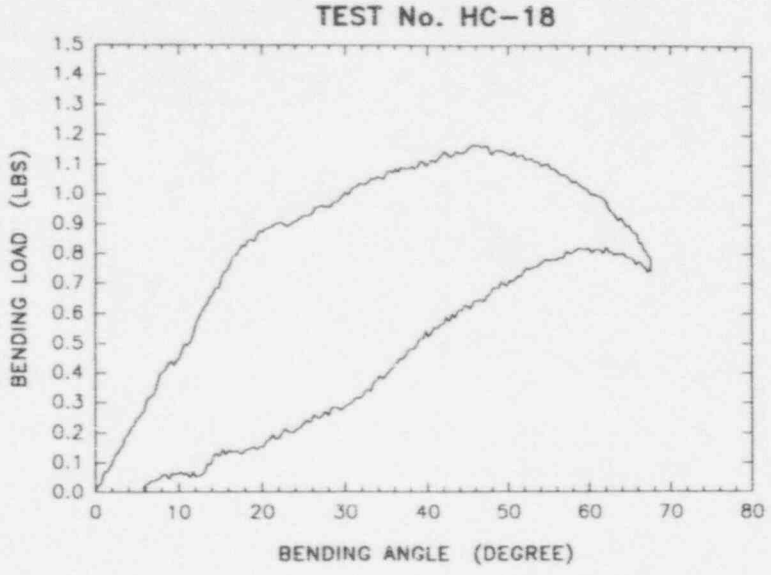

a)

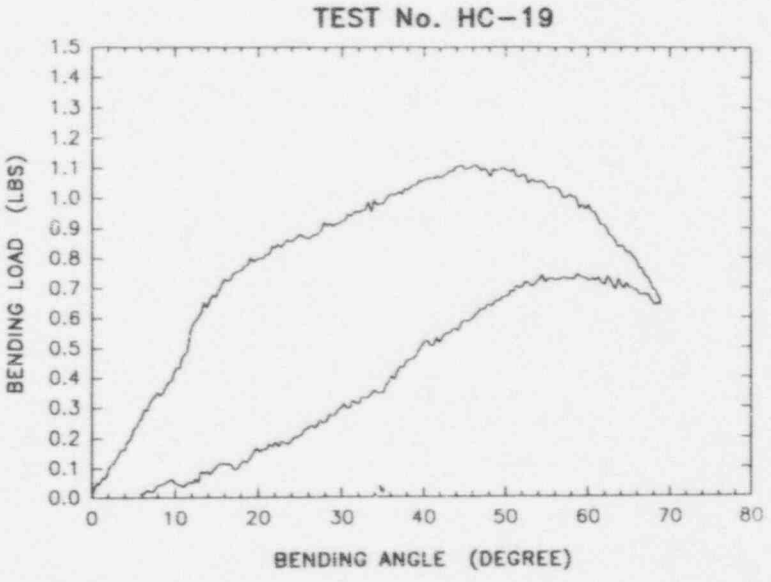

b)

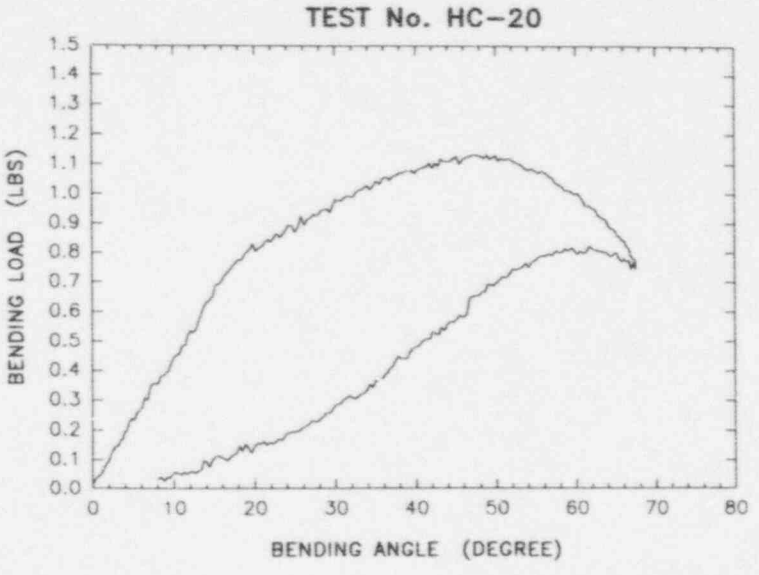

c)

Figure E-9. Plot of Bending Load vs. Angle for Test No. HC-18, HC-19, and HC-2O.

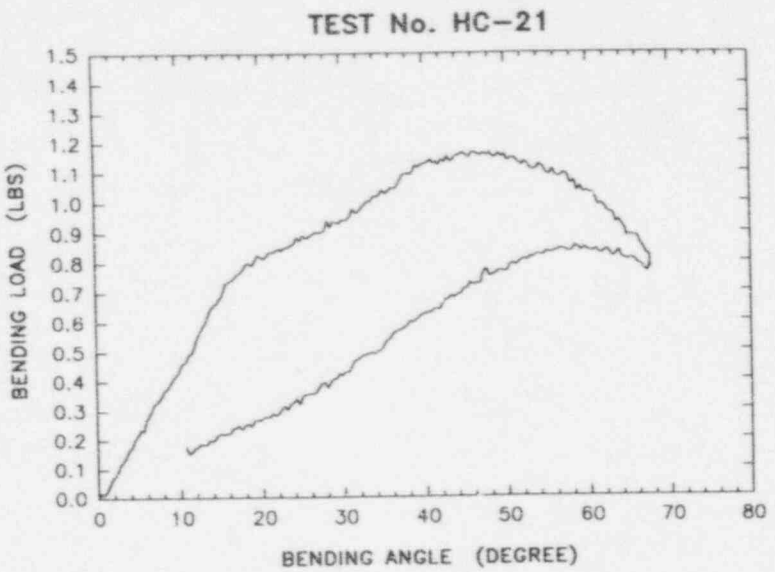

a)

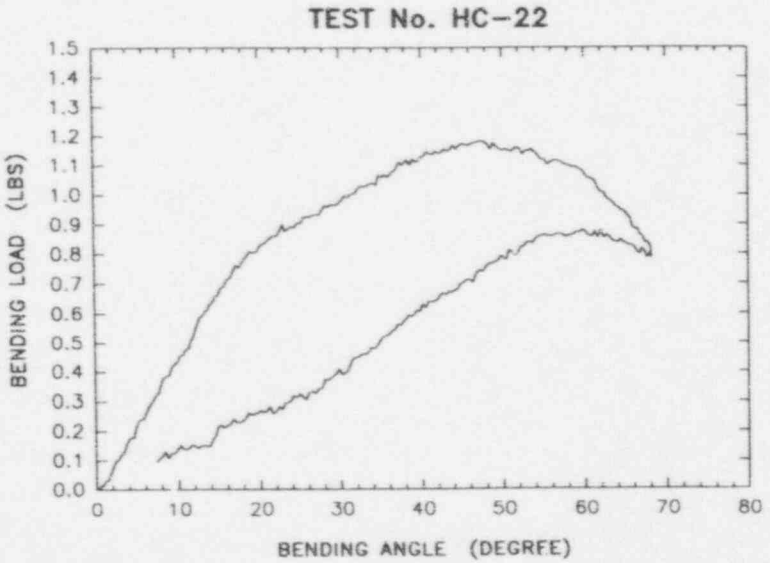

b)

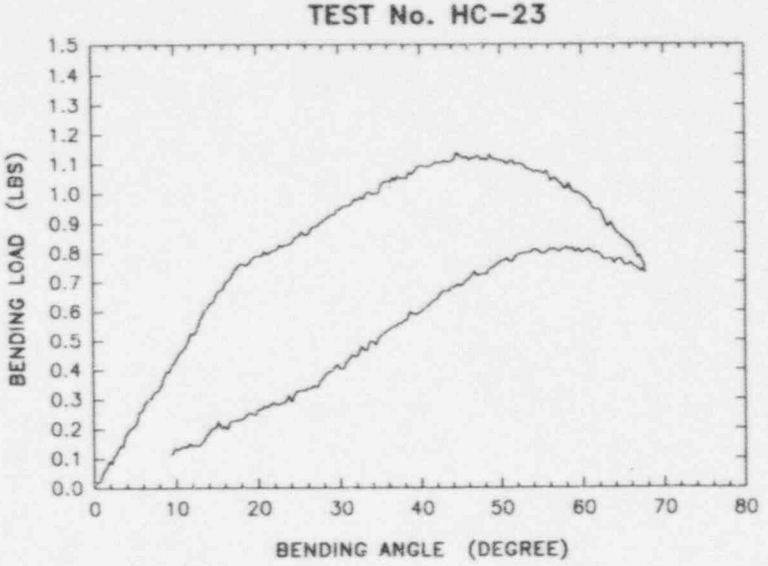

c)

Figure E-10. Plot of Bending Load vs. Angle for Test No. HC-21, HC-22, and HC-23.

APPENDIX F. RADIATION HANDLING AND SAFETY PROCEDURES

Due to the radioactive nature of the wires, all radioactive wires were handled according to SwRI Radiation Safety Regulations. All handling of the wires was by the Radiation Safety Officer (RSO) or under his direct supervision. Persons handling the wires or any parts of the wires that were more than 2 mr/hr (millirem) at a distance of 1 foot wore personnel TLD dosimeters. Persons handling wires that were likely to provide doses greater than 100 mr wore direct reading pocket dosimeters with the TLD dosimeter, ring TLD dosimeters, and a direct reading pocket dosimeter on the hand. No exposures in excess of the Texas Bureau of Radiation Control (TRBC) or SwRI have occurred.

SwRI has a Broad Form license from the TRBC which contains a specific amendment permitting possession of up to 50 Curies of Brachytherapy Ir-192 Sources in any form (to allow handling broken or unsealed sources.)

When the wires were tested, all handling was in a cell designed for up to 100,000 Curies of Co-60 so that non-monitored personnel would be out of the radiation exposure area. The Ir-192 wire was transferred to the wire testing system using long tongs and clamped into position. When the wire was secure in the test system, the excess wire was clipped off (the Ir-192 source cavity was inside the testing system holder.) A catcher was placed on the end of the test system to retain any wires that broke during testing. Testing was watched through a mirror from behind a 2 inches thick lead brick shield between the RSO and the testing equipment. After bend testing, the intact wires were transferred to lead shields designed for the environment selected. The wires remained in the radiation cell during all environmental exposures. Transfers were with rubber tipped tongs for best control of the wires which were often placed into small diameter holes. Broken wires were transferred to small copper tubes held in 2 inches thick lead bricks. When the wires were released, the copper tubes were sealed and transferred to cavities in lead containers for decay and disposal.

Some parts of broken wires were examined by placing them under a microscope mounted in a lead shield with a lead glass viewing window to minimize exposure during handling. For long "looks" in the microscope with really high radiation exposure rates, a pocket dosimeter was taped to the forehead or a baseball cap on the observer. Wires removed for Scanning Electron Microscope view were decontaminated to less than 100 cpm removeable contamination and were all below 2 mr/hr at one foot from the specimen.

After handling the wires, all areas and equipment involved were wiped to detect contamination and decontaminated when removeable contamination was found. When testing was done, the air flow in the radiation cell was from the test system to HEPA filters and then outside to prevent contamination of the person handling the wires. All materials involved in the testing remain in the radiation cell until removeable contamination is removed. All wires, shields, and containers with wires remain in the radiation cell at this time.

APPENDIX G. POTENTIAL PATHWAYS FOR FORMATION OF HF IN STORAGE OF SOURCEWIRES

Teflon is one brand name of poly (tetrafluoro) ethylene (PTFE), which is a polymeric substance with the repeating unit shown below:

$$—[CF_2 - CF_2]_n - \qquad (n \sim 1000)$$

PTFE is a relatively inert material that effectively resists attack by nearly all chemical species. In a radioactive flux of sufficient intensity, the polymer is likely to break down through the formation of radicle or ionic species as outlined in Reactions 1 and 2 below.

Reaction 1

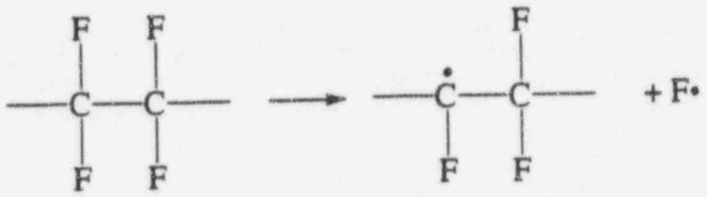

Reaction 2

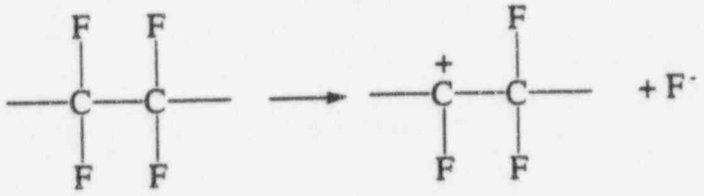

Beta particles, such as those emitted from iridium sources used in oncology, are relatively large and travel at speeds close to the speed of light. They possess sufficient energy to induce the cleavage of the C-F bond in either a homolytic or heterolytic manner. If homolytic cleavage were to occur, fluorine radicles would be produced, while if heterolytic cleavage would produce fluorine anions. Both fluorine species are capable of producing hydrofluoric acid through reaction with any moisture that may be present, as illustrated in Reactions 3 and 4.

(4) $H_2O + F\cdot \rightarrow HF + \cdot OH$

(5) $H_2O + F^- \rightarrow HF + OH-$

While it is difficult to predict the fate of the hydroxy radicle or the hydroxyl anion, either is likely to be stabilized by reaction with whatever oxide species are present on the nearly metal surface. The HF produced would also be in close proximity to the metal, and without a barrier to diffusion, would proceed to attack and embrittle the alloy.

A thin oxide layer exists on the surface of all metal articles that are exposed to air. Unless extreme measures are taken, this oxide layer will contain a certain percentage of hydroxy function. These hydroxy functions can also react with fluorine species to produce HF in a manner similar to that illustrated above with water (Reactions 6 and 7).

(6) $F\cdot$ HO-Metal $\rightarrow$ HF $\cdot$O-Metal

(7) F^- HO-Metal $\rightarrow$ HF $^-$O-Metal

Unless moisture is rigorously excluded from the chamber containing the article, and extreme measures are taken to remove hydroxyl functions from the oxide present on the metal's surface, HF will likely be produced by reaction of radiation-induced PTFE decomposition products with moisture or hydroxy functions on the metal surface.

NRC FORM 335 (2-89) NRCM 1102, 3201, 3202

U.S. NUCLEAR REGULATORY COMMISSION

BIBLIOGRAPHIC DATA SHEET

(See instructions on the reverse)

1. REPORT NUMBER (Assigned by NRC, Add Vol., Supp., Rev., and Addendum Numbers, if any.)
NUREG/CR-6074
04-4448-010
Vol. 2

2. TITLE AND SUBTITLE
Sealed Source and Device Design Safety Testing
Technical Report on the Findings of Task 4
Investigation of Failed Nitinol Brachytherapy Wire

3. DATE REPORT PUBLISHED
MONTH: March
YEAR: 1996

4. FIN OR GRANT NUMBER
D2553

5. AUTHOR(S)
D. J. Benac, H. C. Burghard

6. TYPE OF REPORT

7. PERIOD COVERED *(Inclusive Dates)*

8. PERFORMING ORGANIZATION – NAME AND ADDRESS *(If NRC, provide Division, Office or Region, U.S. Nuclear Regulatory Commission, and mailing address; if contractor, provide name and mailing address.)*
Southwest Research Institute
6220 Culebra Road
San Antonio, TX 78238-5166

9. SPONSORING ORGANIZATION – NAME AND ADDRESS *(If NRC, type "Same as above"; if contractor, provide NRC Division, Office or Region, U.S. Nuclear Regulatory Commission, and mailing address.)*
Division of Industrial and Medical Nuclear Safety
Office of Nuclear Material Safety and Safeguards
U. S. Nuclear Regulatory Commission
Washington, DC 20555-0001

10. SUPPLEMENTARY NOTES
D.H. Tiktinsky, NRC Project Manager

11. ABSTRACT *(200 words or less)*

This report covers an investigation of the nature and cause of failure in Nitinol brachytherapy sourcewires. The investigation was initiated after two clinical incidents in which sourcewires failed during or immediately after a treatment. The investigation determined that the two clinical Nitinol sourcewires failed in a brittle manner, which is atypical for Nitinol. There were no material anomalies or subcritical flaws to explain the brittle failures. The bend tests also demonstrated that neither moist environment, radiation, nor low-temperature structure transformation was a likely root cause of the failures. However, degradation of the PTFE was consistently evident, and those sourcewires shipped or stored with PTFE sleeves consistently failed in laboratory bend tests. On the basis of the results of this study, it was concluded that the root cause of the in-service failures of the sourcewires was environmentslly induced embrittlement due to the breakdown of the PTFE protective sleeves in the presence of the high-radiation field and subsequent reaction or interaction of the breakdown products with the Nitinol alloy.

12. KEY WORDS/DESCRIPTORS *(List words or phrases that will assist researchers in locating the report.)*
safety testing, brachytherapy, Nitinol, sourcewires, PTFE, failed wires

13. AVAILABILITY STATEMENT
unlimited

14. SECURITY CLASSIFICATION
(This Page) unclassified
(This Report) unclassified

15. NUMBER OF PAGES

16. PRICE

Federal Recycling Program

UNITED STATES
NUCLEAR REGULATORY COMMISSION
WASHINGTON, DC 20555-0001

OFFICIAL BUSINESS
PENALTY FOR PRIVATE USE, $300

SPECIAL FOURTH-CLASS MAIL
POSTAGE AND FEES PAID
USNRC
PERMIT NO. G-67